Mathematics for Industry 7

Kazuyuki Aihara
Jun-ichi Imura
Tetsushi Ueta *Editors*

Analysis and Control of Complex Dynamical Systems

Robust Bifurcation, Dynamic Attractors, and Network Complexity

Springer

Mathematics for Industry

Volume 7

Aims & Scope

The meaning of "Mathematics for Industry" (sometimes abbreviated as MI or MfI) is different from that of "Mathematics in Industry" (or of "Industrial Mathematics"). The latter is restrictive: it tends to be identified with the actual mathematics that specifically arises in the daily management and operation of manufacturing. The former, however, denotes a new research field in mathematics that may serve as a foundation for creating future technologies. This concept was born from the integration and reorganization of pure and applied mathematics in the present day into a fluid and versatile form capable of stimulating awareness of the importance of mathematics in industry, as well as responding to the needs of industrial technologies. The history of this integration and reorganization indicates that this basic idea will someday find increasing utility. Mathematics can be a key technology in modern society.

The series aims to promote this trend by (1) providing comprehensive content on applications of mathematics, especially to industry technologies via various types of scientific research, (2) introducing basic, useful, necessary and crucial knowledge for several applications through concrete subjects, and (3) introducing new research results and developments for applications of mathematics in the real world. These points may provide the basis for opening a new mathematics-oriented technological world and even new research fields of mathematics.

More information about this series at http://www.springer.com/series/13254

Kazuyuki Aihara · Jun-ichi Imura
Tetsushi Ueta
Editors

Analysis and Control of Complex Dynamical Systems

Robust Bifurcation, Dynamic Attractors, and Network Complexity

Springer

Editors
Kazuyuki Aihara
The University of Tokyo
Tokyo
Japan

Jun-ichi Imura
Tokyo Institute of Technology
Tokyo
Japan

Tetsushi Ueta
Tokushima University
Tokushima
Japan

ISSN 2198-350X ISSN 2198-3518 (electronic)
Mathematics for Industry
ISBN 978-4-431-55012-9 ISBN 978-4-431-55013-6 (eBook)
DOI 10.1007/978-4-431-55013-6

Library of Congress Control Number: 2015933364

Springer Tokyo Heidelberg New York Dordrecht London

Printed on acid-free paper

Springer Japan KK is part of Springer Science+Business Media (www.springer.com)

Preface

Recent advanced communication and information technologies have attracted our attention to developments of highly dependable, strongly resilient, and energy-efficient systems with applications to intelligent transportation systems (ITS), smart grids, high-level medical diagnosis/treatment systems, and so on. Such systems in general involve complex behavior induced by interactions among subsystems, and complex network structure as well as a large number of components. We need to analyze such complex behavior for capturing the intrinsic properties of the systems and to design control systems for realizing the desirable behavior. Both dynamical systems theory and control systems theory will play indispensable and central roles in addressing such issues.

Dynamical systems theory originated from Newton's motion equations in the seventeenth century, and has been founded by Poincaré's great contributions late in the nineteenth century. After that, various mathematical methods such as ergodic theory, stability theory of periodic solutions including equilibrium points, and bifurcation theory for nonlinear dynamical systems have been developed, and since the late 1970s, they have been extended to different research topics on more complex phenomena/control such as bifurcations to chaos, chaos control, and chaos synchronization.

On the other hand, James Watt's steam engine at the industrial revolution in the eighteenth century has opened the gate to feedback control, and Maxwell's stability analysis late in the nineteenth century, which theoretically analyzed the instability phenomena of steam engines, was the occasion of developing control systems theory. Continuing upon classical control theory dealing with control system design mainly in the frequency domain since the 1920s, modern control theory has been advancing since the 1960s, which enables us to analyze controllability/observability and to design optimal control by means of state equations in the time domain. Moreover, a deep understanding on robustness of the system behavior for dynamic uncertainty including unmodeled dynamics in addition to parametric uncertainty has been gained, and then robust control theory has been developed since the 1980s.

The above two research fields, however, have been developing almost independently so far, although there have been several successes to be related in both fields such as Pontryagin's maximum principle and R.E. Kalman's pioneering contribution on chaos and control theory. The main focus in dynamical systems theory is nonlinear autonomous dynamics with a kind of unstable phenomena like bifurcations and chaos, while the focus in control systems theory is feedback stabilization of linear non-autonomous dynamics at an equilibrium point. This motivates us to develop a new paradigm on analysis and control of complex/large-scale dynamical systems throughout collaborative research between dynamical systems theory and control systems theory.

This book, which is the first trial toward developments of such a new paradigm, presents fundamental and theoretical breakthroughs on analysis and control of complex/large-scale dynamical systems toward their applications to various engineering fields. In particular, this book focuses on the following three topics:

1. Analysis and control of bifurcation under model uncertainty.
2. Analysis and control of complex behavior including quasi-periodic/chaotic orbits.
3. Modeling of network complexity emerging from dynamical interaction among subsystems.

According to the above three topics, this book is organized as follows: In Part I, robust bifurcation analysis, which deals with bifurcation analysis for dynamical systems subject to uncertainty due to unmodeled dynamics, is presented and various kinds of bifurcation control methods based on the degree of stability are proposed. Part II begins with the analysis of chaotic behavior of triangle-folding maps, and presents novel attempts for controlling various kinds of complex behavior, namely feedback stabilization of quasi-periodic orbits and spatial patterns, chaos control, ultra-discretization based control, and control of unstabilizable switched systems. Finally, Part III includes research topics on network model reduction and network structure identification toward control of large-scale network systems.

This book can be beneficial to mathematicians, physicists, biophysicist as well as researchers on nonlinear science and control engineering for a better fundamental understanding of analysis and control synthesis of such complex systems.

We would like to thank the contributors: Shun-ichi Azuma, Ken'ichi Fujimoto, Tomohisa Hayakawa, Yoshito Hirata, Natsuhiro Ichinose, Masaki Inoue, Daisuke Ito, Masato Ishikawa, Takayuki Ishizaki, Kenji Kashima, Takuto Kita, Hiroyuki Kitajima, Miki U. Kobayashi, Mio Kobayashi, Motomasa Komuro, Takuji Kousaka, Jun Nishimura, Toshiyuki Ogawa, Yasuaki Oishi, Masayasu Suzuki, Tomomi Takegami, and Tetsuya Yoshinaga for writing excellent chapters.

This book is the outcome of the Japanese Research Project "the Aihara Innovative Mathematical Modelling Project (2010.3–2014.3)", one of top 30 projects of "Funding Program for World-Leading Innovative R&D on Science and Technology (FIRST Program)" initiated by the Council for Science and Technology Policy (CSTP) in Japan. We would also like to express our sincere gratitude to all members of the international advisory board of this project for their fruitful

suggestions and encouragements toward the developments of this project: Shun-ichi Amari, Miwako Doi, Hiroshi Fujii, Celso Grebogi, Seiichi Ishizu, Kunihiko Kaneko, Hiroshi Kawakami, Hidenori Kimura, Yoshiki Kuramoto, Jürgen Kurths, Henk Nijmeijer, Hugh Robinson, Ichiro Tsuda, Keiji Yamagami, and James A. Yorke.

Tokyo, January 2015

Kazuyuki Aihara
Jun-ichi Imura
Tetsushi Ueta

Contents

Part I
Robust Bifurcation and Control

Chapter 1
Dynamic Robust Bifurcation Analysis

Masaki Inoue, Jun-ichi Imura, Kenji Kashima and Kazuyuki Aihara

1.1 Introduction

In dynamical systems theory, bifurcation phenomena have been studied extensively [1–3]. Bifurcation is a phenomenon whereby a slight parametric perturbation in a dynamical system produces qualitative changes in structure of the solutions. It can be interpreted as bifurcation that because of a slight parameter change a stable equilibrium of differential equations is suddenly destabilized, and a stable periodic orbit can arise near the equilibrium. In order to analyze such phenomena, bifurcation theory has been studied and widely used for analysis and synthesis of complex behavior in many research fields; systems biology and synthetic biology [4–14], power system

This research was done when M.I. was with FIRST, Aihara Innovative Mathematical Modelling Project, Japan Science and Technology Agency/Graduate School of Information Science and Engineering, Tokyo Institute of Technology.

M. Inoue (✉)
Faculty of Science and Technology, Keio University,
3-14-1 Hiyoshi, Kohoku-ku, Yokohama, Kanagawa 223-8521, Japan
e-mail: minoue@appi.keio.ac.jp

J. Imura
Graduate School of Information Science and Engineering,
Tokyo Institute of Technology, 2-12-1 O-Okayama,
Meguro-ku, Tokyo 152-8552, Japan
e-mail: imura@mei.titech.ac.jp

K. Kashima
Graduate School of Informatics, Kyoto University, Yoshida-honmachi,
Sakyo-ku, Kyoto, Japan
e-mail: kashima@bode.amp.i.kyoto-u.ac.jp

K. Aihara
Institute of Industrial Science, The University of Tokyo, 4-6-1 Komaba, Meguro-ku,
Tokyo 153-8505, Japan
e-mail: aihara@sat.t.u-tokyo.ac.jp

K. Aihara et al. (eds.), *Analysis and Control of Complex Dynamical Systems*,
Mathematics for Industry 7, DOI 10.1007/978-4-431-55013-6_1

analysis [15–18], epidemic model analysis [19–22], and so on. For example, bifurcation theory has contributed to recent breakthroughs in systems biology and synthetic biology. Bifurcation analysis methods have been adopted to study the functions or characteristics of artificial bio-molecular systems, such as bio-molecular oscillators [4, 10, 11] and bio-molecular switches [5, 9, 14]. In addition, the robustness of such functions is identified with the volume of a parameter region in which the system has oscillatory property or bistable equilibria.

Conventional bifurcation theory is not always applicable to the analysis and synthesis of dynamical systems with uncertainties. Bifurcation analysis methods assume that mathematical models such as differential equations are completely known. Hence, they are not applicable to dynamical systems with uncertainties, in particular, large dynamic uncertainties . However, practical systems in the real world inevitably involve not only static but dynamic uncertainties [23, 24]. In order to apply the theory to such real-world systems, bifurcation analysis methods for uncertain dynamical systems are required.

In this chapter, we study local bifurcation of an equilibrium for systems with dynamic uncertainties. Note that a bifurcation point, i.e., a parameter value on which bifurcation occurs, depends on each model in general. If a system contains uncertainties and is described by a model set, we cannot find the specific bifurcation point. Therefore, we evaluate the potential bifurcation region: the parameter region that consists of all possible bifurcation points for a given model set. In other words, the region consists of all parameter points on which bifurcation can potentially occur. Evaluating the potential bifurcation region is referred to as the dynamic robust bifurcation analysis problem in this chapter. To this end, we first propose a condition for existence of equilibria independently of uncertainties and evaluate their location. Then, we derive a condition for robust hyperbolicity of potential equilibrium points, which implies that the dimension of unstable manifolds is independent of uncertainties. We consider parameter-dependent nonlinear systems with dynamic uncertainties, and using the robust hyperbolicity condition we identify the region that contains all potential bifurcation points. Finally, illustrative examples for robustness analysis of normal forms for various types of bifurcation are presented.

Notation: The symbols $\overline{\sigma}\{\cdot\}$ and $\rho\{\cdot\}$ represent the maximum singular value and the spectrum radius of a matrix, respectively. RH_∞ is the space that consists of all proper and complex rational stable transfer function matrices. The H_∞ norm and L_∞ norm of a linear system S are defined by

$$\|S\|_{H_\infty} := \sup_{\mathrm{Re}[s]>0} \overline{\sigma}\{\bar{S}(s)\}, \quad \|S\|_{L_\infty} := \sup_{\mathrm{Re}[s]=0} \overline{\sigma}\{\bar{S}(s)\},$$

where $\bar{S}(s)$ is a transfer function matrix representation of S. The poles (system poles) of a linear system $\dot{x} = Ax$ are defined by the roots of the characteristic polynomial $\phi(s) := \det(sI - A)$. In addition, a stable pole, an unstable pole, and a neutral pole are defined as poles lie in the open left half-plane, open right half-plane, and the imaginary axis of the complex plane, respectively.

1.2 Problem Formulation: Dynamic Robust Bifurcation Analysis

Consider the feedback system (Σ, Δ) illustrated in Fig. 1.1. In the figure, Σ is the nominal dynamical system composed of the linear dynamical system Σ_L and the nonlinear static function f. The linear system Σ_L is described by the state equations

$$\Sigma_L : \begin{cases} \dot{x} = A(\mu)x + B_1(\mu)u_1 + B_2(\mu)u_2, \\ y_1 = C_1(\mu)x + D_{11}(\mu)u_1 + D_{12}(\mu)u_2, \\ y_2 = C_2(\mu)x + D_{21}(\mu)u_1 + D_{22}(\mu)u_2, \end{cases} \tag{1.1}$$

where $x \in \mathbb{R}^n$ is the state, $u_1 \in \mathbb{R}^q$ and $u_2 \in \mathbb{R}^m$ are the inputs, $y_1 \in \mathbb{R}^p$ and $y_2 \in \mathbb{R}^\ell$ are the outputs, respectively, $\mu \in \mathscr{P} \subset \mathbb{R}^r$ is a static bifurcation parameter, and $A \in \mathbb{R}^{n\times n}$, $B_1 \in \mathbb{R}^{n\times q}$, $B_2 \in \mathbb{R}^{n\times m}$, $C_1 \in \mathbb{R}^{p\times n}$, $C_2 \in \mathbb{R}^{\ell\times n}$, $D_{11} \in \mathbb{R}^{p\times q}$, $D_{12} \in \mathbb{R}^{p\times m}$, $D_{21} \in \mathbb{R}^{\ell\times q}$, and $D_{22} \in \mathbb{R}^{\ell\times m}$ are parameter-dependent matrices. The input-to-output responses of the system Σ_L can be characterized by the transfer function representation as follows:

$$\begin{bmatrix} \bar{y}_1(s) \\ \bar{y}_2(s) \end{bmatrix} = \bar{\Sigma}_L(s) \begin{bmatrix} \bar{u}_1(s) \\ \bar{u}_2(s) \end{bmatrix}, \quad \bar{\Sigma}_L(s) := \begin{bmatrix} \bar{\Sigma}_{L11}(s) & \bar{\Sigma}_{L12}(s) \\ \bar{\Sigma}_{L21}(s) & \bar{\Sigma}_{L22}(s) \end{bmatrix},$$
$$\bar{\Sigma}_{Lij}(s) = C_i(\mu)(sI_n - A(\mu))^{-1}B_j(\mu) + D_{ij}(\mu),$$
$$(i, j) = (1, 1), (1, 2), (2, 1), (2, 2),$$

where $s \in \mathbb{C}$ and $\bar{u}_1(s)$, $\bar{u}_2(s)$, $\bar{y}_1(s)$, and $\bar{y}_2(s)$ represent the Laplace transformations of the signals $u_1(t)$, $u_2(t)$, $y_1(t)$, and $y_2(t)$, respectively. The function $f : \mathbb{R}^\ell \times \mathbb{R}^r \to \mathbb{R}^m$ is in $C^2(\mathbb{R}^\ell \times \mathbb{R}^r, \mathbb{R}^m)$ and satisfies

$$u_2 = f(y_2, \mu).$$

The symbol Δ in Fig. 1.1 expresses a dynamical system as well, but exact dynamics and even the dimension of the inner state of Δ are uncertain. This Δ is called a dynamic uncertainty. If there is no assumption on the dynamic uncertainty Δ, it is

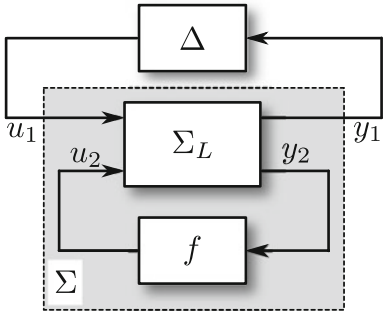

Fig. 1.1 Feedback representation of an uncertain dynamical system: A feedback system is composed of the linear dynamical system Σ_L, nonlinear function f, and dynamic uncertainty Δ

impossible to further analyze the feedback system illustrated in Fig. 1.1. We assume that the uncertainty is in the class of linear time-invariant systems.

$$\Delta : \begin{cases} \dot{\delta} &= A_d\delta + B_d y_1, \\ u_1 &= C_d\delta + D_d y_1, \end{cases} \tag{1.2}$$

where $\delta \in \mathbb{R}^k$ is the state of Δ and the matrices $A_d \in \mathbb{R}^{k\times k}$, $B_d \in \mathbb{R}^{k\times p}$, $C_d \in \mathbb{R}^{q\times k}$, and $D_d \in \mathbb{R}^{q\times p}$ are uncertain. Then, the input-to-output responses of Δ can be characterized by the transfer function matrix $\bar{\Delta}(s) := C_d(sI - A_d)^{-1}B_d + D_d$. In addition, assume that the uncertainty Δ belongs to the given set of linear time-invariant systems as

$$\Delta \in \mathscr{U}.$$

Discussion below is independent of the realization of Δ. The approach of this chapter uses only an input-output relation of the uncertainty as $\Delta \in \mathscr{U}$. Although we assumed above that the dynamic uncertainty Δ is a linear dynamical system for simplifying discussion below, we can extend the results of the paper to nonlinear uncertain cases.

For the uncertain feedback system (Σ, Δ), we consider the bifurcation analysis, i.e., qualitative change of the flow by parametric variations in μ. In this formulation, the uncertain feedback system (Σ, Δ) is described by a model set. Since a bifurcation point depends on each model, we cannot find a specific bifurcation point for such a model set (see Fig. 1.2). For uncertain dynamical systems, the location and even existence of equilibrium points are uncertain as well. We consider the following dynamic robust bifurcation analysis problem of identifying the sets of all potential bifurcation points for a given model set.

Definition 1.1 (*Potential Bifurcation Region*) For a given parameter region $\mathscr{P}$ and a given set of dynamic uncertainties $\mathscr{U}$, the potential bifurcation region $\mathscr{P}_{\mathrm{PB}} \subseteq \mathscr{P}$ is the set of parameter points that are bifurcation points of the feedback system (Σ, Δ) for some $\Delta \in \mathscr{U}$.

Problem 1.1 (*Robust Bifurcation Analysis*) Consider the feedback system (Σ, Δ) and $\Delta \in \mathscr{U}$. Then, find the potential bifurcation region $\mathscr{P}_{\mathrm{PB}} \subseteq \mathscr{P}$.

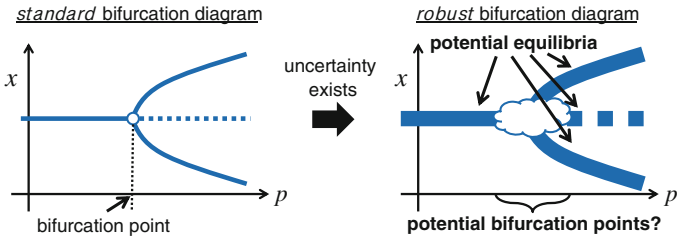

Fig. 1.2 Bifurcation analysis: A pitchfork bifurcation diagram for a nominal dynamical system is illustrated in the *left figure*. A robust bifurcation diagram for an uncertain dynamical system is illustrated in the *right figure*, where the location and hyperbolicity of the equilibria are uncertain

In dynamical systems theory, there is a similar concept called imperfect bifurcation [25], which is a bifurcation phenomenon for dynamical systems with small uncertainties. The uncertainties treated in the imperfect bifurcation problem are restricted to the ones represented by a finite number of uncertain parameters. Thus, our formulation covers a much wider class of uncertainties including dynamic uncertainties.

Bifurcation is defined as qualitative change of the structure of the solution in the state space by small parametric variation in $\mu \in \mathscr{P}$ (see e.g., [3]). In such phenomena, we focus only on local bifurcation of an equilibrium. Suppose that for the feedback system (Σ, Δ) and at a parameter point $\mu_1 \in \mathbb{R}$, the number of equilibria is constant and they are robustly hyperbolic for all $\Delta \in \mathscr{U}$. Further suppose that at a point $\mu_2 (\neq \mu_1) \in \mathbb{R}$ there exists Δ such that the number of equilibria is varied from the nominal system $(\Sigma, 0)$ or an equilibrium loses hyperbolicity. Then, a potential bifurcation point is included in $(\mu_1, \mu_2]$.

In addition, at a bifurcation point, an equilibrium for a dynamical system disappears or loses its hyperbolicity. Therefore, we evaluate the potential bifurcation region by finding the existence and location of an equilibrium and testifying its hyperbolicity for the feedback system (Σ, Δ). The content of the next section is composed of the three parts: Sect. 1.3.1 equilibrium analysis for the feedback system (Σ, Δ), Sect. 1.3.2 hyperbolicity analysis, and Sect. 1.3.3 a solution to the dynamic robust bifurcation analysis.

In the following, we assume that the uncertainty Δ is in the set of norm-bounded linear stable systems $\mathscr{U}(\gamma)$ as follows:

$$\mathscr{U}(\gamma) := \{ \bar{S}(s) \in RH_\infty : \|S\|_{H_\infty} \leq \gamma \},$$

where a positive constant γ is an upper bound of the maximum gain of Δ. The set $\mathscr{U}(\gamma)$ can represent signal distortions, unknown signal delays, approximation errors from PDEs to ODEs, and truncated errors of high index ODEs as long as their gains are bounded [23, 24]. Utilizing this characterization by the value of γ, we solve the dynamic robust bifurcation analysis problem.

Some types of bifurcation phenomena, such as saddle-node bifurcation, are said to be robust. We *qualitatively* know the fact that if the constant γ is small so that $\Delta \in \mathscr{U}(\gamma)$ has little effect to the dynamics of the feedback system (Σ, Δ), then, the same bifurcation can occur generically by parametric variations in μ. On the other hand, in this chapter, we will propose an analysis method to *quantitatively* evaluate the parameter points that can be a bifurcation point for some Δ.

1.3 Equilibrium, Stability/Instability, and Robustness Analysis

In Sects. 1.3.1 and 1.3.2, the parameter value of μ is fixed at a non-bifurcation point in $\mathscr{P}$. We first consider the uncertain feedback system (Σ, Δ) to derive an existence condition for an equilibrium $[x_e^\mathsf{T} \delta_e^\mathsf{T}]^\mathsf{T}$. Then, we derive a robust hyperbolicity condition for nonlinear systems with uncertainty-dependent equilibria.

1.3.1 Equilibrium Analysis

We evaluate the existence and location of equilibria in an uncertain feedback system (Σ, Δ). They are dependent on the steady-state gain of Δ, i.e., $\bar{\Delta}(0)$. To this end, we make an assumption on the system Σ_L.

(A1) Σ_L has no neutral poles.

The assumption A1, i.e., hyperbolicity of the origin of Σ_L, is a technical assumption that is used only for simplifying an existence condition of equilibria. This assumption can be satisfied in any uncertain feedback system applying the loop transformation technique to the feedback loop in Σ_L and f.

If A1 holds, the matrix $A(\mu)$ is nonsingular. Then, we can evaluate the steady state gain of $\bar{\Sigma}_L(s)$ as

$$\bar{\Sigma}_L(0) = -\begin{bmatrix} C_1(\mu) \\ C_2(\mu) \end{bmatrix} A^{-1}(\mu) \begin{bmatrix} B_1(\mu) & B_2(\mu) \end{bmatrix} + \begin{bmatrix} D_{11}(\mu) & D_{12}(\mu) \\ D_{21}(\mu) & D_{22}(\mu) \end{bmatrix}.$$

The steady state gain of $\bar{\Delta}(s)$ can also be defined as

$$\begin{aligned} \bar{\Delta}(0) &= -C_d A_d^{-1} B_d + D_d \in \mathscr{U}_0(\gamma), \\ \mathscr{U}_0(\gamma) &:= \{D_0 \mid \bar{\sigma}(D_0) \in [\,-\gamma,\ \gamma\,]\}. \end{aligned}$$

We focus on the steady state output $y_2 = y_{2e}$ to derive an existence condition for an equilibrium $[\,x_e^{\mathsf{T}}\ \delta_e^{\mathsf{T}}\,]^{\mathsf{T}}$. In the following, we consider the static nonlinear equation

$$y_2 = F_{\mathrm{u}}(\Sigma_L(0), D_0) f(y_2, \mu), \tag{1.3}$$

where $D_0 \in \mathbb{R}^{q \times p}$ is a constant matrix and $F_{\mathrm{u}}(X, Y)$ is the upper LFT representation of matrices X and Y as follows:

$$F_{\mathrm{u}}(X, Y) = X_{21} Y (I - X_{11} Y)^{-1} X_{12} + X_{22}.$$

We also define the matrix

$$M(D_0) := F_{\mathrm{u}} \left\{ \begin{bmatrix} \bar{\Sigma}_{L11}(0) & \bar{\Sigma}_{L12}(0) \\ B_1(\mu) & B_2(\mu) \end{bmatrix}, D_0 \right\}$$

to state the conditions of a theorem. We derive a condition for the existence of equilibria as follows.

Theorem 1.1 *For a given $\gamma > 0$, assume that A1 and $\bar{\sigma}\{\bar{\Sigma}_{L11}(0)\} < 1/\gamma$. Then, for a fixed $\mu \in \mathscr{P}$,* (T1) *holds.*

(T1) *The feedback system (Σ, Δ) has no equilibrium for all $\Delta \in \mathscr{U}(\gamma)$ if and only if* (1.3) *admits no real solution for all $D_0 \in \mathscr{U}_0(\gamma)$.*

In addition, suppose that the matrix $M(D_0)$ is of full column rank for all $D_0 \in \mathscr{U}_0(\gamma)$. Then, (T2) *holds.*

(T2) *The feedback system (Σ, Δ) has $N(\geq 0)$ isolated equilibria for all $\Delta \in \mathscr{U}(\gamma)$ if and only if* (1.3) *admits N isolated real solutions $y_2 = y_2(D_0)$ for all $D_0 \in \mathscr{U}_0(\gamma)$.*

Proof From A1, at the steady state, we have

$$x_e = -A^{-1}\{B_1\bar{\Delta}(0)y_{1e} + B_2 f(y_{2e}, \mu)\}, \tag{1.4}$$

$$\delta_e = -A_d^{-1}B_d y_{1e}, \tag{1.5}$$

$$\begin{bmatrix} y_{1e} \\ y_{2e} \end{bmatrix} = \bar{\Sigma}_L(0)\begin{bmatrix} u_{1e} \\ u_{2e} \end{bmatrix}, \quad u_{1e} = \bar{\Delta}(0)y_{1e}.$$

From the assumption that $\bar{\sigma}\{\bar{\Sigma}_{L11}(0)\} < 1/\gamma$ holds, the matrix $F_{\mathrm{u}}(\bar{\Sigma}_L(0), D_0)$ is well-defined, and we can derive the static equations (1.3) and

$$y_{1e} = \bar{\Sigma}_{L12}(0)\{I_q - \bar{\Delta}(0)\bar{\Sigma}_{L11}(0)\}^{-1} f(y_{2e}, \mu).$$

Then, for fixed $\bar{\Delta}(0)$ and μ, all equilibria $[\,x_e^{\mathsf{T}}\ \delta_e^{\mathsf{T}}\,]^{\mathsf{T}}$ can be parametrized only by the steady state output y_{2e} as (1.4) and (1.5). The existence of a real solution y_{2e} of (1.3) is equivalent to the existence of an equilibrium $[\,x_e{}^{\mathsf{T}}\ \delta_e{}^{\mathsf{T}}\,]^{\mathsf{T}}$. From this equivalence, we can prove (T1).

By using the representation $M(D_0)$, the equilibrium x_e of (1.4) can be written as $x_e = -A^{-1}(\mu)M(\bar{\Delta}(0))f(y_{2e})$. From the assumption that $M(D_0)$ is of full column rank for all $D_0 \in \mathscr{U}_0(\gamma)$, the map from $f(y_{2e})$ to x_e is one-to-one. In other words, two equilibria x_e and $x_e'(\neq x_e)$ are distinguishable by two vectors $f(y_{2e}, \mu)$ and $f(y_{2e}', \mu)(\neq f(y_{2e}, \mu))$. In addition, a solution of the static equation (1.3) is determined by an intersection of linear and nonlinear functions. Then, $f(y_{2e}, \mu) \neq f(y_{2e}', \mu)$ if and only if $y_{2e} \neq y_{2e}'$. The number of the isolated real solutions y_{2e} of (1.3) is equivalent to that of the isolated equilibria x_e. This completes the proof of Theorem 1.1. □

A solution of the static equation (1.3) with $D_0 = \Delta(0) \in \mathscr{U}_0(\gamma)$ is denoted by $y_{2ei}(\Delta)$, $i = \{1, 2, \ldots, N\}$. The sets of such potential steady state outputs $y_{2ei}(\Delta)$, $i = \{1, 2, \ldots, N\}$ for all $\Delta \in \mathscr{U}(\gamma)$ are denoted by

$$\mathscr{Y}_{2ei}(\gamma) := \{y_{2ei}(\Delta) \mid \Delta \in \mathscr{U}(\gamma)\}, \quad i = \{1, 2, \ldots, N\}. \tag{1.6}$$

In the next subsection, we analyze hyperbolicity of the equilibria determined by the elements of $\mathscr{Y}_{2ei}(\gamma)$.

To evaluate the set $\mathscr{Y}_{2ei}(\gamma)$, we need to solve the nonlinear static equation (1.3) for all $D_0 \in \mathscr{U}_0(\gamma)$. In general, it is hard to precisely solve such equations. However, in the case that f is monotonic, we can easily solve the equation. See the following two remarks and two examples with single-input and single-output nonlinear feedback systems.

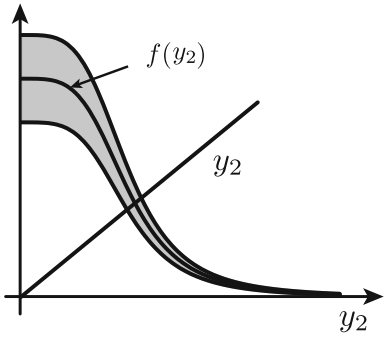

Fig. 1.3 Equilibrium analysis for a monotonically decreasing function: The potential equilibrium of the system is defined by the intersection of the uncertain function $f(y_2)$ and the straight line y_2. A unique equilibrium exists for any uncertainty

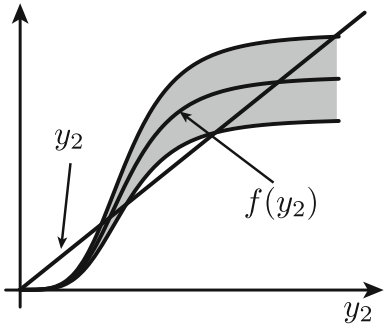

Fig. 1.4 Equilibrium analysis for a monotonically increasing function: The potential equilibria of the system is defined by the intersections of the uncertain function $f(y_2)$ and the straight line y_2. There can exist three equilibria for some uncertainty

Remark 1.1 Assume that $f(y_2, \mu)$, $y_2 \geq 0$, $\ell = m = 1$ is a positive and monotonically decreasing function as illustrated in Fig. 1.3. In that case, there exists a unique equilibrium. In addition, we can evaluate $\mathscr{Y}_{2e1}(\gamma)$ as follows. First, we evaluate the range of the function

$$h(d_0) = \left\{ \frac{d_0 \bar{\Sigma}_{L21}(0) \bar{\Sigma}_{L12}(0)}{1 - d_0 \bar{\Sigma}_{L11}(0)} + \bar{\Sigma}_{L22}(0) \right\}$$

for all $d_0 \in [-\gamma, \gamma]$. If $\min h(d_0) > 0$ holds, then $\mathscr{Y}_{2e1}(\gamma)$ is given by $[y_{2e\min}, y_{2e\max}]$, where $y_{2e\min}$ and $y_{2e\max}$ are the unique solutions of $y_2 = (\min h(d_0)) f(y_2, \mu)$ and $y_2 = (\max h(d_0)) f(y_2, \mu)$, respectively. We can evaluate $\mathscr{Y}_{2e1}(\gamma)$ by simple calculations.

Remark 1.2 Assume that $f(y_2, \mu)$, $y_2 \geq 0$, $\ell = m = 1$ is monotonically increasing and satisfies $f(0) = 0$ as illustrated in Fig. 1.4. Then, the equilibrium uniquely exists and $\mathscr{Y}_{2e}(\gamma_0) = \{0\}$ if there is no solution of $y_2 = (\max h(d_0)) f(y_2, \mu)$ except for $y_2 = 0$. There possibly exist multiple equilibria for such an activation function as illustrated in Fig. 1.4, which connects to the saddle-node bifurcation and its robustness analysis.

1.3.2 Robust Hyperbolicity Analysis

From Theorem 1.1, we can evaluate the region that contains all potential equilibrium points. Suppose that the number of the equilibria is constant for all $\Delta \in \mathscr{U}(\gamma)$. Then, the set of potential equilibrium points associated with $\mathscr{Y}_{2ei}(\gamma)$ is evaluated by (1.4) and (1.5), which are defined in the proof of Theorem 1.1 as

$$\mathscr{X}_{ei}(\gamma) := \{[\, x_e^{\mathsf{T}} \, \delta_e^{\mathsf{T}} \,]^{\mathsf{T}} \text{of (1.4) and (1.5)} \mid y_{2ei} \in \mathscr{Y}_{2ei}(\gamma)\}.$$

In this subsection, we analyze hyperbolicity of potential equilibria in $\mathscr{X}_{ei}(\gamma)$, $i = \{1, 2, \ldots, N\}$.

We define robust hyperbolicity for each $\mathscr{X}_{ei}(\gamma), i = \{1, 2, \ldots, N\}$ of the feedback system (Σ, Δ).

Definition 1.2 (*robust hyperbolicity*) For a given $\gamma > 0$, the set $\mathscr{X}_{ei}(\gamma)$ is said to be $\mathscr{U}(\gamma)$-robustly hyperbolic if the following conditions hold.

(D1) The set $\mathscr{X}_{ei}(\gamma)$ is connected
(D2) The equilibrium $[\, x_e^{\mathsf{T}} \, \delta_e^{\mathsf{T}} \,]^{\mathsf{T}}$ of (1.4) and (1.5) associated with $y_{2ei}(\Delta)$ is hyperbolic for all $\Delta \in \mathscr{U}(\gamma)$.

In the work by the authors [26], the robust hyperbolicity is defined and its analysis method is provided. The paper [26] assumes that the location of the unique equilibrium point x_e is not affected by the uncertainty $\Delta \in \mathscr{U}(\gamma)$. In other words, modeling errors exist only at high-frequencies and $\bar{\Delta}(0) = 0$ holds. On the other hand, in this chapter, the assumption of the steady state gain $\bar{\Delta}(0)$ is removed. In that case, the location and even existence of equilibria are uncertain as studied above.

Remark 1.3 The condition (D2) in Definition 1.2 additionally implies that the dimension of the unstable manifolds at any equilibrium point $[\, x_e^{\mathsf{T}} \, \delta_e^{\mathsf{T}} \,]^{\mathsf{T}} \in \mathscr{X}_{ei}(\gamma)$ of the feedback system (Σ, Δ) is constant for all $\Delta \in \mathscr{U}(\gamma)$ including the nominal case that $\Delta = 0$.

We derive a robust hyperbolicity condition for the set $\mathscr{X}_{ei}(\gamma)$. To this end, we linearize the feedback system (Σ, Δ) at an equilibrium point $[\, x_e^{\mathsf{T}} \, \delta_e^{\mathsf{T}} \,]^{\mathsf{T}} \in \mathscr{X}_{ei}(\gamma)$.

The Jacobian matrix of the function $f(y_2, \mu)$ for a fixed μ is denoted by

$$J_f(y_{2ei}) = \left.\frac{\partial f}{\partial y_2}\right|_{y_2 = y_{2ei}}.$$

Suppose that $I - J_f(y_{2ei})D_{22}(\mu)$ is nonsingular for all $y_{2ei} \in \mathscr{Y}_{2ei}(\gamma)$, i.e., the feedback loop in Σ_L and f is well-posed. Then, the feedback system (Σ, Δ) is linearized at the equilibrium point $[\, x_e^{\mathsf{T}} \, \delta_e^{\mathsf{T}} \,]^{\mathsf{T}}$, and is represented by the feedback system $(\Sigma_{y_{2ei}}, \Delta)$ composed of the linearized system

$$\Sigma_{y_{2ei}} : \begin{cases} \dot{x} &= \hat{A}(\mu)x + \hat{B}(\mu)u_1, \\ y_1 &= \hat{C}(\mu)x + \hat{D}(\mu)u_1, \end{cases}$$

and the uncertainty $\Delta \in \mathscr{U}(\gamma)$, where

$$\begin{bmatrix} \hat{A}(\mu) & \hat{B}(\mu) \\ \hat{C}(\mu) & \hat{D}(\mu) \end{bmatrix} = F_1\left(\left[\begin{array}{cc|c} A(\mu) & B_1(\mu) & B_2(\mu) \\ C_1(\mu) & D_{11}(\mu) & D_{12}(\mu) \\ \hline C_2(\mu) & D_{21}(\mu) & D_{22}(\mu) \end{array}\right], J_f(y_{2ei}) \right),$$

and $F_1(X, Y)$ is the lower LFT representation as follows:

$$F_1(X, Y) = X_{12}Y(I - X_{22}Y)^{-1}X_{21} + X_{11}.$$

For a fixed steady state output y_{2ei} and the linearized feedback system $(\Sigma_{y_{2ei}}, \Delta)$, a robust hyperbolicity condition [26] is proposed based on the Nyquist stability criterion [27]. The proof is essentially equivalent to that of the robust stability condition [23, 24] except the assumption on stability and the norm of $\Sigma_{y_{2ei}}$.

Theorem 1.2 [26] (linear robust hyperbolicity condition) *Consider an equilibrium x_{ei} and its corresponding steady state output y_{2ei} in the feedback system (Σ, Δ) for a fixed μ. Assume that the linearized system $\Sigma_{y_{2ei}}$ has no neutral pole and its realization $(\hat{A}(\mu), \hat{B}(\mu), \hat{C}(\mu))$ is controllable and observable. Then, for a given set $\mathscr{U}(\gamma)$, the set $\{x_{ei}\}$, that is, the equilibrium point x_{ei}, is $\mathscr{U}(\gamma)$-robustly hyperbolic if and only if*

$$\|\Sigma_{y_{2ei}}\|_{L_\infty} < 1/\gamma \tag{1.7}$$

holds.

Proof (*Sufficiency*) We denote the transfer function matrix representation of $\Sigma_{y_{2ei}}$ as

$$\bar{\Sigma}_{y_{2ei}}(s) = \hat{C}(\mu)(sI_n - \hat{A}(\mu))^{-1}\hat{B}(\mu) + \hat{D}(\mu).$$

Since $\|\Sigma_{y_{2ei}}\|_{L_\infty}\|\Delta\|_{H_\infty} < 1$ and

$$\sup_{\mathrm{Re}[s]=0} \rho\{\bar{\Sigma}_{y_{2ei}}(s)\bar{\Delta}(s)\} \le \sup_{\mathrm{Re}[s]=0} \overline{\sigma}\{\bar{\Sigma}_{y_{2ei}}(s)\bar{\Delta}(s)\}$$

hold, there exists a positive constant ε_1 such that

$$\rho\{\bar{\Sigma}_{y_{2ei}}(j\omega)\bar{\Delta}(j\omega)\} \le 1 - \varepsilon_1, \quad \forall \omega \in \mathbb{R}.$$

Then, for some positive constant ε_2,

$$|\det\{I_p - \bar{\Sigma}_{y_{2ei}}(j\omega)\bar{\Delta}(j\omega)\}| \ge \varepsilon_2, \quad \forall \omega \in \mathbb{R}$$

holds. This implies that the linearized feedback system $(\Sigma_{y_{2ei}}, \Delta)$ is well-posed and has no neutral pole.

(*Necessity*) We suppose that (1.7) does not hold, that is, there exists ω_1 such that

$$\|\Sigma_{y_{2ei}}\|_{L_\infty} = \overline{\sigma}\{\bar{\Sigma}_{y_{2ei}}(j\omega_1)\} \geq 1/\gamma$$

holds to show that there exists $\Delta \in \mathscr{U}(\gamma)$ such that either a feedback system is not well-posed or it has a neutral pole. First, by the singular value decomposition, $\Sigma_{y_{2ei}}(j\omega_1)$ can be represented by

$$\bar{\Sigma}_{y_{2ei}}(j\omega_1) = U\Sigma_g V^*, \quad \Sigma_g = \begin{bmatrix} \sigma_1 & & 0 \\ & \ddots & \\ 0 & & 0 \end{bmatrix},$$

where $U \in \mathbb{C}^{p\times p}$, $V \in \mathbb{C}^{q\times q}$ are unitary matrices and $\sigma_1 = \|\Sigma_{y_{2ei}}\|_{L_\infty}$. Since all of the diagonal elements of Σ_g other than the $(1, 1)$ element are not necessary in the following discussion, their descriptions are omitted. Next, we choose $\bar{\Delta}(s) \in RH_\infty$ such that

$$\bar{\Delta}(j\omega_1) = V\Sigma_d U^*, \quad \Sigma_d = \begin{bmatrix} 1/\sigma_1 & 0 & \dots & 0 \\ 0 & 0 & & \\ \vdots & & \ddots & \vdots \\ 0 & & \dots & 0 \end{bmatrix}$$

holds. Since $1/\sigma_1 \leq \gamma$ holds, $\bar{\Delta}(s) \in \mathscr{U}(\gamma)$. In addition, by using $E = \mathrm{diag}\{1, 0, \dots, 0\}$ we have

$$\begin{aligned} \det\{I_p - \bar{\Sigma}_{y_{2ei}}(j\omega_1)\bar{\Delta}(j\omega_1)\} &= \det\{I_\ell - U\Sigma_g V^* V\Sigma_d U^*\} \\ &= |\det(U)|^2 \det\{I_\ell - E\} = 0. \end{aligned}$$

If $\omega_1 = \infty$, the feedback system $(\Sigma_{y_{2ei}}, \Delta)$ is not well-posed. Else if $\omega_1 \in \mathbb{R}$, $\det\{I_p - \bar{\Sigma}_{y_{2ei}}(j\omega)\bar{\Delta}(j\omega)\}$ passes the origin of the complex plane and the feedback system $(\Sigma_{y_{2ei}}, \Delta)$ has the neutral pole $s = j\omega_1$. Then, the equilibrium is not $\mathscr{U}(\gamma)$-robustly hyperbolic. This completes the proof of Theorem 1.2. □

By Theorem 1.2, we can solve the problem of robust hyperbolicity analysis for systems with dynamic uncertainties as well as the robust stability theorem [23]. The theorem is a natural extension of the robust stability theorem [23]. In the above, we use the L_∞ norm to describe the condition of the theorem. The L_∞ norm can be defined for any hyperbolic linear time-invariant system, and is equivalent to the H_∞ norm for stable systems. Then, the condition of the theorem is reduced to the well-known small-gain theorem [28].

Remark 1.4 (*Computation of L_∞ norm*). To determine $\mathscr{U}(\gamma)$-robust hyperbolicity of an equilibrium of an uncertain system, we need to compute the L_∞ norm of a linear system. Some efficient L_∞ norm computational algorithms are presented: for example, the Hamiltonian matrix approach [29] and the Riccati equation and linear matrix inequality approaches [30, 31].

Remark 1.5 (*Implication of L_∞ norm*). By simple calculations [23], we can show that the L_∞ norm of the linearized system $\Sigma_{y_{2ei}}$ is equivalent to the conditional L_2 gain [32, 33]

$$\sup_{u \in L_{2\mathrm{cond}} \setminus \{0\}} \frac{\|\tilde{\Sigma}_{y_{2ei}} u\|_{L_2}}{\|u\|_{L_2}}, \quad L_{2\mathrm{cond}} := \{w \in L_2 \mid \tilde{\Sigma}_{y_{2ei}} w \in L_2\},$$

where $\|\cdot\|_{L_2}$ is the L_2 norm of a signal and $\tilde{\Sigma}_{y_{2ei}}$ is the operator representation of $\Sigma_{y_{2ei}}$. The conditional L_2 gain can be defined even for unstable and nonlinear systems. This fact implies that it is possible to extend Theorem 1.2 as a condition of linear systems for keeping the instability independently of uncertainties to that of nonlinear systems.

From Theorems 1.1 and 1.2, we derive the robust hyperbolicity condition for the nonlinear feedback system (Σ, Δ) with uncertainty-dependent equilibria.

Theorem 1.3 *For a given set $\mathscr{U}(\gamma)$, the set $\mathscr{X}_{ei}(\gamma)$ is $\mathscr{U}(\gamma)$-robustly hyperbolic if the set $\mathscr{X}_{2ei}(\gamma)$ is connected and the following conditions are satisfied for all $y_{2ei} \in \mathscr{X}_{2ei}(\gamma)$.*

(C1) *The linearized system $\Sigma_{y_{2ei}}$ has no neutral pole.*
(C2) *Realization $(\hat{A}(\mu), \hat{B}(\mu), \hat{C}(\mu))$ is controllable and observable.*
(C3) *Inequality* (1.7) *holds.*

We can numerically check (C1)–(C3) by partitioning $\mathscr{X}_{ei}(\gamma)$. To check (C3), we transform the linearized system $(\Sigma_{y_{2ei}}, \Delta)$ into another feedback form composed of the linear system Σ_L and the uncertainty $\mathrm{diag}\{J_f(y_{2ei}), \Delta\}$. The uncertainty part has block-diagonal structure and is included in the set $\mathrm{diag}\{J_f(\mathscr{X}_{ei}(\gamma)), \mathscr{U}(\gamma)\}$. Then, we evaluate the hyperbolicity of the linear feedback system $(\Sigma_L, \mathrm{diag}\{J_f(y_{2ei}), \Delta\})$ by computing the structured singular value [34] of Σ_L instead of the L_∞ norm. Obviously, when the norm of $J_f(y_{2ei})$ is sufficiently small, the theorem is corresponding to the robust stability theorem [23] and the robust instability theorem [26, 35–37] for uncertain linear systems.

1.3.3 Robust Bifurcation Analysis

We propose a method for robust bifurcation analysis that is derived by utilizing Theorem 1.1 for equilibrium analysis and Theorem 1.3 for hyperbolicity analysis. In the method, $\tilde{\mathscr{P}}_{\mathrm{PB}}(\gamma)$ is defined as a region that includes the potential bifurcation region $\mathscr{P}_{\mathrm{PB}}(\gamma)$, i.e., $\mathscr{P}_{\mathrm{PB}}(\gamma) \subseteq \tilde{\mathscr{P}}_{\mathrm{PB}}(\gamma)$.

Procedure for robust bifurcation analysis: Repeat the following Steps (i) and (ii) for all parameter values $\mu \in \mathscr{P}$.

(i) Solve the static equation (1.3) for all $D_0 = \bar{\Delta}(0) \in \mathscr{U}_0(\gamma)$. If the number of the real solutions $y_{2ei}(\Delta)$ is constant for all $\Delta \in \mathscr{U}(\gamma)$ and each set $\mathscr{X}_{ei}(\gamma)$, $i = \{1, 2, \ldots, N\}$ is connected, then, go to Step (ii). Otherwise $\mu \in \mathscr{P}_{\mathrm{PB}}(\gamma)$.
(ii) Define the linearized system $\Sigma_{y_{2ei}}$ and evaluate the L_∞ norm for all $y_{2ei} \in \mathscr{Y}_{2ei}(\gamma)$, $i = \{1, 2, \ldots, N\}$. If all values of the L_∞ norm are strictly less than $1/\gamma$, then, $\mu \in \mathscr{P} \backslash \tilde{\mathscr{P}}_{\mathrm{PB}}(\gamma)$. Otherwise $\mu \in \tilde{\mathscr{P}}_{\mathrm{PB}}(\gamma)$.

By this procedure, we can evaluate the potential bifurcation region $\mathscr{P}_{\mathrm{PB}}(\gamma)$ more widely than the exact region. In general, to identify the type of bifurcation (saddle-node-type, Hopf-type, and so on) that occurs in $\mathscr{P}_{\mathrm{PB}}(\gamma)$, we need additional assumptions. For example, under the assumption that $\bar{\Delta}(0) = 0$, we can show that at a saddle-node bifurcation point μ_{SN} for a nominal feedback system $(\Sigma, 0)$ is *robustly* a saddle-node bifurcation point for all uncertain feedback system (Σ, Δ). We can prove this fact by showing that any uncertain feedback system (Σ, Δ) satisfies saddle-node bifurcation theorem (see e.g., Theorem 2.2 in [1]) as long as $\bar{\Delta}(0) = 0$.

1.4 Examples of Robust Bifurcation Analysis

We illustrate a procedure of dynamic robust bifurcation analysis in the following examples for normal forms of various types of bifurcation.

1.4.1 Robustness Analysis of Saddle-Node Bifurcation

Let us consider the following normal form for saddle-node bifurcation with a dynamic uncertainty:

$$\dot{x} = x^2 + \mu + u_1, \quad u_1 = \Delta x, \quad \Delta \in \mathscr{U}(\gamma).$$

This uncertain model is written by the feedback form illustrated in Fig. 1.1 To evaluate the potential bifurcation region, (1) first we study the existence and location of equilibria and (2) then testify the robust hyperbolicity of potential equilibria.

(1) Note that the equilibria are affected by the steady state gain $D_0 = \Delta(0) \in \mathscr{U}_0(\gamma)$ and are determined by the intersection of $\Delta_0 x$ and $f(x) = x^2 + \mu$. The equilibria exist at

$$x_{ei}(D_0) = -D_0/2 \pm \sqrt{D_0^2/4 - \mu}, \quad i = 1,\ 2$$

for $\mu \leq D_0^2/4$, whereas no point exists for $\mu > D_0^2/4$. For any uncertainty $\Delta \in \mathscr{U}(\gamma)$, two equilibrium points encounter each other and vanish at $\mu \in [\,0, \gamma^2/4\,]$ along the parameter changing as illustrated in Fig. 1.5. This implies that the saddle-node bifurcation occurs, i.e., the number of the equilibria is varied by parameter variation, on $[\,0, \gamma^2/4\,]$ as long as $\Delta \in \mathscr{U}(\gamma)$.

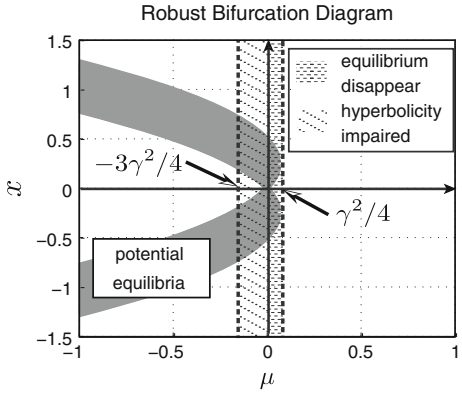

Fig. 1.5 Robust bifurcation analysis for saddle-node bifurcation ($\gamma = 0.5, \mu \in \mathscr{P} := [-1, 1]$): The location and existence of the equilibria are affected by the uncertainties. The hyperbolicity of equilibria can be impaired for some uncertainty in the parameter region $[\,-3\gamma^2/4,\ 0\,]$ and they can disappear and saddle-node bifurcation occurs in $[\,0,\ \gamma^2/4\,]$

(2) We further study the robust hyperbolicity of the equilibria for bifurcation analysis. Even if the equilibria exist, bifurcation can occur by hyperbolicity being impaired. Linearize the nonlinear feedback system at the points $x = x_e$ to obtain

$$\Sigma_{y_{2ei}} : \begin{cases} \dot{\tilde{x}} = 2x_e\tilde{x} + u_1, \\ y_1 = \tilde{x} + x_e, \end{cases}$$

where $\tilde{x} := x - x_e$. From Theorem 1.3 for a fixed μ, the equilibria x_{e1} and x_{e1} are hyperbolic for all $\Delta \in \mathscr{U}(\gamma)$ if the L_∞ norms of the linearized systems are strictly less than $1/\gamma$ for all $D_0 \in \mathscr{U}_0(\gamma)$. Therefore, we can show that the equilibria are hyperbolic for all $\mu < -3\gamma^2/4$ and there is no bifurcation point in the parameter region, although bifurcation occurs at $\mu \in [\,-3\gamma^2/4,\ \gamma^2/4\,]$ as illustrated in Fig. 1.5.

1.4.2 Robustness Analysis of Hopf Bifurcation

Consider the normal form for Hopf bifurcation with a dynamic uncertainty. The uncertain system is represented by the feedback form that is illustrated in Fig. 1.1, where Σ_L, f, and Δ are given by

$$\Sigma_L : \begin{cases} \dot{x} = \begin{bmatrix} \mu & -1 \\ 1 & \mu \end{bmatrix} x + \begin{bmatrix} 0 \\ 1 \end{bmatrix} u_1 + u_2 \\ y_1 = \begin{bmatrix} 1 & 0 \end{bmatrix} x \\ y_2 = x \end{cases}, \quad f(y) = -|y|_2^2 y, \quad \Delta \in \mathscr{U}(\gamma).$$

When $u_1 = 0$, the differential equation composed of Σ_L and f has the unique equilibrium at the origin for any parameter $\mu \in \mathbb{R}$. The existence and location of the equilibrium are independent of the feedback-type uncertainty. We perform dynamic robust bifurcation analysis of the origin. To this end, we have the linearized system $\Sigma_{y_{2ei}}$ that is the same as Σ_L to compute the L_∞ norm

$$\|\Sigma_{y_{2ei}}\|_{L_\infty} = \begin{cases} 1/|2\mu|, & 0 < |\mu| \leq 1, \\ 1/(\mu^2 + 1), & |\mu| > 1. \end{cases}$$

Then, we evaluate the potential bifurcation region for the origin by

$$\mathscr{P}_{\mathrm{PB}}(\gamma) \subseteq \begin{cases} [\,-\gamma/2,\ \gamma/2\,], & 0 < \gamma \leq 2, \\ [\,-\sqrt{\gamma - 1},\ \sqrt{\gamma - 1}\,], & \gamma > 2. \end{cases}$$

1.5 Conclusion

In this chapter, we integrated a concept of bifurcation in dynamical systems theory and that of robustness analysis in control systems theory to propose dynamic robust bifurcation analysis. In the analysis, given an uncertain system described by a model set, we obtain an outer approximation of all the possible bifurcation points.

Acknowledgments The authors gratefully acknowledge Takayuki Arai, Masayasu Suzuki, and Takayuki Ishizaki for their comments and fruitful discussion on this research.

References

1. Robinson, C.: Dynamical Systems: Stability, Symbolic Dynamics, and Chaos. CRC Press, Boca Raton (1998)
2. Wiggins, S.: Introduction to Applied Nonlinear Dynamical Systems and Chaos, 2nd edn. Springer, New York (2003)
3. Kuznetsov, Y.: Elements of Applied Bifurcation Theory, 3rd edn. Springer, New York (2004)
4. Elowitz, M.B., Leibler, S.: A synthetic oscillatory network of transcriptional regulators. Nature **403**, 335–338 (2000)
5. Gardner, T.S., Cantor, C.R., Collins, J.J.: Construction of a genetic toggle switch in Escherichia coli. Nature **403**, 339–342 (2000)
6. Tyson, J.J., Chen, K., Novak, B.: Network dynamics and cell physiology. Nat. Rev. Mol. Cell Biol. **2**(12), 908–916 (2001)
7. Tyson, J.J., Chen, K., Novak, B.: Sniffers, buzzers, toggles and blinkers: dynamics of regulatory and signaling pathways in the cell. Curr. Opin. Cell Biol. **15**(2), 221–231 (2003)
8. Swat, M., Kel, A., Herzel, H.: Bifurcation analysis of the regulatory modules of the mammalian G1/S transition. Bioinformatics **20**(10), 1506–1511 (2004)
9. Angeli, D., Ferrell Jr, J.E., Sontag, E.D.: Detection of multistability, bifurcations, and hysteresis in a large class of biological positive-feedback systems. Proc. Natl. Acad. Sci. USA **101**(7), 1822–1827 (2004)

10. Fung, E., Wong, W.W., Suen, J.K., Bulter, T., Lee, S., Liao, J.C.: A synthetic gene-metabolic oscillator. Nature **435**, 118–122 (2005)
11. Wong, W.W., Tsai, T.Y., Liao, J.C.: Single-cell zeroth-order protein degradation enhances the robustness of synthetic oscillator. Mol. Syst. Biol. **3**, 130 (2007)
12. Chen, L., Wang, R., Li, C., Aihara, K.: Modeling Biomolecular Networks in Cells: Structures and Dynamics. Springer, New York (2010)
13. Cosentino, C., Bates, D.: Feedback Control in Systems Biology. Chapman & Hall, CRC, Boca Raton (2011)
14. Padirac, A., Fujii, T., Rondelez, Y.: Bottom-up construction of in vitro switchable memories. Proc. Natl. Acad. Sci. USA **109**(47), 19047–19048 (2012)
15. Dobson, I.: Observations on the geometry of saddle node bifurcation and voltage collapse in electrical power systems. IEEE Trans. Circuits Syst. I: Fundam. Theory Appl. **39**(3), 240–243 (1992)
16. Dobson, I., Liming, L.: Computing an optimum direction in control space to avoid saddle node bifurcation and voltage collapse in electric power systems. IEEE Trans. Autom. Control **37**(10), 1616–1620 (1992)
17. Ajjarapu, V., Lee, B.: Bifurcation theory and its application to nonlinear dynamical phenomena in an electrical power system. IEEE Trans. Power Syst. **7**(1), 424–431 (1992)
18. Varghese, M., Wu, F., Varaiya, P.: Bifurcations associated with sub-synchronous resonance. IEEE Trans. Power Syst. **13**(1), 139–144 (1998)
19. van den Driessche, P., Watmough, J.: A simple SIS epidemic model with a backward bifurcation. J. Math. Biol. **40**(6), 525–540 (2000)
20. Dodds, P.S., Watts, D.J.: Universal behavior in a generalized model of contagion. Phys. Rev. Lett. **92**(21), 218701 (2004)
21. Gross, T.: DfLima, C.J.D., Blasius, B.: Epidemic dynamics on an adaptive network. Phys. Rev. Lett. **96**(20), 208701 (2006)
22. Wang, W.: Backward bifurcation of an epidemic model with treatment. Math. BioSci. **201**(1–2), 58–71 (2006)
23. Zhou, K., Doyle, J.C., Glover, K.: Robust and Optimal Control. Prentice Hall, Upper Saddle River (1996)
24. Skogestad, S., Postlethwaite, I.: Multivariable Feedback Control: Analysis and Design, 2nd edn. Wiley-Interscience, New York (2005)
25. Ikeda, K., Murota, Z.: Imperfect Bifurcation in Structures and Materials: Engineering Use of Group-Theoretic Bifurcation Theory, 2nd edn. Springer, New York (2010)
26. Inoue, M., Imura, J., Kashima, K., Aihara, K.: Robust bifurcation analysis based on the Nyquist stability criterion. In: Proceedings of 52nd IEEE Conference on Decision and Control, pp. 1768–1773 (2013)
27. Nyquist, H.: Regeneration theory. Bell Syst. Tech. J. **11**(1), 126–147 (1932)
28. Zames, G.: On the input-output stability of nonlinear time-varying feedback systems, Parts I and II. IEEE Trans. Autom. Control **11**, 228–238 and 465–476 (1966)
29. Bruinsma, N.A., Steinbuch, M.: A fast algorithm to compute the H_∞-norm of a transfer function matrix. Syst. Control Lett. **14**(4), 287–293 (1990)
30. Willems, J.C.: Least squares stationary optimal control and the algebraic Riccati equation. IEEE Trans. Autom. Control **16**(6), 621–634 (1971)
31. Stoorvogel, A.A.: Stabilizing solutions of the H_∞ algebraic Riccati equation. Linear Algebra Appl. **240**, 153–172 (1996)
32. Takeda, S., Bergen, A.R.: Instability of feedback systems by orthogonal decomposition of L_2. IEEE Trans. Autom. Control **18**(6), 631–636 (1973)
33. Desoer, C.A., Vidyasagar, M.: Feedback Systems: Input-Output Properties, SIAM (1975)
34. Doyle, J.: Analysis of feedback systems with structured uncertainties. IEE Proc. D (Control Theory Appl.) **129**(6), 242–250 (1982)

35. Inoue, M., Imura, J., Kashima, K., Arai, T., Aihara, K.: An instability condition for uncertain systems toward robust bifurcation analysis. In: Proceedings of European Control Conference 2013, pp. 3264–3269 (2013)
36. Inoue, M., Imura, J., Kashima, K., Aihara, K.: Robust bifurcation analysis of systems with dynamic uncertainties. Int. J. Bifurcat. Chaos **23**(9), 1350157 (2013)
37. Inoue, M., Arai, T., Imura, J., Kashima, K., Aihara, K.: Robust stability and instability of nonlinear feedback system with uncertainty-dependent equilibrium. In: Proceedings of European Control Conference 2014, pp. 1486–1491 (2014)

Chapter 2
Robust Bifurcation Analysis Based on Degree of Stability

Hiroyuki Kitajima, Tetsuya Yoshinaga, Jun-ichi Imura and Kazuyuki Aihara

2.1 Introduction

Consider nonlinear dynamical systems modelled by parameterised differential and difference equations. When the values of the system parameters vary from those at which the system is currently operated, it can exhibit qualitative changes in behaviour and a steady-state may disappear or become unstable through a bifurcation [1, 2]. Bifurcation analysis is clearly useful and a bifurcation diagram composed of bifurcation sets projected into parameter space displays various nonlinear phenomena in dynamical systems. On the other hand, when considering a steady-state which is closely approaching a bifurcation point due to unexpected factors like environmental changes, major incidents, and aging, self recovery is an important strategy for constructing a robust and resilient system. Traditional bifurcation analysis is not effective for this purpose because the global features of a bifurcation diagram in parameter

H. Kitajima
Faculty of Engineering, Kagawa University, 2217-20 Hayashi,
Takamatsu, Kagawa 761-0396, Japan
e-mail: kitaji@eng.kagawa-u.ac.jp

T. Yoshinaga (✉)
Institute of Health Biosciences, Tokushima University, 3-18-15 Kuramoto,
Tokushima 770-8509, Japan
e-mail: yosinaga@medsci.tokushima-u.ac.jp

J. Imura
Graduate School of Information Science and Engineering, Tokyo Institute of Technology,
2-12-1 O-Okayama, Meguro, Tokyo 152-8552, Japan
e-mail: imura@mei.titech.ac.jp

K. Aihara
Institute of Industrial Science, The University of Tokyo, 4-6-1 Komaba, Meguro,
Tokyo 153-8505, Japan
e-mail: aihara@sat.t.u-tokyo.ac.jp

K. Aihara et al. (eds.), *Analysis and Control of Complex Dynamical Systems*,
Mathematics for Industry 7, DOI 10.1007/978-4-431-55013-6_2

space needs to be computed to enable system behaviour to be totally understood with variations in parameters treated as measurable and directly controlled variables.

We present an approach to analyzing the system parameters based on the idea of characterising a steady-state with the degree of stability as a function of the parameters. The robust bifurcation analysis defined in this chapter provides a direct method for finding the values of the parameters at which the dynamical system acquires a steady-state with a high degree of stability using a method of optimization; this makes it possible to avoid bifurcations caused by the adverse effects of unexpected factors, without having to prepare the bifurcation diagrams that are required in advance for methods using traditional bifurcation analysis. As a result, we can design a system that is robust and resilient to unexpected factors.

The bifurcation control [3–10] also deals with modifications to bifurcation characteristics. It requires a feedback system to be constructed by adding control input, whereas our method uses prescribed parameters to optimize the stability.

In the following, after introducing the theoretical results [11] of robust bifurcation analysis, we will present numerical experiments of continuous-time dynamical systems. An example of representative results obtained in a model of the ventricular muscle cell suggests that our method has a possibility to suppress the alternans and reduce the risk of sudden death.

2.2 System Description and Robust Bifurcation Analysis

This section gives an exact definition of robust bifurcation analysis, which we describe both for equilibria in continuous-time dynamical systems and fixed points in discrete-time dynamical systems.

2.2.1 Continuous-Time Systems

We consider parameterised autonomous differential equations for continuous-time systems described by

$$\frac{dx}{dt} = f(x, \lambda), \quad t \in R, \tag{2.1}$$

where $x(t) = (x_1, x_2, \ldots, x_N)^{\mathsf{T}} \in R^N$ is a state vector, $\lambda = (\lambda_1, \lambda_2, \ldots, \lambda_M)^{\mathsf{T}} \in R^M$ is a measurable and directly controlled parameter vector, and f is assumed to be a C^∞ function for simplicity. Suppose that there exists an equilibrium x^* satisfying

$$f(x^*, \lambda) = 0, \tag{2.2}$$

and it can be expressed locally as a function of the parameters λ, namely $x^*(\lambda)$. The Jacobian matrix or the derivative of f with respect to x at $x = x^*$ denoted by

$$D(x^*(\lambda), \lambda) := \left.\frac{\partial f(x, \lambda)}{\partial x}\right|_{x=x^*(\lambda)} \tag{2.3}$$

gives information to determine the stability of the equilibrium. The eigenvalues μ of D at x^* are obtained by solving the characteristic equation

$$\det(\mu I - D(x^*(\lambda), \lambda)) = 0, \tag{2.4}$$

where I is the identity matrix. We call x^* a hyperbolic equilibrium of the system, if D is hyperbolic, i.e., all the real parts of the eigenvalues of D are different from zero. If all eigenvalues lie in the left-half plane, then the equilibrium is asymptotically stable. A local bifurcation occurs if an equilibrium loses its hyperbolicity due to continuous parameter variations. The generic bifurcations of an equilibrium are the saddle-node or tangent bifurcation and the Hopf bifurcation.

The main objective of bifurcation analysis is to find sets of bifurcation values. The bifurcation sets can be obtained by solving simultaneous equations consisting of the equilibrium equation in (2.2) and the characteristic equation in (2.4) for unknown variables x^* and λ_m for $m = 1, 2, \ldots, M$. Thus, the bifurcation sets for all m's need to be computed to enable system behaviour to be totally understood with parameter variations.

2.2.2 Discrete-time Systems

Next, let us consider parameterised difference equations for discrete-time systems

$$x(k+1) = g(x(k), \lambda), \quad k = 1, 2, \ldots,$$

or equivalently, a map defined by

$$g : R^N \times R^M \to R^N \; ; \; (x, \lambda) \mapsto g(x, \lambda), \tag{2.5}$$

where $x(k)$ and x are state vectors in R^N, $\lambda \in R^M$ are the parameters, and the function g is assumed to be C^∞. Note that, for simplicity, we have used the same symbols for the state variables x, the parameters λ, and others in both continuous-time and discrete-time systems. A discrete-time system can be a Poincaré map to take periodic solutions into consideration in autonomous or periodically forced nonautonomous differential equations. The existence of a fixed point x^* satisfying

$$x^* - g(x^*, \lambda) = 0 \tag{2.6}$$

is assumed. The Jacobian matrix of g at the fixed point x^* is indicated by

$$D(x^*(\lambda), \lambda) := \left. \frac{\partial g(x, \lambda)}{\partial x} \right|_{x=x^*(\lambda)}. \tag{2.7}$$

The roots of the characteristic equation denoted by

$$\det(\mu I - D(x^*(\lambda), \lambda)) = 0 \tag{2.8}$$

become the characteristic multipliers of the fixed point. The fixed point is hyperbolic, if all absolute values of the eigenvalues of D are different from unity. If every characteristic multiplier of the hyperbolic fixed point is located inside the unit circle, then it is asymptotically stable. When the hyperbolicity is destroyed by varying the parameters, a local bifurcation occurs. Generic bifurcations are the tangent, period-doubling, and Neimark-Sacker bifurcations, which correspond to the critical distribution of characteristic multiplier μ such that $\mu = +1$, $\mu = -1$, and $\mu = e^{i\theta}$ with $i = \sqrt{-1}$, respectively. Further, a pitchfork bifurcation can appear in a symmetric system as a degenerate case of the tangent bifurcation.

We can simultaneously solve equations consisting of the fixed point equation in (2.6) and the characteristic equation in (2.8) with a fixed μ depending on the bifurcation conditions to obtain unknown bifurcation sets x^* and λ_m.

2.2.3 Robust Bifurcation Analysis

Let $\mu_{\max}(D)$ be the maximum value of the real parts (or the absolute values) of eigenvalues with respect to the matrix D for a continuous-time system in (2.3) (or a discrete-time system in (2.7)). We denote this as a function of the parameters as follows

$$\rho(\lambda) := \mu_{\max}(D(x^*(\lambda), \lambda)).$$

Consider that the dynamics f or g with parameter values λ^* defines a system after being affected by unexpected factors, and the steady-state $x^*(\lambda^*)$ has a low degree of stability, which means that the value of $\rho(\lambda^*)$ is near the condition of a bifurcation. Then, the purpose of robust bifurcation analysis is to find $\lambda \in R^M$ such that

$$\rho(\lambda) < \rho(\lambda^*)$$

for given $\lambda^* \in R^M$ satisfying

$$\left. \frac{\partial \rho(\lambda)}{\partial \lambda_m} \right|_{\lambda=\lambda^*} \neq 0$$

for some m's in $\{1, 2, \ldots, M\}$. We assume that the unexpected factors do not change during the process.

The corresponding eigenvalues can be used to make a contour along which the real part of an eigenvalue is equal to zero to analyze the stability of an equilibrium observed in a continuous-time system. This should be a curve in the parameter plane defining the boundary of a region in which the equilibrium stably exists. The level curves at a fixed maximum eigenvalue in the real part similarly imply the degree of stability in parameter space. Robust bifurcation analysis provides a method for finding the values of the parameters at which stable equilibrium has a higher degree of stability. By obtaining a set of parameters

$$\Lambda := \arg\min_{\lambda \in R^M} \rho(\lambda) \tag{2.9}$$

subject to $\rho(\lambda) < \rho(\lambda^*)$, then it enables us to design a system that has a steady-state with a high degree of stability. The same argument can be applied to a fixed point observed in a discrete-time system by taking into consideration the absolute values of eigenvalues instead of the real parts.

2.3 Method of Robust Bifurcation Analysis

We present a method for finding the set of parameters for the optimization problem in (2.9), assuming that the characteristic multiplier with maximum absolute value is real in the case of discrete-time systems.

Because the eigenvalues are not differentiable with respect to the parameters at points where they coalesce, we consider the optimization problem below instead of directly solving (2.9):

$$\min_{\lambda \in R^M,\ \nu \geq \rho(\lambda)} J(\lambda, \nu),$$

where

$$J(\lambda, \nu) := \det\left(\nu I - D(x^*(\lambda), \lambda)\right). \tag{2.10}$$

The characteristic polynomial J is non-negative for $\nu \geq \rho(\lambda)$ and the optimization problem is formulated to minimise the maximum absolute value of eigenvalues of $D(x^*(\lambda), \lambda)$ for discrete-time systems and the real parts of eigenvalues of $D(x^*(\lambda), \lambda)$ for continuous-time systems by varying the parameter λ. Note that the method provides a uniform treatment of both continuous-time and discrete-time systems according to the above assumption on discrete-time systems, and that, when the characteristic multiplier with maximum absolute value is negative for discrete-time systems, the problem of optimization should be modified to maximise the minimum

real characteristic multiplier (see Sect. 2.4.2 for an example). We use a continuous gradient method to obtain the values of the parameters λ and the supplementary variable ν. The descent flow is given by the initial value problem of the following differential equations:

$$\begin{aligned} \frac{d\lambda}{d\tau} &= -(\nu - \rho(\lambda))\frac{\partial J}{\partial \lambda}^{\mathsf{T}}, \\ \frac{d\nu}{d\tau} &= -(\nu - \rho(\lambda))\frac{\partial J}{\partial \nu}. \end{aligned} \tag{2.11}$$

Here, the solution $(\lambda(\tau), \nu(\tau))$ is a function of the independent variable τ with the initial conditions $\lambda(0) = \lambda^*$ and $\nu(0) > \rho(\lambda^*)$. When $\nu \neq \rho(\lambda)$, the gradient parts of the right hand sides in (2.11) are given by

$$\begin{aligned} \frac{\partial J}{\partial \lambda_m} &= -\mathrm{tr}\left(\mathrm{adj}(\nu I - D)\frac{\partial D}{\partial \lambda_m}\right) \\ &= -J\,\mathrm{tr}\left((\nu I - D)^{-1}\frac{\partial D}{\partial \lambda_m}\right), \end{aligned} \tag{2.12}$$

$$\begin{aligned} \frac{\partial J}{\partial \nu} &= \mathrm{tr}\,(\mathrm{adj}(\nu I - D)) \\ &= J\,\mathrm{tr}\left((\nu I - D)^{-1}\right), \end{aligned} \tag{2.13}$$

for $m = 1, 2, \ldots, M$, where $\mathrm{tr}(\cdot)$ and $\mathrm{adj}(\cdot)$ correspond to the trace and adjugate. We need the derivative of the (i, j) element of D in (2.12) with respect to the parameter λ_m. For the difference system g, this is expressed by

$$\frac{\partial}{\partial \lambda_m}\frac{\partial g_i}{\partial x_j} = \sum_{n=1}^{N}\frac{\partial^2 g_i}{\partial x_j \partial x_n}\frac{\partial x_n^*}{\partial \lambda_m} + \frac{\partial^2 g_i}{\partial x_j \partial \lambda_m}.$$

Here, $\partial x_n^*/\partial \lambda_m$, $n = 1, 2, \ldots, N$ can be obtained by differentiating the fixed point equation in (2.6) with respect to λ_m. Then, we have

$$\frac{\partial x^*}{\partial \lambda_m} = \left(I - \left.\frac{\partial g}{\partial x}\right|_{x=x^*}\right)^{-1}\left.\frac{\partial g}{\partial \lambda_m}\right|_{x=x^*}.$$

A similar argument can be applied to the differential dynamics f.

Let us present a theoretical result for the behaviour of the solution to the dynamical system in (2.11). Note that the subspace of the state $(\lambda, \nu) \in R^{M+1}$ satisfying $\nu = \rho(\lambda)$ is an equilibrium set of (2.11). Therefore, the trajectories cannot pass through the set, according to the uniqueness of solutions for the initial value problem. This leads to the fact that, if we choose initial values $(\lambda(0), \nu(0))$ with $\nu(0) > \rho(\lambda(0))$, any solution $(\lambda(\tau), \nu(\tau))$ stays in the subspace $\nu > \rho(\lambda)$ for all $\tau > 0$. Under this condition, the derivative of J along the solution to (2.11) is given by

$$\left.\frac{dJ}{d\tau}\right|_{(2.11)} = \left(\frac{\partial J}{\partial \lambda} \quad \frac{\partial J}{\partial \nu}\right)\begin{pmatrix}\frac{d\lambda}{d\tau}\\ \frac{d\nu}{d\tau}\end{pmatrix}$$
$$= -(\nu - \rho(\lambda))\left(\left\|\frac{\partial J}{\partial \lambda}\right\|_2^2 + \left(\frac{\partial J}{\partial \nu}\right)^2\right)$$
$$< 0,$$

where the last inequality is obtained because $\nabla J \neq 0$ if $\nu > \rho(\lambda)$. Then, we can see that the value of $J(\lambda(\tau), \nu(\tau))$ with $J > 0$, for all τ, monotonically decreases as time passes.

An interior point method [12] is effective when implementing the algorithm to solve the optimization problem.

2.4 Numerical Examples

Here, we present two representative examples (equilibrium points and periodic solutions) of our robust bifurcation analysis for continuous-time systems. An example of a discrete-time system is shown in [11].

2.4.1 Equilibrium Point

The first example involves the following two-dimensional differential equations, known as the BvP (Bonhöffer-van der Pol) equations:

$$\frac{dx_1}{dt} = \frac{3}{2}(x_1 - \frac{1}{3}x_1^3 + x_2), \tag{2.14}$$
$$\frac{dx_2}{dt} = -\frac{2}{3}(-\lambda_1 + x_1 + \lambda_2 x_2).$$

The result with our method is shown in Fig. 2.1. A contour plot of an eigenvalue with the maximum real part is also presented. The curve T indicates the saddle-node bifurcation of an equilibrium. Equation (2.14) has three equilibria in the gradation region. A pair of stable and unstable equilibria disappears at the saddle-node bifurcation. Here, we try to find the parameter values at which the equilibrium has a high degree of stability. The eigenvalue is -0.04 at the initial parameter values λ^* labeled by a. The eigenvalue becomes -0.47 at the parameter value b after our method was applied. Thus, we can avoid the occurrence of the saddle-node bifurcation and obtain a high degree of stability by automatically changing the parameters when considering

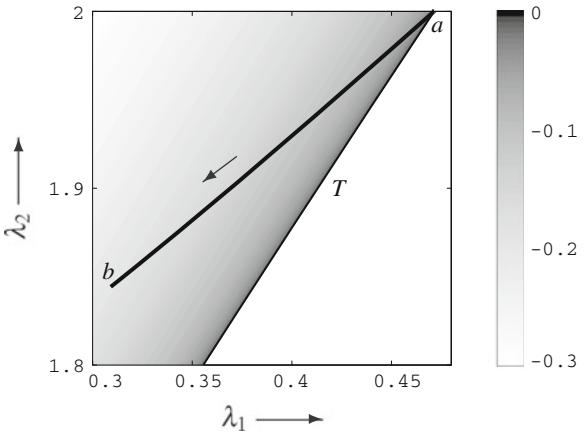

Fig. 2.1 *Bold solid line* indicates the trace of maximum eigenvalue of the equilibrium in BvP equations. Contour plot represents the maximum real part of the eigenvalues, as scaled by the gradation bar. The maximum eigenvalue is equal to 0 on the saddle-node bifurcation *curve* denoted by T

that the situation of the equilibrium with a low degree of stability at the parameter values λ^* near a bifurcation is caused by the effect of unexpected factors.

Figure 2.2 outlines the basins of attraction for the stable equilibrium before and after our method was applied. The phase diagrams in Fig. 2.2a, b correspond to the parameter values a and b in Fig. 2.1. If we put the initial states in the shaded region, we can obtain the targeted equilibrium labeled e in Fig. 2.2 as a steady-state. We can see that our method expanded the basins of attraction by comparing Fig. 2.2a, b.

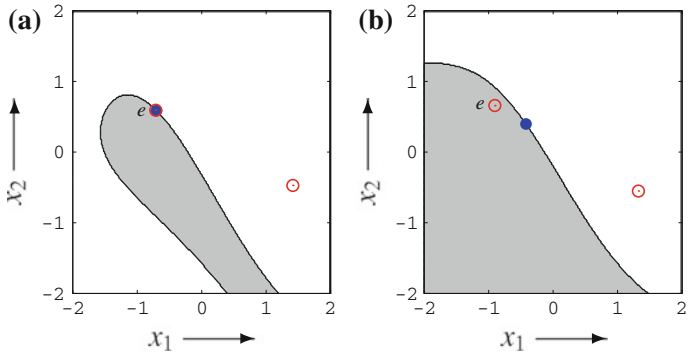

Fig. 2.2 Basins of attraction of equilibria for BvP equations. *Red open* and *blue closed circles* correspond to stable and unstable equilibria. The *red open circle* with label e and the *blue closed circle* are very close in **a** because the parameter value is near the saddle-node bifurcation. The stable manifolds of the saddle-type equilibrium (the *blue closed circle*) form the basin boundary between *shaded* and *unshaded* regions

2.4.2 Periodic Solution

Next, we consider a periodic solution in (2.1). We can reduce it to a fixed point defined by (2.6) by constructing a Poincaré map. Thus, we can use the method described in Sect. 2.3. Here, we study a system of the Luo-Rudy (LR) model [13] with a synaptic input (I_{syn}) described by the following 8-dimensional ordinary differential equations:

$$\begin{aligned} C\frac{dV}{dt} &= -(I_{Na} + I_{Ca} + I_K + I_{K_1} + I_{Kp} + I_b + I_{syn}), \\ \frac{dy}{dt} &= \frac{y_\infty - y}{\tau_y}, \quad (y = m, h, j, d, f, X), \\ \frac{d[Ca]_i}{dt} &= -10^{-4} I_{Ca} + 0.07(10^{-4} - [Ca]_i), \end{aligned} \tag{2.15}$$

where ionic currents are given by

$$\begin{aligned} I_{Na} &= 23m^3hj(V - E_{Na}), \quad I_{Ca} = G_{Ca}df(V - E_{Ca}), \\ I_K &= \overline{G_K} X X_i (V - E_K), \quad I_{K_1} = \overline{G_{K1}} K_{1_\infty}(V - E_{K1}), \\ I_{Kp} &= 0.0183 K_p (V - E_{K_p}), \quad I_b = 0.03921(V + 59.87), \\ I_{syn} &= G_{syn}(V_{syn} - V)\frac{\tau_1}{\tau_2 - \tau_1}\left(-\exp\left(-\frac{t'}{\tau_1}\right) + \exp\left(-\frac{t'}{\tau_2}\right)\right). \end{aligned}$$

Here, we define that the time t' is reset at every basic cycle length (BCL) defined by the period of the external synaptic current I_{syn}. Detailed explanation and normal parameter values for the LR model are given in [13].

The LR model is of the ventricular muscle cell. In a previous study, we clarified alternans corresponding to a two-periodic state that appears by a period-doubling bifurcation through changing the value of the parameter BCL. It is well known that the alternans triggers cardiac electrical instability (ventricular arrhythmias) and may cause sudden cardiac death. Thus, suppressing alternans is important for reducing the risk of sudden death. Here, using our proposed algorithm we show the suppression of the alternans.

Figure 2.3 shows a result of maximising the smallest real characteristic multiplier of the LR model in the parameter plane $\lambda = (\mathrm{BCL}, G_{syn})$. Initial parameter values are marked by the closed circle, which is very close to the period-doubling bifurcation. Then, the smallest real characteristic multiplier is -0.998. In Fig. 2.3, two-periodic solutions generated by the period-doubling bifurcation exist in the shaded parameter region. The waveform of the membrane potential after the period-doubling bifurcation is shown in Fig. 2.4. This waveform shows a typical alternans. From this initial point our algorithm changes the values of the parameters to avoid the bifurcation

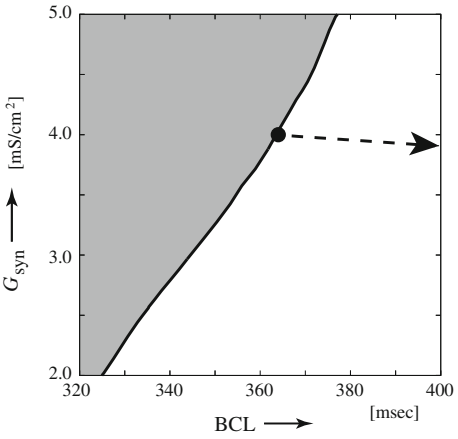

Fig. 2.3 Result of robust bifurcation analysis for the LR model. Initial parameter values are $G_{syn} = 4.0$, BCL $= 362$ and $\nu = -1.15$. The *solid* and *dashed curves* indicate the period-doubling bifurcation set in the parameter plane (BCL, G_{syn}) and the trace of these parameter values while our control method works. In the *shaded region*, stable two-periodic solutions generated by the period-doubling bifurcation exist

Fig. 2.4 Waveforms of the membrane potentials (alternans). BCL $= 376$ and $G_{syn} = 5.0$

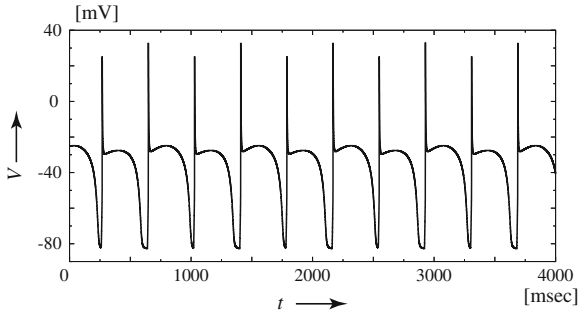

(the trace is shown by the dashed curve.). After that, the smallest real characteristic multiplier becomes -0.434. Thus, our method can avoid the alternans and reduce the risk of sudden death.

2.5 Conclusion

Traditional bifurcation analysis in parameter space deals with contour or level sets of the eigenvalue for a bifurcation, whereas our robust bifurcation analysis is used for finding parameter sets that cause a gradient decrease in the bifurcating eigenvalue. An automatic trace of the gradient based on our method can effectively construct a robust system that has a steady-state with a high degree of stability.

Acknowledgments The proposed method of this research has been published as a paper in IJICIC [11] before. H.K. is partially supported by JSPS KAKENHI (No.23500367).

References

1. Wiggins, S.: Introduction to Applied Nonlinear Dynamical Systems and Chaos, 2nd edn. Springer, Berlin (2003)
2. Kuznetsov, Y.: Elements of Applied Bifurcation Theory, 3rd edn. Springer, Berlin (2004)
3. Chen, G., Moiola, J.L., Wang, H.O.: Bifurcation control: theories, methods, and applications. Int. J. Bifurcat. Chaos **10**(3), 511–548 (2000)
4. Basso, M., Genesio, R., Tesi, A.: A frequency method for predicting limit cycle bifurcations. Nonlinear Dyn. **13**(4), 339–360 (1997)
5. Berns, D.W., Moiola, J.L., Chen, G.: Predicting period-doubling bifurcations and multiple oscillations in nonlinear time-delayed feedback systems. Circ. Syst. I: Fundam. Theory Appl. IEEE Trans. **45**(7), 759–763 (1998)
6. Wu, Z., Yu, P.: A method for stability and bifurcation control. Autom. Control IEEE Trans. **51**(6), 1019–1023 (2006)
7. Xie, Y., Chen, L., Kang, Y.M., Aihara, K.: Controlling the onset of Hopf bifurcation in the Hodgkin-Huxley model. Phys. Rev. E **77**, 061921 (2008)
8. Wen, G., Xu, D.: Control algorithm for creation of Hopf bifurcations in continuous-time systems of arbitrary dimension. Phys. Lett. A **337**, 93–100 (2005)
9. Verduzco, F.: Control of codimension one stationary bifurcations. Int. J. Bifurcat. Chaos **17**(2), 575–585 (2007)
10. Liu, M.K., Suh, C.S.: Simultaneous time-frequency control of bifurcation and chaos. Commun. Nonlinear Sci. Numer. Simul. **17**, 2539–2550 (2012)
11. Kitajima, H., Yoshinaga, T., Imura, J., Aihara, K.: Robust bifurcation analysis based on optimization of degree of stability. Int. J. Innov. Comput. Inf. Control **11**(1), 153–162 (2015)
12. Imae, J., Furudate, T., Sugawara, S.: A simple numerical method for minimizing the maximum eigenvalues of symmetric matrices via nonlinear differential equation solvers. Trans. Japn. Soc. Mech. Eng. **63**(608), 87–92 (1997)
13. Luo, C.H., Rudy, Y.: A model of the ventricular cardiac action potential. Demoralization, repolarization, and their interaction. Circ. Res. **68**, 1501–1526 (1991)

Chapter 3
Use of a Matrix Inequality Technique for Avoiding Undesirable Bifurcation

Yasuaki Oishi, Mio Kobayashi and Tetsuya Yoshinaga

3.1 Introduction

A nonlinear dynamical system often shows a qualitative change in its solution due to the change of the parameter value. This phenomenon is interesting from a theoretical point of view and has been a subject of bifurcation analysis. From an engineering point of view, however, such a qualitative change can be undesirable. For example, an alternating pulse of the heart is claimed to be a consequence of bifurcation [1] and thus it can be suppressed by keeping the heart system from making bifurcation. In order to robustify a system in this sense, it was proposed in Chap. 2 to define a stability index and to update the parameter value so as to minimize this stability index. Here, the stability index is the maximum over the absolute values of the eigenvalues of the linearized dynamics. If the stability index is controlled small, the system is expected not to make bifurcation. A difficulty here is that the stability index is not differentiable in general with respect to the parameter. Indeed, in Chap. 2, the stability index was not directly minimized but a function closely related to it.

In this chapter, we try more direct approach with the technique of a matrix inequality, which is widely used in the field of control theory, and reduce the problem to a differentiable minimization problem. The resulting problem can be solved with the penalty method and gives an update rule of the parameters, which resembles that

Y. Oishi (✉)
Department of Mechatronics, Nanzan University, Seireicho 27, Seto 489-0863, Japan
e-mail: oishi@nanzan-u.ac.jp

M. Kobayashi
Department of Systems and Control Engineering, Anan National College of Technology, Aoki 265, Minobayashicho, Anan 774-0017, Japan
e-mail: kobayashi@anan-nct.ac.jp

T. Yoshinaga
Institute of Health Biosciences, Tokushima University, 3-18-15 Kuramoto, Tokushima 770-8509, Japan
e-mail: yosinaga@medsci.tokushima-u.ac.jp

K. Aihara et al. (eds.), *Analysis and Control of Complex Dynamical Systems*,
Mathematics for Industry 7, DOI 10.1007/978-4-431-55013-6_3

of Chap. 2. The obtained update rule is tested with a simple dynamical system to show its efficacy. Finally, generalization of this approach is considered for keeping the system from falling into chaos. A related result of the same authors can be found in [2].

The following notation is used. The transpose of a matrix or a vector is denoted by $^\mathsf{T}$. The trace of a matrix is expressed by tr and a diagonal matrix is expressed by diag. For a square matrix D, the symbol $\rho(D)$ denotes the maximum of the absolute values of the eigenvalues of D. For a symmetric matrix T, the matrix inequalities $T \succ O$ and $T \succeq O$ stand for positive definiteness (all the eigenvalues are positive) and positive semidefiniteness (all the eigenvalues are nonnegative) of T, respectively.

3.2 Considered Problem

Consider a discrete-time dynamical system

$$z(k+1) = f(z(k), \lambda) \quad (k = 0, 1, 2, \ldots) \tag{3.1}$$

having a state $z \in \mathbb{R}^n$ and a parameter $\lambda \in \mathbb{R}^m$. Here, $f(z, \lambda)$ is some smooth function. Suppose that a fixed point of this system, that is, a state z_λ satisfying $z_\lambda = f(z_\lambda, \lambda)$, is obtained for any λ in some nonempty open set $\Lambda \subseteq \mathbb{R}^m$ and that it is smooth as a function of λ. Then, for the Jacobian matrix of $f(z, \lambda)$ at $z = z_\lambda$, that is,

$$D(\lambda) := \frac{\partial}{\partial z} f(z, \lambda)\Big|_{z=z_\lambda},$$

the maximum over the absolute values of its eigenvalues, i.e., $\rho(D(\lambda))$, is called the *stability index* of the fixed point z_λ. Indeed, it is smaller than unity if and only if the fixed point z_λ is asymptotically stable. In Chap. 2, the following problem was considered:

$$\begin{aligned} S\colon \text{minimize } & \rho(D(\lambda)) \text{ in } \lambda \\ \text{subject to } & \lambda \in \Lambda. \end{aligned}$$

If the parameter λ is updated so as to converge to a local optimal solution of the problem, the dynamical system is driven to increase its stability. Hence, even if the system is subject to unexpected change of the parameter, it is expected to recover its stability.

3.3 Proposed Method

Although the matrix $D(\lambda)$ is smooth with respect to λ, the stability index $\rho(D(\lambda))$ is not differentiable in general with respect to λ and hence its minimization needs some special technique. In Chap. 2, $\rho(D(\lambda))$ was not directly minimized but a smooth function closely related to it.

In this chapter, we use the following result [3, Sect. 4.1.2].

Proposition *For a square matrix D and a positive number ρ, there holds $\rho(D) < \rho$ if and only if there exists a symmetric matrix X that satisfies*

$$\begin{pmatrix} \rho^2 X & D^{\mathsf{T}} X \\ XD & X \end{pmatrix} \succ O.$$

Use this result and rewrite ρ^2 as α to have the following optimization problem equivalent to S:

$$\begin{aligned} S' : \text{minimize } & \alpha \text{ in } (\alpha, \lambda, X) \\ \text{subject to } & \lambda \in \Lambda, \ \begin{pmatrix} \alpha X & D(\lambda)^{\mathsf{T}} X \\ XD(\lambda) & X \end{pmatrix} \succ O. \end{aligned}$$

In this problem, both objective function and constraints are smooth functions of the optimization variables (α, λ, X). Hence, a standard method can be used for the optimization.

Although a similar technique with a matrix inequality is widely used in the field of control theory [3, 4], the objective functions and the constraints are usually affine in the design variables. Our problem S' has a nonlinear matrix inequality constraint and thus cannot be solved with the usual method in control theory. In this chapter, we apply the penalty function method of Kočvara–Stingl [5] to solve S'. Its key idea is to construct a penalty function that has a small value when the matrix inequality constraint is satisfied and a large value when it is not satisfied. Adding this penalty function to the objective function, we can perform minimization without considering the matrix inequality constraint explicitly.

The desired penalty function can be constructed as follows. First, we define a function $\phi_p(t)$ having a positive scheduling parameter p by

$$\phi_p(t) := p\Big(\frac{1}{t/p+1} - 1\Big).$$

For $t \geq 0$, the function $\phi_p(t)$ approaches zero as $p \downarrow 0$; for $t < 0$, it blows up to infinity as $p \downarrow -t$. On the other hand, let T denote the left-hand side matrix of the matrix inequality constraint of S', which is a symmetric matrix of order $2n$. Suppose that this T is diagonalized by some orthogonal matrix Q as $T = Q\,\mathrm{diag}(t_1, t_2, \ldots, t_{2n})Q^{\mathsf{T}}$. Here, we write the matrix $Q\,\mathrm{diag}(\phi_p(t_1), \phi_p(t_2), \ldots, \phi_p(t_{2n}))Q^{\mathsf{T}}$ as $\Phi_p(T)$ and consider $\mathrm{tr}(U\Phi_p(T))$ for some arbitrary positive definite matrix U. Then this function

$\mathrm{tr}(U\Phi_p(T))$ can be used as the desired penalty function. Indeed, for $T \succeq O$, the function $\mathrm{tr}(U\Phi_p(T))$ converges to zero as $p \downarrow 0$; for $T \not\succeq O$, it blows up to infinity as $p \downarrow p_0$, where p_0 is some positive number.

Based on the discussion so far, we can expect that the problem S' can be solved by iteration of the following three steps:

1. Update (α, λ, X) so as to make $\alpha + \mathrm{tr}(U\Phi_p(\begin{pmatrix} \alpha X & D(\lambda)^\mathsf{T} X \\ X D(\lambda) & X \end{pmatrix}))$ smaller,
2. Update U,
3. Update p.

More concretely, the update in Step 1 is performed in the steepest descent direction or in the Newton direction of the objective function with an appropriate step size. The update in Step 2 is carried out so that the Karush–Kuhn–Tucker condition of S' is satisfied. The update in Step 3 is performed so that p approaches zero. See [5] for the details.

3.4 Extension

In the preceding problems S and S', the availability of a fixed point z_λ has been assumed. When this assumption cannot be made, the following problem is considered instead:

$$\begin{aligned} R : \text{minimize } \ & \alpha \ \text{ in } \ (z, \alpha, \lambda, X) \\ \text{subject to } \ & f(z, \lambda) - z = 0, \quad \lambda \in \Lambda, \\ & \begin{pmatrix} \alpha X & D(\lambda)^\mathsf{T} X \\ X D(\lambda) & X \end{pmatrix} \succ O. \end{aligned}$$

In this new problem, z becomes an optimization variable and the equality constraint $f(z, \lambda) - z = 0$ is added.

Just as in the case of S, we can obtain an update rule of (z, α, λ, X). Here, we decompose the newly added equality constraint into two inequality constraints $f(z, \lambda) - z \geq 0$ and $-f(z, \lambda) + z \geq 0$, construct the corresponding penalty functions for each, and add them to the objective function. A similar approach is possible also for a periodic point in place of a fixed point.

For a continuous-time dynamical system $\dot{z} = f(z, \lambda)$, the stability index should be defined as the maximum over the real parts of the eigenvalues of the Jacobian matrix $D(\lambda) := (\partial/\partial z) f(z, \lambda)|_{z=z_\lambda}$ at a fixed point z_λ. In order to minimize it, the following optimization problem is considered:

$$\begin{aligned}&\text{minimize } \alpha \text{ in } (\alpha, \lambda, X)\\ &\text{subject to } \lambda \in \Lambda, \quad X \succ O,\\ &\qquad -X(D(\lambda)-\alpha I)-(D(\lambda)-\alpha I)^{\mathsf{T}} X \succ O.\end{aligned}$$

Application of the penalty function method gives an update rule of (α, λ, X) as before.

3.5 Example

Consider a discrete-time dynamical system based on the Hénon map, that is,

$$\begin{pmatrix} x(k+1) \\ y(k+1) \end{pmatrix} = \begin{pmatrix} 1 + y(k) - ax(k)^2 \\ bx(k) \end{pmatrix}, \tag{3.2}$$

which has the state $z = (x \;\; y)^{\mathsf{T}}$ and the parameter $\lambda = (a \;\; b)^{\mathsf{T}}$. In the parameter region $\Lambda = \{\lambda = (a \;\; b)^{\mathsf{T}} \mid (b-1)^2 + 4a > 0\}$, the system has a fixed point

$$z_\lambda = \begin{pmatrix} (b - 1 + \sqrt{(b-1)^2 + 4a})/2a \\ b(b - 1 + \sqrt{(b-1)^2 + 4a})/2a \end{pmatrix}.$$

The Jacobian matrix at this fixed point z_λ is denoted by $D(\lambda)$. The problem S' is considered in this setting and solved with the method in Sect. 3.3. The result is presented in Fig. 3.1a. Here, the horizontal plane stands for the space of the parameter $\lambda = (a \;\; b)^{\mathsf{T}}$ and the curved surface is the graph of the stability index $\rho(D(\lambda))$.

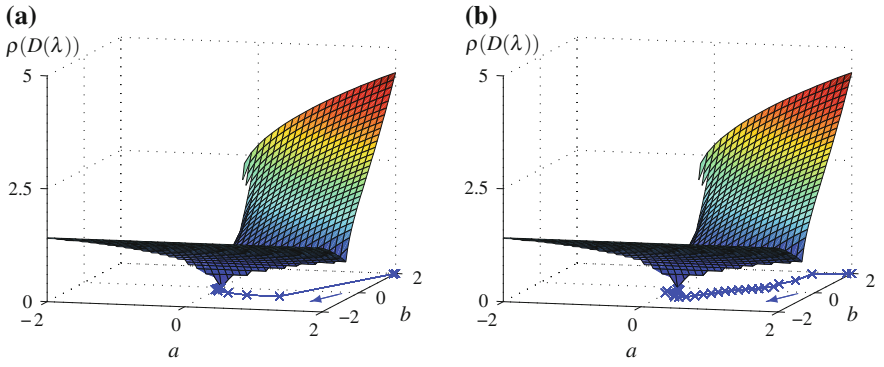

Fig. 3.1 The stability index of a dynamical system based on the Hénon map together with the trajectory of the parameter updated by the proposed method: **a** the case where the fixed point z_λ is available; **b** the case where the fixed point z_λ is not available

(The graph is drawn only for $\lambda \in \Lambda$.) On the horizontal plane, the trajectory of the updated parameter λ is shown. It is seen from the figure that the stability index $\rho(D(\lambda))$ is not differentiable at some point. Nevertheless, the parameter λ is updated without any problem and reaches the neighborhood of a local optimum $\lambda = (0\ \ 0)^{\mathsf{T}}$. Here, in Step 1 of the method, the steepest descent direction is employed with more priority put on the stability of the convergence rather than on its speed. The step size is chosen according to the Armijo rule. The initial value of the scheduling parameter p is 100 and is updated by multiplication of 0.97 in Step 3. The additional constraint $\lambda \in \Lambda$ is guaranteed just by limiting update of the parameter λ in Λ.

Next we consider the case where a fixed point is not available and apply the method of Sect. 3.3 to the problem R in Sect. 3.4. The result is presented in Fig. 3.1b. Although the convergence is slower than in the previous case, the parameter successfully reaches the neighborhood of a local optimum $\lambda = (0\ \ 0)^{\mathsf{T}}$.

3.6 Avoidance of Chaos

The technique of a matrix inequality can be used for more general purpose. In this section, we use it for minimizing the local expansion rate and preventing the system from falling into chaos.

3.6.1 Method for Chaos Avoidance

Let the *maximum Lyapunov exponent* with respect to z_0 be

$$\begin{aligned}\gamma(z_0, \lambda) &:= \lim_{N\to\infty} \frac{1}{N} \log \rho(D^N(z_0, \lambda)) \\ &:= \lim_{N\to\infty} \frac{1}{N} \log \rho\big(D(z_{N-1}, \lambda) \cdots D(z_1, \lambda) D(z_0, \lambda)\big),\end{aligned}$$

where $\{z_0, z_1, \ldots, z_{N-1}\}$ is the trajectory of the dynamical system (3.1) starting from z_0. In the special case that $\{z_0, z_1, \ldots, z_{p-1}\}$ is a periodic orbit of period p, we have

$$\gamma(z_k, \lambda) = \frac{1}{p} \log \rho(D^p(z_0, \lambda)) \quad (k = 0, 1, \ldots, p-1).$$

Since exact computation of the maximum Lyapunov exponent $\gamma(z_0, \lambda)$ is difficult, we may use instead a *finite-time Lyapunov exponent*, or the *local expansion rate*, defined by

$$\Gamma(N, z_0, \lambda) := \frac{1}{N} \log \rho(D^N(z_0, \lambda))$$

for some large positive integer N. The local expansion rate $\Gamma(N, z_0, \lambda)$ usually takes a large value when the system shows chaotic behavior and thus is often regarded as an index of chaos. If we update the parameter λ so as to minimize the local expansion rate, the system is expected to avoid falling into chaos. Note that minimization of the local expansion rate $\Gamma(N, z_0, \lambda)$ is equivalent to that of $\rho(D^N(z_0, \lambda))$, for which the technique of a matrix inequality can be used. In particular, we consider the following optimization problem:

$$\begin{aligned} &\text{minimize } \alpha \ \text{ in } \ (\alpha, \lambda, X) \\ &\text{subject to } \lambda \in \Lambda, \ \begin{pmatrix} \alpha X & D^N(z_0, \lambda)^{\mathsf{T}} X \\ X D^N(z_0, \lambda) & X \end{pmatrix} \succ O. \end{aligned}$$

3.6.2 Experimental Result

We try the proposed method with the system based on the Hénon map (3.2). In the (a, b) parameter space, a grid equally spaced by 0.001 is taken. Each grid point is chosen as an initial parameter λ_0 and is updated according to the method given in the previous section. Figure 3.2a shows the result together with bifurcation parameter sets. The symbols G^p and I^p denote tangent and period-doubling bifurcations for p-periodic points, respectively. Chaotic behavior is observed in the shaded parameter region. The parameters λ_{100} obtained after 100 updates are indicated by the small dots. Four typical trajectories are presented by the solid lines with arrows. The ends of each line correspond to the initial parameter λ_0 and the final parameter λ_{100}. The updates are made in the direction of the arrows.

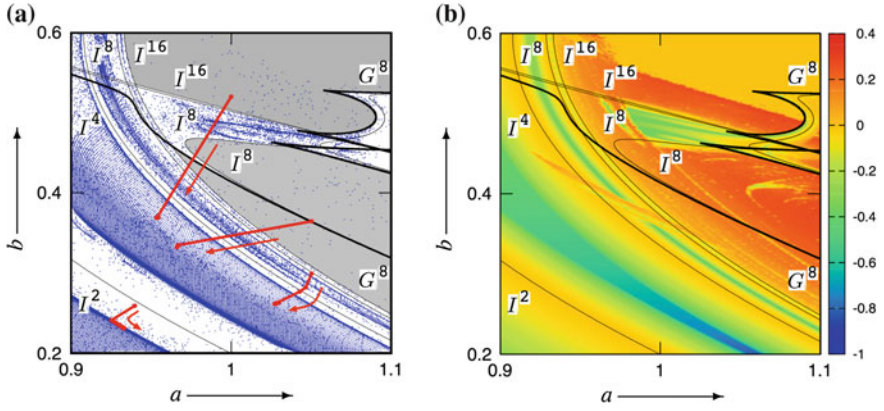

Fig. 3.2 Chaos avoidance in the case of the Hénon map: **a** distribution of the parameters after 100 updates; **b** the local expansion rate in the same parameter region

Figure 3.2b shows an overlapped image of the local expansion rate for attractors and the bifurcation diagram of periodic points. The colored contour plot presents the values of the local expansion rate, as indicated by the color bar. Cold color (blue) expresses a small local expansion rate and then high stability. We see that the small dots in Fig. 3.2a are mainly distributed in the region with a negative local expansion rate in Fig. 3.2b. Thus our method operates the system to avoid chaos.

3.7 Conclusion

In this Chap. 3, robustification of a dynamical system is considered along the approach in the previous chapter and a technique with a matrix inequality is introduced. Although the stability index considered here is not differentiable in general, its optimization can be formulated into a differentiable optimization problem. Since the resulting optimization problem has a nonlinear matrix inequality constraint, we use the penalty function method of Kočvara–Stingl to obtain an update rule of the parameter. The proposed method is applied to a dynamical system based on the Hénon map and is shown to be efficient. It can be generalized for avoiding chaos.

References

1. Kitajima, H., Yazawa, T.: Modified Luo-Rudy model and its bifurcation analysis for suppressing alternans. In: Proceedings of the 2011 International Symposium on Nonlinear Theory and Its Applications (NOLTA 2011), pp. 390–393 (2011)
2. Oishi, Y., Kobayashi, M., Yoshinaga, T.: Robustification of a nonlinear dynamical system with a stability index and a matrix inequality. SICE J. Control Measur. Syst. Integr. (To appear)
3. Duan, G.-R., Yu, H.-H.: LMIs in Control Systems: Analysis, Design and Applications. CRC Press, Boca Raton (2013)
4. Boyd, S., El Ghaoui, L., Feron, E., Balakirishnan, V.: Linear Matrix Inequalities in System and Control Theory. SIAM, Philadelphia (1994)
5. Kočvara, M., Stingl, M.: PENNON: a code for convex nonlinear semidefinite programming. Optim. Methods Softw. **18**(3), 317–333 (2003)

Chapter 4
A Method for Constructing a Robust System Against Unexpected Parameter Variation

Hiroyuki Kitajima and Tetsuya Yoshinaga

4.1 Introduction

The aim of our study is to construct a system that is robust to sudden environmental changes and major incidents. Such changes trigger instabilities in the system, called bifurcations. In biological systems, for example, dynamical diseases such as Cheyne-Stokes respiration and chronic granulocytic leukemia are caused by bifurcations due to variations in system parameters [1, 2]. The ability to predict bifurcations in a parameter space is very important to preventing such diseases. Several methods of predicting and controlling bifurcations have proposed such as, using the averaged harmonic method [3], constructing a feedback system [4–6], and minimizing the maximum eigenvalues of symmetric matrices through optimization [7–9]. The methods in cited studies aim to minimize the maximum eigenvalues of the linearized system (Jacobian matrix), which correspond to rapid recovery from a perturbed state. However, a parameter value with a minimum eigenvalue does not have the longest margin to bifurcations in the parameter space. Dobson proposed a method of calculating the closest-bifurcation from the operating parameter values [10]. This method and its extensions have been applied to hydraulic systems [11], gene systems [12], power systems [13, 14], and bifurcations of arbitrary codimension [15]. Moreover, another method using support vector machine (SVM) and particle swarm optimization (PSO) was proposed [16]. However, in all of the above cases, the considered bifurcations are only for equilibrium points.

H. Kitajima (✉)
Faculty of Engineering, Kagawa University, 2217-20 Hayashi, Kagawa, Takamatsu 761-0396, Japan
e-mail: kitaji@eng.kagawa-u.ac.jp

T. Yoshinaga
Institute of Health Biosciences, Tokushima University, 3-18-15 Kuramoto, Tokushima 770-8509, Japan
e-mail: yosinaga@medsci.tokushima-u.ac.jp

K. Aihara et al. (eds.), *Analysis and Control of Complex Dynamical Systems*, Mathematics for Industry 7, DOI 10.1007/978-4-431-55013-6_4

In this chapter, we propose a method to calculate the closest-bifurcation for periodic solutions by constructing vector fields along bifurcation curves. Moreover, we explain an extended version of the notation of the closest-bifurcation [10] to search for the optimal parameter value meaning the farthest point from the bifurcations in the parameter region under consideration, which has been published in [17]. As a result, we can set appropriate parameter values that correspond to constructing a system which is robust to unexpected parameter changes.

4.2 Method

4.2.1 Dynamical System

We consider the following autonomous dynamical system:

$$\frac{d\xi}{dt} = f_a(\xi, \lambda), \quad \xi \in \mathbb{R}^{N+1}, \lambda \in \mathbb{R}^M, t \in \mathbb{R}, \tag{4.1}$$

where λ is a controllable parameter and ξ is a state variable.We assume that there exists a periodic solution in (4.1) with an initial condition $\xi = \xi_0$ at $t = t_0$, denoted by $\xi(t) = \psi(t, \xi_0, \lambda)$ for all t. We take a local section Γ, that the solution crosses transversely, as follows:

$$\Gamma = \{\xi \in \mathbb{R}^{N+1} | \, z(\xi) = 0\},$$

where $z(\xi)$ is a scalar valued function of ξ in $\mathbb{R}^{N+1}$. Let us define h as a local coordinate of Γ

$$h : \Gamma \to \Pi \subset \mathbb{R}^N; \ \xi \mapsto x = h(\xi)$$

and its inverse h^{-1} as an embedding map

$$h^{-1} : \Pi \to \Gamma; \ x \mapsto \xi = h^{-1}(x),$$

where ξ satisfies $z(\xi) = 0$. Pick a point $\xi \in \Gamma$ and let $\Pi \subset \Gamma$ be some neighborhood of $x = h(\xi)$. Then the Poincaré map T is defined by the following composite map for a point $x \in \Pi$:

$$T : \Pi \to \Pi; \ x \mapsto h(\psi(\tau(h^{-1}(x)), h^{-1}(x), \lambda)),$$

where τ denotes the time during which the trajectory emanating from a point $\xi \in \Gamma$ hits the local cross-section Γ again. The time τ is called the return time.

Similarly, for a non-autonomous system,

$$\frac{dx}{dt} = f_n(x, \lambda, t), \quad x \in \mathbb{R}^N, \lambda \in \mathbb{R}^M, \tag{4.2}$$

we can construct the Poincaré map T as

$$T : \mathbb{R}^N \to \mathbb{R}^N;\ x \mapsto T(x, \lambda) = \psi(L, x, \lambda),$$

where L is the period of the function f_n:

$$f_n(x, \lambda, t + L) = f_n(x, \lambda, t).$$

For a discrete-time system, the map T is directly obtained by

$$T : \mathbb{R}^N \to \mathbb{R}^N;\ x(k) \mapsto x(k+1) = T(x(k), \lambda) = f_d(x(k), \lambda),$$
$$x \in \mathbb{R}^N, \lambda \in \mathbb{R}^M, k \in \mathbb{N}.$$

For all dynamical systems, the fixed point of the map T is given by

$$F(x^*, \lambda) = x^* - T(x^*, \lambda) = 0. \tag{4.3}$$

In the differential equations, we can obtain a one-to-one correspondence between the periodic solution of (4.1) or (4.2) and the fixed point of the map T. Hence, the analysis of the periodic solution can be reduced to an analysis of the fixed point of the map T. The characteristic multiplier μ of the fixed point x^* is obtained by solving

$$G(x^*, \lambda) = \det\left(D(\lambda) - \mu I\right) = 0, \tag{4.4}$$

where

$$D(\lambda) := \left.\frac{\partial T(x, \lambda)}{\partial x}\right|_{x=x^*}. \tag{4.5}$$

If all absolute values of the characteristic multipliers are less than one, then the fixed point is stable. The change in stability due to a parameter perturbation is called a bifurcation. The codimension-one bifurcations are as follows: When $\mu = 1, \mu = -1$ and $\mu = \exp(i\theta)(\theta \neq 0, \pi)$, the tangent, period-doubling, and Neimark-Sacker bifurcations occur, respectively.

4.2.2 Search for Optimal Parameter Values

Here, we describe our method of searching for the optimal parameter values that are farthest points from bifurcations in the parameter region under consideration. For this, we extend the idea of the closest-bifurcation method proposed by Dobson [10].

This method determines the minimum distance to bifurcations along selected directions in the parameter space. It searches a local region of the parameter space in order to find the point on a bifurcation surface. Its searching performance is determined by the initial search direction and local topology of the bifurcation curve. A global search was proposed by Kremer [11]. These methods use the normal vectors at a bifurcation curve in a parameter plane. However, these calculation methods using eigenvectors are only for equilibria.

Here, we show the method of calculating a normal vector to a bifurcation curve for periodic solutions by constructing a vector field along the bifurcation curve. For simplicity, we assume $M = 2$ ($\lambda = (\lambda_1, \lambda_2)^{\mathsf{T}}$). Differentiating (4.3) and (4.4) yields

$$\begin{aligned} \frac{\partial F}{\partial x}dx + \frac{\partial F}{\partial \lambda}d\lambda = 0, \\ \frac{\partial G}{\partial x}dx + \frac{\partial G}{\partial \lambda}d\lambda = 0. \end{aligned} \tag{4.6}$$

We can rewrite (4.6) as

$$\frac{dx_1}{A(x_1)} = \cdots = \frac{dx_i}{(-1)^{i-1}A(x_i)} = \cdots = \frac{d\lambda_1}{(-1)^N A(\lambda_1)} = \frac{d\lambda_2}{(-1)^{N+1}A(\lambda_2)}, \tag{4.7}$$

where

$$A(x_i) = \begin{vmatrix} \frac{\partial F_1}{\partial x_1} & \cdots & \widehat{\frac{\partial F_1}{\partial x_i}} & \cdots & \frac{\partial F_1}{\partial x_N} & \frac{\partial F_1}{\partial \lambda_1} & \frac{\partial F_1}{\partial \lambda_2} \\ \vdots & & \vdots & & \vdots & \vdots & \vdots \\ \frac{\partial F_N}{\partial x_1} & \cdots & \frac{\partial F_N}{\partial x_i} & \cdots & \frac{\partial F_N}{\partial x_N} & \frac{\partial F_N}{\partial \lambda_1} & \frac{\partial F_N}{\partial \lambda_2} \\ \frac{\partial G}{\partial x_1} & \cdots & \frac{\partial G}{\partial x_i} & \cdots & \frac{\partial G}{\partial x_N} & \frac{\partial G}{\partial \lambda_1} & \frac{\partial G}{\partial \lambda_2} \end{vmatrix},$$

where the hat ($\widehat{\ }$) indicates the elimination of the column. Equating (4.7) to ds yields the following vector equations along a bifurcation curve:

$$\begin{cases} \dfrac{dx_i}{ds} = (-1)^{i-1}A(x_i), & (i = 1, 2, \ldots, N), \\ \dfrac{d\lambda_1}{ds} = (-1)^N A(\lambda_1), \\ \dfrac{d\lambda_2}{ds} = (-1)^{N+1}A(\lambda_2). \end{cases}$$

Thus, the normal vector to the bifurcation curve at $(\lambda_{1_0},\lambda_{2_0})$ in the parameter plane is given by

$$\begin{bmatrix} \lambda_{1_0} \\ \lambda_{2_0} \end{bmatrix} = \pm \begin{bmatrix} \frac{d\lambda_2}{ds} \\ -\frac{d\lambda_1}{ds} \end{bmatrix} = \pm \begin{bmatrix} A(\lambda_{2_0}) \\ A(\lambda_{1_0}) \end{bmatrix}. \tag{4.8}$$

Now let us outline our algorithm for obtaining the normal vector to the bifurcation surface of periodic solutions. Note that this algorithm is also applicable to equilibria. We use this normal vector to obtain the optimal parameter values. The procedure is summarized as follows:

1. Set the initial parameter value at which a target solution is stable.
2. Using the normal vectors (4.8), find the closet-bifurcation point [10] by searching several directions. To find a bifurcation point, we use the method described in [18].
3. Change the parameter values in the opposite direction of the closet-bifurcation obtained in Step 2.
4. Repeat Step 2 and Step 3.

4.3 Results

Here, we show the results of our method on discrete-time and continuous-time systems.

4.3.1 Discrete-Time System

We find the parameter values with the largest margin to bifurcation sets in the Kawakami map [19, 20]:

$$T : \mathbb{R}^2 \to \mathbb{R}^2;\ (x_1(k), x_2(k)) \mapsto (x_1(k+1), x_2(k+1)) \\ = (\lambda_1 x_1(k) + x_2(k), x_1(k)^2 + \lambda_2)$$

There are three kinds of bifurcation in the parameter range: $\lambda_1 = [-2.0, 2.0]$ and $\lambda_2 = [-2.0, 1.0]$, as shown in Fig. 4.1a. A stable fixed point exists in the shaded region surrounded by these bifurcations. Note that although the bifurcations curves are shown in Fig. 4.1a, we assume that the bifurcation structure is unknown. We only know the operating point at which the system has a stable fixed point. In the parameter region shown in Fig. 4.1a, our algorithm searches for the optimal parameter values, which means the farthest point from the three bifurcations. The simulation results are shown in Fig. 4.1a. Each circle labeled by A to D is an initial parameter value of our four trials. From Fig. 4.1a, we can see that from any initial parameter value in the shaded region, our method finds the optimal parameter values denoted by the open circle corresponding to almost the center of the gray region. We consider that if the parameter value is set near this point, we can construct a system that is robust to parameter perturbation. Figure 4.1b shows the Euclidean distance between the operating point and the closest bifurcation point as a function of iterations. Black and blue curves correspond to those in Fig. 4.1a. The initial points are very close to bifurcation points, however, our method can find the farthest point from bifurcations.

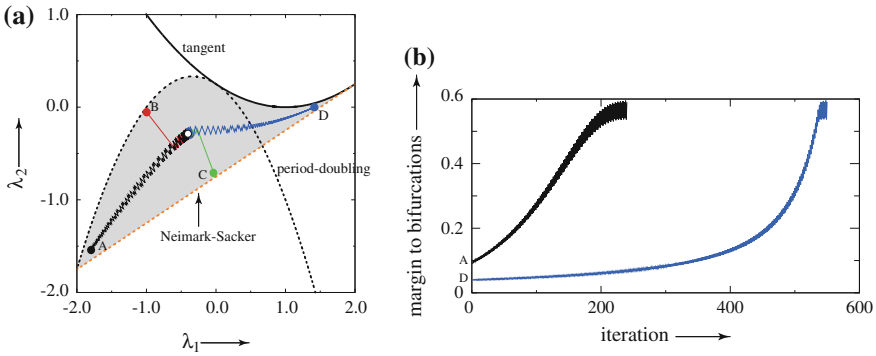

Fig. 4.1 Results for Kawakami map. **a** Bifurcation diagram and result of our method. A stable fixed point exists in the shaded region. The four points labeled by A–D are the initial parameter values. From each initial value, we can obtain the optimal parameter values denoted by the open circle. **b** Margin to bifurcations as a functional of iterations. Two curves correspond to the traces in **a** with different initial values labeled by A and D

4.3.2 Continuous-Time System

An example of a continuous-time system is one described by Duffing's equations:

$$\frac{dx_1}{dt} = x_2,$$
$$\frac{dx_2}{dt} = -\lambda_3 x_2 - x_1^3 + \lambda_2 + \lambda_1 \cos(t), \quad (\lambda_3 > 0).$$

In this system, the Neimark-Sacker bifurcation never appears, because using Liouville's theorem, the product of the two eigenvalues of the Jacobian matrix (4.5) is given by $\exp(-2\pi\lambda_3)$. Typical phenomena observed in this system include nonlinear resonance and chaos due to successive period-doubling bifurcations [21, 22].

Figure 4.2a shows the results of searching for parameter values with the maximum margin to bifurcations when $\lambda_3 = 0.1$. In this parameter region, there are at most three fixed points. Two of them are stable. The solid bifurcation curves in Fig. 4.2 are related to the fixed point which we treat here. Two initial values denoted by the open and closed circles in Fig. 4.2a are chosen. From the open circle, our method can obtain a local optimal parameter value. From the closed circle, our method also reaches a local optimal parameter value: the farthest point from the bifurcations denoted by the solid curves. To achieve a global search, we use the third parameter λ_3. Figure 4.2b shows the results when changing the value of parameter λ_3. The closed circle indicates the initial parameter values when $\lambda_3 = 0.1$. From this point, we can find the optimal parameter values denoted by the star. In this case, our method can escape the complicated bifurcation area and reach parameter values far from them when $\lambda_3 = 0.3$.

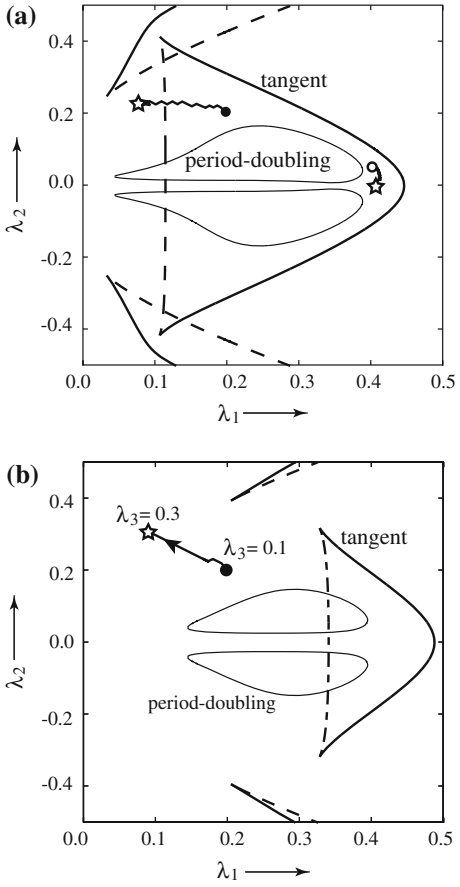

Fig. 4.2 Results for Duffing's equations. Solid curves indicate the bifurcation sets of the fixed point corresponding to the non-resonant state. Chaotic states generated by successive period-doubling bifurcations exist in period-doubling bifurcation sets. **a** $\lambda_3 = 0.1$. **b** Using the third parameter λ_3. Bifurcation sets are for $\lambda_3 = 0.3$

4.4 Conclusion

We proposed a method of determining parameter values that are far from bifurcations in a parameter space. We described the method of calculating the normal vector to the bifurcation curves for periodic solutions. Our decision method uses the normal vector to find parameter values which are far from bifurcations. As illustrated examples, we showed the results of discrete-time and continuous-time systems. Our method could find optimal parameter values in both systems. Open problems are to extend the method so that it can deal with complicated bifurcation structures in a parameter plane and systems including uncertainty.

Acknowledgments The proposed method of this research has been published as a paper in IJMNTA [17] before. H.K. is partially supported by JSPS KAKENHI (No. 23500367).

References

1. Mackey, M., Glass, L.: Oscillation and chaos in physiological control system. Science **197**, 287–289 (1997)
2. Glass, L., Mackey, M.: Pathological conditions resulting from instabilities in physiological control system. Ann. N.Y. Acad. Sci. **316**, 214–235 (1979)
3. Basso, M., Genesio, R., Tesi, A.: A frequency method for predicting limit cycle bifurcations. Nonlinear Dyn. **13**(4), 339–360 (1997)
4. Berns, D.W., Moiola, J.L., Chen, G.: Predicting period-doubling bifurcations and multiple oscillations in nonlinear time-delayed feedback systems. IEEE Trans. Circuits Syst. I: Fundam. Theory Appl. **45**(7), 759–763 (1998)
5. Chen, G., Moiola, J.L., Wang, H.O.: Bifurcation control: theories, methods, and applications. Int. J. Bifurcat. Chaos **10**(3), 511–548 (2000)
6. Xie, Y., Chen, L., Kang, Y.M., Aihara, K.: Controlling the onset of Hopf bifurcation in the Hodgkin-Huxley model. Phys. Rev. E **77**, 061921 (2008)
7. Overton, M.L.: On minimizing the maximum eigenvalue of a symmetric matrix. SIAM J. Matrix Anal. Appl. **9**(2), 256–268 (1988)
8. Shapiro, A., Fan, M.K.H.: On eigenvalue optimization. SIAM J. Optimization **5**(3), 552–569 (1995)
9. Imae, J., Furudate, T., Sugawara, S.: A simple numerical method for minimizing the maximum eigenvalues of symmetric matrices via nonlinear differential equation solvers. Trans. Jpn Soc. Mech. Eng. **63**(608), 87–92 (1997)
10. Dobson, I.: Computing a closest bifurcation instability in multidimensional parameter space. J. Nonlinear Sci. **3**(1), 307–327 (1993)
11. Kremer, G.G.: Enhanced robust stability analysis of large hydraulic control systems via a bifurcation-based procedure. J. Franklin Inst. **338**(7), 781–809 (2001)
12. Lu, J., Engl, H.W., Schuster, P.: Inverse bifurcation analysis: application to simple gene systems. Algorithms Mol. Biol. **1**(11), 1–16 (2006)
13. Dobson, I., Lu, L.: New methods for computing a closest saddle node bifurcation and worst case load power margin for voltage collapse. IEEE Trans. Power Syst. **8**(3), 905–913 (1993)
14. De Souza, A.C.Z., Canizares, C.A., Quintana, V.H.: New techniques to speed up voltage collapse computations using tangent vectors. IEEE Trans. Power Syst. **12**(3), 1380–1387 (1997)
15. Mönnigmann, M., Marquardt, W.: Normal vectors on manifolds of critical points for parametric robustness of equilibrium solutions of ODE systems. J. Nonlinear Sci. **12**, 85–112 (2002)
16. Vahidi, B., Azadani, E.N., Divshali, P.H., Hessaminia, A.H., Hosseinian, S.H.: Novel approach for determination of worst loading direction and fast prediction of stability margin in power systems. Simulation **86**(12), 729–741 (2010)
17. Kitajima, H., Yoshinaga, T.: A method for finding optimal parameter values using bifurcation-based procedure. Int. J. Mod. Nonlinear Theory Appl. **3**(2), 37–43 (2014)
18. Tsumoto, K., Ueta, T., Yoshinaga, T., Kawakami, H.: Bifurcation analyses of nonlinear dynamical systems: from theory to numerical computations. Nonlinear Theory Appl. IEICE **3**(4), 458–476 (2012)
19. Kawakami, H., Kobayashi, K.: Computer experiments on chaotic solutions of $x(t+2)-ax(t+1)-x^2(t)=b$. Bull. Fac. Eng. Tokushima Univ. **16**, 29–46 (1979)
20. Mira, C., Fournier-Prunaret, D., Gardini, L., Kawakami, H., Cathala, J.C.: Basin bifurcations of two-dimensional noninvertible maps: fractalization of basins. Int. J. Bifurcat. Chaos **4**(2), 343–381 (1994)
21. Kawakami, H.: Bifurcation of periodic responses in forced dynamic nonlinear circuits: computation of bifurcation values of the system parameters. IEEE Trans. Circuits Syst. **CAS-31**(3), 248–260 (1984)
22. Kitajima, H., Kawakami, H.: An algorithm tracing out the tangent bifurcation curves and its application to Duffing's equation, IEICE Trans. Fundam. **J78**(7), 806–810 (1995)

Chapter 5
Parametric Control to Avoid Bifurcation Based on Maximum Local Lyapunov Exponent

Ken'ichi Fujimoto, Tetsuya Yoshinaga, Tetsushi Ueta and Kazuyuki Aihara

5.1 Introduction

Discrete-time dynamical systems [2] are widely used for mathematical modeling of various systems. In many cases, desired behavior in nonlinear discrete-time dynamical systems corresponds to stable fixed and periodic points. The values of system parameters can be determined through bifurcation analysis [9, 10, 15] in advance so that desired behavior is produced in a steady state. However, when the parameter values are set far from appropriate values for any reason, the systems may not work correctly owing to undesirable behavior caused by bifurcations of desired behavior, for example, as alternans in the heart model [14].

Control systems to avoid bifurcations can prevent the emergence of undesirable states and keep proper states of dynamical systems. Here, we assume that desired behavior corresponds to a stable periodic point and consider a problem of avoiding its bifurcations in order to construct robust and resilient dynamical systems that are controlled so as not to make bifurcations.

K. Fujimoto (✉) · T. Yoshinaga
Institute of Health Biosciences, Tokushima University, 3-18-15 Kuramoto, Tokushima 770-8509, Japan
e-mail: fujimoto@medsci.tokushima-u.ac.jp

T. Yoshinaga
e-mail: yosinaga@medsci.tokushima-u.ac.jp

T. Ueta
Center for Administration of Information Technology, Tokushima University, 2-1 Minamijyousanjima, Tokushima 770-8506, Japan
e-mail: ueta@tokushima-u.ac.jp

K. Aihara
Institute of Industrial Science, The University of Tokyo, 4-6-1 Komaba, Meguro 153-8505, Japan
e-mail: aihara@sat.t.u-tokyo.ac.jp

K. Aihara et al. (eds.), *Analysis and Control of Complex Dynamical Systems*, Mathematics for Industry 7, DOI 10.1007/978-4-431-55013-6_5

Bifurcations of stable periodic points occur when their degree of stability (stability index) defined in Chap. 2 becomes one, i.e., their bifurcations can be avoided by suppressing the stability index below one. However, as described in Chap. 3, the optimization of the stability index has a difficulty because the stability index is not differentiable with respect to system parameters in general.

In this chapter, by using the maximum Lyapunov exponent (MLE) [11, 13, 16] that is related to the stability index [4, 5, 11, 12], we present a parametric controller that can avoid bifurcations of stable periodic points for unexpected parameter variation [6]. In practice, we substitute the maximum local LE (MLLE) [1, 3] defined in finite time to relieve a difficulty in computation of the MLE. Compared with the stability index, using the MLLE has the following advantages [6]: simple gradient methods can be used to optimize the MLLE, and the calculations of the MLLE and control input to avoid bifurcations can be realized along the passage of time. Experimental results applied to the Hénon map [7] to evaluate whether our parametric controller is effective to avoid bifurcations are also presented.

5.2 Problem Statement

Consider a discrete-time dynamical system described by

$$x(t+1) = f(x(t), p(t), q(t)), \tag{5.1}$$

where t denotes the discrete time, $x \in \mathbb{R}^N$ representing the set of real numbers is the vector of state variables, and $p \in \mathbb{R}^M$ and $q \in \mathbb{R}^L$ are time-variant system parameters. Here, we assume that f is known and differentiable, all states are always observable, and the values of p can be forcibly changed for any reason and are out of control, but q is handleable. We also assume that these parameter values can be changed only at $t = mT$ $(m = 0, 1, 2, \ldots)$ where T represents an interval to get the value of the MLLE and control input to avoid bifurcations, which are defined later.

When all parameter values are constant, fixed and periodic points of f are defined as follows. If a point $x^* \in \mathbb{R}^N$ satisfies $x^* - f(x^*, p, q) = 0$, then x^* is a fixed point of f. In the same way, a periodic point with period n, i.e. an n-periodic point, of f is defined as a point x^* such that $x^* - f^n(x^*, p, q) = 0$ and $x^* - f^k(x^*, p, q) \neq 0$ for $k < n$ where f^n denotes the nth iterate of f. By describing the Jacobian matrix of f as

$$Df(x(t), p, q) = \frac{\partial}{\partial x} f(x(t), p, q), \tag{5.2}$$

we introduce the characteristic equation of an n-periodic point x^* as

$$\chi(x^*, p, q, \mu) = \det\left(\mu I - Df^n(x^*, p, q)\right) = 0, \tag{5.3}$$

where I denotes the $N \times N$ identity matrix; μ is an eigenvalue of $Df^n(x^*, p, q)$ and is called the characteristic multiplier of x^*.

The stability index of an n-periodic point (x^*) is defined by using the maximum modulus of its characteristic multipliers, i.e., it is equivalent to the spectral radius of the Jacobian matrix, $\rho\left(Df^n(x^*, p, q)\right)$, where $\rho(\cdot)$ represents the spectral radius of a matrix. Therefore, a periodic point x^* is stable if and only if $\rho\left(Df^n(x^*, p, q)\right) < 1$ and bifurcations of a stable periodic point occur when $\rho\left(Df^n(x^*, p, q)\right) = 1$. The parameter values at which bifurcations occur can be numerically found by using a powerful computing method [9, 15].

We now assume that desired behavior corresponds to a stable periodic point and treat a situation that bifurcations of desired behavior may emerge owing to the forcible variation of p. For the situation, we consider avoiding bifurcations of desired behavior by adjusting the values of q only when the parameter values approach any bifurcation points. Therefore, this problem resembles the problems treated in Chaps. 2, 3 and 4.

5.3 Proposed Method

From the aforementioned assumptions, the values of p and q are constant for the duration of interval T. When an initial value $x(mT)$ at $t = mT$ $(m = 0, 1, 2, \ldots)$ that converges to a stable periodic point and a small perturbation $w(mT) \in \mathbb{R}^N$ to $x(mT)$ are given, the MLLE is defined as

$$\lambda(x(mT), p, q, T) = \frac{1}{T} \sum_{t=mT}^{(m+1)T-1} \ln\|w(t+1)\|, \tag{5.4}$$

where $\|\cdot\|$ represents the Euclidean norm of a vector. The trajectory of $w(t+1)$ is obtained from the linearized system defined by

$$w(t+1) = Df(x(t), p, q) \cdot v(t), \tag{5.5}$$

where $v(t) = w(t)/\|w(t)\|$. This normalization is to relieve a computational difficulty in (5.4). In the following, we simplify the notation of $\lambda(x(mT), p, q, T)$ as λ.

The problem of avoiding bifurcations of stable periodic points can be formulated as the minimization problem of an objective function defined by

$$G(\lambda) = \frac{1}{2}\left(\lambda - H(\lambda)\right)^2, \tag{5.6}$$

where H is a map described as

$$H(\lambda) = \begin{cases} \lambda & \text{if } \lambda \le \lambda^*, \\ \lambda^* & \text{otherwise.} \end{cases} \tag{5.7}$$

The user-defined parameter λ^* is set to a negative value close to zero; it is used not only to detect the approach of the values of p and q to any bifurcation points but also a set point to control λ when $\lambda^* < \lambda < 0$. Since λ is the function with respect to q, we can obtain a gradient system of (5.6), i.e. the updating rule of q, as

$$q((m+1)T) - q(mT) = -\eta \frac{\partial G(\lambda)}{\partial q} = -\eta(\lambda - \lambda^*)\frac{\partial \lambda}{\partial q}, \tag{5.8}$$

where η is a positive parameter given by users. The formulas to calculate the values of $\partial\lambda/\partial q$ can be explicitly expressed [6, 8] and their computations can be realized in real time without off-line calculation to find the exact position of stable periodic points to be controlled objects. Note that the formulas we derived [6] can be commonly used in a variety of nonlinear discrete-time dynamical systems. By updating the values of q according to (5.8) only when $\lambda^* < \lambda < 0$, the MLLE can remain a negative value, i.e., bifurcations of stable periodic points can be avoided.

5.4 Experimental Results

To evaluate whether the proposed parametric controller is effective, we carried out several experiments for stable periodic points observed in the Hénon map [7]. The dynamics of the Hénon map is described as

$$x_1(t+1) = 1 + x_2(t) - p(t) \cdot x_1(t)^2, \tag{5.9a}$$
$$x_2(t+1) = q(t) \cdot x_1(t), \tag{5.9b}$$

where x_1 and x_2 are state variables and t is the discrete time. We here assumed that p and q correspond to out-of-control and control parameters, respectively. In the following experiments, we set $T = 500$, $\eta = 0.1$, and $\lambda^* = -0.2$ in (5.4) and (5.8).

Before carrying out experiments, we analyzed bifurcations on fixed and periodic points observed in (5.9). As shown in Fig. 5.1, we found a fixed point, n-periodic

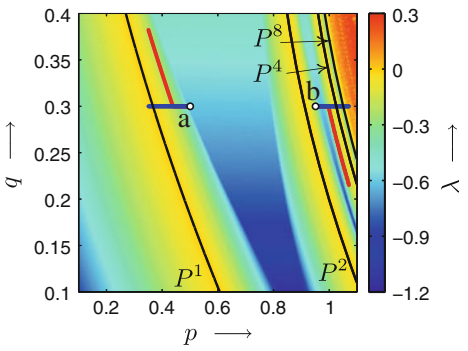

Fig. 5.1 Bifurcation diagram on fixed and periodic points in the Hénon map, MLLE, and *blue horizontal* and *red diagonal curves* corresponding to parameter variation without and with control

points ($n = 2, 4, 8$), and their period-doubling bifurcations where the solid curve with P^n represents the set of bifurcation points of the n-periodic point. The stable fixed point is present in the left-hand-side parameter regions of the curve P^1 and the stable n-periodic point exists in the parameter regions surrounded by the curves of $P^{\frac{n}{2}}$ and P^n. The MLLE on the fixed and periodic points is indicated in color, for example, the color in the parameter regions surrounded by the curves of P^1 and P^2 shows the MLLE on the stable two-periodic point. The relationship between the MLLE and colors is shown in the right bar graph. We note that these analyses are not necessary to avoid bifurcations using our controller, i.e., it was carried out only to demonstrate whether bifurcation points are avoided in space of system parameters.

When we set $(p(0), q(0)) = (0.5, 0.3)$ corresponding to the point "a" in Fig. 5.1 and $(x_1(0), x_2(0)) = (1.43, 0.0)$, the two-periodic point was observed in a steady state. By decreasing the value of p with 0.0015 every T along the blue horizontal line from the initial point "a", the two-periodic point bifurcated on the curve P^1 and instead the fixed point appeared at $t \simeq 93T$ as shown by the blue trajectory of x_1 in Fig. 5.2a. To avoid the period-doubling bifurcation, the proposed controller adjusted the value of q so as to keep $\lambda \simeq \lambda^*$ after $t = 42T$ (Fig. 5.2b). The trajectory of the controlled parameter is also shown as the red diagonal curve branching from the blue horizontal line with the point "a" in Fig. 5.1. Consequently, the stable two-periodic point could be observed for the duration of $0 \leq t \leq 100T$ without bifurcating.

We also analyzed avoiding the period-doubling bifurcation of the stable four-periodic point. The initial values were set to $(x_1(0), x_2(0)) = (1.04, -0.18)$ and $(p(0), q(0)) = (0.95, 0.3)$ corresponding to the point "b" in Fig. 5.1. When we changed the value of p along the blue horizontal line starting from the point "b", we

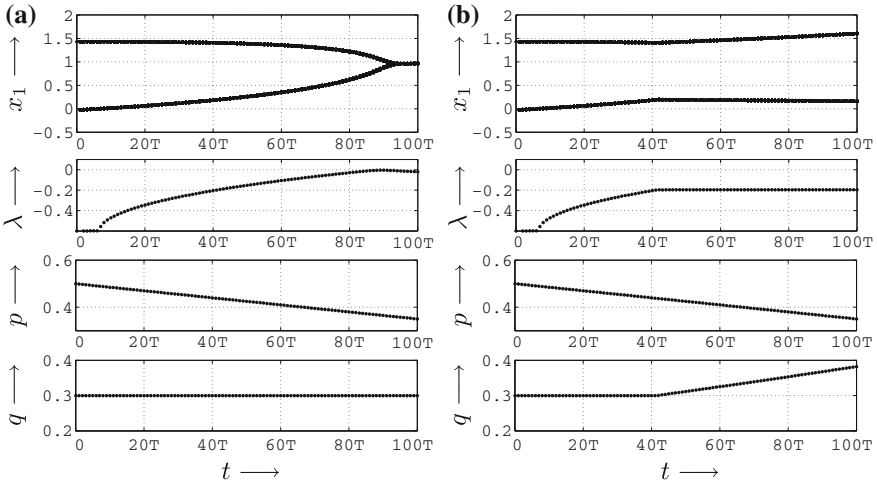

Fig. 5.2 Experimental results of bifurcation avoidance for a two-periodic point in the Hénon map displayed as time series. The *blue* and *red* sequences correspond to the trajectories both without and with control **a** case without control **b** case with control

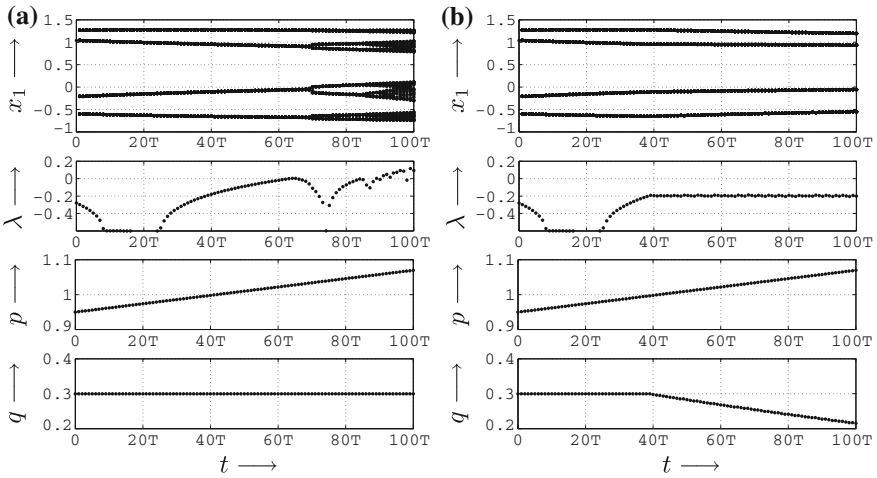

Fig. 5.3 Experimental results of bifurcation avoidance for a four-periodic point in the Hénon map displayed as time series **a** case without control **b** case with control

observed the eight-periodic points and a chaotic state caused by a cascade of period-doubling bifurcations across the curves of P^4 and beyond (Figs. 5.1 and 5.3a). Hence, the stable four-periodic point bifurcated and vanished at $t \simeq 70T$ owing to its period-doubling bifurcation curve P^4. In contrast, the red diagonal curve branching from the blue horizontal line with the point "b" in Fig. 5.1 indicated that the proposed controller was used to avoid the bifurcation curve of P^4. As the results, as shown in Fig. 5.3b, we could observe the four-periodic point for the duration of $0 \leq t \leq 100T$.

5.5 Conclusion

In this chapter, we presented a parametric control system to avoid bifurcations of stable periodic points in nonlinear discrete-time dynamical systems with parameter variation. The parameter updating of our controller is theoretically derived from the minimization of an objective function with respect to the MLLE. The computations of the MLLE and parameter variation to avoid bifurcations can be realized in real time without finding the exact positions of stable periodic points to be controlled objects. Our experimental results showed that the proposed controller effectively worked to avoid bifurcations of stable periodic points in the Hénon map. We note that this control system can be also applied to avoid bifurcations of stable fixed points. Further, the parameter-updating formulas we derived [6] can be widely used to a variety of nonlinear discrete-time dynamical systems.

Acknowledgments This chapter described the basic idea of the paper "Fujimoto, K., and Aihara, K., Bifurcation avoidance control of stable periodic points using the maximum local Lyapunov exponent, Nonlinear Theory and Its Applications, IEICE. vol. 6, "no.1", sects. 2–3, 2015 (Copyright © 2006 IEICE)" with different examples. This research was partially supported by JSPS KAKENHI Grant Number 25330288.

References

1. Abarbanel, H., Brown, R., Kennel, M.: Local Lyapunov exponents computed from observed data. J. Nonlinear Sci. **2**, 343–365 (1992)
2. Alberto, J.M. (ed.): Discrete Time Systems. InTech (2011). http://www.intechopen.com/books/discrete-time-systems
3. Ali, M., Saha, L.: Local Lyapunov exponents and characteristics of fixed/periodic points embedded within a chaotic attractor. J. Zhejiang Univ. Sci. A. **6**, 296–304 (2005)
4. Dingwell, J.B.: Lyapunov exponents. In: Akay M. (ed.) Wiley Encyclopedia of Biomedical Engineering. Wiley, New York (2006)
5. Eckmann, J.P., Ruelle, D.: Ergodic theory of chaos and strange attractors. Rev. Mod. Phys. **57**, 617–656 (1985)
6. Fujimoto, K., Aihara, K.: Bifurcation avoidance control of stable periodic points using the maximum local Lyapunov exponent. Nonlinear Theory Appl. IEICE **6**, 2–14 (2015)
7. Hénon, M.: A two-dimensional mapping with a strange attractor. Commun. Math. Phys. **50**, 69–77 (1976)
8. Honma, N.: Control of the complexity in recurrent neural networks (in Japanese). Bull. Coll. Medi. Sci, Tohoku Univ. **8**, 23–30 (1999)
9. Kawakami, H.: Bifurcation of periodic responses in forced dynamic nonlinear circuits: computation of bifurcation values of the system parameters. IEEE Trans. Circ. Syst. **31**, 248–260 (1984)
10. Kuznetsov, Y.: Elements of Applied Bifurcation Theory, 3rd edn. Applied Mathematical Sciences. Springer, Berlin (2004)
11. Marco, S.: Numerical calculation of Lyapunov exponents. Math. J. **6**, 78–84 (1996)
12. Oseledec, V.I.: A multiplicative ergodic theorem: Lyapunov characteristic numbers for dynamical systems. Trans. Moscow Math. Soc. **19**, 197–231 (1968)
13. Sano, M., Sawada, Y.: Measurement of the Lyapunov spectrum from a chaotic time series. Phys. Rev. Lett. **55**, 1082–1085 (1985)
14. Sun, J., Amellal, F., Glass, L., Billette, J.: Alternans and period-doubling bifurcations in atrioventricular nodal conduction. J. Theor. Biol. **173**, 79–91 (1995)
15. Tsumoto, K., Ueta, T., Yoshinaga, T., Kawakami, H.: Bifurcation analyses of nonlinear dynamical systems: from theory to numerical computations. Nonlinear Theory Appl. IEICE. **3**, 458–476 (2012)
16. Wolf, A., Swift, J.B., Swinney, H.L., Vastano, J.A.: Determining Lyapunov exponents from a time series. Phys. D. **16**, 285–317 (1985)

Chapter 6
Threshold Control for Stabilization of Unstable Periodic Orbits in Chaotic Hybrid Systems

Daisuke Ito, Tetsushi Ueta, Takuji Kousaka, Jun-ichi Imura and Kazuyuki Aihara

6.1 Introduction

Various deterministic dynamical systems including nonlinear electric circuits show chaotic phenomena characterized by the sensitivity to small perturbations, positive Lyapunov exponents, and their complex orbit structure. It is well known that an infinite number of unstable periodic orbits (UPOs)are embedded in a chaotic attractor [1].

Based on the Poincaré mapping, a UPO in a continuous-time system can be expressed as an unstable periodic point (UPP) in the corresponding discrete-time system. The Ott-Grebogi-Yorke (OGY) method was the pioneering attempt to stabilize UPPs [2] by pushing the orbit near the stable manifold of the target UPP with very

D. Ito (✉)
Advanced Technology and Science, System Innovation Engineering,
Tokushima University, 2-1 Minamijyousanjima, Tokushima 770-8504, Japan
e-mail: d-ito@is.tokushima-u.ac.jp

T. Ueta
Center for Administration of Information Technology, Tokushima University,
2-1 Minamijyousanjima, Tokushima 770-8506, Japan
e-mail: ueta@tokushima-u.ac.jp

T. Kousaka
Faculty of Engineering, Oita University, 700 Dannoharu, Oita 870-1192, Japan
e-mail: takuji@oita-u.ac.jp

J. Imura
Graduate School of Information Science and Engineering, Tokyo Institute of Technology,
2-12-1 O-Okayama, Meguro, Tokyo 152-8552, Japan
e-mail: imura@mei.titech.ac.jp

K. Aihara
Institute of Industrial Science, The University of Tokyo, 4-6-1 Komaba, Meguro,
Tokyo 153-8505, Japan
e-mail: aihara@sat.t.u-tokyo.ac.jp

K. Aihara et al. (eds.), *Analysis and Control of Complex Dynamical Systems*,
Mathematics for Industry 7, DOI 10.1007/978-4-431-55013-6_6

small parameter perturbations. If it fails, a retry in near future is expected because of the recurrence property of the chaos, i.e., the uncontrolled orbit will comes close to the target UPP again. With this recurrence, there is a possibility that stabilizing the target UPP with a tiny control input, which is proposed to the distance between the current state and the UPP. In the very small area around the target UPP, this kind of problems can be considered by linear control theory. The controlling chaos by the pole assignment method has been proposed [3]. The feedback gain of this controller can be designed with assigned poles regarding the characteristic equation for the variational equation [4, 5]. Extensions of the methods are applied to chaotic hybrid systems [6]. In these conventional methods, the amplitude of the control input is basically proportional to the error between the current state of the orbit and the UPP. As mentioned above, the recurrence property of chaotic dynamics realizes that the orbit will visit a neighborhood of the UPP in future, thus the control input can be small at that moment.

Other nonlinear control schemes including the delayed feedback control [7] and its extensions [8, 9] have been proposed. Related methods such as external force control [10], and occasional proportional feedback [11–16] are also discussed from a practical view point.

In these methods, the control input is basically added to the state or parameters of the system. Thus the controller must vary these values which may be difficult to change; e.g., in electrical circuits, the controller requires to change the amount of a resistor or a capacitor quickly.

While, hybrid systems has been intensively studied for a decade [17]. In those systems, a flow described by differential equations is interrupted by the discrete events, and then an impulsive jumping or a switching of the governing differential equations happens. Thus the flow may changes non-smoothly, and it may cause peculiar bifurcations [18]; e.g., in chaotic spiking oscillators [19], state-dependent switching generates two different flows where a bifurcation phenomena and a chaotic response are guaranteed theoretically. In general, the switching mechanism is not explicitly described in the differential equations, but it affects certainly dynamical behavior of the system [20, 21]. In electric circuits, a variable threshold is realized by an analog switch (multiplexer); therefore, to choose the threshold value as a control input is reasonable.

For a specific hybrid system, the controlling chaos based on the linear control theory can be realized by applying the Poincaré section on the border [6]. UPPs in the derived discrete-time system are controlled with the same framework of the conventional control method, i.e., the control input is added into a system parameter or the state as a small perturbation successively. In other words, the whole control system spends a certain amount of energy until the control scheme completes the stabilization.

A threshold value in the given hybrid system is not used as the control parameter because dynamical affection with perturbed threshold values has not been evaluated yet. In the previous study [20] we clarified the derivatives and variational equations of the given hybrid systems about threshold values. Thereby we apply these results

to controlling chaos; namely, we try to design a control scheme with variations of threshold values theoretically.

Now let us restate our purpose in this chapter. We stabilize a UPO embedded within a chaotic attractor in a hybrid system by varying its threshold values. The control system compares the current state variable with the threshold value, and updates the threshold value instantly and slightly. The orbit starting from the current Poincaré section (the threshold value) does not receive any control until it reaches the next section. Although Murali and Sinha [22] have proposed a chaos controller by featuring the perturbation of attached threshold values, the objective system is not a hybrid system and the proposed controller stabilizes UPOs by clipping the voltage of a system with a simple circuit. Parameter values of the controller are provided by trial and error. In our method, the control vector is computed systematically by applying the linear control theory. We demonstrate control results of a 1D switching chaotic system and a 2D chaotic neuron, and evaluate its control performances as the controller by specifying basins of attraction. Moreover, a related experiment is given for the former system.

6.2 Design of Controller with Perturbation of the Threshold Value

Let us consider the n-dimensional and m-tuple differential equations described by

$$\frac{dx}{dt} = f_i(x),\ i = 0,\ 1,\ \ldots,\ m-1, \tag{6.1}$$

where $t \in \mathbb{R}$ is time, $x \in \mathbb{R}^n$ is the state and $f_i : \mathbb{R}^n \to \mathbb{R}^n$ is a C^∞ class function.

Suppose that Π_i is a transversal section to the orbit and set $x_0 = x(0) \in \Pi_0$, then the solution of (6.1) is given by

$$x(t) = \varphi(x_0, t).$$

Now we provide Π_i with a threshold value as follows:

$$\Pi_i = \left\{ x \in \mathbb{R}^n \,|\, q_i(x,\ \theta_i) = 0 \right\},$$

where q_i is a differentiable scalar function, and θ_i is a unique parameter that defines the position of Π_i. Note that Π_i becomes also a local section, and θ_i is independent from the vector field in (6.1). When an orbit governed by f_i reaches the section Π_i, the governing function is changed to f_{i+1}. If the orbit passing through several sections reaches Π_0 again, then m local maps are defined as follows:

$$\begin{aligned} T_0 &: \Pi_0 \to \Pi_1, \\ &\quad x_0 \mapsto x_1 = \varphi_0(x_0,\ \tau_0), \\ T_1 &: \Pi_1 \to \Pi_2, \\ &\quad x_1 \mapsto x_2 = \varphi_1(x_1,\ \tau_1), \\ &\quad \vdots \\ T_{m-1} &: \Pi_{m-1} \to \Pi_0, \\ &\quad x_{m-1} \mapsto x_0 = \varphi_{m-1}(x_{m-1},\ \tau_{m-1}), \end{aligned} \tag{6.2}$$

where τ_i is the passage time from Π_i to Π_{i+1}, and depends on the state x_i and the parameter θ_{i+1} of the local section Π_{i+1}. Assume that $y(k) \in \Sigma \subset \mathbb{R}^{n-1}$ is a location on local coordinates, then there is the projection satisfying $\eta(x(k)) = y(k)$. Let the composite map of $T_i,\ i = 0,\ 1, \ldots, m-1$ be the solution starting in $\eta^{-1}(y(0)) = x(0) \in \Pi_0$. From (6.2), the Poincaré map T is given by the following composite map:

$$T(y(k),\ \theta_0,\ \theta_1,\ \ldots,\ \theta_{m-1}) = \eta \circ T_{m-1} \circ \cdots \circ T_1 \circ T_0 \circ \eta^{-1}.$$

Thus

$$y(k+1) = T(y(k),\ \theta_0,\ \theta_1,\ \ldots,\ \theta_{m-1}).$$

When the orbit starting from $x_0 \in \Pi_0$ returns x_0 itself, this orbit forms a periodic orbit and it is defined as the fixed point by using the Poincaré map T as follows:

$$y_0 = T(y_0,\ \theta_0,\ \ldots,\ \theta_{m-1}).$$

The corresponding characteristic equation is given by

$$\chi(\mu) = \det\left(\frac{\partial T(y_0)}{\partial y_0} - \mu I\right) = 0.$$

To apply the pole assignment method, the derivatives of the Poincaré map are required to compute a control gain [3]. The equations in (6.2) are, in fact, differentiable with respect to the state, thus each derivative is given as follows:

$$\begin{aligned} \frac{\partial T_i}{\partial x_i} &= \left[I - \frac{1}{\dfrac{\partial q_{i+1}}{\partial x}\dfrac{\partial \varphi_i}{\partial t}} \frac{\partial q_{i+1}}{\partial \theta_{i+1}} \frac{\partial \varphi_i}{\partial t} \right] \frac{\partial \varphi_i}{\partial x_i}, \\ \frac{\partial T}{\partial y_0} &= \frac{\partial \eta}{\partial x} \left(\prod_{i=1}^{m} \frac{\partial T_{m-i}}{\partial x_{m-i}} \right) \frac{\partial \eta^{-1}}{\partial y}, \end{aligned} \tag{6.3}$$

$$\frac{\partial T_{j-1}}{\partial \theta_j} = \frac{-1}{\dfrac{\partial q_j}{\partial x}\dfrac{\partial \varphi_{j-1}}{\partial t}} \frac{\partial q_j}{\partial \theta_j}\frac{\partial \varphi_{j-1}}{\partial t},$$

$$\frac{\partial T}{\partial \theta_j} = \frac{\partial \eta}{\partial x}\prod_{i=1}^{m-j}\frac{\partial T_{m-i}}{\partial x_{m-i}}\frac{\partial T_{j-1}}{\partial \theta_j}. \tag{6.4}$$

We can suppose here that $(\partial q_{i+1}/\partial x) \times (\partial \varphi_i/\partial t)$ and $(\partial q_j/\partial x) \times (\partial \varphi_{j-1}/\partial t)$ are non-zero unless the orbit and sections are crossed tangentially.

Suppose that $\xi(k)$ is a small perturbation and $u(k)$ is intended to be a control input defined later. When the parameter θ_j is chosen as a controlling parameter, the variational equations around the fixed point are expressed as

$$y(k) = y^* + \xi(k),\ \theta_j(k) = \theta_j + u(k). \tag{6.5}$$

After one iteration of T, we have

$$\begin{aligned} y(k+1) &= T(y^* + \xi(k),\ \theta_j + u(k)) \\ &\approx y^* + \frac{\partial T}{\partial y^*}\xi(k) + \frac{\partial T}{\partial \theta_j}u(k). \end{aligned}$$

Therefore we obtain the difference equation defined by the derivative of T as follows:

$$\xi(k+1) = D_{y^*}\xi(k) + D_{\theta_j}u(k), \tag{6.6}$$

where $D_{y^*} = \partial T/\partial y^*$ and $D_{\theta_j} = \partial T/\partial \theta_j$. Note that (6.6) holds when the state $y(k)$ is located to be adjacent to the fixed point y^*.

To stabilize $\xi(k)$ at the origin, a state feedback control is designed as follows [5]:

$$u(k) = K^{\mathsf{T}}\xi(k), \tag{6.7}$$

where T is a transpose and K is an appropriate $n-1$ dimensional vector designed by the pole assignment method. Thus we have

$$\xi(k+1) = [D_{y^*} + D_{\theta_j}K^{\mathsf{T}}]\xi(k). \tag{6.8}$$

The corresponding characteristic equation is given by

$$\chi(\mu) = \det(D_{y^*} + D_{\theta_j}K^{\mathsf{T}} - \mu I) = 0. \tag{6.9}$$

The stability condition at the origin is $|\mu_i| < 1,\ i = 1,\ 2,\ \ldots,\ n-1$.

In the conventional chaos control methods, a control input is applied into the specific system parameter as a small perturbation. During a transition state, the control system consumes certain control energy given by integration of such perturbations even if small. Thus $\varepsilon = \int_0^\infty ||u(t)||dt$ is regarded as controlling energy.

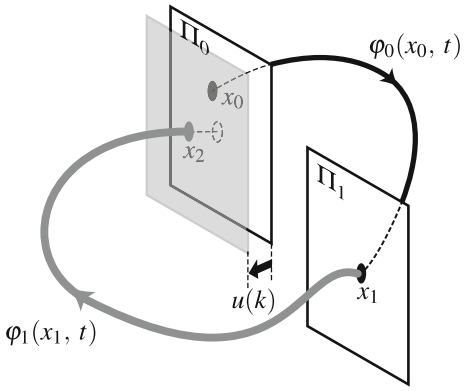

Fig. 6.1 Relationship between the flow and sections. Our method adjusts the position of the local section Π_0 only. The state and vector fields are not affected by the control input

In our method, the control input $u(k)$ is added into θ_j; see (6.5). Figure 6.1 depicts a schematic diagram of the method. The location of the section Π_0 defined by θ_0 is shifted by $u(k)$ instantly when the orbit $\varphi_0(t,\ x_0)$ departs from Π_0. No actual control input is added into the system. The state-feedback is utilized only to determine the dynamic threshold value, thus the orbit starting from the current threshold value reaches the next controlled threshold value without any control energy.

It is noteworthy that this is an energy-saving control scheme. For example, let us suppose that we want to put a ball into a bucket with bouncing once on the wall. In Fig. 6.2a, an electrical fan modifies the trajectory of the ball by blowing against it. The fan consumes electrical energy continuously during transient. The conventional methods look like this situation. On the other hand, changing the position of the wall

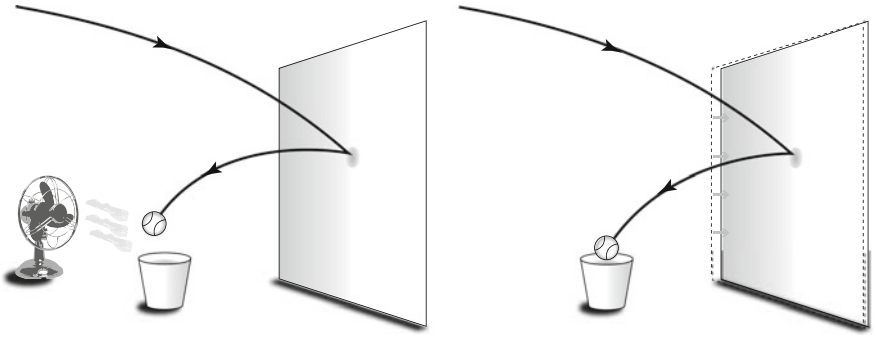

Fig. 6.2 Concepts of controlling schemes. In a conventional method, a controller, e.g. an electrical fan, has to blow the ball to put it to the bucket. Therefore, it requires a powerful controller to move a ball. In the case to use the threshold value as a perturbation parameter, the controller only move the position of a wall or a goal, and does not influence the ball directly

also provides the same effect with (a), i.e., the original position of the wall may cause failure of the shoot, but a desirable trajectory can be realized by letting the wall to be in a proper position, see Fig. 6.2b. Realistically, not a little effort is required to move the wall compared with a short-time operation of the fan, however, in the electric circuit, such movement of the wall is easily realized, e.g., by a change of the value of the threshold for an operational amplifier. Note that no control energy consumed during this scheme. Only small energy is required when the old threshold value is updated. The orbit runs without any control until it reaches the next threshold value.

6.3 A Simple Chaotic System

Let us consider a simple interrupt chaotic system [23] shown in Fig. 6.3 as an example. The switch is flipped by a certain rule depending on the state and the period. Assume that v is the state variable, and then the normalized equation is given as follows:

$$\dot{v} = -v + E,$$
$$\text{if} \quad t = n\rho \quad \text{then} \quad E \leftarrow E_1, \quad \text{if} \quad v > E_r \quad \text{then} \quad E \leftarrow 0$$

where $n \in \mathbb{N}$, E_1 and E_r are a direct voltage bias and a switching threshold value, respectively. ρ is the period of the clock pulse input. Figure 6.4 illustrates the dynamical behavior. If the Poincaré section is defined as $\Pi = \{v \in \mathbb{R};\ t = n\rho\}$, trajectories stroke two types of solutions (Fig. 6.5), and they can be solved exactly, see, [24]. Therefore the system can be discretized by the Poincaré section, and redefined as follows:

$$v'(k+1) = g(v'(k)) = \begin{cases} (v'(k) - E_1)e^{-\rho} + E_1, & \text{if} \quad v'(k) < d, \\ E_r \dfrac{v'(k) - E_1}{E_r - E_1} e^{-\rho}, & \text{otherwise}, \end{cases} \tag{6.10}$$
$$d = (E_r - E_1)e^{\rho} + E_1.$$

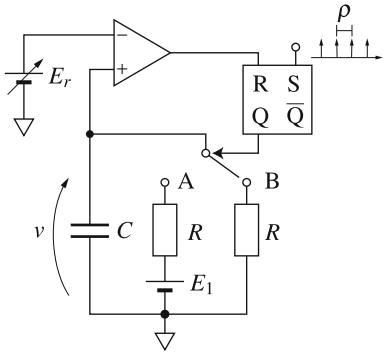

Fig. 6.3 Circuit model of an interrupt chaotic system. ρ and E_r represent the period of the clock pulse input and the switching threshold value, respectively

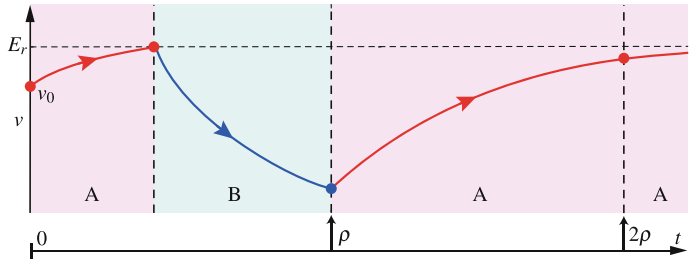

Fig. 6.4 The switching behavior. When the capacitor voltage reaches to the threshold value E_r, the switch is flipped to the position B. If the time t is ρ, the switch is flipped to the position A

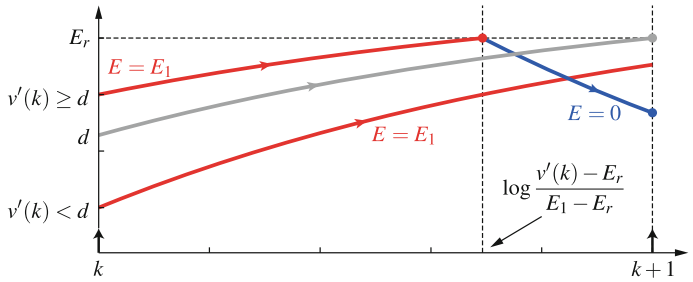

Fig. 6.5 The sketch of a simple chaotic interrupt system. There are two types of trajectories depending on the initial value $v'(k)$. If $v'(k)$ is less than d, the trajectory reaches $v'(k+1)$ without interruption. Otherwise, the trajectory reaches the threshold value E_r, and E is changed to zero

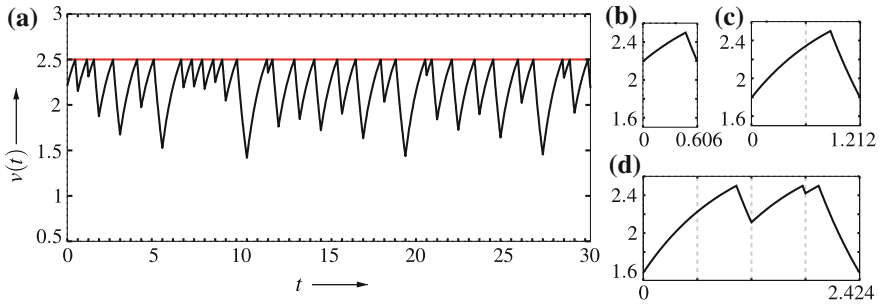

Fig. 6.6 **a** A sample trajectories of a chaotic attractor with $E_1 = 3$, and $E_r = 2.5$. **b**, **c**, and **d**: Period 1, 2 and 4 UPOs embedded in the chaos, respectively

Note that $v'(k) = v(k\rho)$. The solution ψ is defined by (6.11):

$$\psi(v'(0), k) = v'(k), \ \psi(v'(0), 0) = v'(0) = v(0). \tag{6.11}$$

A chaotic attractor and three UPOs with parameters $E_1 = 3$, $E_r = 2.5$ and $\rho = 0.606$ are shown in Fig. 6.6. Table 6.1 lists the periods, states and multipliers of some UPOs. Each orbit is confirmed to be a UPO.

Table 6.1 Periods, states, and multipliers of UPOs in Fig. 6.6b–d

Attractor	Period	v^*	μ
(b) UPO_1	1	2.195202	−2.727643125796
(c) UPO_2	2	1.794216	−1.488007404341
		2.34221	
(d) UPO_4	4	1.580281	−11.070830176867
		2.225503	
		2.112552	
		2.420642	

From Eqs. (6.8) and (6.9), we can choose the control gain as

$$K = \frac{q - D_{v^*}}{D_{E_r}},$$

where $D_{v^*} = \partial T/\partial v^*$ and $D_{E_r} = \partial T/\partial E_r$ are derivatives of T, and can be calculated as follows:

$$\frac{\partial T}{\partial v^*} = \frac{\partial \psi}{\partial v^*}(v^*,\ p),\ \frac{\partial \psi}{\partial v^*}(v^*,\ k+1) = \left.\frac{\partial g}{\partial v'}\right|_{v'=v'(i)} \frac{\partial \psi}{\partial v^*}(v^*,\ k),$$
$$\frac{\partial \psi}{\partial v^*}(v^*,\ 0) = I, \tag{6.12}$$

$$\frac{\partial T}{\partial E_r} = \frac{\partial \psi}{\partial E_r}(v^*,\ p),\ \frac{\partial \psi}{\partial E_r}(v^*,\ k+1) = \left.\frac{\partial g}{\partial v'}\right|_{v'=v'(i)} \frac{\partial \psi}{\partial v^*}(v^*,\ k) + \left.\frac{\partial g}{\partial E_r}\right|_{v'=v'(i)},$$
$$\frac{\partial \psi}{\partial E_r}(v^*,\ 0) = 0, \tag{6.13}$$

where the symbol $p \in \mathbb{N}^+$ is the period of the target trajectory, and q is a desirable pole for the controlling, and $|q| < 1$ is required for stabilization. When the clock pulse is input at $t = k\rho$, $u(t)$ is generated as $K(v^* - v'(k))$ from (6.7), and it is added to the switching threshold E_r. Figure 6.7 shows the behavior of $u(t)$ and the system. When $u(t)$ is applied to the system, the threshold value is changed, and the behavior of the system is controlled.

6.3.1 Numerical Simulation

We show some results of the chaos control by referring to Fig. 6.8, where each graph shows a transition response of the orbit and the threshold value. From this figure, we confirm that each UPO is controlled to become a stable periodic orbit by several

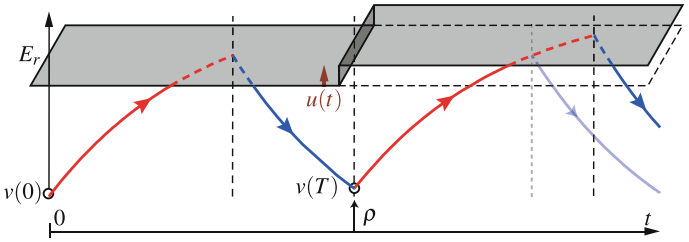

Fig. 6.7 Controller affects the switching threshold E_r, thus the control input $u(t)$ biases E_r. By doing this, the controller can control the trajectory without any effect on the dynamical equations and vector fields

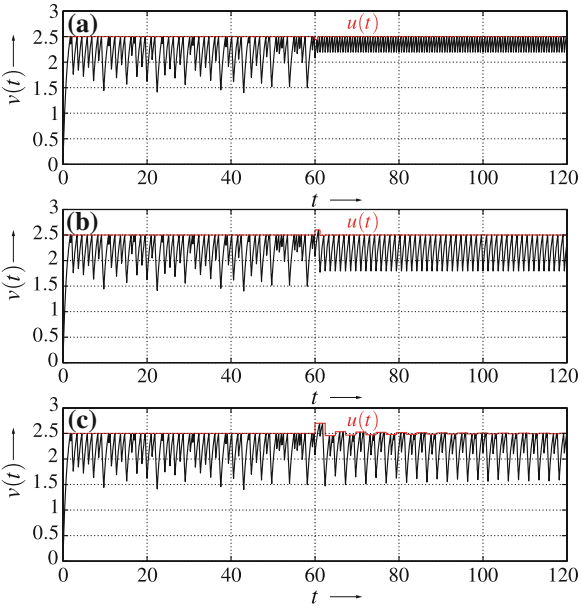

Fig. 6.8 Transition responses of controlled UPOs and the threshold values. **a** Period-1, **b** period-2 and **c** period-4 solutions shown in Table 6.1 are stabilized. Note that $u(t)$ does not affect the state and vector fields directly

renewals of $u(t)$. The UPO_4 in Fig. 6.8c has a longer renewal span than other UPOs because a renewal span depends on the period of the target UPO.

Figure 6.9 shows basins of attraction of UPOs with our controller in the q-$v(0)$ plane. White regions in the figure indicate the initial values in which the UPO could be stabilized, and black regions indicate failure of the controlling. This shows that all UPOs could be stabilized easily with relatively small initial values. Additionally, UPOs can also be stabilized at a negative initial value. However, in larger initial values, the UPO_4 could not be controlled. The pole assignment method renews the control signal on a periodic basis only. Therefore, this technique is less effective for long-period UPOs such as the UPO_4.

Figure 6.6a reveals that the chaotic attractor wanders within $1.3 < v(t) < 2.5$. The basin of attraction in this range is shown by white regions in Fig. 6.9. Thus the

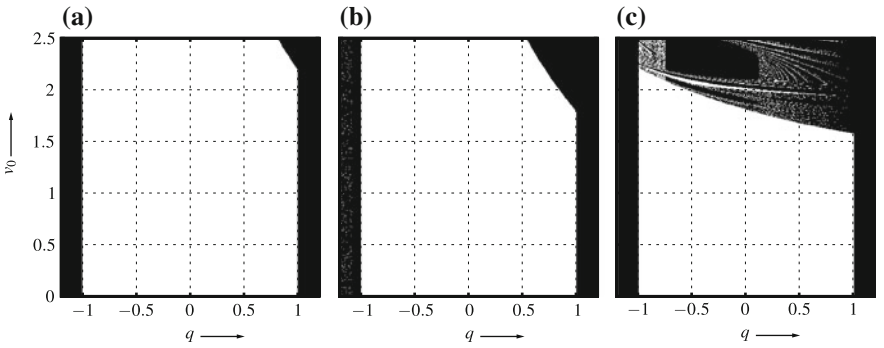

Fig. 6.9 Basins of attraction resulting from a control experiment. (*White* stabilizable regions and *black* unstabilizable regions.) The *horizontal* and *vertical axes* are the parameter q of the controller and the initial state of the system, respectively

UPO_1 and the UPO_2 are stabilized robustly. The threshold control performs well for this simple chaotic system.

6.3.2 Circuit Implementation

Owing to the sample holder synchronized with a clock pulse, our controller is very easy to implement, thus we show the circuit implementation and experimental results.

Figure 6.10 shows the circuit diagram of the system and the controller. The subtractor and the inverter 1 generate $u(t)$, and the adder and the inverter 2 add the control input to the switching threshold. The switching threshold generated by this controller is applied to the system as a perturbation of the reference value E_r.

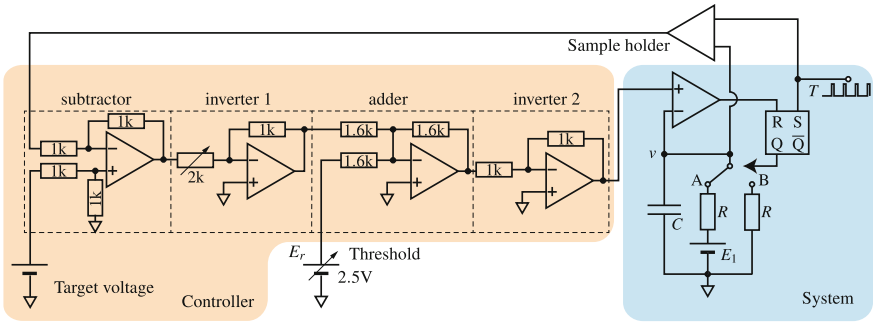

Fig. 6.10 Circuit diagram of a simple chaotic system and the proposed controller. The controller is composed of four parts. The variable resistance defines the controlling gain, and the voltage source is the target voltage v^*

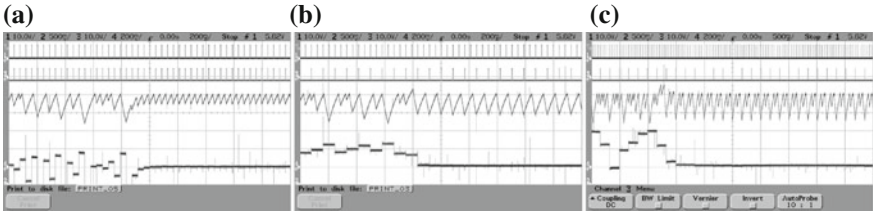

Fig. 6.11 Results of the laboratory experiments. **a** UPO_1, **b** UPO_2, and **c** UPO_4. (*For each shot*: *Top row* the clock pulse input, *2nd row* the timing of the renewal of the controlling signal, *3rd row* the voltage of the capacitor [10V/DIV], and the *bottom* the control input voltage [200mV/DIV]. The *horizontal axis* time [(**a**, **b**) 200 and (**c**) 500 ms/DIV].) The controlling started at 800 ms. The circuit is quickly converged to each periodic orbit after the control transition

We use ICs TC4053BP and LM325M as the logic switch and the comparator in this experiment.

Figure 6.11 shows a transition response of the circuit experiment. In these figures, the top, 2nd, 3rd and bottom time series show the clock pulse input, the timing of the renewal of the control signal, the voltage of the capacitor as the orbit v and the control signal, respectively. It is confirmed that control inputs converged to zero, and orbits are certainly stabilized at UPOs.

6.4 Izhikevich Model

Let us consider the Izhikevich model [25] as the second example. As is well known that this model is two dimensional, and behaves chaotically in certain parameter setting [26]. The equations are given as follows:

$$\dot{z}(t) = \begin{pmatrix} 0.04v + 5v + 140 - w + I \\ a(bv - w) \end{pmatrix},$$

$$\text{if} \quad v = \theta, \quad \text{then} \quad v \leftarrow c, \quad w \leftarrow w + d,$$

where $z = (v,\ w)$ is the state, and I, a, b, c, d and θ are parameters. Especially, c and d show the jumping dynamics, and θ defines the threshold value of the jumping. Figure 6.12 illustrates the dynamical behavior.

A chaotic attractor and three UPOs that are involved in it with parameters $a = 0.2$, $b = 2$, $c = -56$, $d = -16$, $I = -99$ and $\theta = 30$ are shown in Fig. 6.13. Table 6.2 lists the periods, states and multipliers of several UPOs. Each orbit is confirmed to be a UPO.

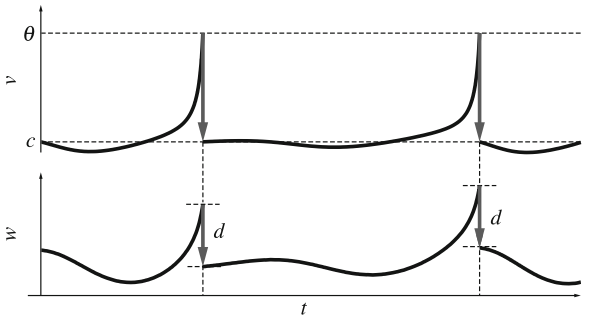

Fig. 6.12 The sketch of the typical behavior of the Izhikevich model. If the state $z(t)$ reaches the threshold value θ, the state $z(t) = (\theta,\ w(t))$ jumps to $z(t) = (c,\ w(t) + d)$

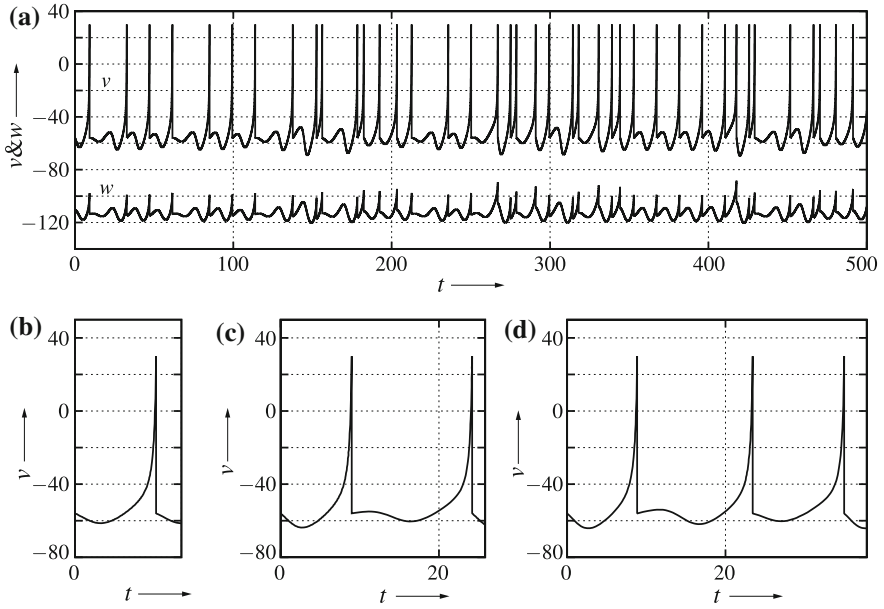

Fig. 6.13 Phase portraits of a chaotic attractor and UPOs by the numerical simulation, where $a = 0.2$, $b = 2$, $c = -56$, $d = -16$, $I = -99$, and $\theta = 30$. These UPOs are embedded in the chaotic attractor

6.4.1 Controller

The stabilizing control is applied to UPOs in Table 6.2. The Poincaré section is defined as: $\Pi = \left\{z \in \mathbb{R}^2 |\, q(z) = v - \theta = 0\right\}$.

Table 6.2 Periods, states, and multipliers of UPOs in Fig. 6.13

Attractor	Period	w^* ($v^* = c = 56$)	μ
UPO_1	1	−111.734371227672	−2.192843924301
UPO_2	2	−114.280257572631	−9.910331534347
		−109.950121533113	
UPO_3	3	−114.603487249294	+25.322864600880
		−112.427919143969	
		−109.602553091223	

From (6.8) and (6.9), the control gain is computed as follows:

$$K = \frac{q - D_{w^*}}{D_\theta},$$

where $D_{w^*} = \partial T/\partial w^*$ and $D_\theta = \partial T/\partial \theta$. The derivatives of the Poincaré map are obtained by (6.3) and (6.4). Now q is a desirable pole for the controller, and $|q| < 1$ is required for stabilization. The control input $u(k)$ is generated by the gain $K \in \mathbb{R}$ and the state $z(t)$ as $K(w^* - w(\tau))$ from (6.7). It is renewed after the jumping dynamics, and added to the threshold value θ as a perturbation. Since θ is only referred as the threshold value of the jumping dynamics, $u(k)$ does not affect the dynamical equations during the transition state.

6.4.2 Numerical Simulation

We show some results of the chaos control in Fig. 6.14, where each diagram shows a transition response of the orbit and the threshold value with the controlling signal. From these figures, we confirmed that each UPO has been controlled to become a stable periodic orbit by several renewals of $u(t)$. To prevent generating big amplitude of the control, a limiter is provided in the controller. The condition is given as follows:

$$\text{if} \quad |u(t)| \geq 20 \quad \text{then} \quad u(t) \leftarrow 0.$$

Figure 6.15 shows the basins of attraction of UPOs with our controller in the q-$w(0)$ plane. White regions in Fig. 6.15 indicate the initial values in which the UPO can be stabilized, and black regions indicate failure of the controlling.

Figure 6.13 reveals that the chaotic attractor wanders within $-125 < w < -100$ on the Poincaré section. The basin of attraction in this range is shown by the white regions in Fig. 6.15. Thus UPOs are stabilized robustly, and the threshold control for the piecewise nonlinear system performs well.

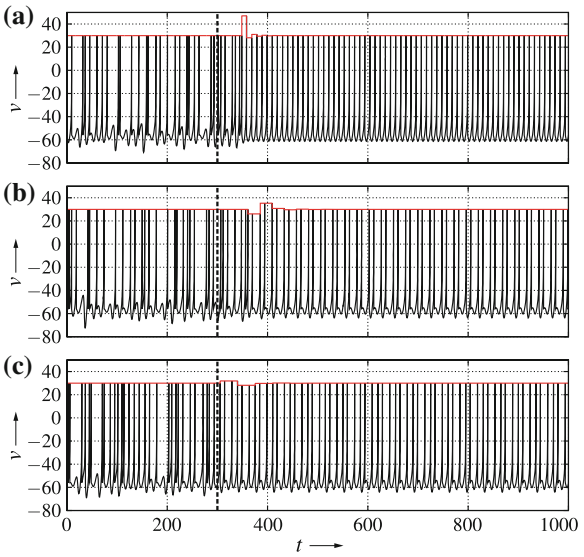

Fig. 6.14 Transition responses of controlled UPOs and the threshold values. **a** Period-1, **b** period-2 and **c** period-3 solutions shown in Table 6.2 are stabilized, and the final threshold value is 30 [mV]. Note that $u(t)$ is not applied to the system as a continuous input, but only updates the threshold value

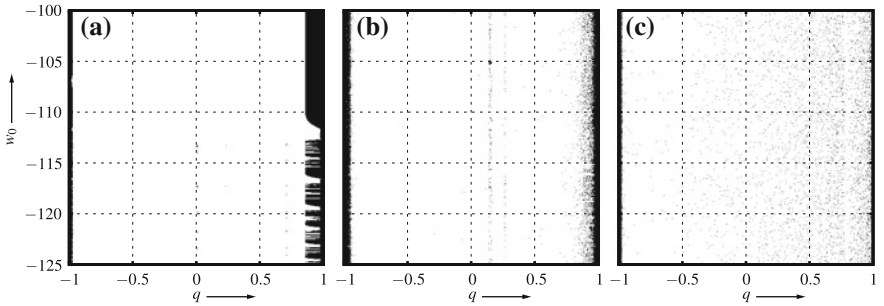

Fig. 6.15 Basins of attraction resulting from a control experiment. (*White* stabilizable regions and *black* unstabilizable regions.) The *horizontal* and *vertical axes* are the parameter q of the controller and the initial state of the system, respectively

6.5 Conclusion

We have proposed a control method for UPOs embedded in hybrid chaotic systems by variable threshold values. First, we have explained how to design the controlling gain of assigning poles with the perturbation of a switching threshold value. The pole assignment method requires the derivatives of the Poincaré map about threshold values, for which we have proposed the technique to calculate. We have also

demonstrated the design of a controller and numerical simulations of the controlling for a 1D switching chaotic system and a 2D chaotic neuron model. Some simulation results indicate that our controller stabilizes target UPOs well. Additionally, we have implemented our controller in a real circuit and presented experimental results. From them, it is confirmed that our controller can be implemented in a real circuit, and also well performed without technical difficulties.

For modeling biological and medical systems, the hybrid dynamical systems are widely used [27]. For example, Akakura et al. [28] reported that the intermittent hormone therapy could be effective in the hormone treatment of prostate cancer. This therapy switches the treatment on and off based on the observation of the serum prostate-specific antigen (PSA) level. Therefore, the therapy can be represented as a hybrid dynamical system, and some PSA levels are defined as the switching threshold values. The mathematical modeling of the intermittent hormone therapy has been investigated intensively [29]. Since our method is available for general piecewise nonlinear systems and the threshold perturbation seems to be related to the intermittent hormone therapy, it is worth investigating a possibility whether our method is applicable for the prostate cancer treatment or not.

Acknowledgments The authors wish to thank International Journal of Bifurcation and Chaos, World Scientific Publishing for granting permission to present here a modified version of the material published in "Controlling chaos of hybrid systems by variable threshold values," D. Ito, T. Ueta, T. Kousaka, J. Imura, and K. Aihara, International Journal of Bifurcation and Chaos, Vol. 24, No. 10, http://www.worldscientific.com/doi/abs/10.1142/S0218127414501259 ©2014 World Scientific Publishing Company [30].

References

1. Auerbach, D., Cvitanović, P., Eckmann, J.-P., Gunaratne, G.: Exploring chaotic motion through periodic orbits. Phys. Rev. Lett. **23**, 2387–2389 (1987)
2. Ott, E., Grebogi, C., Yorke, J.A.: Controlling chaos. Phys. Rev. Lett. **64**, 1196–1999 (1990)
3. Romeiras, F.J., Grebogi, C., Ott, E., Dayawansa, W.P.: Controlling chaotic dynamical systems. Physica D **58**(1–4), 165–192 (1992)
4. Kousaka, T., Ueta, T., Kawakami, H.: Controlling chaos in a state-dependent nonlinear system. Int. J. Bifurcat. Chaos **12**(5), 1111–1119 (2002)
5. Ueta, T., Kawakami, H.: Composite dynamical system for controlling chaos. IEICE Trans. Fundam **E78-A**(6), 708–714 (1995)
6. Kousaka, T., Ueta, T., Ma, Y., Kawakami, H.: Control of chaos in a piecewise smooth nonlinear system. Chaos, Solitons Fractals **27**(4), 1019–1025 (2006)
7. Pyragas, K.: Delayed feedback control of chaos. Phil. Trans. R. Soc. A **15**, **364**(1846), 2309–2334 (2006)
8. Perc, M., Marhl, M.: Detecting and controlling unstable periodic orbits that are not part of a chaotic attractor. Phys. Rev. E **70**, 016204 (2004)
9. Perc, M., Marhl, M.: Chaos in temporarily destabilized regular systems with the slow passage effect. Chaos, Solitons Fractals **7**(2), 395–403 (2006)
10. Pyragas, K.: Continuous control of chaos by self-controlling feedback. Phys. Lett. A **70**(6), 421–428 (1992)
11. Myneni, K., Barr, T.A., Corron, N.J., Pethel, S.D.: New method for the control of fast chaotic oscillations. Phys. Rev. Lett. **83**, 2175–2178 (1999)

12. Rajasekar, S., Lakshmanan, M.: Algorithms for controlling chaotic motion: application for the BVP oscillator. Physica D **67**(1–3), 282–300 (1993)
13. Roy, R., Murphy, T.W., Maier, T.D., Gills, Z., Hunt, E.R.: Dynamical control of a chaotic laser: Experimental stabilization of a globally coupled system. Phys. Rev. Lett. **68**, 1259–1262 (1992)
14. Sabuco, J., Zambrano, S., Sanjuán, M.A.F.: Partial control of chaotic transients using escape times. New J. Phys. **12**, 113038 (2010)
15. Starrett, J.: Control of chaos by occasional bang-bang. Phys. Rev. E **67**, 036203 (2003)
16. Zambrano, S., Sanjuán, M.A.F.: Exploring partial control of chaotic systems. Phys. Rev. E **79**, 026217 (2009)
17. Leine, R., Nijmeijer, H.: Dynamics and Bifurcations of Non-smooth Mechanical Systems. Springer, Berlin (2004)
18. Bernardo, M., Budd, C.J., Champneys, A.R., Kowalczyk., P.: Piecewise-Smooth Dynamical Systems: Theory and Applications. Springer, London (2008)
19. Inagaki, T., Saito, T.: Consistency in a chaotic spiking oscillator. IEICE Trans. Fundam. **E91-A**(8), 2040–2043 (2008)
20. Ito, D., Ueta, T., Aihara, K.: Bifurcation analysis of two coupled Izhikevich oscillators. Proc. IEICE/NOLTA2010, 627–630 (2010)
21. Kousaka, T., Ueta, T., Kawakami, H.: Bifurcation of switched nonlinear dynamical systems. IEEE Trans. Circ. Syst. **CAS-46**(7), 878–885 (1999)
22. Murali, K., Sinha, S.: Experimental realization of chaos control by thresholding. Phys. Rev. E **68**, 016210 (2003)
23. Kousaka, T., Tahara, S., Ueta, T., Abe, M., Kawakami, H.: Chaos in simple hybrid system and its control. Electron. Lett. **37**(1), 1–2 (2001)
24. Kousaka, T., Kido, T., Ueta, T., Kawakami, H., Abe, M.: Analysis of border-collision bifurcation in a simple circuit. Proc. IEEE/ISCAS **2**, 481–484 (2000)
25. Izhikevich, E.M.: Simple model of spiking neurons. IEEE Trans. Neural Netw. **14**(6), 1569–1572 (2003)
26. Tamura, A., Ueta, T., Tsuji, S.: Bifurcation analysis of Izhikevich neuron model. Dyn. Continuous, Discrete Impulsive Syst. **16**(6), 849–862 (2009)
27. Aihara, K., Suzuki, H.: (2010) Theory of hybrid dynamical systems and its applications to biological and medical systems. Phil. Trans. R. Soc. A. **13**(368), 4893–4914 (1930)
28. Akakura, K., Bruchovsky, N., Goldenberg, S.L., Rennie, P.S., Buckley, A.R., Sullivan, L.D.: Effects of intermittent androgen suppression on androgen-dependent tumors. Apoptosis and serum prostate-specific antigen. Cancer **71**, 2782–2790 (1993)
29. Tanaka, G., Hirata, Y., Goldenberg, S.L., Bruchovsky, N., Aihara, K.: Mathematical modelling of prostate cancer growth and its application to hormone therapy. Phil. Trans. R. Soc. A. **13**, **368**(1930), 5029–5044 (2010)
30. Ito, D., Ueta, T., Kousaka, T., Imura, J., Aihara, K.: Controlling chaos of hybrid systems by variable threshold values. Int. J. Bifurcat. Chaos **24**(10), 1450125 (2014) (12 pages)

Part II
Dynamic Attractor and Control

Chapter 7
Chaotic Behavior of Orthogonally Projective Triangle Folding Map

Jun Nishimura and Tomohisa Hayakawa

7.1 Introduction

Chaotic behavior embedded in dynamical systems has been attracting huge attention in the field of nonlinear dynamical systems theory since 1960s. Wide variety of results have also been reported concerning chaotic systems in many areas such as fundamental field of physics and biology as well.

One of the major objectives of investigating chaos is to elucidate the mechanism of generating chaotic behavior. A mathematical approach to address analysis problems of chaotic systems is to observe simple nonlinear dynamics and find key factors that give rise to chaos. The simplicity of the nonlinear models to consider is central in obtaining better understanding of complicated behaviors. Notable examples of such relatively simple dynamic models are the logistic map, the tent map, the Horseshoe map [12, 13], to cite but a few (see also [1–5, 7–9, 11] and the references therein).

In our earlier paper [6], we considered a *simple* folding map for equilateral triangles (which we call the *triangle folding map*) that has sensitivity with respect to the initial conditions. The operation is shown in Fig. 7.1 and defined by the the following procedure:

[1] Fold along NL and bring A to M.
[2] Fold along LM and bring B to N.
[3] Fold along MN and bring C to L.
[4] Rotate LMN around its center by π radian.
[5] Enlarge LMN by double so that MNL coincides with ABC.

Specifically, we provided fixed point analysis and periodic point analysis associated with this mapping operation by sequentially partitioning a restricted domain. Furthermore, we discussed some connections of the folding map to the Sierpinski gasket,

J. Nishimura · T. Hayakawa (✉)
Graduate School of Information Science and Engineering,
Tokyo Institute of Technology, 2-12-1 Oh-Okayama, Meguro-ku, Tokyo 152-8552, Japan
e-mail: hayakawa@mei.titech.ac.jp

K. Aihara et al. (eds.), *Analysis and Control of Complex Dynamical Systems*,
Mathematics for Industry 7, DOI 10.1007/978-4-431-55013-6_7

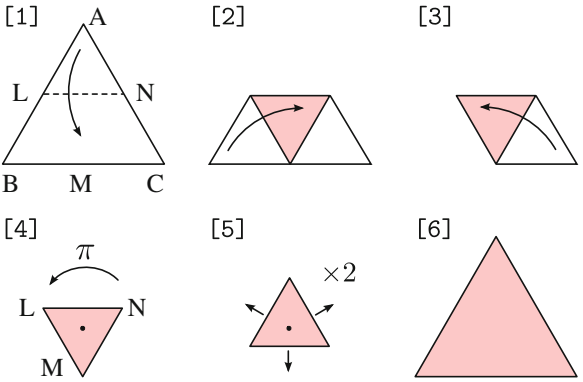

Fig. 7.1 Triangle folding map [6]. The map was defined as a surjective map

which is well known to be composed of self-homothetic triangles, and proposed a scheme to construct other interesting fractals by removing certain regions of the equilateral triangle.

In this article, we introduce a bifurcation parameter for the folding angle and generalize this triangle folding map so that the operation in [6] reduces to a special case of the new map. In particular, we call the operation the orthogonally projective triangle folding map and provide a similar analysis given in [6] in terms of the fixed points. We note that the preliminary results of this article can be found in [10].

7.2 Orthogonally Projective Triangle Folding Map

For the orthogonally projective triangle folding map, consider the equilateral triangle ABC given by [4] in Fig. 7.1. In order to introduce the bifurcation parameter in the folding operation, let θ be the folding angle in operation [2] and [3] in Fig. 7.1 and the sequence of operation is given by Fig. 7.2.

After the folding operation above, the resulting triangle in [5] becomes identical to the equilateral triangle in [1]. We denote this folding operation [1]–[5] by $F : \mathscr{T} \to \mathscr{T}$. For example, the point $\mathrm{P} \in \mathscr{T}$ shown in [1] of Fig. 7.3 is mapped by

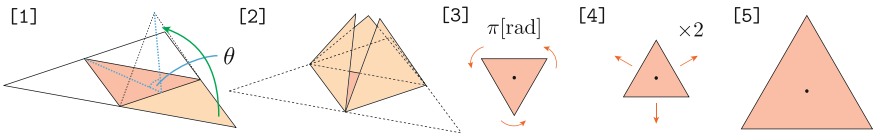

Fig. 7.2 Orthogonally projective triangle folding map. The triangle folding map in Fig. 7.1 is modified to introduce the bifurcation parameter θ. The case of $\theta = 0$ corresponding to the the triangle folding map defined in Fig. 7.1

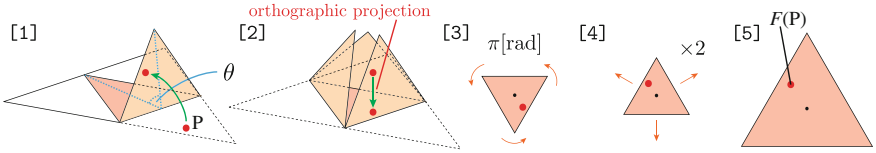

Fig. 7.3 Visualization of the mapping scheme for a given point in $\mathscr{T}$. This map will be redefined from the map from $\mathscr{D}$ to $\mathscr{D}$ as in Definition 7.1

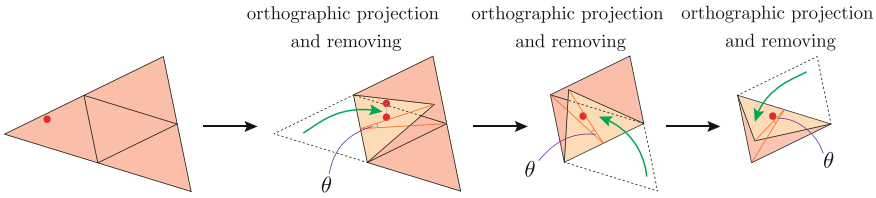

Fig. 7.4 Mapping with small θ

the function F to another point $F(\mathrm{P})$ in [5]. For the case where the folding angle θ is small, i.e., $\cos^{-1}\frac{1}{3} < \theta < \frac{\pi}{2}$, the operation is shown in Fig. 7.4. Note that the operation given by Fig. 7.1 corresponds to the case of $\theta = 0$. It is immediate that the map F is surjective as discussed below.

Now, it is important to note that there are several variations of prescribing the operation from [3] to [4] in Fig. 7.2 in order to define the surjective map from $\mathscr{T}$ to $\mathscr{T}$. For example, by rotating the triangle by $\frac{\pi}{6}$ radian, instead of π radian, counterclockwise (or clockwise), we can obtain a similar map to the original map $\mathscr{T}$. Or, more easily, the triangle in [3] can be flipped upside down to arrive at [4] through which we can construct a surjective map from $\mathscr{T}$ to $\mathscr{T}$. This commonality is due to the reflective and the rotational symmetry that the equilateral triangles possess and it is preferable to characterize the map that describes the essential dynamics of the folding operation. The following notion precludes the ambiguity of the operation F.

Definition 7.1 (*Equivalence relation on* $\mathscr{T}$) Consider the map $F : \mathscr{T} \to \mathscr{T}$ defined by Fig. 7.2. Two points P, Q $\in \mathscr{T}$ are considered to be equivalent if P is transformed to Q via rotation by $2\pi/3$ or $4\pi/3$ radians, or reflection with respect to the symmetric axis of the equilateral triangle, or the combination of the rotation and the reflection. Specifically, we denote by

$$\mathrm{equiv}\,\mathscr{X} \triangleq \{t \in \mathscr{T} : t \text{ has the equivalence relation with a point in } \mathscr{X}\}, \quad (7.1)$$

the equivalence set associated with the set $\mathscr{X} \subset \mathscr{T}$.

Note that the center of the equilateral triangle has its equivalence relation with itself, and any point on the symmetric axis (except for the center) has 2 other points (on the other symmetric axes) that have equivalence relation with it. Otherwise, a point on $\mathscr{T}$ has 5 other points that have equivalence relation to each other (see

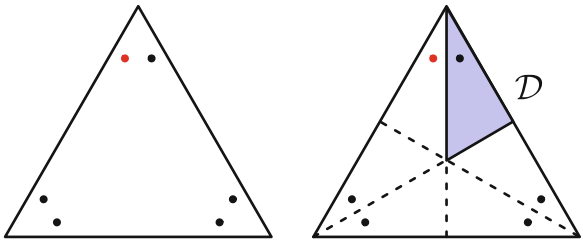

Fig. 7.5 Equivalence relation for the triangle folding map. The 6 points in the *left triangle* is identified as the same point and hence the *top left point* (*marked in red*) in the *left figure* is considered as the point in $\mathscr{D}$ in the *right figure*

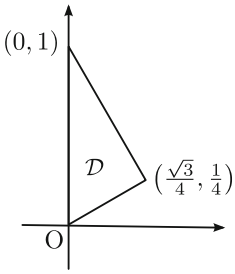

Fig. 7.6 Domain $\mathscr{D}$ in the coordinate system

Fig. 7.5, left). In any case, it is important to note that any point $\mathrm{P} \in \mathscr{T}$ has a *unique* point in $\mathscr{D}$ that has the equivalence relation with P, where the closed subset $\mathscr{D} \subset \mathscr{T}$ is given by partitioning $\mathscr{T}$ with the three symmetric axes (Fig. 7.5, right). Note that the 6 partitioned sets are right triangles and are all identical to each other in the shape and the size so that the choice of the partitioned set is not important.

Now, from the analysis above, we restrict the domain and the codomain into $\mathscr{D}$, instead of the original equilateral triangle $\mathscr{T}$, and define a new map $f : \mathscr{D} \to \mathscr{D}$ associated with the folding map F under the equivalence relation given by Definition 7.1. Note that for a point $\mathrm{R} \in \mathscr{D}$, $f(\mathrm{R}) \in \mathscr{D}$ has the equivalence relation with $F(\mathrm{R}) \in \mathscr{T}$.

In order to describe the map f more clearly, we define the x-y coordinate system to the triangle. Specifically, let the length of the edges of $\mathscr{T}$ be $2\sqrt{3}$ and, as shown in Fig. 7.6, let the center of the equilateral triangle be placed at the origin, and let the bottom edge be parallel to the x-axis. In this case, the map f is described by a piecewise affine function given in Definition 7.2 below.

For the statement of the following results, let the domain $\mathscr{D}$ be further partitioned into the 4 closed subdomains $\mathscr{D}_i$, $i = 0, 1, 2, 3$, for the case of $0 \le \theta < \cos^{-1}\frac{1}{3}$ as given by Fig. 7.7 (left) and the 2 closed subdomains $\mathscr{D}_i$, $i = 2, 3$, for the case of $\cos^{-1}\dfrac{1}{3} < \theta < \dfrac{\pi}{2}$ as given by Fig. 7.7 (right).

Definition 7.2 (*Orthogonally projective triangle folding map*) For the point $p = [x, y]^{\mathrm{T}}$ in the closed domain $\mathscr{D} \subset \mathbb{R}^2$, the folding map $f^\theta : \mathscr{D} \to \mathscr{D}$ for the equilateral triangle is given by

$$f^\theta(p) \triangleq f_i^\theta(p), \quad p \in \mathscr{D}_i^\theta, \quad i = 0, 1, 2, 3, \tag{7.2}$$

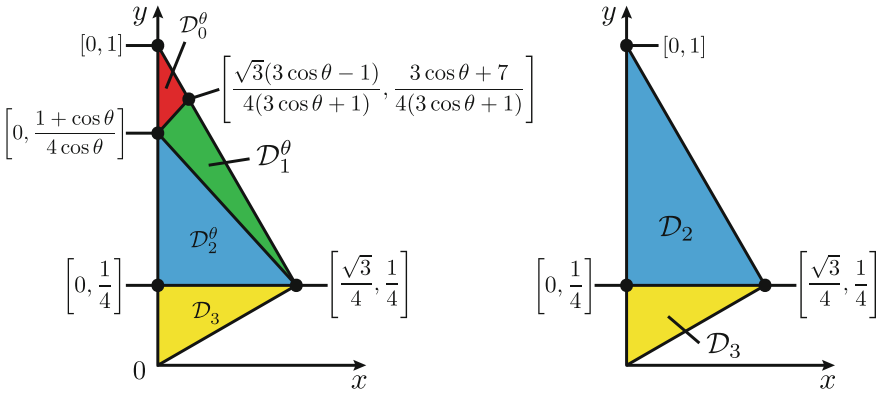

Fig. 7.7 Partitioned domains of $\mathscr{D}$ with respect to θ; (*left*) $0 \le \theta < \cos^{-1}\frac{1}{3}$; (*right*) $\cos^{-1}\frac{1}{3} < \theta < \frac{\pi}{2}$. When $\theta \searrow \cos^{-1}\frac{1}{3}$, the domains $\mathscr{D}_0^\theta$ and $\mathscr{D}_1^\theta$ in the *left figure* degenerate

where

$$f_0^\theta(p) \triangleq \begin{bmatrix} 2 & 0 \\ 0 & 2\cos\theta \end{bmatrix} p - \frac{1+\cos\theta}{4}\begin{bmatrix} 0 \\ 2 \end{bmatrix},$$

$$f_1^\theta(p) \triangleq \begin{bmatrix} 1 & \sqrt{3}\cos\theta \\ \sqrt{3} & -\cos\theta \end{bmatrix} p + \frac{1+\cos\theta}{4}\begin{bmatrix} -\sqrt{3} \\ 1 \end{bmatrix},$$

$$f_2^\theta(p) \triangleq \begin{bmatrix} -1 & -\sqrt{3}\cos\theta \\ \sqrt{3} & -\cos\theta \end{bmatrix} p + \frac{1+\cos\theta}{4}\begin{bmatrix} \sqrt{3} \\ 1 \end{bmatrix},$$

$$f_3^\theta(p) \triangleq \begin{bmatrix} -1 & \sqrt{3} \\ \sqrt{3} & 1 \end{bmatrix} p.$$

Since each subdomain $\mathscr{D}_i^\theta$ is defined as a closed set for all $i = 0, 1, 2, 3$, adjacent domains share the points on their boundaries. Note, however, that the map f^θ defined in Definition 7.2 has no ambiguity in that when $p \in (\mathscr{D}_i^\theta \cap \mathscr{D}_j^\theta)$ it follows that $f_i^\theta(p) = f_j^\theta(p)$ so that the point p on the intersection of the domains is mapped to the same point in $\mathscr{D}$.

Henceforth, for a subset $S \subset \mathscr{D}$, $f^\theta(S)$ denotes the set of points $f(p)$, $p \in \mathscr{D}$, which is also a subset of $\mathscr{D}$.

7.3 Tetrahedron Map

In this section, we consider the special case of the orthogonally projective triangle folding map. Specifically, consider the map f^θ for the case of $\theta = \cos^{-1}\frac{1}{3}$. This value is the critical value for the expression of the piecewise affine function and the folding in [2] of Fig. 7.3 is characterized by the tetrahedron as shown in Fig. 7.8. For this specialized map, we write $f^\triangle$ to denote $f^{\cos^{-1}\frac{1}{3}}$.

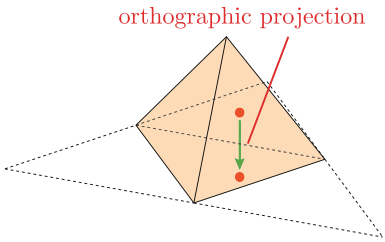

Fig. 7.8 Regular tetrahedron map (procedure [2] of Fig. 7.3). This is the special case of the orthogonal triangle folding map f^{θ} with $\theta = \cos^{-1}\frac{1}{3}$

Definition 7.3 (*Tetrahedron map*) For the point $p = [x, y]^{\mathrm{T}}$ in the closed domain $\mathscr{D} \subset \mathbb{R}^2$, the tetrahedron map $f^{\triangle} : \mathscr{D} \to \mathscr{D}$ for the equilateral triangle is given by

$$f^{\triangle}(p) \triangleq f_i^{\triangle}(p), \quad p \in \mathscr{D}_i, \quad i = 2, 3, \tag{7.3}$$

where

$$\begin{aligned} f_2^{\triangle}(p) &\triangleq A_2^{\triangle} p + b_2^{\triangle}, \\ f_3^{\triangle}(p) &\triangleq A_3^{\triangle} p, \\ A_2^{\triangle} &\triangleq \begin{bmatrix} -1 & \frac{-\sqrt{3}}{3} \\ \sqrt{3} & -\frac{1}{3} \end{bmatrix}, \quad b_2^{\triangle} \triangleq \frac{1}{3}\begin{bmatrix} \sqrt{3} \\ 1 \end{bmatrix}, \\ A_3^{\triangle} &\triangleq \begin{bmatrix} -1 & \sqrt{3} \\ \sqrt{3} & 1 \end{bmatrix}. \end{aligned}$$

7.3.1 Fixed Point and Periodic Point Analysis on the Boundary of $\mathscr{D}$

In this section, we restrict our attention on the boundary $\partial\mathscr{D}$ of the domain $\mathscr{D}$ and provide analysis in regards to the fixed points and the periodic points. Specifically, note that the folding map f maps every point on $\partial\mathscr{D}$ onto $\partial\mathscr{D}$. In other words, the set $\partial\mathscr{D}$ is a positively invariant set with respect to f.

For the analysis presented in this section, we define the map $f_{\partial}^{\triangle} : \partial\mathscr{D} \to \partial\mathscr{D}$ as

$$f_{\partial}^{\triangle}(p) = f_i^{\triangle}(p), \quad p \in (\mathscr{D}_i \cap \partial\mathscr{D}), \quad i = 2, 3, \tag{7.4}$$

where $f_i^{\triangle}(\cdot)$, $i = 2, 3$, are given by (7.4). Furthermore, for the statement of the following result, let the points A, B, C, D be placed on the boundary of $\mathscr{D}$ as shown in Fig. 7.9.

Theorem 7.1 *Consider the tetrahedron map $f_{\partial}^{\triangle}$ given by (7.4). For $\partial\mathscr{D}$, let* A, B, C, D *denote the points shown in* Fig. 7.9. *Then the map $f_{\partial}^{\triangle} : \partial\mathscr{D} \to \partial\mathscr{D}$ satisfies the following properties:*

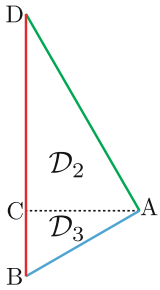

Fig. 7.9 Definition of the points A, B, C, D on the boundary of $\mathscr{D}$

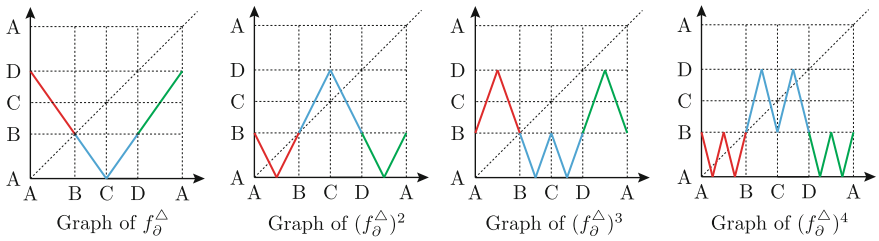

Fig. 7.10 The mapping relation of the points on the boundary of $\mathscr{D}$ for the maps $f_\partial^\triangle$, $(f_\partial^\triangle)^2$, $(f_\partial^\triangle)^3$, and $(f_\partial^\triangle)^4$. The point B can be seen as a fixed point for the map $(f_\partial^\triangle)^k$, $k \in \mathbb{N}$

1. *For k even, the k-times composite map* $(f_\partial^\triangle)^k$ *has* $2^{k/2}$ *fixed points on the edge A-B.*
2. *For k even, the k-times composite map* $(f_\partial^\triangle)^k$ *has* $2^{k/2}$ *fixed points on the edge B-D.*
3. *For k even, the k-times composite map* $(f_\partial^\triangle)^k$ *has* $2^{k/2+1} - 1$ *fixed points on* $\partial\mathscr{D}$.
4. *For k odd, the k-times composite map* $(f_\partial^\triangle)^k$ *has a unique fixed point on* $\partial\mathscr{D}$*, which is the vertex B.*

Proof The results can be shown from the relationship given in Fig. 7.10 where f_∂ is surjective from $\partial\mathscr{D}$ to $\partial\mathscr{D}$. □

7.4 Extended Fixed Point and Periodic Point Analysis for Tetrahedron Map

7.4.1 Geometric Interpretation of the Triangle Folding Map

In this section, we provide characterization of the fixed and the periodic points of the tetrahedron map $f^\triangle$ over the domain $\mathscr{D}$ and compute the Lyapunov exponent of the map. In the following, we give mathematical representation of the partitioned domains and characterize the relationship between the partitioned domains and the map $f^\triangle$.

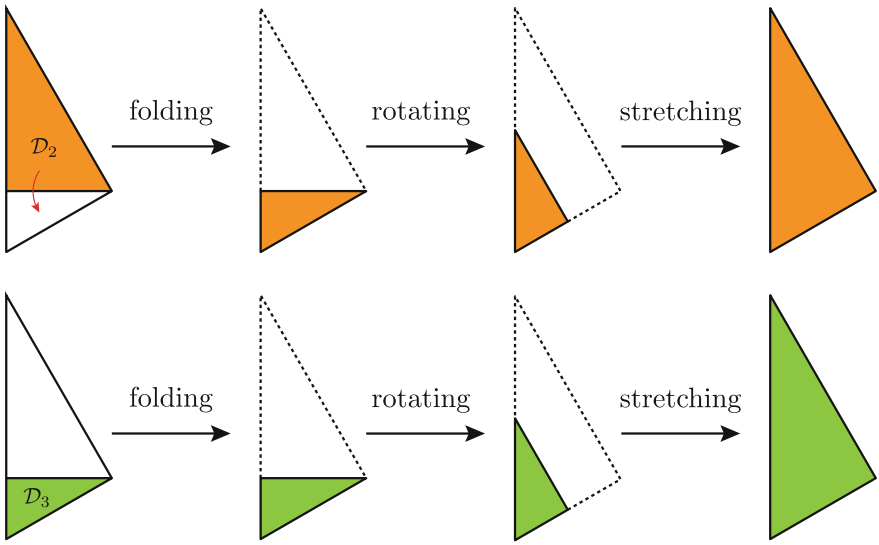

Fig. 7.11 Transition of $\mathscr{D}_2$ and $\mathscr{D}_3$. For both of the domains, they are mapped to the domain $\mathscr{D}$

Definition 7.4 (*Sequentially partitioned set by a sequence*) For a given $k \in \mathbb{N}$, consider the collection of finite sequences $\mathscr{S}_k$ given by

$$\mathscr{S}_k \triangleq \left\{ s = \{s_i\}_{i=0}^{k-1} : s_i \in \{2, 3\},\ i = 0, 1, \ldots, k-1 \right\}. \tag{7.5}$$

Then the subset $\mathscr{D}_s$, where $s = \{s_0, s_1, \ldots, s_{k-1}\} \in \mathscr{S}_k$, is defined as

$$\mathscr{D}_s \triangleq \{p \in \mathscr{D}_{s_0} : f^{\triangle}(p) \in \mathscr{D}_{s_1}, (f^{\triangle})^2(p) \in \mathscr{D}_{s_2}, \ldots, (f^{\triangle})^{k-1}(p) \in \mathscr{D}_{s_{k-1}}\}. \tag{7.6}$$

For simplicity of exposition, we write $\mathscr{D}_{ij\ldots k}$ to denote $\mathscr{D}_{\{i,j,\ldots,k\}}$.

Consider the partitioned domains for the map $(f^{\triangle})^2$. Note that $f^{\triangle}$ maps $\mathscr{D}_2$ and $\mathscr{D}_3$ to $\mathscr{D}$ (see Fig. 7.11).

In other words, by taking the inverse map in Fig. 7.11, we can characterize the partitioned domains for the map $(f^{\triangle})^2$, which are shown in Fig. 7.12.
In a similar manner, it is possible to characterize the partitioned domains for the map $(f^{\triangle})^k$ by applying the similar procedure `[1]` in Fig. 7.12 to the partitioned domains for the map $(f^{\triangle})^{k-1}$. As an example, the partitioned domains for the map $(f^{\triangle})^3$ is shown in Fig. 7.13.

In summary, the partitioned domains for $f^{\triangle}$, $(f^{\triangle})^2$, $(f^{\triangle})^3$, $(f^{\triangle})^4$ are shown in Fig. 7.14.

Remark 7.1 According to this definition, the notation $\mathscr{D}_i$ used in the previous sections stands for $\mathscr{D}_{\{i\}}$.

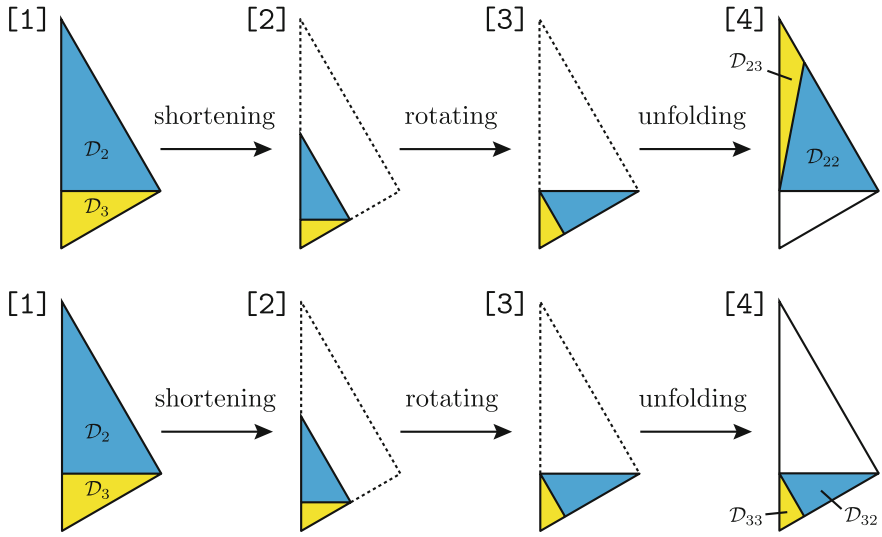

Fig. 7.12 Domain of $(f^{\triangle})^2$, which are twice inverse maps of the domain $\mathscr{D}$. There are two cases to be mapped to the domain $\mathscr{D}_2$ (*above*) and $\mathscr{D}_3$ (*below*)

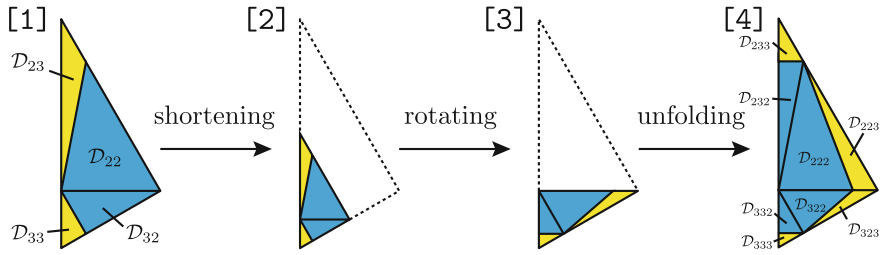

Fig. 7.13 Domain of $(f^{\triangle})^3$. The domains $\mathscr{D}_{223}, \mathscr{D}_{233}, \mathscr{D}_{323}, \mathscr{D}_{333}$ in [4] are mapped to the domains $\mathscr{D}_{23}$ and $\mathscr{D}_{33}$ in [1] by $f^{\triangle}$

Definition 7.5 Let $k, l \in \mathbb{Z}^+$ and let $u = \{u_0, u_1, \ldots, u_{k-1}\} \in \mathscr{S}_k$ and $v = \{v_0, v_1, \ldots, v_{l-1}\} \in \mathscr{S}_l$. Then the operation $\oplus : \mathscr{S}_k \times \mathscr{S}_l \to \mathscr{S}_{k+l}$ is defined as

$$u \oplus v \triangleq \{u_0, u_1, \ldots, u_{k-1}, v_0, v_1, \ldots, v_{l-1}\}. \tag{7.7}$$

Theorem 7.2 *For any $s \in \mathscr{S}_k$, $k \in \mathbb{Z}^+$, it follows that*

$$\Pi_2(\mathscr{D}_s) = \mathscr{D}_{s\oplus\{2\}}, \tag{7.8}$$
$$\Pi_3(\mathscr{D}_s) = \mathscr{D}_{s\oplus\{3\}}. \tag{7.9}$$

Next, we define a left shift operation for the sequence s.

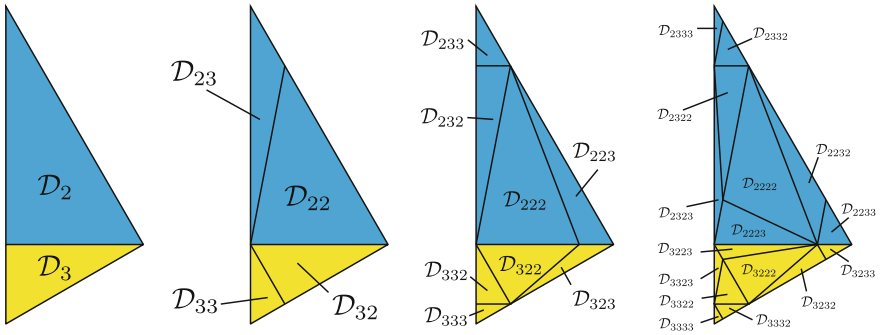

Fig. 7.14 Domains of $\mathscr{D}_{s_0,\ldots,s_k}$ for $k = 1, 2, 3, 4$

Definition 7.6 (*Left shift operation of sequences*) For a given $k \in \mathbb{N}$ and the finite sequence $s = \{s_0, s_1, \ldots, s_{k-1}\} \in \mathscr{S}$, let $i \in \mathbb{N}$ be $i < k$. The left shift operation for s is defined as the binary operation $\ll : \mathscr{S} \times \mathbb{N} \to \mathscr{S}$ given by

$$s \ll i \triangleq \{s_i, s_{i+1}, \ldots, s_{k-1}\}. \tag{7.10}$$

This definition makes it possible to simply represent the tetrahedron map for the equilateral triangle.

Theorem 7.3 *For a given $k \in \mathbb{N}$ and the finite sequence $s = \{s_0, s_1, \ldots, s_{k-1}\} \in \mathscr{S}$, let $i \in \mathbb{N}$ be $i < k$. Then it follows that*

1. $(f^{\triangle})^i (D_s) = D_{s \ll i}$,
2. $(f^{\triangle})^i (p) \in \mathscr{D}_{s \ll i}$, $p \in \mathscr{D}_s$.

Proof We show the case of $i = 1$ in (i) because the result of (i) can be shown by applying the case of $i = 1$ and the result of (ii) is immediate from (i).

Note from Definition 7.4 that

$$\begin{aligned} f(\mathscr{D}_s) &= f^{\triangle} \circ \Pi_{s_{n-1}} \circ \cdots \circ \Pi_{s_1} \circ \Pi_{s_0}(\mathscr{D}) \\ &= f^{\triangle} \circ \Pi_{s_{n-1}} \circ \cdots \circ \Pi_{s_1}(\mathscr{D}_{s_0}) \\ &= \Pi_{s_{n-1}} \circ \cdots \circ \Pi_{s_1} \circ f^{\triangle}(\mathscr{D}_{s_0}). \end{aligned}$$

Note that $f^{\triangle}(\mathscr{D}_{s_0}) = \mathscr{D}$ for every $s_0 \in \{2, 3\}$. Hence, it follows that

$$f^{\triangle}(\mathscr{D}_s) = \Pi_{s_{n-1}} \circ \cdots \circ \Pi_{s_1}(\mathscr{D}) = \mathscr{D}_{s \ll 1},$$

which completes the proof. □

The result (i) in Theorem 7.3 indicates the fact that applying the tetrahedron map f is equivalent to shifting left the subscript s of $\mathscr{D}_s$ by 1, while (ii) suggests that the mapped point $(f^{\triangle})^k(p)$ of $p \in \mathscr{D}$ by $(f^{\triangle})^k$ may be estimated.

Theorem 7.4 (Grey code property) *Let $k \in \mathbb{Z}^+$. For the partitioned domains $\mathscr{D}_s$ and $\mathscr{D}_{s'}$ for the map $(f^{\triangle})^k$ with $s' = \{s'_0, s'_1, \ldots, s'_{k-1}\} \in \mathscr{S}_k$, there exists $0 \leq \alpha \leq k-1$ such that*

$$s_\alpha \neq s'_\alpha, \tag{7.11}$$

$$s_i = s'_i, \quad i \neq \alpha, \quad 0 \leq i \leq k-1. \tag{7.12}$$

Proof The result is proven by invoking induction. □

7.4.2 Periodic Points of the Tetrahedron Map

The main result of this section is shown in Theorems 7.5 and 7.6 below. Before stating the result, we need to provide several preliminary lemmas.

Lemma 7.1 *Let $g^{\triangle}$ denote $(f^{\triangle})^k$. Then, for any $s \in \mathscr{S}_k$, $k \in \mathbb{Z}^+$, the map $g^{\triangle}_{\mathrm{dom}(\mathscr{D}_s)}$ is bijective.*

Lemma 7.2 *Let $l \in \mathbb{Z}$ and $k \in \mathbb{Z}^+$ be such that k is even and $0 \leq l \leq k$, and let $s = \{s_0, s_1, \ldots, s_{k-1}\} \in \mathscr{S}_k$. Then it follows that*

$$A^{\triangle}_{s_{k-1}} A^{\triangle}_{s_{k-2}} \cdots A^{\triangle}_{s_0} = 2^k \begin{bmatrix} 1 & 0 \\ 0 & (-1/3)^l \end{bmatrix}. \tag{7.13}$$

Theorem 7.5 *The k-times tetrahedron map $(f^{\triangle})^k : \mathscr{D} \to \mathscr{D}$ has a unique fixed point on $\mathscr{D}_s$, $s \in \mathscr{S}_k$, $k \in \mathbb{Z}^+$.*

Proof The fixed point of the map $(f^{\triangle})^k$ on $\mathscr{D}_s$ can be obtained by solving the equation $g^{\triangle} = (f^{\triangle})^k(p) = p$ or, equivalently,

$$A^{\triangle}_{s_{k-1}} A^{\triangle}_{s_{k-2}} \cdots A^{\triangle}_{s_0} p + C = p. \tag{7.14}$$

Now, since

$$\det\left(A^{\triangle}_{s_{k-1}} A^{\triangle}_{s_{k-2}} \cdots A^{\triangle}_{s_0} - I\right) \neq 0, \tag{7.15}$$

it follows that (7.14) has a unique solution p. □

Lemma 7.3 *Let p be the fixed point for $(f^{\triangle})^k$. Then there do not exist two distinct sequences α and β of length k such that $p \in \mathscr{D}_\alpha$ and $p \in \mathscr{D}_\beta$.*

Theorem 7.6 *The map $(f^{\triangle})^k$ possesses 2^k fixed points on $\mathscr{D}$.*

Proof It follows from Theorem 7.5 and Lemma 7.3 that $(f^{\triangle})^k$ possesses a fixed point on the boundary or the interior of $\mathscr{D}_s$. Note that these fixed points are not shared by 2 different domains. Hence, the number of fixed points is equal to the number of the partitioned domains. □

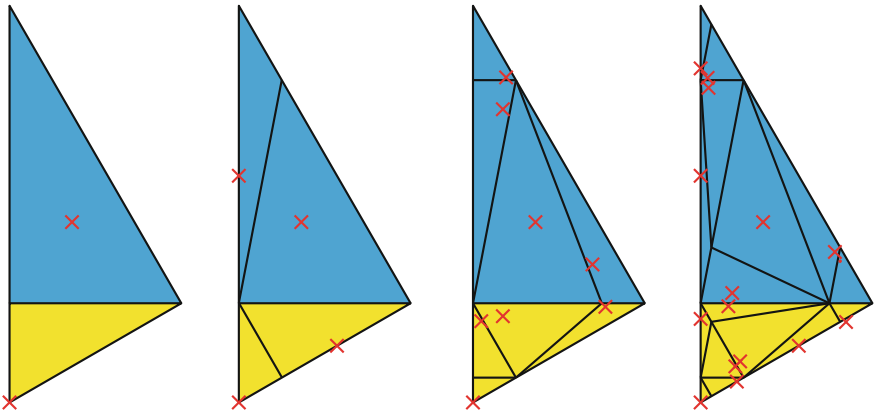

Fig. 7.15 Domain separation and fixed points of $f^{\triangle}$, $(f^{\triangle})^2$, $(f^{\triangle})^3$, $(f^{\triangle})^4$. There are 2 fixed points for the map $f^{\triangle}$ (*left*). Similarly, the fixed points for the map $(f^{\triangle})^2$ are shown in the *middle left figure* but the ones in the *left figure* are also included in the figure. The same comment applies to the figures for $(f^{\triangle})^3$ and $(f^{\triangle})^4$

7.4.3 Chaos by the Tetrahedron Map

In this section, we show that the tetrahedron map exhibits chaotic behavior.

Theorem 7.7 *The tetrahedron map $f^{\triangle} : \mathscr{D} \to \mathscr{D}$ is topologically transitive on $\mathscr{D}$ and possesses dense periodic points on $\mathscr{D}$.*

Hence, the tetrahedron map $f^{\triangle}$ exhibits chaotic behavior on $\mathscr{D}$.

Figure 7.15 shows the partitioned domains and the corresponding fixed points for $f^{\triangle}$, $(f^{\triangle})^2$, $(f^{\triangle})^3$, $(f^{\triangle})^4$.

Theorem 7.8 *Let $k \in \mathbb{Z}^+$ and let $i \leq k$ be an integer. Furthermore, define the circular function* $\mathrm{Circ}_i^k : \mathscr{S}^k \to \mathscr{S}^k$ *given by*

$$\mathrm{Circ}_i^k(s) \triangleq \{s_i, s_{i+1}, \ldots, s_{k-1}, s_0, s_1, \ldots, s_{i-1}\}. \tag{7.16}$$

Then there exists $s \in \mathscr{S}_k$ such that

$$\begin{aligned} f^{\triangle}(x_s) &= x_{\mathrm{Circ}_1^k(s)}, \\ f^{\triangle}(x_{\mathrm{Circ}_1^k(s)}) &= x_{\mathrm{Circ}_2^k(s)}, \\ &\vdots \\ f^{\triangle}(x_{\mathrm{Circ}_{k-1}^k(s)}) &= x_{\mathrm{Circ}_k^k(s)} = x_s, \end{aligned}$$

where x_s denotes a fixed point for the map $(f^{\triangle})^k$.

Proof It suffices to show $f^{\triangle}(x_s) = x_{\mathrm{Circ}_1^k(s)}$. For any $s = \{s_0, s_1, \ldots, s_{k-1}\} \in \mathscr{S}_k$, it follows that

$$f^{\triangle}_{s_{k-1}} \circ f^{\triangle}_{s_{k-2}} \circ \cdots \circ f^{\triangle}_{s_0}(x_s) = x_s,$$

and hence

$$f^{\triangle}_{s_0} \circ f^{\triangle}_{s_{k-1}} \circ f^{\triangle}_{s_{k-2}} \circ \cdots \circ f^{\triangle}_{s_0}(x_s) = f^{\triangle}_{s_0}(x_s).$$

On the other hand, it follows that for $x_{\mathrm{Circ}_1^k(s)}$,

$$f^{\triangle}_{s_0} \circ f^{\triangle}_{s_{k-1}} \circ f^{\triangle}_{s_{k-2}} \circ \cdots \circ f^{\triangle}_{s_1}(x_{\mathrm{Circ}_1^k(s)}) = x_{\mathrm{Circ}_1^k(s)}.$$

By comparing the above two equations, we obtain

$$f^{\triangle}_{s_0}(x_s) = x_{\mathrm{Circ}_1^k(s)},$$

and hence $f^{\triangle}(x_s) = x_{\mathrm{Circ}_1^k(s)}$. □

Corollary 7.1 *The number T_k of periodic orbits with the fundamental period k is given by $T_1 = 2$ and*

$$T_k = \frac{1}{k}\left(2^k - \sum_{i \in \mathscr{M}_k} i T_i\right). \tag{7.17}$$

Figure 7.16 shows the periodic orbits of period 1, 2, 3, and 4.

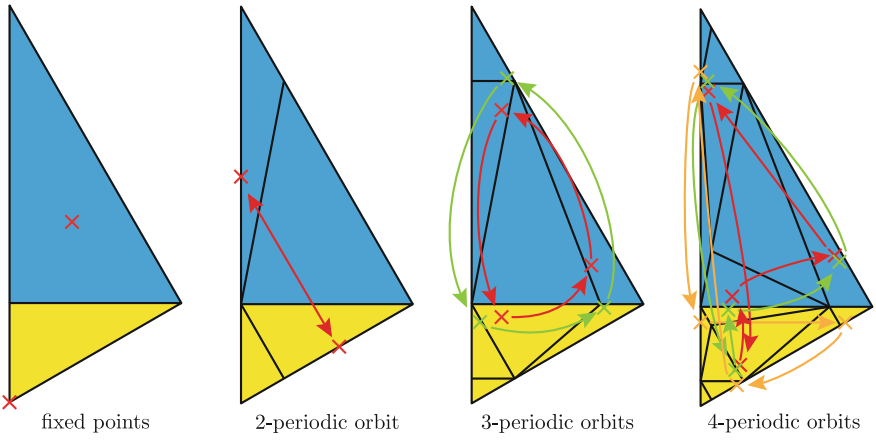

Fig. 7.16 Domain separation and true periodic orbits of $f^{\triangle}$, $(f^{\triangle})^2$, $(f^{\triangle})^3$, $(f^{\triangle})^4$. There are 2, 1, 2, 3 periodic orbits for the periods 1, 2, 3, and 4, respectively

7.5 Conclusion

In this article, we proposed a simple folding map associated with the equilateral triangle and provided intensive analysis for the case where the folding leads to form the tetrahedron. Specifically, we showed that each partitioned domain possesses a unique fixed point for the map $(f^{\triangle})^k$ and the labels of the domains satisfy the grey code property. Furthermore, we showed that when θ is less than the value of $\cos^{-1}\frac{1}{3}$, the $f^{\triangle}$ exhibits chaotic behavior in the sense of Devaney. Future works include investigating the connections and the differences between the folding map and the well-known horseshoe map, which also has the notion of 'folding' in its operation.

References

1. Amaral, G.F.V., Letellier, C., Aguirre, L.A.: Piecewise affine models of chaotic attractors: the Rossler and Lorenz systems. Interdisc. J. Nonlinear Sci., Chaos **16** (2006)
2. Chen, G., Yu, X.: Chaos Control: Theory and Applications. Springer, Berlin (2003)
3. Devaney, R.: An Introduction to Chaotic Dynamical Systems. Addison-Wesley Studies in Nonlinearity. Westview Press, Reading (2003)
4. Guckenheimer, J., Holmes, P.: Nonlinear oscillations dynamical systems, and bifurcations of vector fields. J. Appl. Mech. **51** (1984)
5. Guckenheimer, J., Holmes, P.: Nonlinear Oscillations, Dynamical Systems, and Bifurcations of Vector Fields. Springer, New York (1983)
6. Ishikawa, T., Hayakawa, T.: Chaotic behavior of the folding map on the equilateral triangle. In: Proc. Sympo. Nonlin. Contr. Syst., 767–772 (2013)
7. May, R.M.: Simple mathematical models with very complicated dynamics. Nature **261**(5560), 459–467 (1976)
8. Melnikov, V.K.: On the stability of the center for time periodic perturbations. Trans. Moscow Math. **12**, 1–57 (1963)
9. Mielke, A., Holmes, P., O'Reilly, O.: Cascades of homoclinic orbits to, and chaos near, a hamiltonian saddle-center. J. Dyn. Diff. Eqn. **4**(1), 95–126 (1992)
10. Nishimura, J., Hayakawa, T.: Chaotic dynamics of orthogonally projective triangle folding map. In: Proc. IEEE Conf. Dec. Contr., 813–815 (2014)
11. Robinson, C.: Dynamical Systems: Stability, Symbolic Dynamics, and Chaos. CRC Press, Boca Raton (1998)
12. Smale, S.: Diffeomorphisms With Many Periodic Points. Department of Mathematics, Columbia University, New York (1963)
13. Smale, S.: The Mathematics of Time: Essays on Dynamical Systems. Economic Processes and Related Topics. Springer, New York (1980)

Chapter 8
Stabilization Control of Quasi-periodic Orbits

Natushiro Ichinose and Motomassa Komuro

8.1 Introduction

A quasi-periodic orbit possesses the properties of both a periodic orbit and a chaotic orbit. Let x_n be a quasi-periodic orbit in a discrete-time system. The quasi-periodic orbit is aperiodic in the sense that we cannot choose a period d such that $x_{n+d} = x_n$. Aperiodicity is the main property of a chaotic orbit. At the same time, the quasi-periodic orbit is almost periodic in the sense that we can choose a recurrence time d such that $||x_{n+d} - x_n|| < \varepsilon$ for a small positive ε and any n. Since the definition of almost periodicity holds for a periodic orbit in which $x_{n+d} = x_n$, a periodic orbit is a special case in almost periodicity.

In dynamical system theory, several control methods are available to stabilize an unstable periodic orbit, such as the OGY method [10] and the delayed feedback control [13]. In control theory, control methods to stabilize a fixed point (or an equilibrium) have been discussed from various viewpoints. Especially, in discrete-time systems, since a periodic orbit can be described by a fixed point by using a composition of a map, the stabilization is reducible to that of a fixed point. In this sense, the stabilization of a quasi-periodic orbit presents a challenging problem because the stabilization is not reducible to a fixed point due to the aperiodicity of the quasi-periodic orbit.

In general, quasi-periodic orbits are dynamics defined on a high-dimensional invariant torus [2]. In this chapter, we focus on the simplest case of dynamics defined on an invariant closed curve in discrete-time systems. In this case, a quasi-periodic

N. Ichinose (✉)
Graduate School of Informatics, Kyoto University,Yoshida-Honmachi,
Sakyo-ku, Kyoto 606-8501, Japan
e-mail: ichinose@i.kyoto-u.ac.jp

M. Komuro
Center for Fundamental Education, Teikyo University of Science,
2525 Yatsusawa, Uenohara-shi, Yamanashi 409-0193, Japan
e-mail: komuro@ntu.ac.jp

K. Aihara et al. (eds.), *Analysis and Control of Complex Dynamical Systems*,
Mathematics for Industry 7, DOI 10.1007/978-4-431-55013-6_8

orbit is characterized by its rotation number. We explain that a quasi-periodic orbit is associated with an irrational rotation via its rotation number, which is reflected in the design of control methods.

We apply the external force control, the delayed feedback control, and the pole assignment method, to stabilize an unstable quasi-periodic orbit. These control methods have been used to stabilize an unstable periodic orbit. We show that these control methods are also applicable to an unstable quasi-periodic orbit.

8.2 Properties of Quasi-periodic Orbit on Invariant Closed Curve

In this section, we summarize the properties of a quasi-periodic orbit on an invariant closed curve. The rotation number introduced by Poincaré is an important invariant in a quasi-periodic orbit on an invariant closed curve [14]. If a certain phase is determined in the quasi-periodic orbit, the rotation number is defined by the average phase difference for an iterate of a map. We consider a one-dimensional map:

$$\theta_{n+1} = f(\theta_n),$$

where θ_n is the phase and $f : \mathbb{S} \to \mathbb{S}$ is the orientation preserving homeomorphism of the circle $\mathbb{S} = \mathbb{R}/\mathbb{Z}$. The circle $\mathbb{S}$ implies the set of real numbers modulo integers, i.e., only the fractional part of the phase θ_n is considered. To calculate the phase difference, we lift f to a map $F : \mathbb{R} \to \mathbb{R}$ such that $f(\theta) = F(\theta)$ modulo integers and $F(\theta + m) = F(\theta) + m$ for any integer m. By considering the lifted dynamics $\theta_{n+1} = F(\theta_n)$ and averaging the phase difference $(\theta_{n+1} - \theta_n)$, the rotation number $\omega \in [0, 1]$ is calculated by:

$$\omega = \lim_{N\to\infty} \frac{\sum_{n=0}^{N-1}(\theta_{n+1} - \theta_n)}{N} = \lim_{N\to\infty} \frac{F^N(\theta_0) - \theta_0}{N}.$$

It has been proved that the rotation number ω is unique independently of the initial phase θ_0. Although this is the simplest case of a one-dimensional system, several numerical approximation methods of rotation numbers have been proposed [1, 11, 14] and we can obtain the rotation number from higher-dimensional systems.

We consider an M-dimensional discrete-time system having a quasi-periodic orbit on an invariant closed curve:

$$x_{n+1} = F(x_n),$$

where $x_n \in \mathbb{R}^M$ is the M-dimensional state vector and $F : \mathbb{R}^M \to \mathbb{R}^M$ is the function representing the system. If the rotation number is irrational, the quasi-periodic orbit is topologically conjugate to the irrational rotation [9]:

$$\theta_{n+1} = \theta_n + \omega, \tag{8.1}$$

where $\theta_n \in \mathbb{S}$. If the state x_n is in the quasi-periodic orbit, the following relation holds:

$$x_n = \psi(\theta_n), \tag{8.2}$$

where $\psi : \mathbb{S} \to \mathbb{R}^M$ is the homeomorphism from the phase to the state.

Using the irrational rotation, we can understand that the quasi-periodic orbit is aperiodic. The irrational rotation (8.1) is solved as follows:

$$\theta_n = \theta_0 + n\omega.$$

We first consider the case that ω is rational, i.e., $\omega = p/q$ for coprime integers p and q. Then, $\theta_q = \theta_0 + p$. In the circle $\mathbb{S}$, the integer p implies zero because the rotation returns to the same phase. Therefore, the dynamics are periodic ($\theta_q = \theta_0$). On the other hand, in the case of the irrational rotation number, $n\omega$ is never an integer for any n. Therefore, there is no period d such that $\theta_d = \theta_0$ and $x_d = x_0$ from the topological conjugacy (8.2).

We can also understand that the quasi-periodic orbit is almost periodic. The irrational rotation number ω can be approximated by a rational number:

$$\omega = \frac{p}{q} + \varepsilon,$$

where p and q are coprime integers. If we consider the period q, the following relation holds:

$$\theta_q = \theta_0 + p + q\varepsilon.$$

Since the integer p is regarded as zero in $\mathbb{S}$, the difference between these phases is $q|\varepsilon|$. In general, we can choose a specific q such that the order of $|\varepsilon|$ is limited [8] by:

$$|\varepsilon| < \frac{1}{2q^2}. \tag{8.3}$$

Since the difference $q|\varepsilon|$ is less than $1/(2q)$, we can obtain a smaller difference for a larger q. From the topological conjugacy (8.2), we can choose a period q for a small $\varepsilon' > 0$ and any n:

$$||x_{n+q} - x_n|| < \varepsilon'.$$

Therefore, the quasi-periodic orbit is almost periodic in the period q.

The approximation theory of irrational numbers by rational numbers shows that a continued fraction gives us a good representation [8]. The irrational rotation number is represented by the infinite continued fraction:

$$\omega = \cfrac{1}{a_1 + \cfrac{1}{a_2 + \cfrac{1}{a_3 + \cdots}}},$$

where $a_1, a_2, a_3, \ldots$ are positive integers. If we stop the continuation of fractions in a finite order, the resulting continued fraction is a rational number. This finite continued fraction is called a *convergent*. The convergent gives us a good approximation of the irrational rotation number. Actually, the rational number p/q in which (8.3) holds is a convergent [8]. Therefore, the almost periodicity of the quasi-periodic orbit is associated with the continued fraction expansion of its rotation number.

8.3 Unstable Quasi-periodic Orbit

As an example of systems, we use a coupled map lattice with asymmetric connections [7]:

$$\begin{aligned} x_{n+1} &= f(x_n) + \tfrac{1}{2}(\beta - \delta)(f(z_n) - f(x_n)) + \tfrac{1}{2}(\beta + \delta)(f(y_n) - f(x_n)), \\ y_{n+1} &= f(y_n) + \tfrac{1}{2}(\beta - \delta)(f(x_n) - f(y_n)) + \tfrac{1}{2}(\beta + \delta)(f(z_n) - f(y_n)), \\ z_{n+1} &= f(z_n) + \tfrac{1}{2}(\beta - \delta)(f(y_n) - f(z_n)) + \tfrac{1}{2}(\beta + \delta)(f(x_n) - f(z_n)), \end{aligned} \tag{8.4}$$

where $x_n, y_n, z_n \in \mathbb{R}$ are the states of the system and f is the logistic map $f(x) = 1 - \alpha x^2$. In this section, we discuss the mechanism for the generation of unstable quasi-periodic orbits of the system.

If the three states synchronize, i.e., $x_n = y_n = z_n$, the system (8.4) is reduced to the one-dimensional logistic map:

$$x_{n+1} = f(x_n).$$

Therefore, the system (8.4) has all possible solutions of the logistic map as the synchronization solutions although those solutions may be unstable. Using the solutions of the logistic map, we represent a synchronization fixed point as follows:

$$x_n = y_n = z_n = x^*, \quad x^* = f(x^*) = \frac{-1 + \sqrt{4\alpha + 1}}{2\alpha}.$$

The stability of the fixed point is determined by the eigenvalues of a Jacobian matrix of the system. The Jacobian matrix J^* at the fixed point is represented as follows:

$$J^* = \gamma \begin{pmatrix} 1-\beta & \frac{\beta+\delta}{2} & \frac{\beta-\delta}{2} \\ \frac{\beta-\delta}{2} & 1-\beta & \frac{\beta+\delta}{2} \\ \frac{\beta+\delta}{2} & \frac{\beta-\delta}{2} & 1-\beta \end{pmatrix},$$

where $\gamma = f'(x^*) = 1 - \sqrt{4\alpha + 1}$. The Jacobian matrix has a real eigenvalue and a conjugate pair of complex eigenvalues:

$$\mu_1 = \gamma, \quad \mu_{2,3} = \gamma \frac{2 - 3\beta \pm i\sqrt{3}\delta}{2}.$$

If the absolute values of all eigenvalues are less than one, the fixed point is stable.

We consider two cases in which the fixed point is destabilized by the distinct settings of the eigenvalues: (a) $|\mu_1| < 1 < |\mu_{2,3}|$ and (b) $|\mu_1|, |\mu_{2,3}| > 1$. We show the dynamics of cases (a) and (b) in Fig. 8.1a and b, respectively. The dashed line shows the synchronization set ($x_n = y_n = z_n$) in which all synchronization solutions occur. The fixed point exists in the synchronization set (shown as the gray dot). In case (a), since the absolute value of the complex eigenvalue $|\mu_{2,3}|$ is greater than one, the Neimark-Sacker bifurcation occurs. Then, the system is desynchronized and the stable quasi-periodic orbit emerges around the unstable fixed point (Fig. 8.1a).

In case (b), a quasi-periodic orbit exists similarly to case (a) because $|\mu_{2,3}| > 1$. However, since μ_1 is less than -1, the period-doubling bifurcation occurs at the same time. The quasi-periodic orbit is stable on its stable manifold as shown in Fig. 8.1b. However, the outer states except the stable manifold converge to the stable period-2 points. Therefore, this quasi-periodic orbit is unstable and has saddle-type instability. Using the control methods, we aim to stabilize this unstable quasi-periodic orbit.

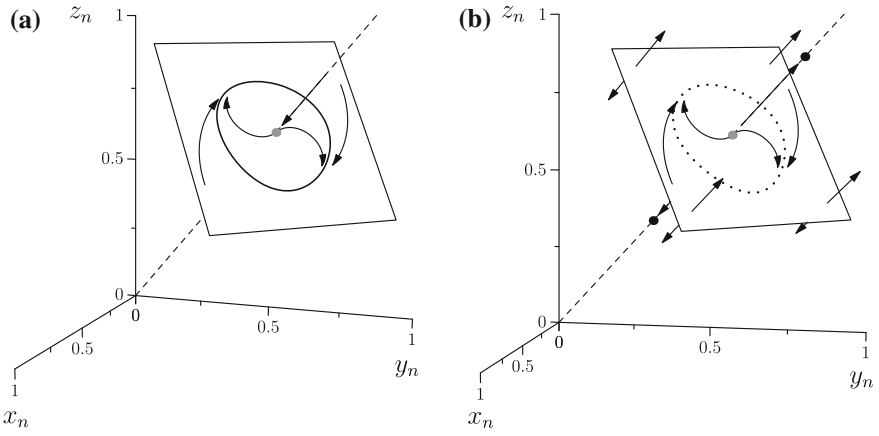

Fig. 8.1 Stable and unstable quasi-periodic orbits of the coupled map lattice (8.4). **a** The parameters are fixed at $(\alpha, \beta, \delta) = (0.7, 0.02, 0.5)$, in which the eigenvalues are $|\mu_1| < 1 < |\mu_{2,3}|$. The *solid circle* shows the stable quasi-periodic orbit. The *gray dot* shows the unstable fixed point. The *dashed line* shows the synchronization set. **b** $(\alpha, \beta, \delta) = (0.79, 0.02, 0.06)$, in which $|\mu_1|, |\mu_{2,3}| > 1$. The *dotted circle* shows the unstable quasi-periodic orbit. The period-2 points are stable in this case (shown as *black dots*)

8.4 External Force Control

The external force control was proposed by Pyragas to stabilize unstable periodic orbits [13]. The feedback input is defined by the difference between the current state and the external force that is the unstable periodic orbit itself. The control system is defined by:

$$x_{n+1} = F(x_n) + Ku_n, \tag{8.5}$$

where K is the matrix of the feedback coefficients, u_n is the feedback input,

$$u_n = y_n - x_n,$$

and y_n is the external force. If the unstable periodic orbit is stabilized, the feedback input vanishes (i.e., $y_n - x_n = 0$). Therefore, only a small external force is used to stabilize the unstable periodic orbit [13].

To apply the external force control to stabilize the unstable quasi-periodic orbit, it is necessary to determine the orbit itself in advance. If we find the stable manifold, we would be able to determine the unstable quasi-periodic orbit because the orbit is stable on it. In general, however, it is difficult to determine the stable manifold analytically. Fortunately, a method that numerically estimates the orbit on the stable manifold has been proposed based on a bisection method [6].

We consider two initial points on either side of the stable manifold and their midpoint (Fig. 8.2). When each point is mapped by the system equation, the midpoint and the initial point 2 approach each other, whereas the initial point 1 is separated from them. Therefore, by observing the dynamics, we can identify the side on which the midpoint is located relative to the stable manifold. We replace the initial points with the midpoint and the initial point 1, which are more proximately located on either side of the stable manifold than the two initial points. These two points approximate

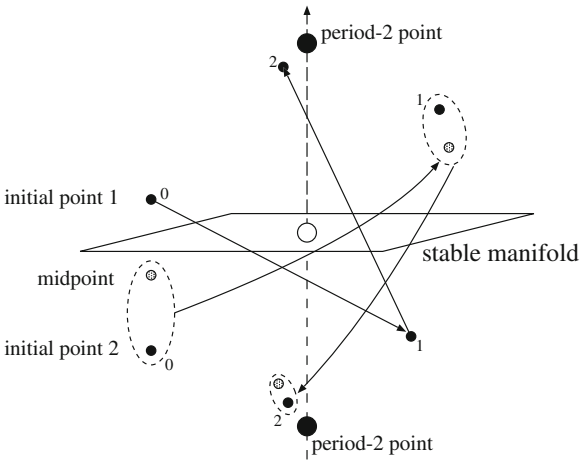

Fig. 8.2 Bisection method to find the stable manifold. The two initial points are given. When each point is mapped (shown as *0*, *1*, and *2*), the midpoint and the initial point 2 approach each other. The initial point 1 and the midpoint are more proximately located on either side of the stable manifold than the two initial points

a point on the stable manifold with arbitrary precision by iterating this process. Furthermore, by mapping the approximated point, we can obtain the orbit on the stable manifold [6]. We use the unstable quasi-periodic orbit estimated numerically by this bisection method as the external force y_n.

To understand the structure of the external force control, we assume that the external force y_n is derived from a system identical to the control-free system:

$$y_{n+1} = F(y_n). \tag{8.6}$$

Note that (8.6) holds for the orbit y_n, although it is unstable. We introduce the following transformation [4, 12]:

$$U_n = \frac{y_n + x_n}{2}, \quad V_n = \frac{y_n - x_n}{2}.$$

The control system represented by (8.5) and (8.6) is rewritten as follows:

$$\begin{aligned} U_{n+1} &= F(U_n + V_n)/2 + F(U_n - V_n)/2 + KV_n, \\ V_{n+1} &= F(U_n + V_n)/2 - F(U_n - V_n)/2 - KV_n. \end{aligned} \tag{8.7}$$

If the stabilization is achieved, $U_n = y_n$ and $V_n = 0$.

This transformation has been discussed from the viewpoint of synchronization in dynamical systems [4, 12]. In synchronization theory, the manifold $V_n = 0$ corresponds to a synchronization hyperplane on which the two systems (8.5) and (8.6) synchronize. If the origin of V_n is stable, i.e., the transverse direction of the synchronization hyperplane is stable, the synchronization between the two systems is stable. Although the driving orbit is assumed to be an attractor in synchronization theory, this discussion holds even if it is an unstable orbit.

To evaluate the stability of the external force control, we calculate the Lyapunov exponents of the subsystem (8.7). Since we evaluate the stability on $V_n = 0$, we linearize (8.7) at the origin of V_n:

$$V_{n+1} = (F'(y_n) - K)V_n, \tag{8.8}$$

where F' is the Jacobian matrix of F. The largest Lyapunov exponent λ_1 of (8.8) is defined by:

$$\lambda_1 = \lim_{N\to\infty} \frac{1}{N} \log \left\| \prod_{n=0}^{N} (F'(y_n) - K)v \right\|,$$

for almost any vector v [3]. If the largest Lyapunov exponent is negative, the origin of V_n is stable and hence the external force control stabilizes the unstable quasi-periodic orbit. These Lyapunov exponents are called *conditional Lyapunov exponents* because they are calculated for the subsystem driven by the external force [12].

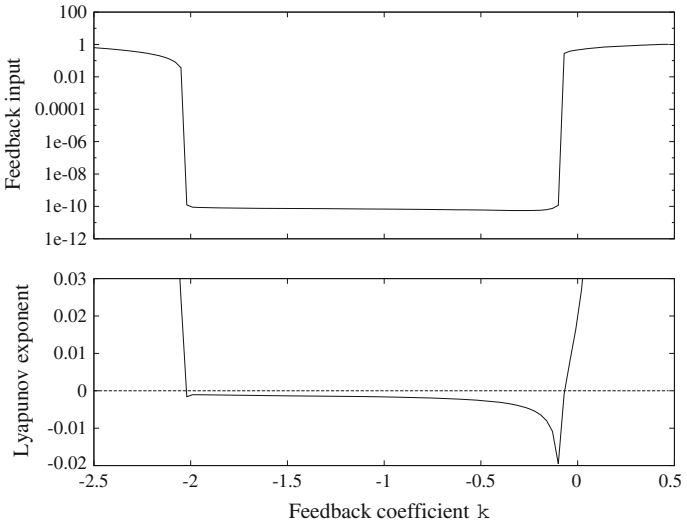

Fig. 8.3 Results of the external feedback control for the coupled map lattice (8.4). We show the average feedback input (*top*) and the largest Lyapunov exponent (*bottom*) as a function of the feedback coefficient k. The parameters are fixed at $(\alpha, \beta, \delta) = (0.79, 0.02, 0.06)$

In Fig. 8.3, we show the results of the external feedback control for the coupled map lattice (8.4). We assume that the feedback input is given to only the state x_n:

$$K = \begin{pmatrix} k & 0 & 0 \\ 0 & 0 & 0 \\ 0 & 0 & 0 \end{pmatrix}, \tag{8.9}$$

where k is the feedback coefficient. The average feedback input is defined by the average of the input strength $||u_n||$. If the average feedback input is sufficiently small, the stabilization is achieved. In Fig. 8.3, the unstable quasi-periodic orbit is stabilized when the largest Lyapunov exponent is negative.

8.5 Delayed Feedback Control

The delayed feedback control was also proposed by Pyragas to stabilize unstable periodic orbits [13]. The feedback input u_n is defined by the difference between the d-past state and the current state:

$$u_n = x_{n-d} - x_n,$$

where d is equal to the period of the unstable periodic orbit. The control system is the same as (8.5). Similarly to the external force control, if the stabilization is achieved, the feedback input vanishes. However, whereas the external force control requires the target orbit itself, the delayed feedback control does not require any exact information of the unstable periodic orbit except its period.

Unfortunately, there is no delay d such that the feedback input vanishes in the unstable quasi-periodic orbit because of its aperiodicity. However, since the quasi-periodic orbit is almost periodic, we can choose a delay d in which the feedback input is always small. The delayed feedback control may be applicable to the unstable quasi-periodic orbit by using such a delay in the same way as the periodic case [5].

Using the unstable quasi-periodic orbit y_n, we observe the average of the distance $||y_{n-d} - y_n||$ between the d-past state and the current state. In Fig. 8.4, we show the average distance for the coupled map lattice (8.4). When $d \leq 200$, the delay that gives the smallest distance is $d = 59$, which corresponds to a denominator of a convergent explained in Sect. 8.2. In this sense, we can also choose such a delay by using only the rotation number that generates convergents. We use the delays giving the five smallest distances as the candidates for the feedback delay (circles in Fig. 8.4).

In Fig. 8.5, we compare the unstable quasi-periodic orbit to an orbit of the delayed feedback control with the delay $d = 59$. The matrix of the feedback coefficients K is the same as (8.9). In this case, the stabilization is achieved in the sense that the orbit of the delayed feedback control lies in the neighborhood of the unstable quasi-periodic orbit. However, since the feedback input does not vanish, the difference between the two orbits does not disappear.

In Fig. 8.6, we show the average feedback input for $d = 59$, 175, and 177. The other candidates $d = 118$ and 116 are even numbers and the system has stable period-2 points. Since the feedback input vanishes for the period-2 points in these cases, we exclude them. Whereas the average feedback input of $d = 59$ is sufficiently small, the stabilization is not achieved for $d = 175$ and 177.

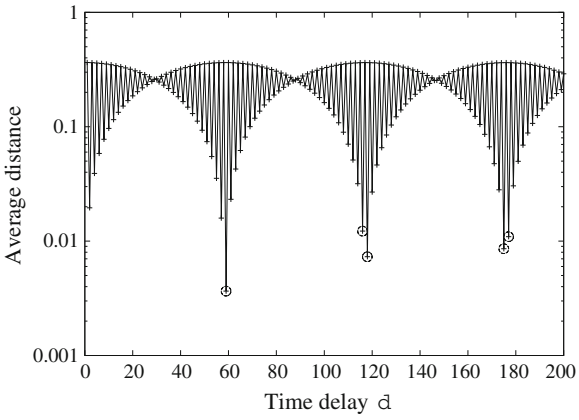

Fig. 8.4 Average distance between d-past state and current state for the coupled map lattice (8.4). When $d \leq 200$, the delays giving the five smallest distances are 59, 118, 175, 177, and 116 (indicated by *circles*). The parameters are fixed at $(\alpha, \beta, \delta) = (0.79, 0.02, 0.06)$

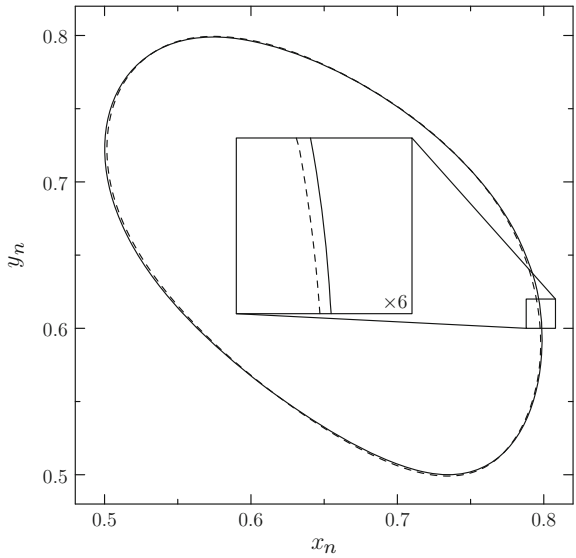

Fig. 8.5 Unstable quasi-periodic orbit (*solid circle*) and orbit of the delayed feedback control (*dashed circle*) for the coupled map lattice (8.4). The orbits are projected onto the x–y plane. A partial area of the orbits is enlarged to indicate the difference between them. The delay is $d = 59$ and the feedback coefficient is $k = -0.4$. The parameters are fixed at $(\alpha, \beta, \delta) = (0.79, 0.02, 0.06)$

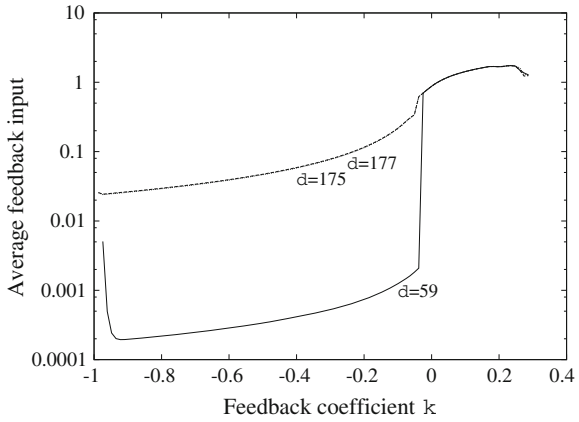

Fig. 8.6 Average feedback input of the delayed feedback control for the coupled map lattice (8.4). We use the delays $d = 59$, 175, and 177. The profiles of $d = 175$ and 177 almost overlap with each other. The parameters are fixed at $(\alpha, \beta, \delta) = (0.79, 0.02, 0.06)$

From the viewpoint of the stabilization of the unstable quasi-periodic orbit, a smaller feedback input is required. We here attempt to realize a small feedback input by using multiple feedback delays. As mentioned in Sect. 8.2, the quasi-periodic orbit is topologically conjugate to the irrational rotation. We consider a delayed phase θ_{n-d} in the phase domain. Using the irrational rotation, we can represent the current phase by the delayed phase:

$$\theta_n = \theta_{n-d} + d\omega, \tag{8.10}$$

where ω is the rotation number. Let $\langle d\omega \rangle$ be the fractional part of $d\omega$. Intuitively, the phase difference between θ_n and θ_{n-d} is defined by $\langle d\omega \rangle$ from (8.10). However, we

require that the phase difference represents the lead and lag of the delayed phase for the current phase. Therefore, we define the phase difference by:

$$D(\theta_n, \theta_{n-d}) = \begin{cases} \langle d\omega \rangle & \text{if } \langle d\omega \rangle < 0.5 \\ \langle d\omega \rangle - 1 & \text{otherwise} \end{cases}. \tag{8.11}$$

We consider two delays, d_1 and d_2, and their phase differences from the current phase:

$$D_1 = D(\theta_n, \theta_{n-d_1}), \quad D_2 = D(\theta_n, \theta_{n-d_2}).$$

From the definition of the phase difference (8.11), D_1 and D_2 are constant and independent of time n. If both delays give small feedback inputs, D_1 and D_2 are also small.

The state of the quasi-periodic orbit is represented by the phase via the homeomorphism ψ. Thus, we represent the current state y_n by using a linear interpolation of the delayed phases:

$$y_n = \psi(\theta_n) \approx \frac{\psi(\theta_{n-d_2}) - \psi(\theta_{n-d_1})}{\theta_{n-d_2} - \theta_{n-d_1}} (\theta_n - \theta_{n-d_1}) + \psi(\theta_{n-d_1}). \tag{8.12}$$

Equation (8.12) can be rewritten by using the phase differences D_1 and D_2 (Fig. 8.7):

$$y_n \approx \left(1 - \frac{D_1}{D_1 - D_2}\right) y_{n-d_1} + \frac{D_1}{D_1 - D_2} y_{n-d_2}, \tag{8.13}$$

where $y_{n-d_1} = \psi(\theta_{n-d_1})$ and $y_{n-d_2} = \psi(\theta_{n-d_2})$. As shown in Fig. 8.7, the interpolated state is closer to the current state y_n than either of the delayed states y_{n-d_1} and y_{n-d_2} if D_1 and D_2 are sufficiently small. Therefore, by using two delays, we can obtain a smaller feedback input than that of a single delay.

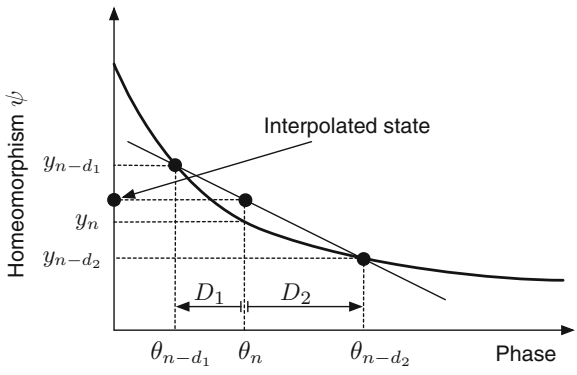

Fig. 8.7 Linear interpolation of current state. Although the homeomorphism ψ is a vector function, we show only a component in it. The phase domain is enlarged at the current phase θ_n. The interpolated state is closer to the current state than either of the delayed states

Since D_1 and D_2 are constant, we introduce a constant parameter τ:

$$\tau = \frac{D_1}{D_1 - D_2}. \tag{8.14}$$

Using (8.13), we construct the feedback input:

$$u_n = (1-\tau)x_{n-d_1} + \tau x_{n-d_2} - x_n.$$

Note that we require no information of the homeomorphism ψ in the feedback input. The parameter τ can be determined if the rotation number ω is given.

In the unstable quasi-periodic orbit of Fig. 8.5, the rotation number is estimated to be $\omega \approx 2622/5335 = 0.491\ldots$. Using (8.11), we calculate the phase differences of the delayed states from the current state (Table 8.1). To apply the linear interpolation method to the delayed states, it is necessary that the phase differences of the two delays have different signs. Therefore, we use pairs of the delays $(d_1, d_2) = (59, 175)$, $(59, 116)$, $(118, 175)$, $(175, 177)$, and $(177, 116)$. Although the above condition holds for the pair $(d_1, d_2) = (118, 116)$, we exclude this pair because the feedback input vanishes for the stable period-2 points. The parameter τ is calculated for each pair by using (8.14).

In Fig. 8.8, we show the results of the delayed feedback control with the two delays. Since the feedback input is sufficiently small except that for the case of $(d_1, d_2) = (175, 177)$, the stabilization is achieved. In the delays except (175, 177) and (177, 116), we obtain a smaller feedback input than that of the single delay.

Table 8.1 Phase differences of delayed states for the coupled map lattice (8.4)

Delay d	59	118	175	177	116
Phase difference D ($\times 10^{-3}$)	−3.19	−6.37	7.50	−9.56	10.7

Parameters $(\alpha, \beta, \delta) = (0.79, 0.02, 0.06)$

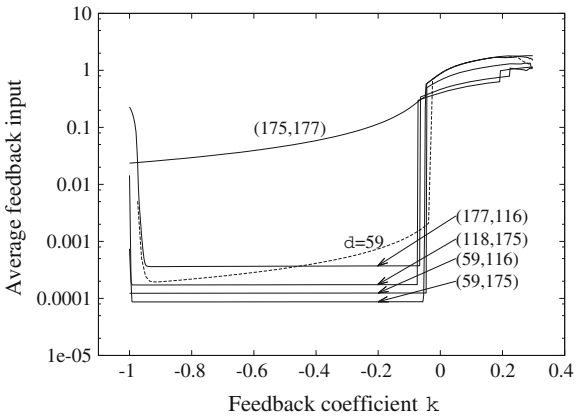

Fig. 8.8 Average feedback input of the delayed feedback control with two delays for the coupled map lattice (8.4). The pairs of numbers show the delays (d_1, d_2). For comparison, we show the profile of the single delay $d = 59$ (*dashed curve*). The parameters are fixed at $(\alpha, \beta, \delta) = (0.79, 0.02, 0.06)$

8.6 Pole Assignment Method

As mentioned in Sect. 8.3, in the coupled map lattice, if the absolute value of the complex eigenvalue $|\mu_{2,3}|$ at the fixed point is greater than one, the quasi-periodic orbit occurs. At the same time, if the absolute value of the real eigenvalue $|\mu_1|$ is greater than one, the period-2 points are stable and the quasi-periodic orbit is unstable. Therefore, if we can stabilize only the real eigenvalue μ_1, a stable quasi-periodic orbit is realized. This type of control method is known as the pole assignment method and is widely used in control theory [15].

The eigenvalues of the Jacobian matrix J^* at the fixed point are given by solutions of s in the following equation:

$$\det(sI - J^*) = 0,$$

where I is the identity matrix, $\det(\cdot)$ implies the determinant of a matrix, and the left side of the equation corresponds to the characteristic polynomial of J^*. Thus, if $\mu_1, \mu_2, \ldots, \mu_M$ are the eigenvalues of J^*, the characteristic polynomial is given by:

$$\det(sI - J^*) = (s - \mu_1)(s - \mu_2)\cdots(s - \mu_M).$$

Since a quasi-periodic orbit is assumed to exist, there is at least a conjugate pair of complex eigenvalues whose absolute values are greater than one. We here assume that only μ_1 is an unstable real eigenvalue ($|\mu_1| > 1$). The aim of the control is to replace μ_1 with a stable real eigenvalue $\hat{\mu}$ where $|\hat{\mu}| < 1$. If such a fixed point is realized, its characteristic polynomial is expressed by:

$$q(s) = (s - \hat{\mu})(s - \mu_2)(s - \mu_3)\cdots(s - \mu_M). \tag{8.15}$$

The feedback input is defined by the difference between the fixed point and the current state:

$$u_n = x^* - x_n,$$

where x^* is the fixed point. The control system is the same as (8.5). Then, the characteristic polynomial of the control system is given by:

$$r_K(s) = \det(sI - F'(x^*) + K). \tag{8.16}$$

If we can design the feedback coefficients K such that $r_K(s) = q(s)$, the fixed point of the control system (equivalent to x^*) has the objective eigenvalues. It is necessary that all coefficients of $r_K(s)$ and $q(s)$ are equivalent. Since we do not change the eigenvalues except μ_1, the quasi-periodic orbit can be stabilized.

Strictly speaking, this control method does not imply the stabilization of the unstable quasi-periodic orbit itself. Since x^* is a constant and x_n is a quasi-periodic orbit, the feedback input is large and hence the controlled quasi-periodic orbit is

obviously distinct from the unstable quasi-periodic orbit. However, since the control can be carried out by using only the information of the fixed point, the design of the control system is markedly simple in comparison with the previous control methods.

In the coupled map lattice, we consider a restricted matrix of feedback coefficients:

$$K = k \begin{pmatrix} 1 & 1 & 1 \\ 1 & 1 & 1 \\ 1 & 1 & 1 \end{pmatrix}.$$

We find the feedback coefficient k such that $r_K(s) = q(s)$ holds. For example, the coefficients of s^2 in $r_K(s)$ and $q(s)$ are respectively given by:

$$3k - 3\gamma(1-\beta), \quad \gamma(3\beta - 2) - \hat{\mu}.$$

Since these coefficients are equivalent to each other, we obtain the feedback coefficient k:

$$k = \frac{\gamma - \hat{\mu}}{3}.$$

This relationship holds for the other coefficients of the characteristic polynomials. Although this is a restricted case, the necessary and sufficient conditions for the existence of K and the efficient design methods in general cases have been discussed in control theory [15].

In Fig. 8.9, we show an orbit of the pole assignment method. Although a difference from the unstable quasi-periodic orbit is noticeable, a stable quasi-periodic orbit can be observed by using the pole assignment method. Since the feedback coefficient is

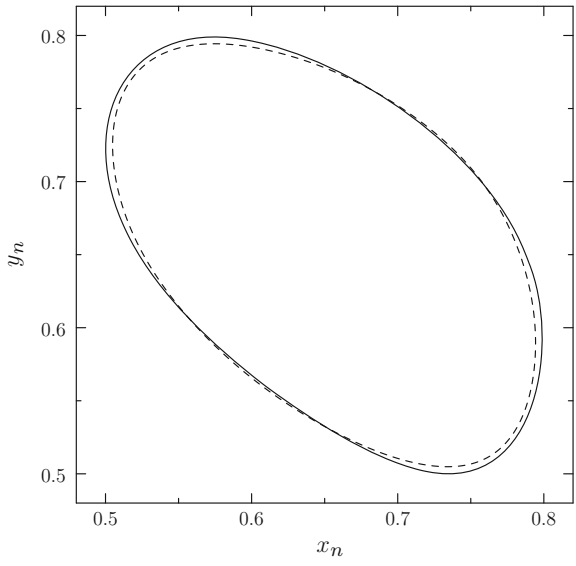

Fig. 8.9 Unstable quasi-periodic orbit (*solid circle*) and orbit of the pole assignment method (*dashed circle*) for the coupled map lattice (8.4). The orbits are projected onto the x–y plane. The controlled eigenvalue is assigned to $\hat{\mu} = -0.9$ and the feedback coefficient is calculated to be $k = -0.0465$. The parameters are fixed at $(\alpha, \beta, \delta) = (0.79, 0.02, 0.06)$

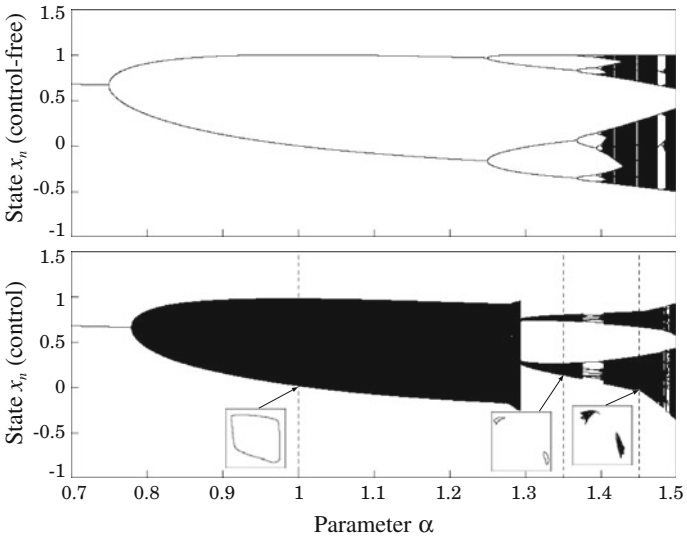

Fig. 8.10 Bifurcation diagrams of control-free system (*top*) and control system by the pole assignment method (*bottom*). We use α as the bifurcation parameter. *Boxes* show orbits on the x–y plane for corresponding α shown by *vertical dashed lines*. The controlled eigenvalue is $\hat{\mu} = -0.9$. The other parameters are fixed at $(\beta, \delta) = (0.02, 0.06)$

determined directly from the system parameters, the control method can be applied to a variety of parameter values more easily than the previous methods. In Fig. 8.10, we compare the bifurcation diagram of the control system to that of the control-free system. In the control-free system, the period-doubling bifurcation to chaotic orbits is observed. In the control system, a quasi-periodic orbit on an invariant closed curve, which is the target orbit, can be observed for a wide range of parameter values. However, besides the invariant closed curve, we observe a period-2 quasi-periodic orbit (double closed curves) and a chaotic orbit. Since this control method does not stabilize the quasi-periodic orbit directly, nor does it prevent the orbit from changing its stability, the orbit stabilization is not always guaranteed. In general, this control method is applicable to only parameter values in neighborhood of the Neimark-Sacker bifurcation in which the unstable quasi-periodic orbit does not disappear.

8.7 Conclusions

We have applied three control methods, the external force control, the delayed feedback control, and the pole assignment method, to stabilize an unstable quasi-periodic orbit. From the viewpoint of stabilization control, the reproducibility of the unstable quasi-periodic orbit is an important factor. In the delayed feedback control, however, there is an inevitable difference between the controlled and unstable quasi-periodic

Table 8.2 Reproducibility of unstable quasi-periodic orbit and prior knowledge of control

	External force control	Delayed feedback control	Pole assignment
Reproducibility	High	Middle	Low
Prior knowledge	Large (orbit)	Middle (rotation number)	Small (fixed point)

orbits because a quasi-periodic orbit is almost periodic and there is a delay mismatch between the delayed state and the current state. In the pole assignment method, since the control is applied to a fixed point, the stabilization of the unstable quasi-periodic orbit is indirect and an intrinsically distinct quasi-periodic orbit is stabilized.

On the other hand, prior knowledge required to stabilize the unstable quasi-periodic orbit is also an important factor. The external force control is the most direct method for the stabilization. However, this method requires the unstable quasi-periodic orbit itself as the external force constructed in advance. In the delayed feedback control, although calculation of the rotation number from the unstable quasi-periodic orbit is required, suitable delays may be found by applying the delayed feedback control exhaustively to many delays. On the other hand, since the pole assignment method involves the control to a fixed point, we can apply advanced control theory in which the control is feasible even if there is no adequate knowledge of the system. In Table 8.2, we summarize the three control methods from the viewpoint of the reproducibility of the unstable quasi-periodic orbit and the prior knowledge to control it. Since these factors have a trade-off relationship, it is necessary to choose a method by considering the required reproducibility.

References

1. Bruin, H.: Numerical determination of the continued fraction expansion of the rotation number. Physica D: Nonlinear Phenomena **59**(1–3), 158–168 (1992). http://dx.doi.org/10.1016/0167-2789(92)90211-5
2. Ciocci, M.C., Litvak-Hinenzon, A., Broer, H.: Survey on dissipative KAM theory including quasi-periodic bifurcation theory based on lectures by Henk Broer. In: Montaldi, J., Ratiu, T. (eds.) Peyresq Lectures in Geometric Mechanics and Symmetry. Cambridge University Press, Cambridge (2005)
3. Eckmann, J.P., Ruelle, D.: Ergodic theory of chaos and strange attractors. Rev. Mod. Phys. **57**, 617–656 (1985). doi:10.1103/RevModPhys.57.617
4. Fujisaka, H., Yamada, T.: Stability theory of synchronized motion in coupled-oscillator systems. Prog. Theor. Phys. **69**(1), 32–47 (1983). doi:10.1143/PTP.69.32
5. Ichinose, N., Komuro, M.: Delayed feedback control and phase reduction of unstable quasi-periodic orbits. Chaos: Interdisc. J. Nonlinear Sci. **24**, 033137 (2014). http://dx.doi.org/10.1063/1.4896219
6. Kamiyama, K., Komuro, M., Endo, T.: Algorithms for obtaining a saddle torus between two attractors. I. J. Bifurcat. Chaos **23**(9), 1330032 (2013). http://dx.doi.org/10.1142/S0218127413300322
7. Kaneko, K.: Overview of coupled map lattices. Chaos: Interdisc. J. Nonlinear Sci. **2**(3), 279–282 (1992). http://dx.doi.org/10.1063/1.165869

8. Khinchin, A., Eagle, H.: Continued Fractions. Dover Books on Mathematics. Dover Publications, New York (1997)
9. MacKay, R.: A simple proof of Denjoy's theorem. Math. Proc. Cambridge Philos. Soc. **103**(2), 299–303 (1988)
10. Ott, E., Grebogi, C., Yorke, J.A.: Controlling Chaos. Phys. Rev. Lett. **64**, 1196–1199 (1990). doi:10.1103/PhysRevLett.64.1196
11. Pavani, R.: The numerical approximation of the rotation number of planar maps. Comput. Math. Appl. **33**(5), 103–110 (1997). http://dx.doi.org/10.1016/S0898-1221(97)00023-0
12. Pecora, L.M., Carroll, T.L., Johnson, G.A., Mar, D.J., Heagy, J.F.: Fundamentals of synchronization in chaotic systems, concepts, and applications. Chaos: Interdisc. J. Nonlinear Sci. **7**(4), 520–543 (1997). http://dx.doi.org/10.1063/1.166278
13. Pyragas, K.: Continuous control of chaos by self-controlling feedback. Phys. Lett. A **170**(6), 421–428 (1992). http://dx.doi.org/10.1016/0375-9601(92)90745-8
14. Veldhuizen, M.V.: On the numerical approximation of the rotation number. J. Comput. Appl. Math. **21**(2), 203–212 (1988). http://dx.doi.org/10.1016/0377-0427(88)90268-3
15. Wonham, W.: On pole assignment in multi-input controllable linear systems. IEEE Trans. Autom. Control **12**(6), 660–665 (1967). doi:10.1109/TAC.1967.1098739

Chapter 9
Feedback Control Method Based on Predicted Future States for Controlling Chaos

Miki U. Kobayashi, Tetsushi Ueta and Kazuyuki Aihara

9.1 Introduction

Control theory is established and interdisciplinary fields in engineering, physics, life science and mathematics and so on. The main purpose of control theory is to make a system desirable by putting inputs to the system.

In the past two decades, chaos control for changing a chaotic state to a periodic state in a system got attention in control theory [1]. There are two main methods of chaos control. The strategy of both control methods is that a chaotic state is changed to a periodic state in a system by stabilizing an unstable periodic orbit embedded in a chaotic attractor. The first one which was proposed by Ott, Grebogi and Yorke (the OGY method) is based on the stable manifold structure of an unstable periodic orbit embedded in a chaotic attractor [2]. The advantage of this method is that the control method is available with small control inputs. However, the OGY method requires the solution of the unstable periodic orbit, which is very hard in experiments. Many extensions and applications of the OGY method have been studied [1, 3, 4]. The second one which was proposed by Pyragas (the DFC method) is based on the time-delayed control inputs [5]. The DFC method is the simple but efficient tool to control

M.U. Kobayashi (✉)
WPI-AIMR, Tohoku University,
2-1-1 Katahira Aoba-ku, Sendai, Miyagi 980-8577, Japan
e-mail: miki@wpi-aimr.tohoku.ac.jp

T. Ueta
Center for Administration of Information Technology, Tokushima University,
2-1 Minamijosanjima, Tokushima 770-8506, Japan
e-mail: ueta@tokushima-u.ac.jp

K. Aihara
Institute of Industrial Science, The University of Tokyo,
4-6-1 Komaba, Tokyo, Japan
e-mail: aihara@sat.t.u-tokyo.ac.jp

K. Aihara et al. (eds.), *Analysis and Control of Complex Dynamical Systems*,
Mathematics for Industry 7, DOI 10.1007/978-4-431-55013-6_9

a chaotic state to a periodic one [1, 6–8]. In contrast to the former one, the DFC method can be easily applied to experiments, because the solution of the unstable periodic orbit is not required. However, it is difficult to analyze the linear stability for a system with delayed feedback control inputs due to infinite dimension of the system with the inputs. Furthermore, there is the limitation in the DFC method that unstable periodic orbits with an odd number of real Floquet multipliers greater than unity cannot be stabilized with the DFC method [9, 10]. Recently, several methods are proposed in order to circumvent this limitation, e.g. by suitable choices of feedback gain [11] and an oscillating feedback [12].

The prediction-based feedback control is also presented as a method for refuting the odd-number limitation [13, 14]. In the prediction-based feedback control, the control inputs $u(k)$ for stabilization of an unstable periodic orbit with the period T are determined by the difference between the future state and the current state: $u(k) = K(x(k+T) - x(k))$, where $x(k)$ denotes a state vector in a chaotic system at time k and K is a feedback gain. Note that $x(k+T)$ is the future state of the variable $x(k)$ in the system without control inputs. One of the advantages of this method is that the stability analysis for the prediction-based feedback control method is easier than that for the delayed feedback control method. Because the dimension of a system with the prediction-based feedback control inputs is the same with the dimension of the original system without the control inputs. Control parameters, e.g. the control gain, can be set up easily with the stability analysis. However, the exact future states in a chaotic system cannot be predicted in general because of unpredictability in a chaotic system. Without knowing the perfect model of the chaotic system, it would be impossible to predict the exact future state.

In order to avoid the difficulty, we propose a combined method of the prediction-based feedback control method and the nonlinear time series analysis for the prediction of future states in a system. Namely, we introduce the control inputs $u(k) = K(x_p(k+T) - x(k))$, where $x_p(k+T)$ is the state vector in a system without control inputs at $k+T$ which is predicted with a time series analysis. The difference from the prediction-based feedback control method is that our control inputs are based not on the exact future state $x(k+T)$ but on the predicted future state $x_p(k+T)$. There are many nonlinear time series analyses for the prediction of states in chaotic systems [15, 16]. In this chapter, we use the method of analogues which is the most fundamental method [17].

This chapter is organized as follows. In Sect. 9.2, we propose a new method for controlling chaos. In our method, we introduce control inputs on the basis of the predicted future states with the method of analogues which is one of the nonlinear time series analyses. In Sect. 9.3, we validate performance of our method by applying it to the logistic map and the Hénon map. Finally, in Sect. 9.4, we summarize our results.

9.2 Method

We consider an n-dimensional chaotic dynamical system with a p-dimensional control inputs $u(t)$:

$$x(k+1) = f(x(k), u(k)). \tag{9.1}$$

We choose control inputs to stabilize an unstable periodic orbit with period T which is embedded in a chaotic attractor as follow:

$$u(k) = K(x_p(k+T) - x(k)),$$

where K is a feedback gain and $x_p(k+T)$ is a predicted T-future state of the variable $x(k)$ in the system without control inputs. When the control inputs are chosen as $u(t) = K(x(k-T) - x(k))$, this control scheme corresponds to the delayed feedback control method [5], and when the control inputs are chosen as $u(t) = K(x(k+T) - x(k))$, this control scheme corresponds to the prediction-based feedback control method [13, 14]. Note that $x(k+T)$ is the future state of the variable $x(k)$ in the system without control inputs, that is $x(k+T) = f^T(x(k), 0)$.

In order to perform our control method, we predict a T-future state of the variable $x_{\text{system}}(k)$ in the system without control inputs, that is $x_{\text{system}}(k+1) = f(x_{\text{system}}(k), 0)$, by using the method of analogues which is a nonlinear time series analysis proposed by Lorenz as follows [17]. We define $x_p(k+T)$ as the predicted future state of $x_{\text{system}}(k)$ in the system without control inputs. First, we obtain time series data $x_{\text{data}}(k)$ in a chaotic dynamical system without control inputs, $x_{\text{data}}(k+1) = f(x_{\text{data}}(k), 0)(0 \leq k < t_p)$. The parameter t_p indicates the number of the data. Note that the initial condition of the time series data $x_{\text{data}}(0)$ is not necessarily the same with the initial condition of the system variables $x_{\text{system}}(0)$. Our purpose is to predict a future state of $x_{\text{system}}(k)$ in the system without control inputs from the time series data $x_{\text{data}}(k)$. Next, we find the nearest state $x_{\text{data}}(k^*)$ from the state vector $x(k)$ in the controlled system (Eq. (9.1)) in the sense of the Euclidean distance from the time series data $x_{\text{data}}(k)(0 \leq k < t_p)$. Finally, we assume $x_{\text{data}}(k^* + T)$ as the predicted future state $x_{\text{system}}(k+T)$ in the system without control inputs. Namely, we use $x_{\text{data}}(k^* + T)$ as the predicted future state $x_p(k+T)$. We apply $x_p(k+T)$ which is obtained by the method of analogues to the control inputs; namely, $u(k) = K(x_p(k+T) - x(k))$.

Here, we demonstrate the prediction with the method of analogues to discuss the accuracy of the method. Let's consider the logistic map; $x(k+1) = 3.99x(k)(1 - x(k))$. Now, we predict the future state of the variables $x_{\text{system}}(k)$ from the time series data $x_{\text{data}}(k)$, $(0 \leq k < t_p)$ by using the method of analogues. We take 0.31 as the initial condition of time series data $x_{\text{data}}(k)$ we use to predict dynamics of the logistic map. Namely, in order to obtain the data $x_{\text{data}}(k)$, we calculate the system $x_{\text{data}}(k+1) = f(x_{\text{data}}(k), 0)$, $(0 \leq k < t_p)$ with $x_{\text{data}}(0) = 0.31$, where $f(x(k), 0) = 3.99x(k)(1 - x(k))$. As a test, we predict $x_{\text{system}}(T)$ $(x_{\text{system}}(k+1) =$

Table 9.1 Dependence of the prediction error on the number of data t_p

t_p	$x_{\text{data}}(0)$	$x_{\text{system}}(0)$	Error between exact and predicted future states
$T = 1$			
1000	0.31	0.21	0.001
100	0.31	0.21	0.004
50	0.31	0.21	0.0252
10	0.31	0.21	0.151
$T = 5$			
1000	0.41	0.11	0.002
100	0.41	0.11	0.061
50	0.41	0.11	0.048
10	0.41	0.11	0.945
$T = 10$			
10,000	0.41	0.11	0.003
1000	0.41	0.11	0.198
100	0.41	0.11	0.536

$x_{\text{data}}(0)$ is the initial condition of the time series data we use for the prediction. $x_{\text{system}}(0)$ is the current state in the system we try to predict, that is we predict the state vector $x_{\text{system}}(T)$

$3.99x_{\text{system}}(k)(1 - x_{\text{system}}(k))$, $x_{\text{system}}(0) = 0.21$) from the time series data $x_{\text{data}}(k)$ $(0 \leq k < t_p)$ by the method of analogues. It is clear from Table 9.1 that the accuracy of the prediction become better and better as the number of data t_p gets larger and larger. Furthermore, longer time series data are needed in order to predict the longer-term future state.

The advantage of our control method is that we do not need to know the exact future states in a system without the control inputs, because we use the predicted future state $x_p(k+T)$ in stead of the exact future states $x(k+T)$. Thus, we can apply our method to experiments when we have long time series data in the experiments.

9.3 Application

9.3.1 Logistic Map

We stabilize unstable periodic orbits in the logistic map $x(k+1) = ax(k)(1-x(k))$ by our method which is explained in Sect. 9.2. It is found that the logistic map with some parameter a shows chaos. In this chapter, a is chosen as 3.99. The behavior of $x(k)$ with $a = 3.99$ is shown in Fig. 9.1. It shows that the system is fully developed chaos.

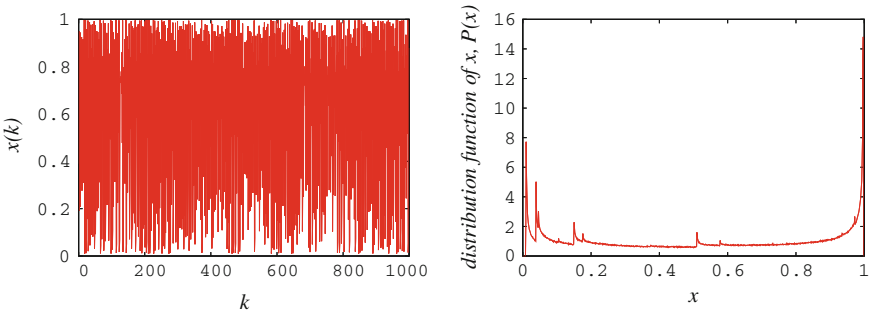

Fig. 9.1 *Left* Uncontrolled behavior $x(k)$ with $a = 3.99$. The system shows fully developed chaos. *Right* Distribution function of uncontrolled behavior

The controlled system is described as follow:

$$x(k+1) = ax(k)(1-x(k)) + K(x_p(k+T) - x(k)),$$

where $x_p(k+T)$ is the predicted future state of $x(k)$ in the system without control inputs, and K is a feedback gain. Since control inputs should be put in a neighborhood of the target orbit, we use the following switching control:

$$u(k) = \begin{cases} K(x_p(k+T) - x(k)), & \text{if} \quad |x(k-T) - x(k)| \leq 0.1, \\ 0, & \text{otherwise.} \end{cases} \tag{9.2}$$

As a numerical example, we demonstrate the stabilization of a fixed point x_{fp} of the logistic map. In order to determine a suitable feedback gain K, we perform the stability analysis of the fixed point in the system with the control inputs based on the exact future state. In the case of the control inputs based on the exact future state, we can solve the stability analysis easily. Here, we perform the stability analysis of a fixed point x_{fp} of the logistic map. The controlled system is described by $x(k+1) = ax(k)(1-x(k)) + K(ax(k)(1-x(k)) - x(k))$. The linearized system around the fixed point x_{fp} is given by

$$\delta x(k+1) = (-2a(1+K)x_{\text{fp}} + a + aK - K)\delta x(k),$$

where $\delta x(k) = x(k) - x_{\text{fp}}$. If K satisfies the following inequality

$$|(-2a(1+K)x_{\text{fp}} + a + aK - K)| < 1,$$

the fixed point x_{fp} is locally stable. In this chapter, in the case with $a = 3.99$, the fixed point $x_{\text{fp}} = 0.7493$, and K is chosen as -0.5 as the inequality is hold. Note that in our control scheme, this choice of K is neither a necessary nor sufficient condition for the stability of the fixed point, because our control inputs are not based on the

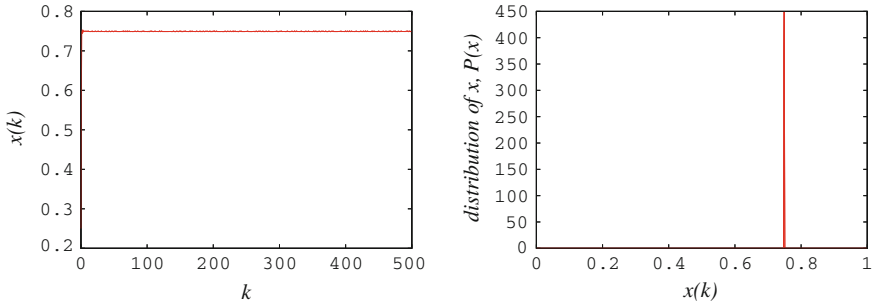

Fig. 9.2 *Left* Controlled behavior $x(k)$ with $a = 3.99$, $K = -0.5$, and $t_p = 1000$. *Right* Distribution function of controlled behavior

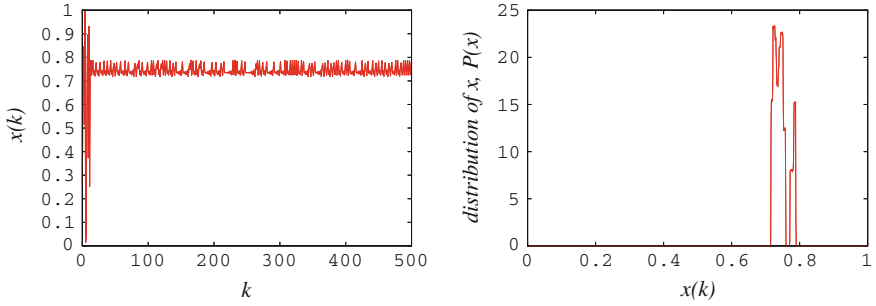

Fig. 9.3 *Left* Controlled behavior $x(k)$ with $a = 3.99$, $K = -0.5$, and $t_p = 50$. *Right* Distribution function of controlled behavior

exact future state but the predicted future state. However, it must be valid to choose K as the inequality is hold, if the prediction is good enough.

Figure 9.2 (left) shows the controlled behavior $x(k)$ with $a = 3.99$ where the prediction is estimated with time series data with $t_p = 1000$. The variable $x(k)$ of the controlled system is static. Figure 9.2 (right) shows the distribution function of $x(k)$ after putting the control inputs. The distribution has the sharp peak around the fixed point $x_{\mathrm{fp}} = 0.7493$. The distribution function indicates that the unstable fixed point in the uncontrolled system can be stabilized and the attractor in the controlled system is the fixed point.

Figure 9.3 (left) shows controlled behavior $x(k)$ with $a = 3.99$ where the prediction is estimated with time series data with $t_p = 50$. The variable $x(k)$ of the controlled system is not static but oscillate chaotically. In fact, the distribution function of $x(k)$ distributes around the fixed point $x_{\mathrm{fp}} = 0.7493$ in Fig. 9.3 (right). From the distribution function, it is clear that the controlled system is still chaotic. However, the distribution function is bounded in a narrow region, which means that this chaos is much "weaker" than one in the original system without the control inputs (see Fig. 9.1 (right)). In this sense, the control is still successful.

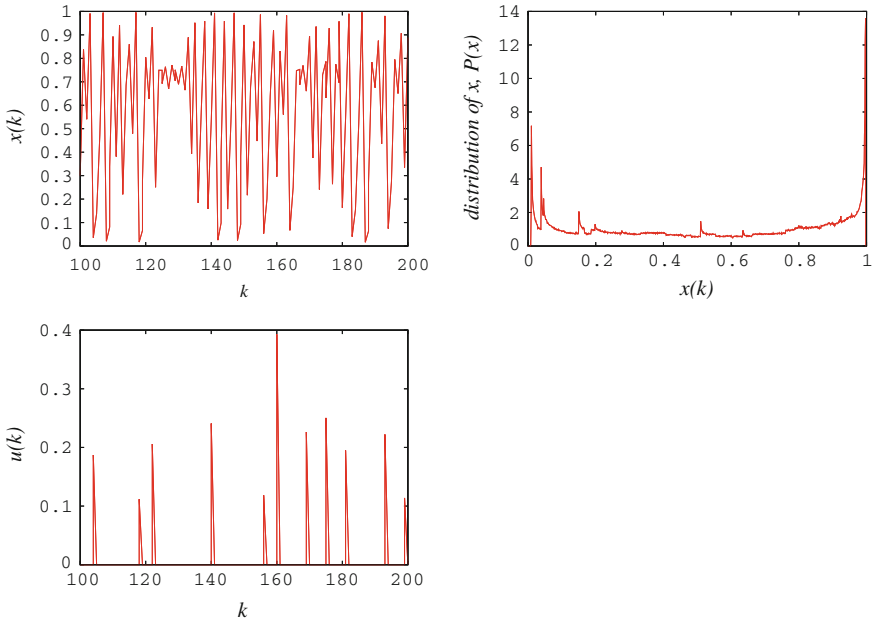

Fig. 9.4 *Upper left* Controlled behavior $x(k)$ with $a = 3.99$, $K = -0.5$, and $t_p = 10$. *Upper right* Distribution function of controlled behavior. *Lower left* Control input behavior

Figure 9.4 (upper left) shows the controlled behavior $x(k)$ with $a = 3.99$ where the prediction is estimated with time series data with $t_p = 10$. The variable $x(k)$ of the controlled system oscillates chaotically. The distribution function of $x(k)$ shows fully developed chaos as in Fig. 9.4 (upper right). In this case $t_p = 10$, the control inputs is applied to the system many times (see Fig. 9.4 (lower left)), but the control fails because of the small number of data.

We discuss how long the time series data we use for the prediction should be to stabilize the fixed point. Table 9.2 shows dependence of the success rate of our

Table 9.2 Dependence of the success rate of the method on the number of data t_p

The number of data t_p	The success rate of the method with various time series data (%)
1000	100
500	100
100	100
50	60
20	30
10	0

We define that the control becomes successful when the dispersion of the distribution of controlled behavior is smaller than 0.01

method on the number of data t_p. We define that the system is successfully controlled when the dispersion of the variable $x(k)$ in the controlled system is less than 0.01. We discuss the rate that the method becomes successful by using 10 different time series data which are calculated with randomly chosen 10 different initial conditions. We define the rate as the percentage that the control trials with 10 time series data become successful. From Table 9.2, the method is completely available when the number of data t_p is larger than 100.

In the case $a = 3.99$, the correlation time of this system is about 8. It is indicated that system does not become chaotic by using time series data with longer time than the correlation time.

9.3.2 Hénon Map

Here, we stabilize unstable periodic orbits in the Hénon map $x(k+1) = 1.4 - x(k)^2 + 0.3y(k)$, $y(k+1) = x(k)$. The Hénon map is a typical non-hyperbolic chaotic map (see Fig. 9.5).

we use the following switching control as is the case in the logistic map:

$$u(k) = \begin{cases} K(x_p(k+T) - x(k)), & \text{if } |x(k-T) - x(k)| \leq 0.1, \\ 0, & \text{otherwise.} \end{cases} \tag{9.3}$$

Fig. 9.6 (left) shows the controlled behavior $x(k)$ with $K = -0.5$ where the prediction is estimated with time series data with $t_p = 1000$. Figure 9.6 (right) shows the distribution function of $x(k)$ which has the sharp peak around the fixed point $x_{\text{fp}} = 0.63$. The distribution function indicates that the unstable fixed point in the controlled system is stabilized and the attractor in the controlled system is the fixed point.

Figure 9.7 (left) shows controlled behavior $x(k)$ with $K = -0.5$ where the prediction is estimated with time series data with $t_p = 100$. The variable $x(k)$ of the

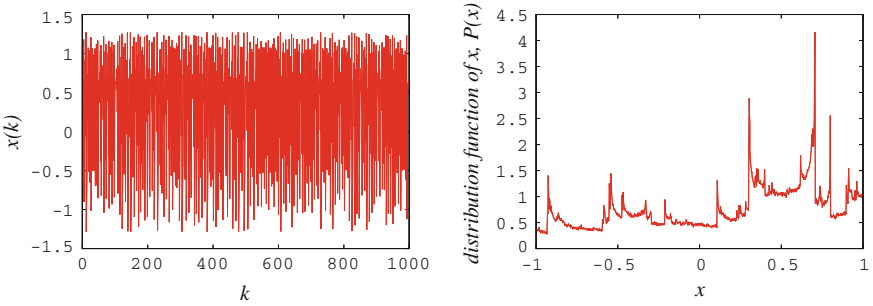

Fig. 9.5 *Left* Uncontrolled behavior $x(k)$. The system shows fully developed chaos. *Right* Distribution function of uncontrolled behavior

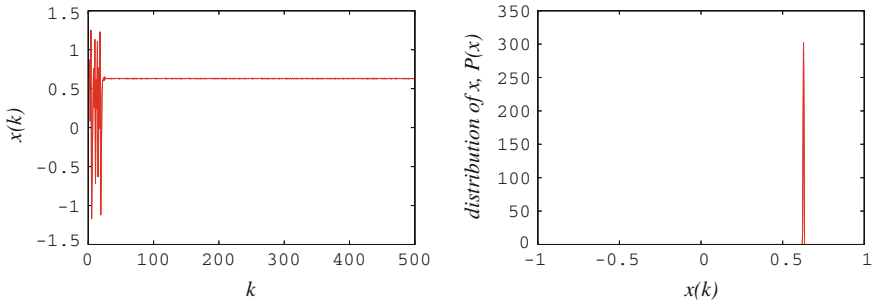

Fig. 9.6 *Left* Controlled behavior $x(k)$ with $K = -0.5$, and $t_p = 1000$. *Right* Distribution function of the controlled behavior

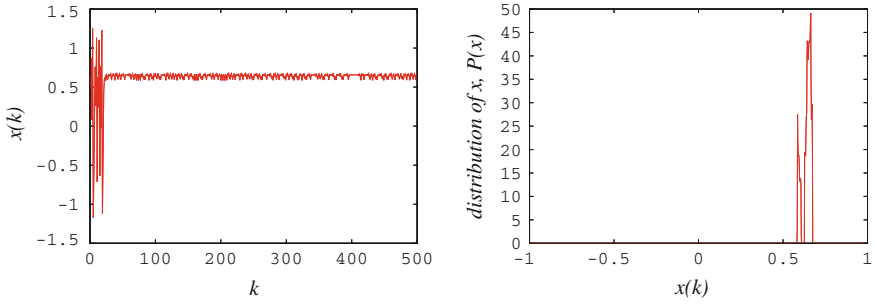

Fig. 9.7 *Left* Controlled behavior $x(k)$ with $K = -0.5$, and $t_p = 100$. *Right* Distribution function of the controlled behavior

controlled system is not static but oscillate chaotically. In fact, the distribution function of $x(k)$ distributes around the fixed point $f_{\text{fp}} = 0.63$ in Fig. 9.7 (right). From the distribution function, it is clear that that the controlled system is still chaotic. However, the distribution function is bounded in a narrow region, which means that chaos is much "weaker" than the original system without the control inputs as the same with the logistic map.

Figure 9.8 shows controlled behavior $x(k)$ with $K = -0.5$ where the prediction is estimated with time series data with $t_p = 10$. The variable $x(k)$ of the controlled system oscillates chaotically. The distribution function of $x(k)$ shows fully developed chaos in Fig. 9.8 (right). In this case $t_p = 10$, the control fails because of the lack of the enough number of data.

We discuss how long the time series we use should be to stabilize the fixed point. Table 9.3 shows dependence of the success rate of our method on the number of data t_p. We define that the system is successfully controlled when the dispersion of the variable $x(k)$ in the controlled system is less than 0.01. The rate that the control trials become successful is defined by the same way with the logistic map. From Table 9.3, the method is completely available when the number of data t_p is larger than 200.

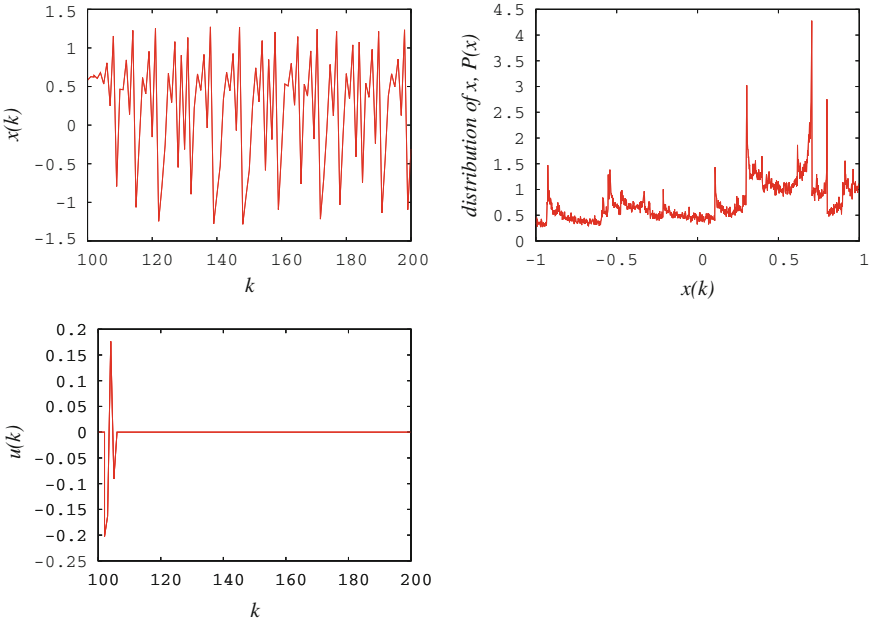

Fig. 9.8 *Upper left* Controlled behavior $x(k)$ with $K = -0.5$, and $t_p = 10$. *Upper right* Distribution function of the controlled behavior. *Lower left* Control input behavior

Table 9.3 Dependence of the success rate of the method on the number of data t_p

The number of data t_p	The success rate of the method with various time series data (%)
1000	100
500	100
200	100
100	80
50	30
20	0
10	0

We define that the control becomes successful when the dispersion of the distribution of controlled behavior is smaller than 0.01

9.4 Conclusions

We have proposed a new control method with a combination of the prediction-based feedback control method and the method of analogues which is one of nonlinear time series analyses.

The prediction-based feedback control method is useful when we can obtain the exact future states of a system. In general, it is impossible to obtain the exact future

states in a chaotic system, especially in experiments, due to its orbital instability. On the other hand, our method is applicable even if we do not know the exact future states. The only necessary information for our control scheme is enough long time series data in the system to predict future states. Whether our scheme becomes successful or not depends on how good we can predict the future states in the system. In this chapter, we use the method of analogues in order to predict the future states. The method is the simplest method for the prediction of time series in chaotic systems. Nevertheless, our control scheme with the method of analogues is useful in chaotic systems. When we use more advanced methods for the prediction, e.g. the nonlinear time series analysis based on radial basis function [16], our control scheme must be improved.

The Prediction-based control method can be also applied to continuous-time chaotic systems [18]. We will report applications of our method to continuous-time chaotic systems and chaotic systems with a large degrees of freedom in another paper.

Acknowledgments M.U.K is partially supported by World Premier International Research Center Initiative (WPI), MEXT, Japan, and T.U. is partially supported by JSPS KAKENHI Grant Number 25420373.

References

1. Schuster, H.F. (ed.): Handbook of Chaos Control. Wiley, Weinheim (1999)
2. Ott, E., Grebogi, C., Yorke J.A.: Controlling chaos. Phys. Rev. Lett. **64**, 1196–1199 (1990)
3. Romeiras, F.J., Grebogi, C., Ott, E., Dayawansa, W.P.: Controlling chaotic dynamical systems. Phys. D **58**, 165–192 (1992)
4. Shinbrot, T., Grebogi, C., Ott, E., Yorke, J.A.: Using small perturbation to control chaos. Nature **363**, 411–417 (1993)
5. Pyragas, K.: Continuous control of chaos by self-controlling feedback. Phys. Lett. A **170**, 421–428 (1992)
6. Just, W.: Delayed feedback control of periodic orbits in autonomous systems. Phys. Rev. Lett. **81**, 562–565 (1998)
7. Bielawski, S., Derozier, D., Glorieux, P.: Controlling unstable periodic orbits by a delayed continuous feedback. Phys. Rev. E **49**, R971 (1994)
8. Kobayashi, U.M., Aihara, K.: Delayed feedback control method for dynamical systems with chaotic saddles. AIP Conf. Proc. **1468**, 207–2015 (2012)
9. Just, W., Bernard, T., Ostheimer, M., Reibold, E., Benner, H.: Mechanism of time delayed feedback control. Phys. Rev. Lett. **78**, 203–206 (1997)
10. Nakajima. H.: On analytical properties of delayed feedback control of chaos, Phys. Lett. A. **232** 207–210 (1997)
11. Fiedler, B., Flunkert, V., Georgi, M., Hövel, P., Schöll, E.: Refuting the odd-number limitation of time-delayed feedback control. Phys. Rev. Lett. **98** 114101-1–114101-4 (2007)
12. Schuster, H.G., Stemmler, M.B.: Control of chaos by oscillating feedback. Phys. Rev. E **56**, 6410 (1997)
13. Vieira, M.de S., Lichtenberg, A.J.: Controlling chaos using nonlinear feedback with delay. Phys. Rev. E **54**, 1200–1207 (1996)
14. Ushio, T., Yamamoto, S.: Prediction-based control of chaos. Phys. Lett. A **264**, 30–35 (1999)
15. Sugihara, G., May, R.M.: Nonlinear forecasting as a way of distinguishing chaos from measurement error in time series. Nature **344**, 734–741 (1990)

16. Casdagli, M.: Nonlinear prediction of chaotic time series. Phys. D **35**, 335–356 (1989)
17. Lorenz, E.N.: Atmospheric predictability as revealed by naturally occurring analogues. J. Atmos. Sci. **26**, 636–646 (1969)
18. Boukabou, A., Chebbah, A., Mansouri, N.: Predictive control of continuous chaotic systems. Int. J. Bifurcat. Chaos **18**, 587–592 (2008)

Chapter 10
Ultra-discretization of Nonlinear Control Systems with Spatial Symmetry

Masato Ishikawa and Takuto Kita

10.1 Introduction

Nonlinear control systems, as well as nonlinear dynamical systems in general, are usually referred to nonlinear ordinary differential equations expressed by $\dot{x} = f(x, u)$, where $x \in M$ is its state, M is a smooth manifold of states, $u \in U \subset \mathbb{R}^m$ is the control input included in the set of admissible controls U, and f if a smooth mapping $f : M \times U \to TM$.

Now, let us think of its *discrete alternative in full sense*, i.e., behavior of a system whose variables are all discrete with respect to *spacio-temporal* axes. Suppose M_d is a finite set corresponding to a discrete version of the state space, U_d is also a finite set of admissible control symbols. Then consider a discrete-valued *difference* equation

$$x[k+1] = f_d(x[k], u[k]), \quad x \in M_d,\ u \in U_d,\ f_d : M_d \times U_d \to M_d$$

where $k \in \mathbb{Z}$ denotes the time step instead of the continuous time $t \in \mathbb{R}$. This approach is often called em ultra-discretization, mainly along the context of mathematical analysis of integrable systems such as various soliton equations [3]. The prefix *ultra*-distinguishes the problem from so-called discrete-time systems, in the sense that the dependent variable x is supposed discrete, as well as the independent variable k. Upon facing to these ultra-discrete control systems, we are naturally led to discuss which sort of controller *design* framework (i.e., how to design a state

M. Ishikawa (✉) · T. Kita
Department of Mechanical Engineering, Osaka University,
2-1 Yamadaoka, Suita, Osaka 565-0871, Japan
e-mail: ishikawa@mech.eng.osaka-u.ac.jp

T. Kita
Denso Co. Ltd., Kosai, Japan

K. Aihara et al. (eds.), *Analysis and Control of Complex Dynamical Systems*,
Mathematics for Industry 7, DOI 10.1007/978-4-431-55013-6_10

feedback law $u[k] = k(x[k])$ to fulfill the design requirement) can be established. This is the central motivation in this chapter.

It would be technically possible to develop systems theory for *general* class of M_d, U_d and f_d. However, in this chapter, we dare to confine ourselves to a specific class of systems in the following manners:

- M_d is not only a mere collection of elements, but is associated with some structure such as *symmetry*.
- There exist some *first principles* behind the system dynamics. In other words, f_d should be derived from some discrete version of first principles, not by straightforward discretization of f (see Fig. 10.4 below).

From these points of view, in this chapter, we consider to discuss discrete-valued alternative of *planar locomotion* of rigid bodies. Planar locomotion is inherently symmetric under isometric transformation, i.e., invariant under action of translation and rotation without mirror reflection. The set of such a transformation is identified with the special Euclidean transformation group, say $\mathbb{SE}(2)$, parameterized by $\{(x, y, \theta) | x \in \mathbb{R}, y \in \mathbb{R}, \theta \in \mathbb{S}\} \simeq \mathbb{R}^2 \times \mathbb{S}$. The configuration space of the vehicle $\mathbb{SE}(2)$ is supposed to be discretized as a hexagonal cellular space [6], while the shape space (or joint space, usually referred to $\mathbb{T}^n$) is also discretized as $\mathbb{Z}_6^n$ of modular arithmetic.

Control problems in planar locomotion have been attracting much interest of nonlinear control theorists and robotics researchers since early 90s. Some notable properties of such a system include: (1) the set of equilibria forms a submanifold of the state space rather than an isolated point, (2) any equilibrium cannot be asymptotically stabilized by continuous state feedback as pointed out by Brockett [2], (3) nevertheless the equilibrium can be reached from its neighborhood if it satisfies the Lie algebra rank condition [10]. As the conventional control theory of planar locomotion is based on nonintegrable nature of kinematic constraints, we start from considering a discrete-valued version of nonholonomic constraints (an integer-valued equation of integer variables), then discuss how the admissible motion that satisfies the constraint look, compared to the continuous ones. Here we re-emphasize that the issue addressed here is (relevant, though) different from a *discretization* of continuous nonlinear systems or nonlinear *sampled-data* systems [1, 7, 9, 13]. In other words, the resulting behavior can rather be viewed as a special class of *cellular automata* [11, 12]. Our standpoint is just to observe what should happen, starting from the discrete constraints as principal rules. This chapter partially includes the results obtained by the authors, reported in [4].

In the rest of the chapter, $t \in \mathbb{R}$ denotes the time in continuous case, while $k \in \mathbb{Z}$ denotes the time *step* in discrete case. Moreover, we often use the following short-form notation, $C_i := \cos\theta_i$, $S_i := \sin\theta_i$, $C_{ij} := \cos(\theta_i - \theta_j)$ and $S_{ij} := \sin(\theta_i - \theta_j)$ to save the space.

10.2 Basic Properties on the Hexagonal Cellular Space

10.2.1 Coordinate Settings

Suppose a tessellation of two-dimensional euclidean space $\mathbb{R}^2$ with *unit hexagons*, as shown in Fig. 10.1. Let O be a center of a hexagon. The x-axis is the line passing through O which is assumed perpendicular to the edge of a hexagon, while y-axis passes through one of its vertex (alternative definition can be possible). Here we introduce the following three constants will play important roles throughout this chapter,

$$\alpha = \frac{1}{2},\ \beta = \frac{\sqrt{3}}{2},\ \gamma = \frac{\pi}{3},$$

which satisfy following elementary relations

$$\alpha^2 + \beta^2 = 1,\ \alpha^2 - \beta^2 = -\alpha.$$

Each cell is identified with the (x, y)-position of its center, e.g., (α, β), $(1 + \alpha, \beta)$ or $(2, 2\beta)$ in Fig. 10.1.

For θ refers to an angle on this space, it should be confined to $0, \pm\gamma, \pm 2\gamma, \pm 3\gamma, \ldots$, where 3γ and -3γ are identified to each other. As slight abuse of notation, we identify γi ($i \in \mathbb{Z}$) with i itself, as long as it causes no confusion. In other words, the space of angles is identified with the set of integers modulo 6:

$$\mathbb{Z}_6 = \{0, 1, 2, 3, 4, 5\} \equiv \{0, \pm 1, \pm 2, 3\},$$

The integer $3 \in \mathbb{Z}_6$ will be treated as discrete counterpart of $\pi \in \mathbb{S}$. Similarly, $\cos\theta$ actually implies $\cos\gamma\theta$ for any discrete angle $\theta \in \mathbb{Z}_6$. The cosine and sine of discrete angles are summarized in Fig. 10.2. Fundamental trigonometric identities, such as angle addition formulae, naturally hold as in the continuous case.

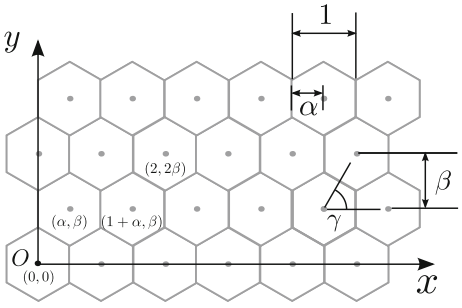

Fig. 10.1 Coordinate settings on the hexagonal cellular space and the unitary constants used for the coordinates

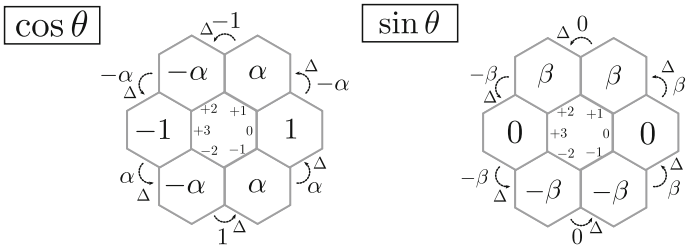

Fig. 10.2 Cosine (*left*) and sine (*right*) functions defined on the hexagonal cells. The symbols shown in the cells indicate values of functions at corresponding direction (e.g., $\cos(1) = \alpha$). Symbols shown between two cells indicate their differences (e.g., $\cos(2) - \cos(1) = (-\alpha) - \alpha = -1$.)

In summary, we define the whole configuration space of planar rigid body, say $\mathbb{SE}_H(2)$, as follows:

$$\mathbb{SE}_d(2) = \left\{ \begin{bmatrix} x \\ y \\ \theta \end{bmatrix} = \begin{bmatrix} n_x + \mathrm{odd}(y)\alpha \\ n_y \beta \\ n_\theta \end{bmatrix} \middle| \, n_x, n_y \in \mathbb{Z}, n_\theta \in \mathbb{Z}_6 \right\} \simeq \mathbb{Z} \times \mathbb{Z} \times \mathbb{Z}_6, \tag{10.1}$$

where $\mathrm{odd}(y)$ is 1 if y is an odd integer, 0 otherwise.

10.2.2 Basics of Difference Calculus in Concern

For a function $f(\theta)$, we define

$$\Delta_\theta f := f(\theta + \Delta\theta) - f(\theta),$$

where $|\Delta\theta| \leq 1$. $\Delta_\theta f$ is simply denoted by Δf if the argument is obvious. Note that Δf depends on both θ and $\Delta\theta$. By definition, $\Delta f = 0$ if $\Delta\theta = 0$.

Differentiation of trigonometric functions are derived as follows. First, note that cosine and sine of small angles are formulated by (see Fig. 10.2)

$$\cos\Delta\theta = 1 - \alpha\Delta\theta^2, \ \sin\Delta\theta = \beta\Delta\theta \quad (\text{if } |\Delta\theta| \leq 1).$$

Therefore

$$\begin{aligned} \cos(\theta + \Delta\theta) - \cos\theta &= \cos\theta\cos\Delta\theta - \sin\theta\sin\Delta\theta - \cos\theta \\ &= -\sin\Delta\theta\sin\theta + (\cos\Delta\theta - 1)\cos\theta \\ &= -\beta\Delta\theta\sin\theta - \alpha\Delta\theta^2\cos\theta, \end{aligned}$$

Table 10.1 Discrete version of calculus; differences of trigonometric functions for $|\Delta\theta| = 1$

$\Delta\cos\theta$						
	$\theta=-2$	$\theta=-1$	$\theta=0$	$\theta=1$	$\theta=2$	$\theta=3$
$\Delta\theta=1$ (i.e., $\cos(\theta+1)-\cos\theta$)	1	α	$-\alpha$	-1	$-\alpha$	α
$\Delta\theta=-1$ (i.e., $\cos(\theta-1)-\cos\theta$)	$-\alpha$	-1	$-\alpha$	α	1	α
$\Delta\sin\theta$						
$\Delta\theta=1$ (i.e., $\sin(\theta+1)-\sin\theta$)	0	β	β	0	$-\beta$	$-\beta$
$\Delta\theta=-1$ (i.e., $\sin(\theta-1)-\sin\theta$)	β	0	$-\beta$	$-\beta$	0	β

$$\begin{aligned}\sin(\theta+\Delta\theta)-\sin\theta &= \sin\theta\cos\Delta\theta+\cos\theta\sin\Delta\theta-\sin\theta\\ &= \sin\Delta\theta\cos\theta+(\cos\Delta\theta-1)\sin\theta\\ &= \beta\Delta\theta\cos\theta-\alpha\Delta\theta^2\sin\theta.\end{aligned}$$

Thus we have the basic difference formulae

$$\Delta\cos\theta = -\beta\Delta\theta\sin\theta-\alpha\Delta\theta^2\cos\theta, \tag{10.2}$$

$$\Delta\sin\theta = \beta\Delta\theta\cos\theta-\alpha\Delta\theta^2\sin\theta. \tag{10.3}$$

In contrast to continuous differentiation, we should note that the differences are *neither linear nor symmetric with respect to* $\Delta\theta$, due to the presence of $\Delta\theta^2$. This asymmetry will yield the discrepancy between the continuous and discrete cases in the following discussion. Moreover, differential algebraic relations such as $(\sin\theta)' = \cos\theta$ and $(\cos\theta)' = -\sin\theta$ do not hold in the discrete case, while the following phase shift relations are satisfied (Table 10.1):

$$\begin{aligned}\Delta\cos\theta &= \cos(\theta+2\Delta\theta),\\ \Delta\sin\theta &= \sin(\theta+2\Delta\theta).\end{aligned}$$

10.3 Locomotion Under Nonholonomic Constraints

10.3.1 Derivation of the Continuous Single-Cart Model

Let us start with a simple example concerning planar locomotion of single rigid body, which we call a *single cart*, shown in Fig. 10.3(left). The state vector of this system is $\xi = (x_0, y_0, \theta_0) \in \mathscr{X}$, $\mathscr{X} := \mathbb{SE}(2)$ where (x_0, y_0) implies its position and θ_0 implies its orientation angle relative to the x-axis. We assume that the cart is not permitted to slide sideways. This means the *nonholonomic constraint*

$$\dot{y_0}\cos\theta_0 - \dot{x_0}\sin\theta_0 = 0 \tag{10.4}$$

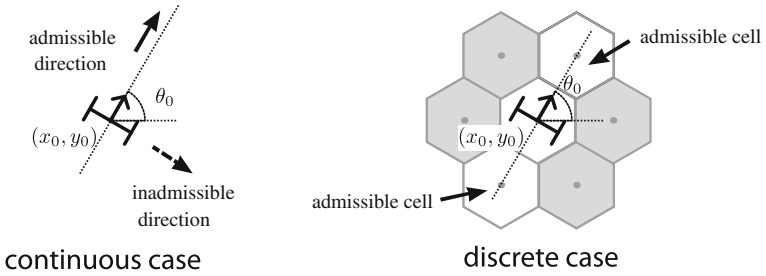

Fig. 10.3 Single cart: nonholonomic constraint imposed by the rolling wheels

should be satisfied. The state equation, derived from the kinematic relation, is given by the following differential equation

$$\dot{\xi} = g_1(\xi)u_1 + g_2(\xi)u_2, \tag{10.5}$$

$$g_1(\xi) := \begin{pmatrix} \cos\theta_0 \\ \sin\theta_0 \\ 0 \end{pmatrix}, \quad g_2(\xi) := \begin{pmatrix} 0 \\ 0 \\ 1 \end{pmatrix},$$

where $u_1 \in \mathbb{R}$ is the forwarding velocity and $u_2 \in \mathbb{R}$ is the heading angular velocity. Each point $\xi \in \mathscr{X}$ can be an equilibrium by setting $u = 0$. Brockett's stabilizability theorem [2] tells us that this system is *not asymptotically stabilizable* by any smooth time-invariant state feedback law. This system, in turn, is called *controllable* if any two equilibria can be reached from each other [10]. This is indeed satisfied since its controllability Lie algebra

$$\mathscr{C}(\xi) := \mathrm{span}\{g_1(\xi), g_2(\xi), [g_1, g_2](\xi)\} \tag{10.6}$$

has dimension 3 at $\forall\xi \in \mathscr{X}$, where

$$[g_1, g_2](\xi) := \frac{\partial g_2}{\partial \xi} g_1 - \frac{\partial g_1}{\partial \xi} g_2 = \begin{pmatrix} \sin\theta_0 \\ -\cos\theta_0 \\ 0 \end{pmatrix}.$$

10.3.2 Derivation of the Discrete Version

Now let us discuss what happens if the single cart is placed on the hexagonal cellular space (Fig. 10.3, right). The state vector of this system is $\xi = (x_0, y_0, \theta_0)$ as the same as in the continuous case, but it must be an element of $\mathscr{X} = \mathbb{SE}_H(2)$.

Next, let us think of a condition which prevents the cart from sliding sideways. Let Δx_0 denote the progress of the variable x_0 from the current step k to the next step $k + 1$, i.e.,

$$\Delta x_0 = x_0[k+1] - x_0[k]. \tag{10.7}$$

Δy_0 and $\Delta\theta_0$ are defined in the same manner. Then the discrete version of the nonholonomic constraint is given by

$$\Delta y_0 \cos\theta_0 - \Delta x_0 \sin\theta_0 = 0. \tag{10.8}$$

Suppose $u_1 \in \{-1, 0, 1\}$ is the forwarding velocity and $u_2 \in \{-1, 0, 1\}$ is the heading angular velocity. Then the state equation of the cart is immediately obtained as

$$\begin{pmatrix} \Delta x_0 \\ \Delta y_0 \\ \Delta\theta_0 \end{pmatrix} = \begin{pmatrix} \cos\theta_0 \\ \sin\theta_0 \\ 0 \end{pmatrix} u_1 + \begin{pmatrix} 0 \\ 0 \\ 1 \end{pmatrix} u_2, \tag{10.9}$$

or equivalently,

$$\Delta\xi = g_1(\xi)u_1 + g_2(\xi)u_2, \tag{10.10}$$

$$g_1(\xi) := \begin{pmatrix} \cos\theta_0 \\ \sin\theta_0 \\ 0 \end{pmatrix}, \quad g_2(\xi) := \begin{pmatrix} 0 \\ 0 \\ 1 \end{pmatrix}.$$

The process of this derivation is summarized in Fig. 10.4. What we have derived here is an integer-valued difference equation *that satisfies the discrete nonholonomic constraint* (10.8), which should be distinguished from a direct discretization of the continuous differential equation (10.5) although it apparently seems to be.

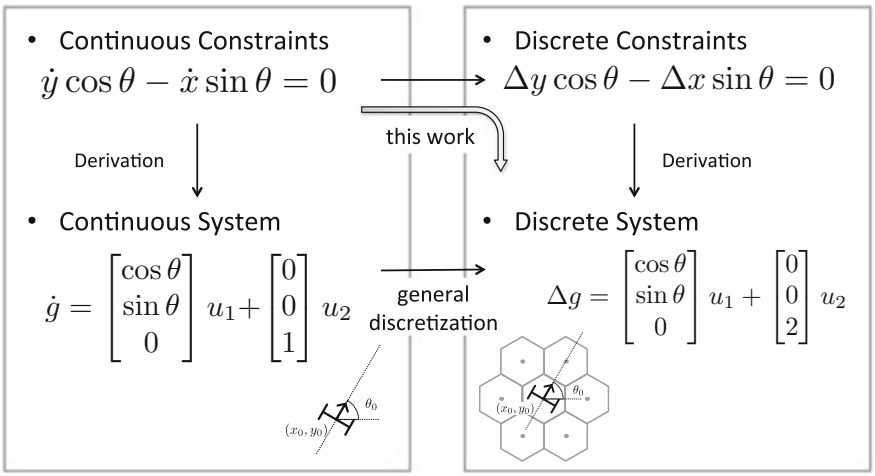

Fig. 10.4 Overview of the discretization approach in this work. At first, the continuous constraint (nonholonomic velocity constraint) is replaced by its discrete couterpart, then the description of dynamics (state equation) is derived which conform to the constraint

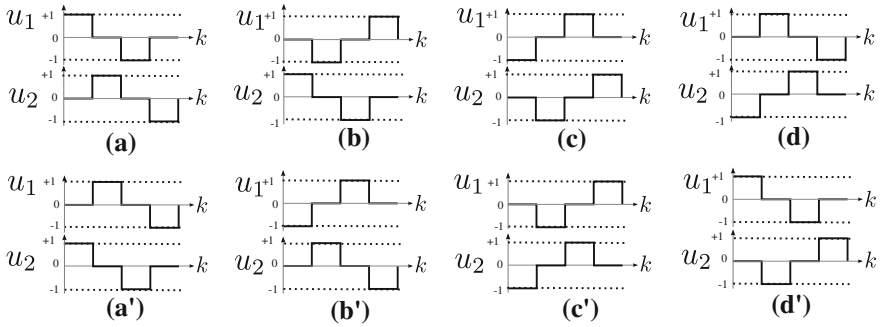

Fig. 10.5 Primitive periodic input patterns. Sequence of control inputs $u_1[k], u_2[k] \in \{1, 0, -1\}$ are chosen so that each of their average over a period is zero

10.3.3 Holonomy and the Lie Bracket Motion

Using the discrete model of a single cart obtained above, let us investigate discrete version of *holonomy*, i.e., the net effect of periodic inputs. Figure 10.5 shows primitive 8 patterns of four step periodic input signals with unit amplitude. The input (a′) is the time-reversal signal of (a′) and vice versa, and so for other pairs.

Figure 10.6 shows the effect of these inputs starting from the origin. The effect of (a′) is just the opposite to that of (a) and so for the other pairs. In essence, the holonomy is split into two types, the effect of (a)(b) and that of (c)(d).

As an analogy from the continuous case, we expect it possible to analyze this effect by some discrete counterpart of Lie bracket. For this purpose, let us first define discrete version of Jacobian matrix.

$$\Delta g_1 = g_1(\xi + \Delta\xi) - g_1(\xi) = \begin{pmatrix} -\beta\Delta\theta_0 S_0 - \alpha\Delta\theta_0^2 C_0 \\ \beta\Delta\theta_0 C_0 - \alpha\Delta\theta_0^2 S_0 \\ 0 \end{pmatrix},$$

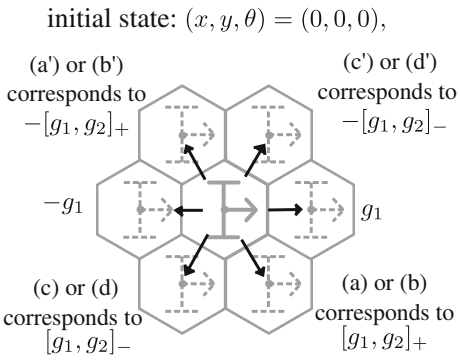

Fig. 10.6 Effect of Lie bracket; motions of the single cart resulting from the periodic input patterns

where $S_0 = \sin\theta_0, C_0 = \cos\theta_0$. The problem here is that Δg_1 is not linear with respect to $\Delta\xi$ due to the presence of $\Delta\theta_0^2$. Now, let us remember that $\Delta\theta_0^2$ may be replaced by the linear term, i.e., $\Delta\theta_0^2 = \Delta\theta_0$ if $\Delta\theta_0 \geq 1$, while $\Delta\theta_0^2 = -\Delta\theta_0$ if $\Delta\theta_0 \leq -1$. Then this leads us to define *two branches* of Jacobians $J_+(g_1)$ and $J_-(g_1)$, as follows:

$$J_+(g_1) := \begin{pmatrix} 0 & 0 & -\beta S_0 - \alpha C_0 \\ 0 & 0 & \beta C_0 - \alpha S_0 \\ 0 & 0 & 0 \end{pmatrix}, \quad J_-(g_1) := \begin{pmatrix} 0 & 0 & -\beta S_0 + \alpha C_0 \\ 0 & 0 & \beta C_0 + \alpha S_0 \\ 0 & 0 & 0 \end{pmatrix},$$

which enable us to rewrite Δg_1 as

$$\Delta g_1 = \begin{cases} J_+(g_1)\Delta\xi, & \text{if } \Delta\theta_0 \geq 0, \\ J_-(g_1)\Delta\xi, & \text{if } \Delta\theta_0 \leq 0. \end{cases}$$

Using J_+ and J_-, we can define the following two branches of Lie brackets:

$$[g_1, g_2]_+(\xi) := J_+(g_2)g_1 - J_+(g_1)g_2 = \begin{pmatrix} \beta S_0 + \alpha C_0 \\ -\beta C_0 + \alpha S_0 \\ 0 \end{pmatrix},$$

$$[g_1, g_2]_-(\xi) := J_-(g_2)g_1 - J_-(g_1)g_2 = \begin{pmatrix} \beta S_0 - \alpha C_0 \\ -\beta C_0 - \alpha S_0 \\ 0 \end{pmatrix}.$$

Their values at $\xi = 0$ are:

$$g_1(0) = \begin{pmatrix} 1 \\ 0 \\ 0 \end{pmatrix}, \; g_2(0) = \begin{pmatrix} 0 \\ 0 \\ 1 \end{pmatrix}, \; [g_1, g_2]_+(0) = \begin{pmatrix} \alpha \\ -\beta \\ 0 \end{pmatrix}, \; [g_1, g_2]_-(0) = \begin{pmatrix} -\alpha \\ -\beta \\ 0 \end{pmatrix},$$

which are consistent with the actual displacements shown in Fig. 10.6.

10.4 Connected Rigid Bodies: Locomotion Under both Nonholonomic and Holonomic Constraints

10.4.1 Cart-Trailer Systems

In this section, we consider planar locomotion of multiple rigid bodies connected to each other. Suppose a cart towing ℓ trailers as shown in Fig. 10.7(left). Each of the carts $0, \ldots, \ell - 1$ has a free joint on the center of its wheel axis, which connects the following cart to itself. The length of each connecting link is supposed to be 1. The state vector is

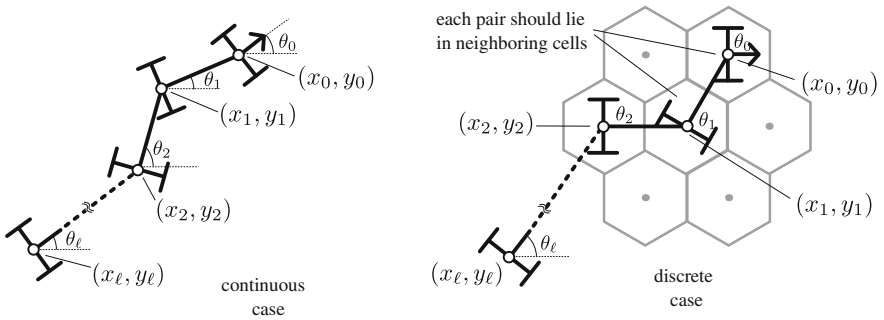

Fig. 10.7 Cart-trailer system is composed of a heading cart with articulated trailers, which undergoes holonomic constraints due to rigid linkage

$$\begin{aligned} \xi &= (x_0, y_0, \theta_0, \ldots, \theta_\ell)^{\mathsf{T}} \in \mathscr{X}, \\ \mathscr{X} &:= \mathbb{SE}(2) \times \mathbb{T}^{\ell-1}, \end{aligned}$$

where (x_0, y_0) denotes the position of the truck (cart 0) and θ_i denotes the orientation of the cart i for $i = 0, \ldots, \ell$. This system undergoes $\ell + 1$ nonholonomic constraints

$$\dot{y}_i \cos\theta_i - \dot{x}_i \sin\theta_i = 0, \quad i = 0, \ldots, \ell - 1 \tag{10.11}$$

and ℓ *holonomic constraints* of rigid linkage as well:

$$\begin{cases} x_i = x_{i+1} + \cos\theta_{i+1}, \\ y_i = y_{i+1} + \sin\theta_{i+1}, \end{cases} \quad i = 0, \ldots, \ell - 1.$$

We also have to pay attention to the joint limitation

$$|\theta_{i+1} - \theta_i| < \pi, \quad i = 0, \ldots, \ell - 1.$$

By taking all the constraints into account, the state equation is obtained as

$$\dot{\xi} = g_1(\xi)u_1 + g_2(\xi)u_2, \tag{10.12}$$

$$g_1(\xi) := \begin{pmatrix} \cos\theta_0 \\ \sin\theta_0 \\ 0 \\ -\sin(\theta_1 - \theta_0) \\ -\sin(\theta_2 - \theta_1)\cos(\theta_1 - \theta_0) \\ \vdots \end{pmatrix}, \quad g_2(\xi) := \begin{pmatrix} 0 \\ 0 \\ 1 \\ 0 \\ 0 \\ \vdots \end{pmatrix},$$

where u_1 is the forwarding velocity and u_2 is the heading angular velocity of the truck (cart 0). It is easy to show that this system is also controllable by analyzing its controllability Lie algebra.

10.4.2 Derivation of the Discrete Version

Now let us turn to consider the discrete counterpart (Fig. 10.7, right). Each cart is placed on the hexagonal cells, thus each joint angle is the difference between adjoining cart orientation, e.g., $\theta_{i+1} - \theta_i$. We also assume that the joint angles are limited to

$$|\theta_{i+1} - \theta_i| < 3, \quad i = 0, \ldots, \ell - 1.$$

The state vector is

$$\begin{aligned} \xi &= (x_0, y_0, \theta_0, \ldots, \theta_\ell)^{\mathsf{T}} \in \mathscr{X}, \\ \mathscr{X} &:= \mathbb{SE}_H(2) \times \mathbb{Z}_6^{\ell-1}. \end{aligned}$$

Control inputs are assigned to the velocity of the trucks, i.e., u_1 is the forwarding velocity and u_2 is the heading angular velocity of the front cart, respectively:

$$\begin{aligned} &\Delta x_0 C_0 + \Delta y_0 S_0 = u_1, \\ &\Delta\theta_0 = u_2 of. \end{aligned} \tag{10.13}$$

Nonholonomic constraint for the wheels are

$$\Delta y_i \, C_i - \Delta x_i \, S_i = 0, \quad i = 0, \ldots, \ell. \tag{10.14}$$

Holonomic constraints for rigid linkage are

$$\begin{cases} x_{i-1} = x_i + C_i, \\ y_{i-1} = y_i + S_i, \end{cases} \quad i = 1, \ldots, \ell. \tag{10.15}$$

The holonomic constraints should be kept satisfied in every step; hence the constraints in the next step

$$\begin{cases} (x_{i-1} + \Delta x_{i-1}) = (x_i + \Delta x_i) + \cos(\theta_i + \Delta\theta_i), \\ (y_{i-1} + \Delta y_{i-1}) = (y_i + \Delta y_i) + \sin(\theta_i + \Delta\theta_i) \end{cases} \tag{10.16}$$

should also hold for $i = 1, \ldots, \ell$. The state vector of this system is

$$\xi = (x_0, y_0, \theta_0, \ldots, \theta_\ell) \in \mathbb{SE}_H(2) \times \mathbb{Z}_6^{\ell-1}.$$

In order to obtain a difference equation for this system, we have to eliminate $\Delta x_1, \ldots, \Delta x_\ell,\ \Delta y_1, \ldots, \Delta y_\ell,\ x_1, \ldots, x_\ell,\ y_1, \ldots, y_\ell$ from (10.13)–(10.16) and derive explicit expression of $\Delta\xi$. (We eliminate 4ℓ variables from $5\ell + 3$ equations, resulting in $\ell + 3$ solutions). First, substituting (10.2), (10.3) and (10.15) into (10.16), we have

$$\begin{cases} \Delta x_{i-1} = \Delta x_i - \beta\Delta\theta_i S_i - \alpha\Delta\theta_i^2 C_i, \\ \Delta y_{i-1} = \Delta y_i + \beta\Delta\theta_i C_i - \alpha\Delta\theta_i^2 S_i, \end{cases}$$

or equivalently,

$$\begin{cases} \Delta x_i = \Delta x_0 + \sum_{j=1}^{i} \left(\beta\Delta\theta_i S_i + \alpha\Delta\theta_i^2 C_i\right), \\ \Delta y_i = \Delta y_0 + \sum_{j=1}^{i} \left(-\beta\Delta\theta_i C_i + \alpha\Delta\theta_i^2 S_i\right). \end{cases}$$

Computing $\Delta y_{i-1} C_i - \Delta x_{i-1} S_i$ leads us

$$\Delta y_{i-1} C_i - \Delta x_{i-1} C_i = \Delta y_i C_i - \Delta x_i S_i + \beta\Delta\theta_i = \beta\Delta\theta_i,$$

where the nonholonomic constraints (10.14) are used. Thus $\Delta\theta_i$ can be obtained by recursive computation

$$\begin{aligned} \beta\Delta\theta_i &= \Delta y_{i-1} C_i - \Delta x_{i-1} S_i \\ &= \Delta y_0 C_i - \Delta x_0 S_i - \sum_{j=1}^{i-1} \left(\beta\Delta\theta_j (C_i C_j + S_i S_j) + \alpha\Delta\theta_j^2 (S_i C_j - C_i S_j)\right) \\ &= -S_{i0} u_1 - \sum_{j=1}^{i-1} \left(\beta\Delta\theta_j C_{ij} - \alpha\Delta\theta_j^2 S_{ij}\right), \end{aligned} \tag{10.17}$$

where $C_{ij} = \cos(\theta_i - \theta_j)$, $S_{ij} = \sin(\theta_i - \theta_j)$.

10.4.2.1 Single Trailer

The simplest case is a single trailer system ($\ell = 1$), whose state vector is $\xi = (x_0, y_0, \theta_0, \theta_1)^\mathsf{T}$. The state equation is given by

$$\Delta\xi = g_1(\xi) u_1 + g_2(\xi) u_2,$$

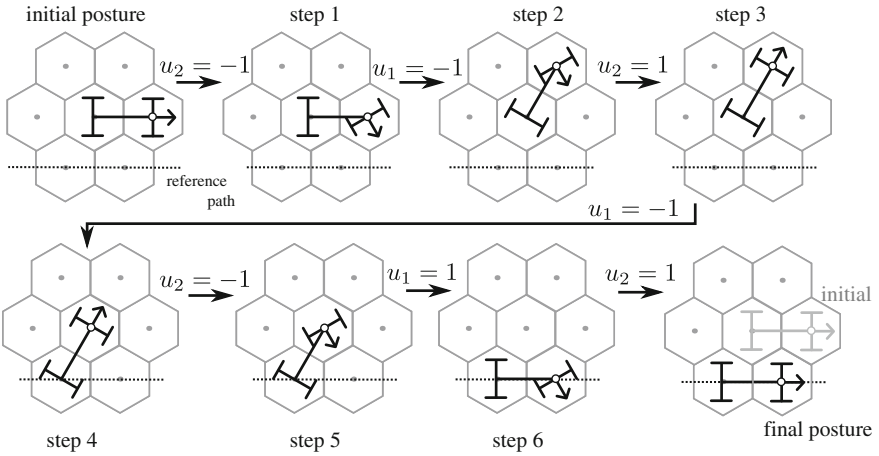

Fig. 10.8 Backward parking of the single trailer for linear reference path. The vehicle moves rightward in parallel from the initial position

$$g_1(\xi) = \begin{pmatrix} C_0 \\ S_0 \\ 0 \\ -S_{10}/\beta \end{pmatrix}, \quad g_2(\xi) = \begin{pmatrix} 0 \\ 0 \\ 1 \\ 0 \end{pmatrix}. \tag{10.18}$$

Forwarding motion this trailer system is not difficult to imagine from the single cart case. Backward motion is also possible, e.g., by a skillful steering shown in Fig. 10.8.

10.4.2.2 Double Trailers

When the cart is towing two trailers, i.e., if $\ell = 2$, the state vector is $\xi = (x_0, y_0, \theta_0, \theta_1, \theta_2)$. Behavior of the first four state variables is as exactly the same as in the previous case (10.18), while $\Delta\theta_2$ can be derived using (10.17) as follows:

$$\begin{aligned} \beta\Delta\theta_2 &= -S_{20}u_1 - \beta\Delta\theta_1 C_{21} - \alpha\Delta\theta_1^2 S_{21} \\ &= -S_{20}u_1 + \beta S_{21}C_{10}u_1\beta - \frac{\alpha}{\beta^2}S_{21}S_{10}^2u_1^2 \\ &= -S_{21}C_{10}u_1 - \frac{\alpha}{\beta^2}S_{21}S_{10}^2u_1^2. \end{aligned}$$

Note that the state equation is not linear with respect to u_1 any longer; this implies the system behavior changes depending on the sign of u_1.

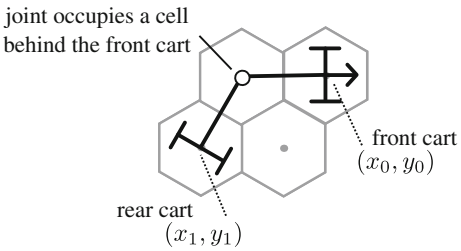

Fig. 10.9 Trailer with off-axle hitching; the joint is located in the middle of two carts

10.4.2.3 Trailer with Off-Axle Hitching

Suppose that the hinge joint is not precisely at the center of the rear axis (see Fig. 10.9). This configuration is so-called *off-axle hitching*, where its behavior is slightly different from the previous case. In this case, the holonomic constraint (10.15) is replaced by

$$\begin{cases} x_{i-1} = x_i + C_i + C_{i-1}, \\ y_{i-1} = y_i + S_i + S_{i-1}, \end{cases} \quad i = 1, \ldots, \ell. \tag{10.19}$$

The state equation is obtained by solving (10.19) and (10.14) for $(\Delta x_0, \Delta y_0, \Delta\theta_0, \ldots, \Delta\theta_\ell)$. The single trailer case ($\ell = 1$) is given as follows:

$$\Delta\xi = \begin{pmatrix} C_0 \\ S_0 \\ 0 \\ -S_{10}/\beta \end{pmatrix} u_1 + \begin{pmatrix} 0 \\ 0 \\ u_2 \\ -C_{10}u_2 - \alpha S_{10}u_2^2/\beta \end{pmatrix}. \tag{10.20}$$

Unlike the on-axle case, the right-hand side is not linear in u_2 any longer, and the steering input u_2 affects both $\Delta\theta_0$ and $\Delta\theta_1$.

10.5 Reachability Issues

Now we proceed to discuss a crucial problem to observe the region that the mobile robots can reach from given initial state. In the case of continuous systems, we could apply continuous-valued inputs to mobile robots. In the discrete-valued cases, however, we can give only discrete-valued inputs and robots placed on the hexagonal cellular space. This causes essential differences of reachable state between continuous systems and discrete-valued nonholonomic mobile robot systems. In this section, we define a *stepwise reachability set* as the collection of all reachable states within the given number of steps.

10.5.1 Definitions

We restart with a slightly general formulation of system dynamics, where the state equation of a discrete-valued nonholonomic mobile robot systems is expressed as the following difference equation of integral values:

$$\xi[k+1] = \xi[k] + \Delta\xi = \mathbf{G}(\xi[k], u[k]). \tag{10.21}$$

Let $\{u[k] | k \in \mathbb{Z}_+\}$ be a series of inputs to be applied. Then the stepwise evolution of the system state is given by

$$\begin{aligned}
\xi[1] &= \mathbf{G}(\xi[0], u[0]) &&= \mathbf{G}_1(\xi[0], u[0]),\\
\xi[2] &= \mathbf{G}(\xi[1], u[1]) &&= \mathbf{G}_2(\xi[0], u[0], u[1]),\\
&\vdots &&\vdots\\
\xi[k] &= \mathbf{G}(\xi[k-1], u[k-1]) &&= \mathbf{G}_k(\xi[0], u[0], \ldots, u[k-1]),
\end{aligned}$$

where $\mathbf{G}_k$ is recursively defined by

$$\begin{aligned}
\mathbf{G}_{k+1}(\xi[0], u[0], \ldots, u[k-1]) &:= \mathbf{G}(\mathbf{G}_{k-1}(\xi[0], u[0], \quad \ldots, u[k-2]), u[k-1]),\\
\mathbf{G}_1(\xi[0], u[0]) &:= \mathbf{G}(\xi[0], u[0]).
\end{aligned}$$

Definition 10.1 (*Stepwise Reachability Set*) For the integer-valued difference equations (10.21), the k-stepwise reachability set from the state $\xi[0]$, denoted by $\Lambda(\xi[0], k)$, is defined as

$$\Lambda(\xi[0], k) := \{\mathbf{G}_k(\xi[0], u[0], \ldots, u[k-1]), u[j] \in \Omega, j = 0, \ldots, k-1\},$$

where Ω is the set of all admissible inputs.

Definition 10.2 (*Neighborhood*) For an integer-valued state $\xi \in \mathbb{Z}^N$, its neighborhood is defined as

$$N(\xi) := \{\xi + (\delta_1, \ldots, \delta_N)^\mathsf{T}, \quad \delta_i \in \{-1, 0, 1\}, i = 1, \ldots, N\}.$$

10.5.2 Application

Let us turn to consider how the k-stepwise reachability set grows as k increases, when applied to the case of wheeled mobile robot we discussed in Sect. 10.3. Figure 10.10 shows a visualization of the k-stepwise reachability set of the single cart from $\xi[0] = (0, 0, 0)^\mathsf{T}$.

In Fig. 10.10, thick-lined hexagons imply the reachable cells by k steps for $k = 1, 2, 3, 4$. These cells contain some colored triangles, which imply the reachable "orientation" by k steps. For instance, the 1-step reachability set consists of

$$(0, 0, 0)^\mathsf{T}, (0, 0, 1)^\mathsf{T}, (0, 0, -1)^\mathsf{T}, (1, 0, 0)^\mathsf{T}, (-1, 0, 0)^\mathsf{T}.$$

At $k = 1$, the cart can move only in the initial orientation due to the nonholonomic constraint (10.8), namely, it cannot step sideways. Next, in the 2-stepwise reachability set, the cart can move to cells around the initial cell. However, the orientation of the cart is different from the initial orientation. Therefore, the cart can not take any state. Finally, the 4-stepwise reachability set shows that the cart can move to all the neighboring cells around the initial one with arbitrary orientations there. This analysis results in the fact

$$\arg\min_k \{\Lambda(\xi[0, k]) \supseteq N(\xi[0])\} = 4.$$

This indicates us a sufficient condition for controllability. By repeating these primitive motions to neighboring cells, each of which is composed of 4 steps at most, the state of the single cart can be transferred to *any* desired state in the whole hexagonal space. In addition, the 4-step reachability set in Fig. 10.10 indicates the same property as the continuous case that it is easy for the cart to move in the same direction as the initial orientation.

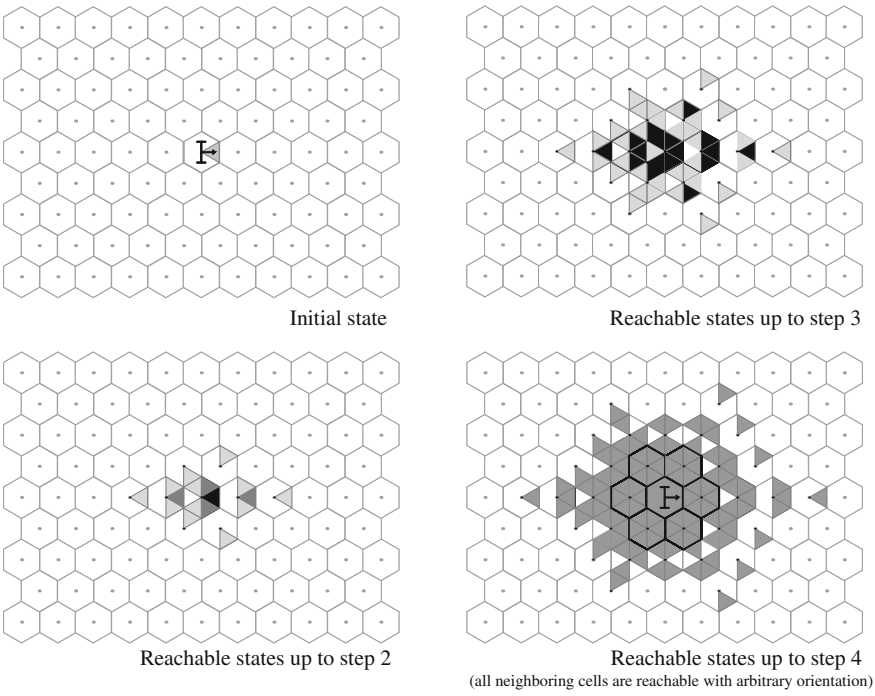

Fig. 10.10 Stepwise reachability set planar locomotion under discrete nonholonomic constraint. the *grey triangles* indicate the reachable states (considering its position and orientation) within the specified steps. All the neighboring cells are reachable up to 4 steps with arbitrary orientation

10.6 Other Possibilities of Cellular Tesselation

Thus far, we adopt regular hexagons for spatial discretization, mainly focusing on its preferable properties such as isotropy, e.g., distance between neighboring centers is always 1. Of course, this is not the only choice. The $\mathbb{R}^2$ can also be filled with regular squares or regular triangles as shown in Fig. 10.11. In this final section, let us pursuit the possibility of square tesselation.

Positions of the cells can be addressed by the usual Cartesian coordinate system (Fig. 10.11). Here we have two choices in defining adjacency; one is the so-called *Neumann neighborhood*, where each square cell is adjacent to 4 cells via its edges (i.e., its top, bottom, right and left sides). Then the discrete space is associated with 4 directions, namely,

$$\mathbb{SE}_N(2) = \left\{ \begin{pmatrix} x \\ y \\ \theta \end{pmatrix} = \begin{pmatrix} n_x\alpha \\ n_y\beta \\ n_\theta\gamma \end{pmatrix} \middle| \, n_x, n_y \in \mathbb{Z}, n_\theta \in \mathbb{Z}_4 \right\} \simeq \mathbb{Z} \times \mathbb{Z} \times \mathbb{Z}_4,$$

where $\mathbb{Z}_4 = \{0, 1, 2, 3\} \equiv \{0, \pm 1, 2\}$ and $\alpha = 1, \beta = 1, \gamma = \frac{\pi}{2}$. The other is the so-called *Moore neighborhood*, where each square cell is adjacent to 8 cells via its vertices as well as edges (i.e., all the surrounding cells). Then the discrete space is associated with 8 directions, namely,

$$\mathbb{SE}_M(2) = \left\{ \begin{pmatrix} x \\ y \\ \theta \end{pmatrix} = \begin{pmatrix} n_x\alpha \\ n_y\beta \\ n_\theta\gamma \end{pmatrix} \middle| \, n_x, n_y \in \mathbb{Z}, n_\theta \in \mathbb{Z}_8 \right\} \simeq \mathbb{Z} \times \mathbb{Z} \times \mathbb{Z}_8,$$

where $\mathbb{Z}_4 = \{0, 1, 2, 3, 4, 5, 6, 7\} \equiv \{0, \pm 1, \pm 2, \pm 3, 4\}$ and $\alpha = 1, \beta = 1, \gamma = \frac{\pi}{4}$.

The cosine and sine function and its derivatives can be defined as before, shown in Fig. 10.12 and Tables 10.2 and 10.3. Note that all the values concerned here are limited to $+1, 0, -1$.

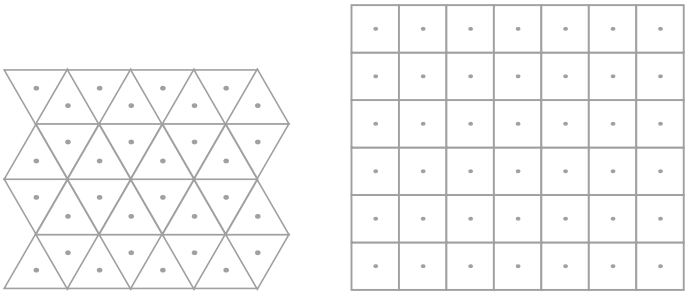

Fig. 10.11 Alternate choices of regular tessellations for $\mathbb{R}^2$ (*left* triangular, *right* square)

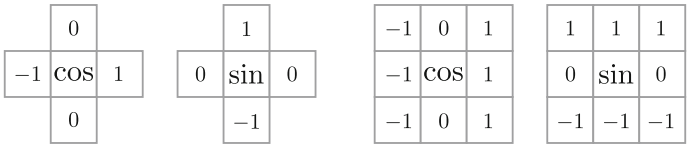

Fig. 10.12 Cosine and sine on square cells (*left* Neumann, *right* Moore)

Table 10.2 Discrete trigonometric calculus on square cells (Neumann neighborhood)

$\Delta\cos\theta$				
	$\theta=-1$	$\theta=0$	$\theta=1$	$\theta=2$
$\Delta\theta=1$	1	-1	-1	1
$\Delta\theta=-1$	-1	-1	1	1
$\Delta\sin\theta$				
$\Delta\theta=1$	1	1	-1	-1
$\Delta\theta=-1$	1	-1	-1	1

Table 10.3 Discrete trigonometric calculus on square cells (Moore neighborhood)

$\Delta\cos\theta$								
	$\theta=-3$	$\theta=-2$	$\theta=-1$	$\theta=0$	$\theta=1$	$\theta=2$	$\theta=3$	$\theta=4$
$\Delta\theta=1$	1	1	0	0	-1	-1	0	0
$\Delta\theta=-1$	0	-1	-1	0	0	1	1	0
$\Delta\sin\theta$								
$\Delta\theta=1$	0	0	1	1	0	0	-1	-1
$\Delta\theta=-1$	1	0	0	-1	-1	0	0	1

Now the discrete version of nonholonomic wheel constraint for a single cart is expressed as

$$\Delta y_0 \cos\theta_0 - \Delta x_0 \sin\theta_0 = 0$$

for both cases of the Neumann and Moore neighborhood. This leads us to derive the corresponding cart kinematics

$$\Delta\xi = g_1(\xi)u_1 + g_2(\xi)u_2, \tag{10.22}$$

$$g_1(\xi) := \begin{pmatrix} \cos\theta_0 \\ \sin\theta_0 \\ 0 \end{pmatrix}, \quad g_2(\xi) := \begin{pmatrix} 0 \\ 0 \\ 1 \end{pmatrix},$$

which is apparently the same as the hexagonal version (10.10). Notable difference can be found in the corresponding Lie-bracket motions, as shown in Fig. 10.13

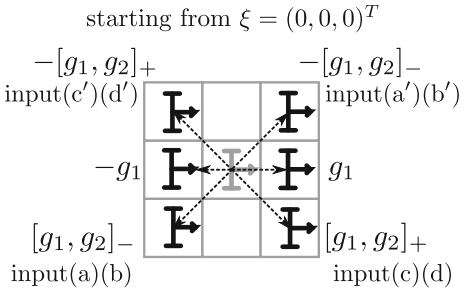

Fig. 10.13 Lie bracket motions of the single cart on square cells (Neumann neighborhood)

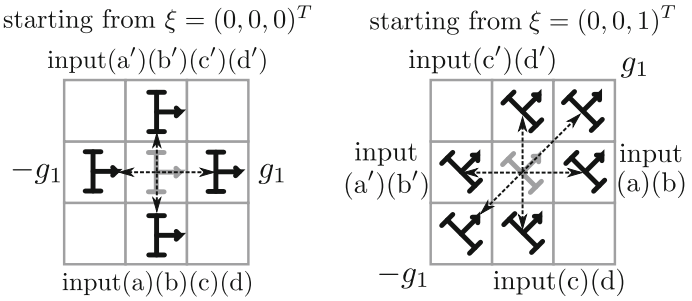

Fig. 10.14 Lie bracket motions of the single cart on square cells (Moore neighborhood)

and Fig. 10.14. In particular, for the case of Moore neighborhood, the net effects are different between $\theta = 0, 2, 4, 6$ and $\theta = 1, 3, 5, 7$, depending on multi-valuedness of the corresponding Lie bracket operations (see Fig. 10.6 for comparison).

10.7 Conclusion

In this chapter, we discussed possibility of discrete-valued version of locomotion of rigid bodies on the horizontal plane. We showed that, many *intrinsic properties consistent with the continuous case* can be derived starting from simply defined discrete constraints. We also examined the k-stepwise reachability set $\Lambda(\xi[0], k)$ for these systems, to confirm possibility to maneuver the system state to any states. Other cases including both holonomic and nonholonomic constraints, and alternate possibilities on cellular tessellation were also discussed.

We showed only a clue to respond to the authors' primitive motivations in this chapter. It is not surprising that a lot of unsolved problems to be discussed are left for the future works; For example, stability and stabilization issues are not discussed at all. Characterization of stability must be crucial in developing theoretical analysis of system behavior. The typical Lyapunov approach may have a difficulty, in the sense

that the converse theorem is not likely to hold in discrete-valued (i.e., discontinuous) cases. Moreover, discrete version of Brockett's theorem [2] must be a quite interesting issue. Other topics contain control *design* theory, e.g., design of discontinuous, time-varying or hybrid controllers have been central issues of continuous nonholonomic systems. Some ideas of existing design approaches, e.g., time-varying approaches [8], may remain effective in discrete cases.

The authors believe it important to discuss if there exists any *underlying mechanics/physics as first principle*, i.e., discrete equivalents of energy, Lagrangian, Hamiltonian or variational principle that are consistent with the current results. It would also be interesting to relate it with discrete mechanics proposed by Marsden et al. [5]. The current work can be considered a *Lebesgue*-type approach to discrete mechanics, in contrast that the aforementioned one [5] can be regarded as a *Riemann*-type approach.

The authors expect the current work to be a first step toward establishment of discrete-valued nonlinear system theory under spatial symmetry.

Acknowledgments The authors are grateful to continuous encouragement by Professor Koichi Osuka.

References

1. Barraquand, J., Latombe, J.C.: Nonholonomic multibody mobile robots: controllability and motion planning in the presence of obstacles. Algorithmica **10**, 121–155 (1993)
2. Brockett, R.W.: Asymptotic stability and feedback stabilization. In: Brockett, R.W., Millman, R.S., Sussman, H. (eds.) Differential Geometric Control Theory, pp. 181–191. Birkhauser, Boston (1983)
3. Hirota, R., Takahashi, D.: Discrete and Ultradiscrete Systems. Kyoritsu Publishing, Tokyo (2003) (in Japanese)
4. Kita, T., Ishikawa, M., Osuka, K.: On discrete-valued modeling of nonholonomic mobile robot systems. In: 2012 IEEE International Conference on Robotics and Biomimetics (ROBIO2012), pp. 2024–2031 (2012)
5. Marsden, J.E., West., M.: Discrete mechanics and variational integrators. Acta Numerica **10**, 357–514 (2001)
6. Middleton, L., Sivaswamy, J.: Hexagonal Image Processing. Advances in Computer Vision and Pattern Recognition. Springer, New York (2005)
7. Monaco, S., Noman-Cyrot, D.: A unified representation for nonlinear discrete-time and sampled dynamics. J. Math. Syst. Estim. Control **7**(4), 477–503 (1997)
8. Morin, P., Samson, C.: Practical stabilization of driftless systems on lie groups: the transverse function approach. IEEE Trans. Autom. Control **48**(9), 1496–1508 (2003)
9. Nesic, D., Teel, A.: A framework for stabilization of nonlinear sampled-data systems based on their approximate discrete-time models. IEEE Trans. Autom. Control **49**(7), 1103–1122 (2004)
10. Nijmeijer, H., van der Schaft, A.J.: Nonlinear Dynamical Control Systems. Springer, New York (1990)
11. Schiff, J.: Cellular Automata: A Discrete View of the World. Wiley, Hoboken (2008)
12. Wolfram, S.: Cellular Automata and Complexity: Collected Papers. Westview, Boulder (1994)
13. Yuz, J.I., Goodwin, G.C.: On sampled-data models for nonlinear systems. IEEE Trans. Autom. Control **50**(10), 1477–1489 (2005)

Chapter 11
Feedback Control of Spatial Patterns in Reaction-Diffusion Systems

Kenji Kashima and Toshiyuki Ogawa

11.1 Introduction

There have been plenty of studies on pattern formation such as thermal convection problems, Turing patterns in reaction-diffusion systems, phase transitions in material sciences, and so on (see [1]). There, one can tune a parameter so that the uniform stationary solution loses its stability against perturbations with certain non-zero wavelength. As a result, a spatially non-uniform stationary solution may appear. Thus the local bifurcation analysis is a first step to understand the onset of the pattern formation.

Let us consider an activator-inhibitor system of reaction-diffusion equations as follows.

$$\begin{cases} u_t = D_u \Delta u + f(u, v), \\ v_t = D_v \Delta v + g(u, v), \quad x \in \Omega. \end{cases} \tag{11.1}$$

Here, the typical reaction part of (11.1) is the following:

$$\begin{cases} f(u, v) = u - u^3 - v, \\ g(u, v) = 3u - 2v. \end{cases} \tag{11.2}$$

K. Kashima (✉)
Graduate School of Informatics, Kyoto University, Yoshida-honmachi, Sakyo-ku, Kyoto 606-8501, Japan
e-mail: kk@i.kyoto-u.ac.jp

T. Ogawa
Graduate School of Advanced Study of Mathematical Sciences, Meiji University, 4-12-1 Nakano, Tokyo 164-8525, Japan
e-mail: togw@meiji.ac.jp

K. Aihara et al. (eds.), *Analysis and Control of Complex Dynamical Systems*, Mathematics for Industry 7, DOI 10.1007/978-4-431-55013-6_11

This reaction-diffusion system (11.1) has a trivial stationary solution $u = v = 0$ under the Neumann boundary condition:

$$\frac{\partial u}{\partial n} = \frac{\partial v}{\partial n} = 0, \quad x \in \partial\Omega$$

or the periodic boundary condition. Here, Ω is a bounded interval or a rectangle in $\mathbb{R}$ or $\mathbb{R}^2$. Although the origin $u = v = 0$ is asymptotically stable under the ODE:

$$\begin{cases} \dot{u} = f(u, v), \\ \dot{v} = g(u, v), \end{cases} \tag{11.3}$$

it might be possible to become unstable in the sense of (11.1). This is the so-called Turing instability or diffusion induced instability which is realized by taking the diffusion constants appropriately as we shall review in the following section.

Once we understand the linearized instability mechanism it turns out that non-trivial patterns may appear from the trivial solution by a standard bifurcation analysis. As one can see in Fig. 11.1, solutions of (11.1) may become closer and closer to stripe patterns. Now if the non-linear terms are not symmetric as in (11.2) and moreover they include quadratic terms as

$$\begin{cases} f(u, v) = u - u^3 - au^2 - v, \\ g(u, v) = 3u - 2v, \end{cases} \tag{11.4}$$

the dot-like patterns may appear rather than stripe.

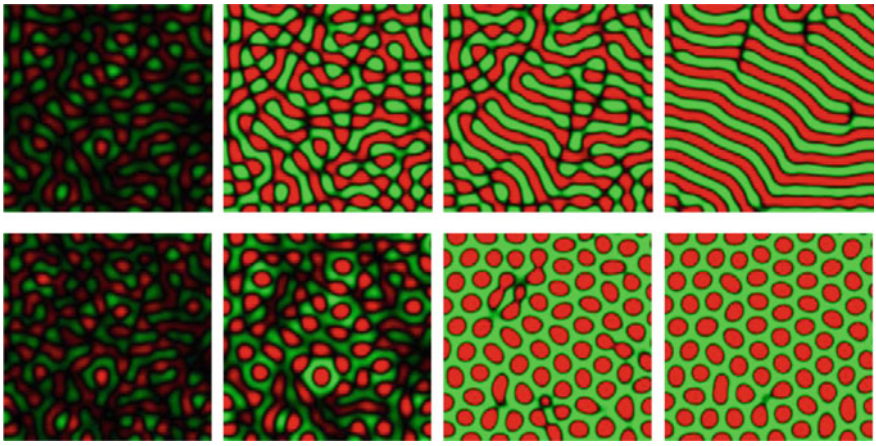

Fig. 11.1 Time sequences of the numerical simulation for (11.1) and (11.4) in a square region with the periodic boundary condition. The coefficient of the quadratic term $a = 0$ and $a = 0.1$ for the *upper* and *lower lines*, respectively. The columns correspond to the time sequences $t = 4, 10, 20, 50$ from the left to right and only the value of u is displayed

In Sect. 11.2, after reviewing the Turing instability from the linearized analysis we introduce the idea which helps us understand the Turing instability mechanism more clearly. In fact we can consider that the inhibitor in the 2-component reaction-diffusion system plays a role of negative global feedback to the activator. By extending this idea we can construct 3-component reaction-diffusion systems which have different types of instabilities.

Since we are considering the bounded interval or a rectangle with Neumann or periodic boundary conditions the problem has the so-called SO(2) symmetry which basically comes from translation invariance. Therefore at the bifurcation point more than one critical modes may interact with each other. As a result, different types of patterns emerge simultaneously. However, the stability of these solutions depends on the nonlinear terms. Now the question is whether we can stabilize each non-trivial pattern or not. Section 11.3 is devoted to partially answer to this question. We formulate and solve a feedback stabilization problem of unstable non-uniform spatial pattern in reaction-diffusion systems. By considering spatial spectrum dynamics, we obtain a finite dimensional approximation that takes over the semi-passivity of the original partial differential equation. By virtue of this property, we can show the diffusive coupling in the spatial frequency domain achieves the desired pattern formation.

11.2 Pattern Formation by Global Feedback

11.2.1 Turing Instability

Turing instability is known to be the fundamental mechanism for the onset of pattern formations. Let us first review the reason why the uniform stationary solution $u = v = 0$ in the reaction-diffusion system (11.1) loses its stability. In fact the linearized stability of the Fourier mode with wavenumber k is characterized by the matrix:

$$M_k = \begin{pmatrix} f_u - k^2 D_u & f_v \\ g_u & g_v - k^2 D_v \end{pmatrix}.$$

Since the fixed point $u = v = 0$ is assumed to be stable in the sense of the ODE (11.3), it turns out that $\mathrm{trace} M_0 = f_u + g_v < 0$ and $\det M_0 = f_u g_v - f_v g_u > 0$ hold true. Therefore, M_k has real part positive eigenvalues if and only if $\det M_k < 0$, and M_k has one real positive eigenvalue in this case. Now $\det M_k$ is given by

$$\det M_k = f_u g_v - f_v g_u - (D_v f_u + D_u g_v)k^2 + D_u D_v k^4.$$

Therefore, if $D_v f_u + D_u g_v > 0$ and $(D_v f_u + D_u g_v)^2 - 4(f_u g_v - f_v g_u) D_u D_v > 0$ hold, then $\det M_k < 0$ for some non-zero wavenumber k and, as a result, M_k has a

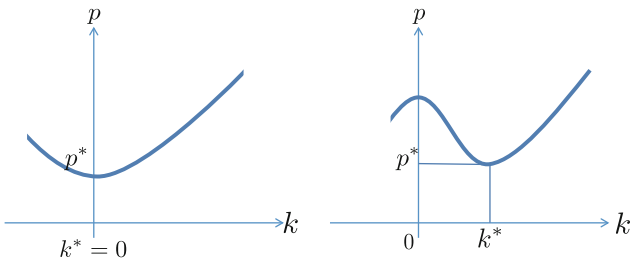

Fig. 11.2 Two types of neutral stability *curves*. The onset of the pattern formation can be observed when the neutral stability *curve* has the shape as in the *right figure*

positive eigenvalue. We have only to take D_v sufficiently large compared to D_u to satisfy these conditions. At the moment of stability change the Fourier mode with a wave-number $k \approx k_c = (\frac{f_u g_v - f_v g_u}{D_u D_v})^{1/4}$ may become unstable.

11.2.2 Interpretation of Turing Instability by Global Feedback

We shall introduce the idea that one can control the onset of pattern formation by a global feedback (see also [2]). Or we can even explain the Turing instability mechanism from the viewpoint of global feedback. Suppose we observe pattern formation from a uniform rest state by changing a parameter p. More precisely, the uniform stationary solution is stable when p is less than a critical value p^* and becomes unstable against certain wavenumber $k^* > 0$ when $p > p^*$. Therefore pattern formation can be observed in the system where the neutral stability curve $p = \phi(k)$ has the property such that $\phi(k)$ attains its minimum at k^* (see Fig. 11.2). Here, the neutral stability curve is the stability boundary in the (k, p)-plane. In other words, it is equivalent to say that the uniform stationary solution is stable against perturbations of wavenumber k when $p < \phi(k)$ and it is unstable when $p > \phi(k)$. Let us consider the following scalar reaction-diffusion equation as a simple example

$$u_t = Du_{xx} + pu, \tag{11.5}$$

where D is a diffusion constant and p is a parameter. Since it is equivalent to

$$\frac{d\tilde{u}}{dt} = (p - Dk^2)\tilde{u}$$

by Fourier transformation, the neutral stability curve is $p - Dk^2 = 0$. Now, it is clear that $\phi(k) = Dk^2$ does not attain its minimum at positive k and the instability for $k = 0$ takes place earlier than any other non-trivial perturbation. Therefore we can not observe pattern formations in scalar reaction-diffusion equations.

Since the scalar reaction-diffusion equation is not sufficient to produce the onset of patterns as we saw above let us consider the following activator-inhibitor type reaction-diffusion equations:

$$\begin{cases} u_t = D_1 u_{xx} + pu - sw, \\ \tau w_t = D_2 w_{xx} + u - w. \end{cases} \tag{11.6}$$

Here, s is assumed to be positive so that species w has negative feedback effect to the species u. On the contrary, u gives positive effects to w. Moreover suppose that the time constant for w is sufficiently small. Let us just plug 0 into τ for simplicity. Then we have the following equations by using the Fourier transformation.

$$\begin{cases} \dfrac{d\tilde{u}}{dt} = (p - D_1 k^2)\tilde{u} - s\tilde{w}, \\ 0 = (-1 - D_2 k^2)\tilde{w} + \tilde{u}. \end{cases} \tag{11.7}$$

Since $\tilde{w}$ is solved as $\tilde{w} = \dfrac{\tilde{u}}{1 + D_2 k^2}$, it turns out that the system (11.7) is equivalent to the following scalar equation:

$$\frac{d\tilde{u}}{dt} = \left(p - D_1 k^2 - \frac{s}{1 + D_2 k^2} \right) \tilde{u}.$$

Therefore the neutral stability curve is given by

$$p = \phi(k) := D_1 k^2 + \frac{s}{1 + D_2 k^2}. \tag{11.8}$$

Moreover we have the following inequality:

$$\begin{aligned} p &= \frac{D_1}{D_2}(1 + D_2 k^2) + \frac{s}{1 + D_2 k^2} - \frac{D_1}{D_2} \\ &\geq 2\sqrt{\frac{D_1 s}{D_2}} - \frac{D_1}{D_2}. \end{aligned}$$

Since the last equality holds true if and only if $(1 + D_2 k^2)^2 = \dfrac{D_2 s}{D_1}$, we have

Theorem 11.1 *The following two conditions are equivalent to each other for the system* (11.6)*:*

- *The neutral stability curve $p = \phi(k)$ attains its minimum at $k = k_0 > 0$.*
- *The constants s, D_1, and D_2 satisfy*

$$\frac{D_2 s}{D_1} > 1. \tag{11.9}$$

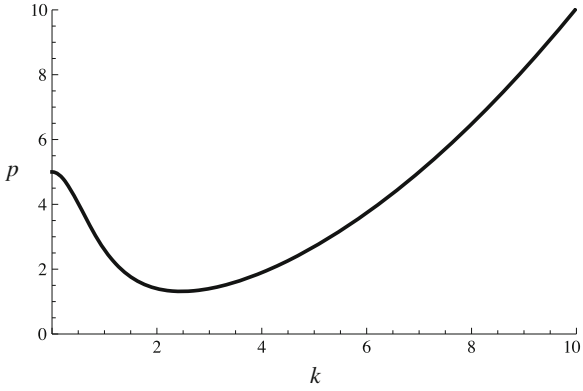

Fig. 11.3 The neutral stability *curve* (11.8). Here, $D_1 = 0.1$, $D_2 = 1$, and $s = 5$

Therefore the neutral stability curve has the desired property when the condition (11.9) is satisfied (see Fig. 11.3).

We can study the bifurcation structure for the system (11.6) with nonlinear terms:

$$\begin{cases} u_t = D_1 u_{xx} + pu - sw + f(u, w) \\ \tau w_t = D_2 w_{xx} + u - w \end{cases} \tag{11.10}$$

on a finite interval $x \in [0, L]$ with periodic boundary condition. Here, $f(u, w)$ denotes higher order terms of u, w. Notice that the bifurcation structure with the Neuman boundary condition is included in the periodic case. By the periodicity we have only to consider countable Fourier modes with the fundamental wavenumber $k_0 = \frac{2\pi}{L}$. We need to take into account wavenumber of the form $k = mk_0$ where $m \in \mathbb{Z}$. It is convenient to draw the neutral stability curves C_m for each mode $m > 0$ in the (k_0, p)-plane:

$$C_m := \{(k_0, p) | p = \phi(mk_0)\}.$$

If the condition (11.9) is satisfied we can conclude that three different neutral stability curves don't intersect at the same point except for $(0, 0)$. This means at most two Fourier modes can be critical at the same time. We call these intersection points degenerate bifurcation points. Moreover, it turns out that there are only degenerate bifurcation points with adjacent modes $n, n+1$ on the first instability (see Fig. 11.4). Therefore the dynamics near the first instability point is governed by the normal form as follows:

Theorem 11.2 *Assume the condition* (11.9) *is satisfied for* (11.6). *Suppose the system size* $L > 2\pi\sqrt{\frac{D_1 D_2}{sD_2 - D_1}}$ $(k_0 < \sqrt{\frac{sD_2 - D_1}{D_1 D_2}})$ *there is one critical point* p *where the first instability takes place for* n *mode* $(n > 0)$. *There are the following two cases:*

(I) $m = \pm n$ *are the only critical modes.*
(II) $m = \pm n, \pm n'$ *are the only critical modes.*

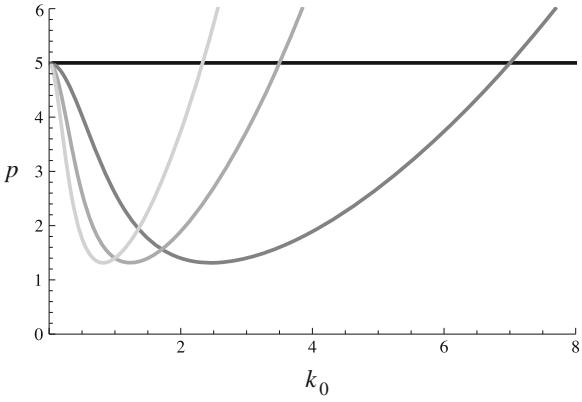

Fig. 11.4 The neutral stability *curves* C_m for $m = 0, 1, 2$ and 3 modes (from *black* to *light gray*). It turns out that more modes become unstable when $k_0 = 2\pi/L$ is small

Here, $n' = n + 1$ *or* $n' = n - 1$. *Dynamics of the solutions to* (11.10) *close to first instability points can be reduced to those on the center manifolds. Moreover they are generically governed by the normal form by taking appropriate real numbers* a, b, c, d.:

$$\text{(I)}\quad \dot{\alpha_n} = \lambda\alpha_n + a|\alpha_n|^2\alpha_n + O(4),$$

$$\text{(II)}\quad \begin{cases} \dot{\alpha_n} = \lambda\alpha_n + (a|\alpha_n|^2 + b|\alpha_{n'}|^2)\alpha_n + O(4), \\ \dot{\alpha_{n'}} = \mu\alpha_{n'} + (c|\alpha_n|^2 + d|\alpha_{n'}|^2)\alpha_{n'} + O(4). \end{cases}$$

Here, $\{\alpha_m \in \mathbb{C};\ |m| = n\}$ *and* $\{\alpha_m \in \mathbb{C};\ |m| = n, n'\}$ *are the critical modes for the cases* (I) *and* (II)*, respectively. Moreover, n is assumed to be larger than 1 in the case* (II).

Proof Since (11.10) is translation invariant the center manifold and its dynamics can be constructed so that they have SO(2) symmetry. Therefore the normal form dose not have quadratic terms.

Remark 11.1 Dynamics close to the degenerate point between 1 and 2 is the exception of the above theorem. Armbruster, Guckenheimer and Holmes [3] studied the interaction of two steady-state bifurcations in a system with O(2)-symmetry, assuming 1:2 resonance for the wavenumbers associated with the critical modes. They found there are rich variety of dynamics in the 1:2 resonance normal form:

$$\begin{aligned} \dot{a_1} &= \overline{a_1}a_2 + a_1(\mu_1 + e_{11}|a_1|^2 + e_{12}|a_2|^2), \\ \dot{a_2} &= ca_1^2 + a_2(\mu_2 + e_{21}|a_1|^2 + e_{22}|a_2|^2) \end{aligned}$$

when the coefficient of the quadratic term c is negative. However, in this case, the two coefficients of quadratic terms have the same sign and, as a result, $c = +1$ which means there are no nontrivial dynamics.

Notice that we solved $(1 - D_2\partial_x^2)w = u$ in the Fourier space. Since the inverse Fourier image of $\dfrac{1}{1 + D_2k^2}$ is $\mathrm{e}^{-\frac{|x|}{\sqrt{D_2}}}$, w can be written as

$$w = \frac{1}{2\pi} \int_{-\infty}^{+\infty} \mathrm{e}^{-\frac{|x-y|}{\sqrt{D_2}}} u(y) dy.$$

Theorem 11.3 *The reaction-diffusion system* (11.6) *is equivalent to the following equation when* $\tau = 0$*:*

$$u_t = D_1 u_{xx} + pu - \frac{s}{2\pi} \int_{-\infty}^{+\infty} \mathrm{e}^{-\frac{|x-y|}{\sqrt{D_2}}} u(y) dy. \tag{11.11}$$

It should be mentioned that Britton [4] studied the ecological pattern formation also with global feedback. In the population growth model it is natural that intra-specific competition for resources depends not simply on population density at one point in space and time but on a weighted average involving values at all previous points and at all points in space. Therefore he considered

$$u_t = D\Delta u + u\,[p + \alpha u - (1+\alpha) G * *u] \tag{11.12}$$

instead of

$$u_t = D\Delta u + u(p - u), \tag{11.13}$$

where, $G * *u$ is a weighted average of u:

$$G * *u := \int_{\mathbb{R}} \int_{-\infty}^{t} G(x - y, t - s) u(y, s) ds dy.$$

Here, G is assumed to be positive, L^1 and moreover,

$$\int_{\mathbb{R}} \int_{-\infty}^{t} G(x, t) dt dx = 1.$$

Notice that the Eq. (11.12) is equivalent to (11.11) when $G(x, t) = \delta(t)\tilde{G}(x)$ with an appropriate $\tilde{G}$. Also (11.12) is equivalent to (11.14) when $G(x, t) = \delta(x)\delta(t)$.

11.2.3 0:1:2-Mode Interaction

We have seen in the previous subsection that the normal form analysis for double degenerate bifurcation points is sufficient to study the Eq. (11.10). On the other hand, we can realize the triple degeneracy if we take another component into account in a three component system as follows:

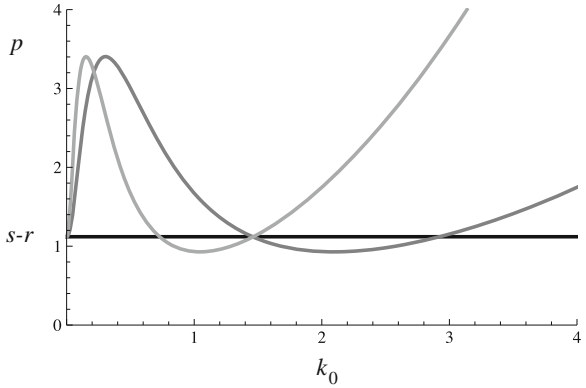

Fig. 11.5 The neutral stability *curves* $C_m = \{(k_0, p) | p = \phi(mk_0)\}$ for $m = 0, 1, 2$ modes (*black*, *gray*, *light gray*, respectively). Here, ϕ is given by (11.15). *Three curves* $C_0,\ C_1,\ C_2$ intersect at the same point for $k_0 \neq 0$ by taking the constants $s,\ t,\ D_1,\ D_2,\ D_3$ appropriately. For instance, $s = 5,\ t = 3.88,\ D_1 = 0.1,\ D_2 = 2.0,\ D_3 = 40.0$ in the figure

$$\begin{aligned} u_t &= D_1 u_{xx} + pu - sv + rw, \\ \tau v_t &= D_2 v_{xx} + u - v, \\ \tau w_t &= D_3 w_{xx} + u - w. \end{aligned} \tag{11.14}$$

Here, τ is again assumed to be small positive number. We also assume negative feedback ($s > 0$) effect from v and positive feedback ($r > 0$) from w. As a consequence of similar discussions in the previous subsection the neutral stability curve for (11.14) is given by

$$p = \phi(k) := D_1 k^2 + \frac{s}{1 + D_2 k^2} - \frac{r}{1 + D_3 k^2}. \tag{11.15}$$

Now, by taking $D_3 \gg D_2 \gg 1$ we can tune the parameters so that the system (11.14) has triple degeneracy of 0:1:2 modes (see Fig. 11.5). The degenerate dynamics by 0:1:2 modes has been studied also by using the normal form analysis. In fact, Smith, Moehlis and Holmes [5] studied the generic quadratic normal form:

$$\begin{aligned} \dot{a_0} &= \mu_0 a_0 + 2(B_1 |a_1|^2 + B_2 |a_2|^2), \\ \dot{a_1} &= \overline{a_1} a_2 + a_1(\mu_1 - B_1 a_0), \\ \dot{a_2} &= -a_1^2 + a_2(\mu_2 - B_2 a_0). \end{aligned}$$

They conclude there are a wide variety of dynamics including heteroclinic cycles. On the other hand, Ogawa and Okuda [6] studied the cubic normal form also with resonance terms under the up-down symmetry:

$$\begin{aligned} \dot{z}_0 &= (\mu_0 + a_1 z_0^2 + a_2 z_1^2 + a_3 z_2^2) z_0 + a_4 z_1^2 z_2, \\ \dot{z}_1 &= (\mu_1 + b_1 z_0^2 + b_2 z_1^2 + b_3 z_2^2) z_1 + b_4 z_0 z_1 z_2, \\ \dot{z}_2 &= (\mu_2 + c_1 z_0^2 + c_2 z_1^2 + c_3 z_2^2) z_2 + c_4 z_0 z_1^2 \end{aligned}$$

and they showed the existence of oscillatory bifurcation from the 1-mode stationary solution not only in the general normal form but also in a particular 3-component reaction-diffusion system.

11.2.4 Wave Instability

Let us introduce pattern formation by an oscillatory instability. We shall start with a 2-dimensional ODE system which has the Hopf bifurcation point:

$$\begin{pmatrix} \dot{u} \\ \dot{v} \end{pmatrix} = \begin{pmatrix} p & -p \\ q & -1 \end{pmatrix} \begin{pmatrix} u \\ v \end{pmatrix} + \begin{pmatrix} O(2) \\ O(2) \end{pmatrix}.$$

Here, $q > 1$ is a given constant and we control the parameter p. The linearized matrix $M = \begin{pmatrix} p & -p \\ q & -1 \end{pmatrix}$ has a characteristic polynomial $\lambda^2 - (\mathrm{trace}M)\lambda + \det M$. Therefore M has a pair of purely imaginary eigenvalues when $p = 1$. Now we are interested in the bifurcation in the following reaction-diffusion system:

$$\begin{pmatrix} u_t \\ v_t \end{pmatrix} = \begin{pmatrix} D_1 u_{xx} \\ D_2 v_{xx} \end{pmatrix} + \begin{pmatrix} p & -p \\ q & -1 \end{pmatrix} \begin{pmatrix} u \\ v \end{pmatrix} + \begin{pmatrix} f(u,v) \\ g(u,v) \end{pmatrix}. \tag{11.16}$$

Here, f, g are assumed to consist of higher order terms of u and v. It turns out from the linearized eigenvalue problem about 0 the stability of the trivial solution against perturbation with wavenumber k can be controlled by the matrix

$$M_k = \begin{pmatrix} p - D_1 k^2 & -p \\ q & -1 - D_2 k^2 \end{pmatrix}.$$

Since the oscillatory instability takes place when $\mathrm{trace}M_k = 0$, the neutral stability curve for the Hopf bifurcation is given by $p = 1 + (D_1 + D_2)k^2$. Therefore, we can not observe any stable spatially non-trivial oscillating patten.

Let us introduce the third component w which has the negative feedback effect to the activator u and consider the following three component reaction-diffusion system instead of (11.16):

$$\begin{pmatrix} u_t \\ v_t \\ \tau w_t \end{pmatrix} = \begin{pmatrix} D_1 u_{xx} \\ D_2 v_{xx} \\ D_3 w_{xx} \end{pmatrix} + \begin{pmatrix} p & -p & -s \\ q & -1 & 0 \\ 1 & 0 & -1 \end{pmatrix} \begin{pmatrix} u \\ v \\ w \end{pmatrix} + \begin{pmatrix} f(u,v) \\ g(u,v) \\ 0 \end{pmatrix}. \tag{11.17}$$

Here, we also assume $\tau > 0$ is sufficiently small. By a similar argument to (11.7) we can obtain the linearized matrix for the wavenumber k when $\tau = 0$ as follows:

$$A_k = \begin{pmatrix} p - D_1k^2 - \frac{s}{1+D_3k^2} & -p \\ q & -1 - D_2k^2 \end{pmatrix}.$$

Thus, a necessary condition for the Hopf instability is given by

$$\mathrm{trace} A_k = p - 1 - (D_1 + D_2)k^2 - \frac{s}{1 + D_3k^2} = 0.$$

Let us also call it the neutral stability curve for the Hopf instability

$$p = \phi(k) := 1 + (D_1 + D_2)k^2 + \frac{s}{1 + D_3k^2}, \tag{11.18}$$

although it is just a necessary condition. Because it has the same form as (11.8) we have the following theorems.

Theorem 11.4 *The following two conditions are equivalent to each other for the system* (11.17)*:*

- *The neutral stability curve* $p = \phi(k)$ *attains its minimum at* $k = k_0 > 0$.
- *The constants* s, D_1 *and* D_2 *satisfy*

$$\frac{sD_3}{D_1 + D_2} > 1. \tag{11.19}$$

Theorem 11.5 *The reaction-diffusion system* (11.17) *is equivalent to the following equations when* $\tau = 0$*:*

$$\begin{aligned} u_t &= D_1\Delta u + pu - pv + O(2) - \frac{s}{2\pi}\int_{-\infty}^{+\infty} \mathrm{e}^{-\frac{|x-y|}{\sqrt{D_3}}} u(y)dy, \\ v_t &= D_2\Delta v + qu - v + O(2). \end{aligned} \tag{11.20}$$

We may have spatio-temporal oscillating patterns if the system (11.17) satisfies the condition (11.19) and this is called "wave instability" (see also [7]).

If we consider the system on a finite interval $(0, L)$ similarly to the above discussion there are three cases in the sense of bifurcation analysis.

Theorem 11.6 *Assume the condition* (11.19) *is satisfied for* (11.17)*. For a given system size* L *(or fundamental wavenumber* k_0*) there is one critical point* p *where the first instability takes place for* n *mode* ($n > 0$)*. There are the following three cases:*

(I) $m = \pm n$ *are the only critical modes.*
(II) $m = 0, \pm n$ *are the only critical modes.*
(III) $m = \pm n, \pm n'$ *are the only critical modes.*

Here, $n' = n + 1$ *or* $n' = n - 1$ *and all the critical modes are of the Hopf type.*

We need to distinguish two critical modes $\{\alpha_m \in \mathbb{C}; |m| = n\}$ in this case since they are the Hopf type critical modes. We introduce the normal form only for the case (I) for the simplicity.

Theorem 11.7 *Under the same setting as* Theorem 11.6 *dynamics of the solutions to* (11.17) *close to first instability points can be reduced to those on the center manifolds. Moreover they are generically governed by the normal form by taking appropriate real numbers* a, b *in the case* (I)*:*

$$\begin{cases} \dot{\alpha_n} = \mu\alpha_n + (a|\alpha_n|^2 + b|\alpha_{-n}|^2)\alpha_n + O(4), \\ \dot{\alpha_{-n}} = \mu\alpha_{-n} + (b|\alpha_n|^2 + a|\alpha_{-n}|^2)\alpha_{-n} + O(4). \end{cases}$$

Notice that we don't need any non-resonance condition in this theorem in contrast to the standard double Hopf theorem since we have SO(2) symmetry. We can conclude that there are two typical oscillating solutions: rotating wave and standing wave solutions. Stability for both solutions depends on the normal form coefficients a, b. It turns out from simple calculations that $(a, b) = (-3, -6)$ when $f(u, v) = -u^3$, $g(u, v) = 0$. Therefore the rotating wave solution is stable while the standing wave solution is unstable in this case (Fig. 11.6).

Notice that the wave instability criterion depends on s, D_3 and $D_1 + D_2$. Therefore we can realize the situation where both Turing and wave instabilities take place at the same value of p by changing the ratio between D_1 and D_2 without changing $D_1 + D_2$. We draw the neutral stability curves for Turing instability ($\det A_k = 0$) and wave instability ($\mathrm{trace} A_k = 0$) in Fig. 11.7 .

Again it should be mentioned that Gourley and Britton [8] studied the similar 2-component reaction-diffusion system with the global feedback from the population dynamics.

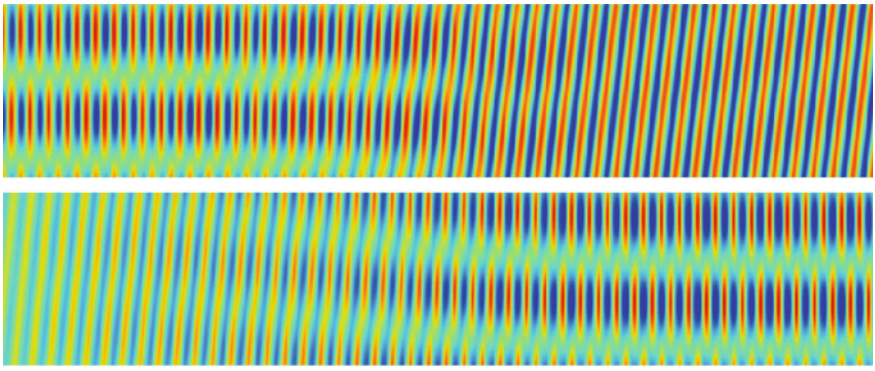

Fig. 11.6 Numerical simulations for (11.17) under the parameters $L = 2\pi$, $p = 2.01$, $q = 1.5$, $s = 2.0$, $D_1 = 0.8$, $D_2 = 0.2$, $f(u, v) = -u^3$, and $g(u, v) = 0$ in the *upper figure*. Therefore the standing wave is unstable and the solution converges to the rotating wave. By taking another nonlinear terms such as $f(u, v) = 0$ and $g(u, v) = uv$

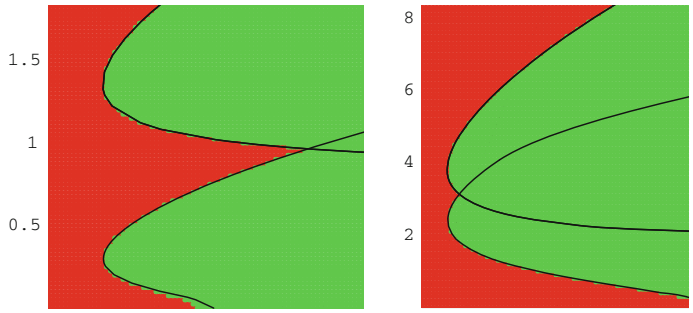

Fig. 11.7 *Two curves* of $\det A_k = 0$ (*upper curve*) and $\mathrm{trace} A_k = 0$ (*lower*) are described in the (k, p)-plane. Parameter sets are $(s, D_1, D_2, D_3, \tau) = (0.6, 0.24, 0.76, 50, 0.1)$ and $(s, D_1, D_2, D_3, \tau) = (20, 0.2, 0.23, 1, 0.01)$ in *left* and *right figures*, respectively

11.2.5 Summary

In this section we introduce the idea that helps us understand the mechanism of the Turing instability from the viewpoint of global feedback. It turns out that not only the Turing instability but also other instabilities relating to pattern formation can be obtained by the global feedback although it might not be described in the system explicitly.

11.3 Selective Stabilization of Turing Patterns

11.3.1 Reaction-Diffusion Systems

In this section, we consider (11.1) with

$$\begin{cases} f(u, v) = a_{11}u - a_{12}v - u^3, \\ g(u, v) = a_{21}u - a_{22}v, \end{cases} \tag{11.21}$$

where the spatial domain $\Omega := [0, L_x] \times [0, L_y]$ with the periodic boundary condition. We denote (Fig. 11.8)

$$z(t, x, y) = \begin{bmatrix} u(t, x, y) \\ v(t, x, y) \end{bmatrix} \in \mathbb{R}^2.$$

This reaction-diffusion system has a trivial equilibrium pattern

$$z_{eq}(x, y) \equiv 0 \text{ on } \Omega. \tag{11.22}$$

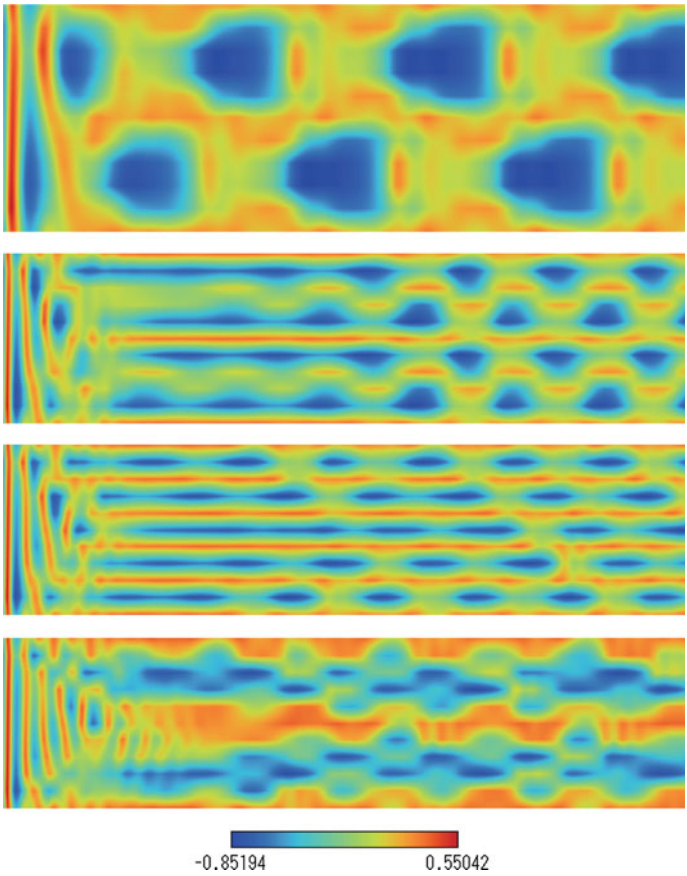

Fig. 11.8 Oscillating patterns observed when both Turing and wave instabilities coexist. *Vertical* and *horizontal axis* denote the interval $(0, L)$ and time, respectively

Even if the reaction term is globally stable, this trivial equilibrium of reaction-diffusion system is not necessarily stable [9].

Consider the spatial Fourier transform

$$z_m(t) := \begin{bmatrix} u_m(t) \\ v_m(t) \end{bmatrix} := \int_\Omega \boldsymbol{z}(t, x, y) p_m(x, y)^* dx dy \in \mathbb{C}^2 \tag{11.23}$$

for *wave number* $m = (m_x, m_y) \in \mathbb{Z}^2$, where

$$p_m(x, y) := \frac{1}{\sqrt{L_x L_y}} \mathrm{e}^{2\pi j \left(\frac{m_x x}{L_x} + \frac{m_y y}{L_y}\right)}$$

and p_m^* is its complex conjugate. This satisfies

$$z(t,x,y) = \sum_{m\in\mathbb{Z}^2} z_m(t) \mathrm{e}^{2\pi j(\frac{m_x x}{L_x}+\frac{m_y y}{L_y})}.$$

Note that

$$z_m = z_{-m}^* \quad \text{for all} \quad m \in \mathbb{Z}^2 \tag{11.24}$$

since the dynamics of our interest is real-valued. Then, it is useful to investigate the dynamics of each spatial component $\{z_m(t)\}_{m\in\mathbb{Z}^2}$ instead of $\{z(t,x,y)\}_{(x,y)\in\Omega}$.

Let us consider the localized dynamics around the trivial pattern z_{eq}. It should be emphasized that each wave number has its *decoupled* local dynamics:

$$\frac{d}{dt} z_m(t) = A_m z_m(t), \tag{11.25}$$

$$A_m := A - s_m D =: \begin{bmatrix} \bar{a}_{11} & -a_{12} \\ a_{21} & -\bar{a}_{22} \end{bmatrix}, \tag{11.26}$$

$$A := \begin{bmatrix} a_{11} & -a_{12} \\ a_{21} & -a_{22} \end{bmatrix}, \quad D := \begin{bmatrix} D_u & 0 \\ 0 & D_v \end{bmatrix}, \tag{11.27}$$

$$s_m := \left(\frac{2\pi m_x}{L_x}\right)^2 + \left(\frac{2\pi m_y}{L_y}\right)^2. \tag{11.28}$$

Note that when $D_u \neq D_v$, stability of A does not necessarily guarantee stability of A_m. In such a case, the corresponding spatial wave p_m *grows* around the z_{eq}. Further discussion on the pattern formation needs to consider the effect of nonlinearity.

11.3.2 Problem Formulation

Let us formulate a stabilization problem of unstable spatial patterns. We define the set of wave numbers for which the local dynamics is unstable: We assume that the finite set $\mathscr{M} \subset \mathbb{Z}^2$ satisfies

1. A_m has at least one eigenvalue in $\mathbb{C}_+$ if $m \in \mathscr{M}$,
2. A_m is stable if $m \notin \pm\mathscr{M} := \{\pm m : m \in \mathscr{M}\}$, and
3. if $m \in \mathscr{M}$, then $-m \notin \mathscr{M}$.

Because $A_m = A_{-m}$ and (11.24), we imposed the condition (3) in order to avoid redundancy. It should be emphasized that $s_{m_1} = s_{m_2}$ can hold for $m_1 \neq m_2$.

Next, for the feedback control problem [10], we assume that we can observe and also manipulate u in a spatially distributed manner. Thus, the controlled reaction-diffusion system is given by

$$\begin{cases} u_t = D_u \Delta u + f(u, v) + \boldsymbol{w}, \\ v_t = D_v \Delta v + g(u, v), \\ \boldsymbol{w} = W(\boldsymbol{u}), \end{cases} \qquad (x, y) \in \Omega. \tag{11.29}$$

Problem 11.1 Let $\theta_m \in \mathbb{R},\ m \in \mathscr{M}$ be given. Under definitions and assumptions above, find a feedback control law $W(\cdot)$ such that

1. z does not diverge,
2. z_m for $m \notin \pm\mathscr{M}$ asymptotically vanishes,
3. $\mathrm{e}^{j\theta_m} z_m$ for $m \in \mathscr{M}$ converges to the same nonzero value, and
4. $\boldsymbol{w}(t, x, y)$ asymptotically vanishes.

11.3.3 Feedback Control of Center Manifold Dynamics

In view of the assumption on the stability of A_m, let us assume that z_m is negligible for $m \notin \pm\mathscr{M}$ to avoid infinite-dimensionality [11]. We analyze the dynamics that z_m should obey when there exists no third order resonance: If $n_1,\ n_2,\ n_3 \in \mathscr{M}$ satisfy $n_1 + n_2 + n_3 = m \in \pm\mathscr{M}$, then at least one of n_i's is equal to m.

By putting $z_m \approx 0$ for $m \notin \pm\mathscr{M}$, the wave number m component appears only from the combination $(n_1, n_2, n_3) = (m, n, -n)$ and its permutation, where $n \in \pm\mathscr{M}$ is arbitrary. Therefore, we obtain the following approximation in the spatial frequency domain:

$$\frac{d}{dt}\begin{bmatrix} u_m \\ v_m \end{bmatrix} = A_m \begin{bmatrix} u_m \\ v_m \end{bmatrix} + \begin{bmatrix} -u_m \left(3|u_m|^2 + 6 \sum_{n \neq m} |u_n|^2 \right) \\ 0 \end{bmatrix} + \begin{bmatrix} w_m \\ 0 \end{bmatrix}, \tag{11.30}$$

where

$$w_m(t) := \int_\Omega w(t, x, y)\, p_m^*(x, y) dx dy.$$

Now, Problem 11.1 is naturally rephrased in this domain:

Problem 11.2 Consider the complex-valued system (11.30) and $\theta_m \in \mathbb{R},\ m \in \mathscr{M}$. Then, find a feedback control law

$$w_m(t) = W_m((u_n(t))_{n \in \mathscr{M}})$$

such that,

(1′) z_m is *ultimately bounded*, that is, there exists (initial state independent) $R > 0$ such that

$$\limsup_{t\to\infty} \|z_m\| < R \quad \text{for all} \quad m \in \mathscr{M}, \tag{11.31}$$

(3′-a)

$$\lim_{t\to\infty} |e^{j\theta_m} z_m(t) - e^{j\theta_n} z_n(t)| = 0 \quad \text{for all} \quad m, n \in \mathscr{M}, \tag{11.32}$$

(3′-b) the origin is locally unstable, and

(4′)

$$\lim_{t\to\infty} w_m(t) = 0 \quad \text{for all} \quad m \in \mathscr{M}. \tag{11.33}$$

For this problem, we can simply obtain a desired control law by considering the specific structure of Problem 11.2.

Theorem 11.8 *For* Problem 11.2*, consider the following diffusive coupling on* $\mathscr{M}$

$$w_m(t) = \sigma \sum_{n\in\mathscr{M}, n\neq m} \gamma_{mn}(e^{j\theta_n - j\theta_m} u_n(t) - u_m(t)), \tag{11.34}$$

where $\gamma_{mn} \geq 0$*. If* γ_{mn} *is associated to a strongly connected*[1] *graph on* $\mathscr{M}$*, then there exists* $\underline{\sigma} > 0$ *such that the control law* (11.34) *with any strength* $\sigma > \underline{\sigma}$ *satisfies the following:*

- *the condition* (1′) *in* Problem 11.2 *holds.*
- *If* $s_m = \bar{s}$ *(see* (11.28)*for the definition) for all* $m \in \mathscr{M}$*, then* (3′-a), (3′-b), (4′) *are also satisfied.*

Proof When we redefine $e^{j\theta_m} z_m$ as z_m, this theorem is equivalent to [12, Theorem1].

As a next step, we need to embed this proposed control law onto the original partial differential equation. The corresponding input pattern should be given as

$$w(t, x, y) := 2\sigma \sum_{m\in\mathscr{M}} Re\left(p_m \left(\sum_{n\neq m,\ n\in\mathscr{M}} \gamma_{mn}(e^{j(\theta_n - \theta_m)} u_n - u_m) \right) \right), \tag{11.35}$$

where u_m for $m \in \mathscr{M}$ is defined by (11.23). We have already verified numerically that this control law achieves the expected pattern formation.

[1] For any $m_i, m_j \in M$, there exists a sequence $\{i_1, i_2, \ldots, i_K\}$ on $\mathscr{M}$ such that $\gamma_{i_k, i_{k+1}} > 0$ for all $k = 1, \ldots, K-1$ and $i_1 = i, i_K = j$.

11.3.4 Numerical Example

The simulation in this section is executed under the following parameter settings: We take

$$A = \begin{bmatrix} 1 & -1 \\ 3 & -2 \end{bmatrix}, \tag{11.36}$$

$$D_u = 0.2, \tag{11.37}$$

$$D_v = 1.5, \tag{11.38}$$

and

$$L_x = \frac{8\pi}{\sqrt{1.8}}, \quad L_y = \frac{L_x}{\sqrt{3}}. \tag{11.39}$$

For these parameters, A_m has one (real) unstable eigenvalue for $m = \pm m_i$

$$m_1 = (4, 0), \quad m_2 = (2, 2), \quad m_3 = (2, -2), \tag{11.40}$$

and A_m stable otherwise.

The initial patterns are randomly generated but sufficiently close to z_{eq}. We can expect this reaction-diffusion system can generate three roll patterns corresponding to m_i's in (11.40). Figure 11.9 is the snapshots of $\boldsymbol{u}(t, x, y)$ for the uncontrolled ($\boldsymbol{w} = 0$) reaction-diffusion dynamics. Actually, all of observed patterns (including transient ones) look like superpositions of these roll patterns.

Next, we attempt to stabilize another spacial pattern by feedback control. We implement the distributed actuation (11.35) where

$$\theta_{m_1} = 0, \quad \theta_{m_2} = 2\pi/3, \quad \theta_{m_3} = 4\pi/3$$

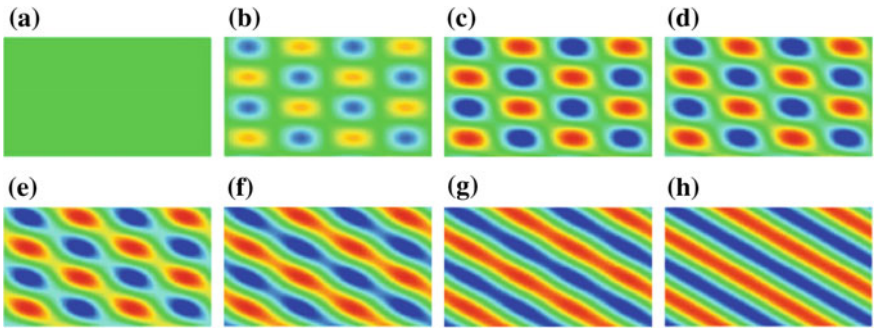

Fig. 11.9 Spatial pattern formation in uncontrolled reaction-diffusion systems. Depending on the initial profile, only one of the three base roll patterns appears. **a** $t = 0$. **b** $t = 3000$. **c** $t = 3500$. **d** $t = 3600$. **e** $t = 3700$. **f** $t = 4000$. **g** $t = 4300$. **h** $t = 5000$

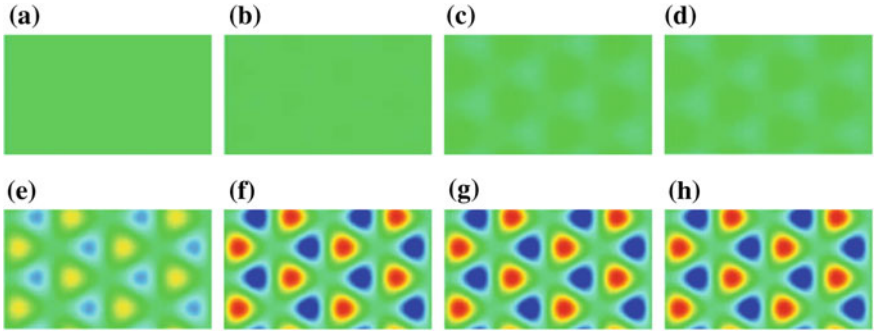

Fig. 11.10 Spatial pattern formation in controlled reaction-diffusion systems. Independent of the initial profile, the rotational symmetry is achieved. **a** $t = 0$. **b** $t = 2000$. **c** $t = 2500$. **d** $t = 2750$. **e** $t = 3000$. **f** $t = 3500$. **g** $t = 4000$. **h** $t = 5000$

and

$$\gamma_{mn} = 1, \quad m \neq n, \quad \sigma = 0.1. \tag{11.41}$$

Figure 11.10 shows the snapshots of $u(t, x, y)$ for the controlled dynamics. We can observe the convergence to another spatial pattern consisting of the three spatial spectra.

11.3.5 Summary

In this section, we formulated a feedback stabilization problem of unstable non-uniform spatial pattern in the reaction-diffusion systems. This problem was solved in the finite dimensionally approximated system. The proposed law, which is a diffusive coupling in the spatial spectrum, achieves desired spectrum consensus while preserving the instability of the trivial equilibrium pattern.

Acknowledgments The authors would like to thank Mr. Yusuke Umezu of Graduate School of Engineering Science, Osaka University for his help for numerical simulation of the controlled reaction-diffusion dynamics.

References

1. Cross, M., Hohenberg, P.: Pattern formation outside of equilibriums. Rev. Mod. Phys. **65**(3) (1993)
2. Ogawa, T.: Nonlinear Phenomenon and Differential Equations, SGC-74. SAIENSU-SHA Co., Ltd (2010) (in Japanese)

3. Armbruster, D., Guckenheimer, J., Holmes, P.: Heteroclinic cycles and modulated travelling waves in systems with O(2) symmetry. Phys. D **29**(3), 257–282 (1988)
4. Britton, N.F.: Spatial structures and periodic travelling waves in an integro-differential reaction-diffusion population model. SIAM J. Appl. Math. **50**(6), 1663–1688 (1990)
5. Smith, T.R., Moehlis, J., Holmes, P.: Heteroclinic cycles and periodic orbits for the O(2)-equivariant 0:1:2 mode interaction. Phys. D **211**(3–4), 347–376 (2005)
6. Ogawa, T., Okuda, T.: Oscillatory dynamics in a reaction-diffusion system in the presence of 0:1:2 resonance. Netw. Heterog. Media **7**(4), 893–926 (2012)
7. Yang, L., Dolnik, M., Zhabotinsky, A.M., Epstein, I.R.: Pattern formation arising from interactions between Turing and wave instabilities. J. Chem. Phys. **117**, 7259 (2002)
8. Gourley, S.A., Britton, N.F.: A predator-prey reaction-diffusion system with nonlocal effects. J. Math. Biol. **34**(3), 297–333 (1996)
9. Turing, A.M.: The chemical basis of morphogenesis. Philo. Trans. Royal Soc. B: Biol. Sci. **237**(641), 37–72 (1952)
10. Mikhailov, A.S., Showalter, K.: Control of waves, patterns and turbulence in chemical systems. Phys. Rep. **425**(2–3), 79–194 (2006)
11. Curtain, R.F., Zwart, H.J.: An Introduction to Infinite-Dimensional Linear Systems Theory. Springer, Berlin (1995)
12. Kashima, K., Ogawa, T., Sakurai, T.: Feedback stabilization of non-uniform spatial pattern in reaction-diffusion systems. In: Proceedings of American Control Conference 2013, pp. 3759–3764 (2013)

Chapter 12
Control of Unstabilizable Switched Systems

Shun-ichi Azuma, Tomomi Takegami and Yoshito Hirata

12.1 Introduction

In the past half a century, the control theory has focused on *stabilization* problems of *stabilizable* systems, for which a number of results have been derived so far. On the other hand, the control of *unstabilizable* systems, which has never been actively studied in the control community, has become increasingly important in a wide range of applications. For instance, as easily imagined, cancer treatment with medication is a kind of "control" but the controlled object is often an unstabilizable system in the sense that cancer cells may not be stopped from growing by medication. For such an application, it is strongly desired to delay cancer cell growth for the extension of life.

This paper thus addresses a control problem of a class of unstabilizable systems. The systems to be studied are switched systems with controlled switching, which can describe, for example, the aforementioned cancer dynamics. For the systems, we aim at delaying the divergence as long as possible.

First, we formulate a divergence delay problem and explain its hardness. Next, we propose an approximate solution based on discrete abstraction. The proposed framework reduces the divergence delay problem into the longest path problem of

S. Azuma (✉)
Graduate School of Informatics, Kyoto University,
Yoshida Honmachi, Sakyo-ku 606-8501, Japan
e-mail: sazuma@i.kyoto-u.ac.jp

T. Takegami
Mitsubishi Electric Corporation, Chiyoda, Japan

Y. Hirata
Institute of Industrial Science, The University of Tokyo,
4-6-1 Komaba, Meguro-ku, Tokyo 153-8505, Japan
e-mail: yoshito@sat.t.u-tokyo.ac.jp

K. Aihara et al. (eds.), *Analysis and Control of Complex Dynamical Systems*,
Mathematics for Industry 7, DOI 10.1007/978-4-431-55013-6_12

a directed graph, which allows us to approximately solve the hard problem in an efficient way. The proposed framework is then applied to the scheduling problem of intermittent androgen suppression to delay the relapse of prostate cancer. By using the mathematical model given by Hirata et al. [1, 2], it is demonstrated that, compared with the continuous treatment, the relapse of prostate cancer is delayed for more than 10 years for a patient.

Finally, it should be noticed that this paper is based on our preliminary version [3] published in a conference proceedings.

Notation: Let $\mathbf{R}$, $\mathbf{R}_+$, and $\mathbf{N}$ be the real number field, the set of positive real numbers, and the set of natural numbers (note that $0 \notin \mathbf{N}$), respectively. The logarithm of a to base 10 is simply denoted by $\log a$. For the vector x and the matrix M, we use $\|x\|$ and $\|M\|$ to represent the ∞-norm (the induced norm for M).

12.2 Problem Formulation

12.2.1 Unstabilizable Switched Systems

Consider the switched system

$$\Sigma : \begin{cases} x(t+1) = A_{s(t)}x(t), \\ y(t) \quad\ = Cx(t), \end{cases} \tag{12.1}$$

where $x(t) \in \mathbf{R}^n$ is the state, $s(t) \in \mathbf{S} := \{0, 1, \ldots, m-1\}$ is the input, $y(t) \in \mathbf{R}$ is the output (which is scalar-valued), and $A_s \in \mathbf{R}^{n\times n}$ $(s = 0, 1, \ldots, m-1)$ and $C \in \mathbf{R}^{1\times n}$ are constant matrices.

For the system Σ and a given time interval $\{0, 1, \ldots, \tau\}$, we denote by $x(t, x_0, \sigma_\tau)$ the state $x(t)$ for the time $t \in \{0, 1, \ldots, \tau\}$, the initial state $x(0) = x_0 \in \mathbf{R}^n$, and the input sequence $(s(0), s(1), \ldots, s(\tau-1)) = \sigma_\tau \in \mathbf{S}^\tau$. The corresponding output $y(t)$ is represented by $y(t, x_0, \sigma_\tau)$, i.e., $y(t, x_0, \sigma_\tau) = Cx(t, x_0, \sigma_\tau)$ from (12.1).

The switched system Σ is said to be *unstabilizable* if there exists an $x_0 \in \mathbf{R}^n$ such that

$$\lim_{t\to\infty} \|y(t, x_0, \sigma_\infty)\| = \infty \tag{12.2}$$

for every $\sigma_\infty \in \mathbf{S}^\infty$, where $\mathbf{S}^\infty := \prod_{i=1}^{\infty} \mathbf{S} = \mathbf{S} \times \mathbf{S} \times \cdots$.

12.2.2 Divergence Delay Problem

In this paper, we consider a problem of delaying the divergence of the unstabilizable switched system Σ. The problem is formulated as follows.

Suppose that $\tau \in \mathbf{N}$, $\gamma \in \mathbf{R}_+$, $x_0 \in \mathbf{R}^n$, and $\sigma_\tau \in \mathbf{S}^\tau$ are given for the unstabilizable system Σ. If $\gamma \leq y(t, x_0, \sigma_\tau)$ holds for some $t \in \{0, 1, \ldots, \tau\}$, we denote by $J(x_0, \sigma_\tau)$ the minimum $t \in \{0, 1, \ldots, \tau\}$ such that $\gamma \leq y(t, x_0, \sigma_\tau)$. Otherwise (i.e., $\gamma > y(t, x_0, \sigma_\tau)$ for every $t \in \{0, 1, \ldots, \tau\}$), let $J(x_0, \sigma_\tau) := \tau$. The number $J(x_0, \sigma_\tau)$ quantifies the slowness of the divergence of the unstabilizable system Σ for the initial state x_0 and the input sequence σ_τ. Then the divergence delay problem is described as follows.

Problem 12.1 For the unstabilizable system Σ, suppose that $\tau \in \mathbf{N}$, $\gamma \in \mathbf{R}_+$, and $x_0 \in \mathbf{R}^n$ are given. Then, find an input sequence $\sigma_\tau \in \mathbf{S}^\tau$ maximizing $J(x_0, \sigma_\tau)$. □

Since $\mathbf{S}^\tau$ is a finite set of cardinality m^τ, Problem 12.1 is a combinatorial optimization problem whose feasible solution set exponentially grows with τ. So it is in general hard to derive a solution for a large τ. This motivates us to find a sub-optimal solution.

12.3 Discrete Abstraction of Switched Systems

In order to derive a sub-optimal solution to Problem 12.1, we introduce the following system as an approximation of the system Σ:

$$\Sigma_d : \begin{cases} z(t+1) = Q(A_{s(t)} z(t)), \\ w(t) \quad\;\; = Cz(t), \end{cases} \tag{12.3}$$

where $z(t) \in \mathbf{R}^n$ is the state, $s(t) \in \mathbf{S} := \{0, 1, \ldots, m-1\}$ is the input, $w(t) \in \mathbf{R}$ is the output, $Q : \mathbf{R}^n \to \mathbf{Z}$ is a quantizer for a (given) discrete set $\mathbf{Z} \subset \mathbf{R}^n$, and A_s ($s = 0, 1, \ldots, m-1$) and C are the constant matrices given for (12.1).

Since $z(t+1) \in \mathbf{Z}$ by the quantizer Q, the state z always takes a value on the discrete set $\mathbf{Z}$. That is, the system Σ_d is a discrete-state system. Such a discrete abstraction technique has been proposed in [4] and it can be easily shown that, if a sufficiently fine quantizer is employed as Q, Σ_d can capture the dynamics of Σ in a finite time interval.

In a similar way to Sect. 12.2, the divergence delay problem is formulated for the system Σ_d. We use $z(t, z_0, \sigma_\tau)$ and $w(t, z_0, \sigma_\tau)$ to express the state $z(t)$ and the output $w(t)$ for the time $t \in \{0, 1, \ldots, \tau\}$, the initial state $z(0) = z_0 \in \mathbf{Z}$, and the input sequence $(s(0), s(1), \ldots, s(\tau-1)) = \sigma_\tau \in \mathbf{S}^\tau$. Moreover, we similarly define the notion of unstabilizability and the number $J(z_0, \sigma_\tau)$ for the output $w(t, z_0, \sigma_\tau)$. Then the divergence delay problem for Σ_d is given as follows.

Problem 12.2 For the unstabilizable system Σ_d, suppose that $\tau \in \mathbf{N}$, $\gamma \in \mathbf{R}_+$, and $z_0 \in \mathbf{Z}$ are given. Then, find an input sequence $\sigma_\tau \in \mathbf{S}^\tau$ maximizing $J(z_0, \sigma_\tau)$. □

12.4 Divergence Delay Control Based on Discrete Abstraction

Now, we give a solution to Problem 12.2 as an approximate solution to Problem 12.1.

It is clear that the discrete-state system Σ_d in (12.3) corresponds to the edge-labeled directed graph G (which is an infinite graph) with

- the node set $\mathbf{Z}$,
- the edge set $\bigcup_{s\in\mathbf{S}}\{(z, z_+) \in \mathbf{Z} \times \mathbf{Z} \mid z_+ = Q(A_s z)\}$, and
- the labeling function L which maps the edge (z, z_+) to $s \in \mathbf{S}$ satisfying $z_+ = Q(A_s z)$.

The graph G represents all the state transitions of Σ_d, where the edge labels corresponds to the input for the transition. An example of G is shown in Fig. 12.1. Note for G that the nodes are of outdegree m and there may exist multiple edges of different labels.

For the graph G, we further introduce the directed graph G_γ (which is unlabeled) given by removing all the edge labels and performing the vertex contraction with respect to all the nodes $z \in \mathbf{Z}$ satisfying $Cz \geq \gamma$. The resulting contracted node is denoted by z_γ. The graph G_γ is illustrated in Fig. 12.2.

Then the following result is obtained.

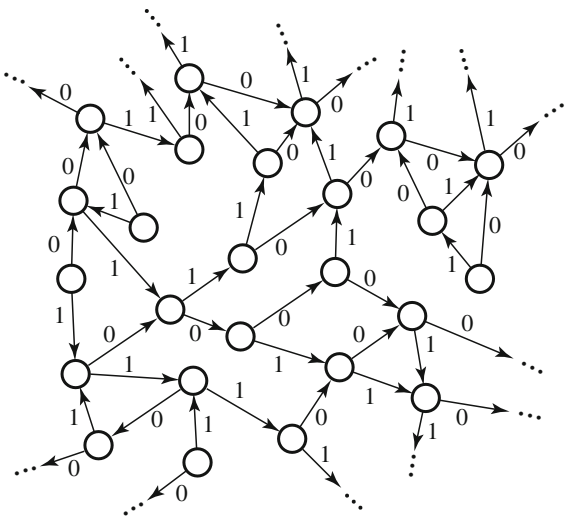

Fig. 12.1 Example of graph G for $m = 2$. It represents all the state transitions of Σ_d where the edge labels corresponds to the input for the transition

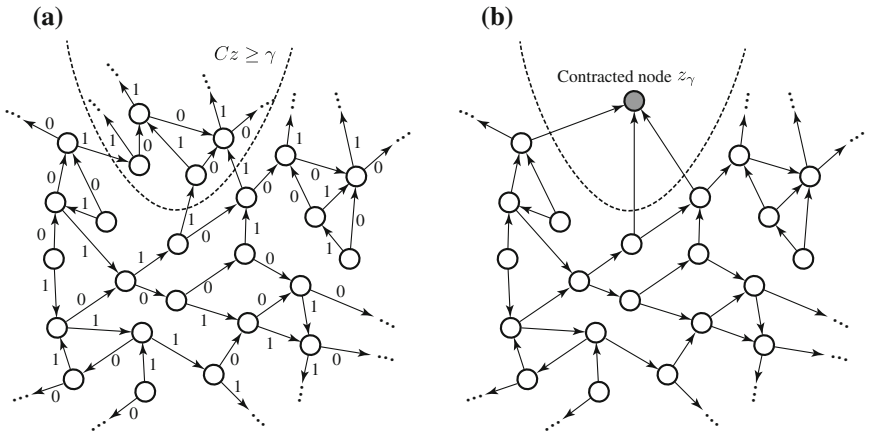

Fig. 12.2 Example of graph G_γ. It is generated from G so as to remove all the edge labels and perform the vertex contraction with respect to all the nodes $z \in \mathbf{Z}$ satisfying $Cz \geq \gamma$. **a** Graph G and nodes $z \in \mathbf{Z}$ satisfying $Cz \geq \gamma$. **b** Graph G_γ

Theorem 12.1 *For the unstabilizable system Σ_d, consider the directed graph G_γ. Let $(z_0, z_1^*, z_2^*, \ldots, z_p^*, z_\gamma)$ be a longest path from node z_0 to node z_γ (in G_γ). Then the following statements hold:*
(i) A solution to Problem 12.2 is given by

$$\sigma_\tau^* = \begin{cases} (L(z_0, z_1^*), L(z_1^*, z_2^*), L(z_2^*, z_3^*), \ldots, L(z_{\tau-1}^*, z_\tau^*)), & \text{if } p+1 \geq \tau, \\ (L(z_0, z_1^*), L(z_1^*, z_2^*), L(z_2^*, z_3^*), \ldots, L(z_{p-1}^*, z_p^*), L(z_p^*, z_\gamma), & \\ \qquad s_{p+2}, s_{p+3}, \ldots, s_{\tau-1}), & \text{otherwise,} \end{cases} \tag{12.4}$$

where L is the labeling function of the the edge-labeled directed graph G, z_τ^* expresses z_γ only if $p+1 = \tau$, and $(s_{p+2}, s_{p+3}, \ldots, s_{\tau-1}) \in \boldsymbol{S}^{\tau-p-1}$ is arbitrarily given.
(ii) The number $J(x_0, \sigma_\tau^*)$ is given by

$$J(x_0, \sigma_\tau^*) = \begin{cases} \tau, & \text{if } p+1 \geq \tau, \\ p+1, & \text{otherwise.} \end{cases} \tag{12.5}$$

□

It follows from this result that Problem 12.2 is reduced into the longest path problem for the directed graph G_γ.

It is well-known that there exist efficient solutions to the longest path problems for acyclic graphs (see e.g., [5]). Moreover, G_γ is acyclic if Q is appropriately selected (so that, in G, there exists no self-loop for the nodes z satisfying $Cz \geq \gamma$). So, as long as n is not so large (i.e., Σ is a low-dimensional system), the proposed framework gives an efficient approximate solution to Problem 12.1.

12.5 Application to Optimal Scheduling Intermittent Androgen Suppression for Treatment of Prostate Cancer

Let us apply the proposed framework to the scheduling problem of intermittent androgen suppression (ISA) to delay the relapse of prostate cancer [1, 2, 6].

ISA is a treatment of prostate cancer which alternately starts and stops androgen suppression in certain periods. The key point for success is the scheduling of the on-treatment period and off-treatment period. So the scheduling problem is an important issue of ISA. On the other hand, in ISA, the dynamics of tumor progression switches between the on-treatment mode and off-treatment mode, which implies that the dynamics is modeled as a switched system.

Here, we deal with this scheduling problem for patients whose relapse cannot be avoided but can be delayed by the intermittent androgen suppression (called *Type 2* in [1]) as the divergence delay problem.

12.5.1 Mathematical Model of ISA

A mathematical model [6] of the tumor progression dynamics is given by (12.1) where $n = 3$, $m = 2$, $x(t) := [x_1(t)\ \ x_2(t)\ \ x_3(t)]^{\mathsf{T}}$, and

$$A_0 := \begin{bmatrix} a_{011} & a_{012} & 0 \\ 0 & a_{022} & 0 \\ 0 & 0 & a_{033} \end{bmatrix}, \quad A_1 := \begin{bmatrix} a_{111} & 0 & 0 \\ a_{121} & a_{122} & 0 \\ a_{131} & a_{132} & a_{133} \end{bmatrix},$$
$$C := [1\ \ 1\ \ 1].$$

Here, the unit of t is the month, $x_i(t)$ $(i = 1, 2, 3)$ are the amount of three kinds of cancer cells, $u(t)$ is the input expressing the on-treatment and off-treatment modes, and $y(t)$ $(= x_1(t) + x_2(t) + x_3(t))$ corresponds to (an approximated value of) the prostate specific antigen (PSA) level. The matrices A_s $(s = 0, 1)$ are for the on-treatment period and for the off-treatment period, respectively, and the elements a_{0ij} and a_{1ij} are constant numbers which depend on patients. For example, they are given by $a_{011} := 1.1374$, $a_{012} := 3.1466$, $a_{022} := 1.2538$, $a_{033} := 0.7802$, $a_{111} := 8.833 \times 10^{-2}$, $a_{121} := 3.8767 \times 10^{-3}$, $a_{122} := 8.6119 \times 10^{-1}$, $a_{131} := 8.3344 \times 10^{-6}$, $a_{132} := 2.9161 \times 10^{-3}$, and $a_{133} := 1.2059$, which are used in this paper.

12.5.2 Sub-optimal Scheduling Based on Discrete Abstraction

For the above system, let us consider Problem 12.1 for $\tau = 200$ (approximately 17 years) and $\gamma = 1$.

We first introduce the discrete-state system Σ_d with the discrete set $\mathbf{Z} \subset \mathbf{R}^3$ and the quantizer $Q : \mathbf{R}^3 \to \mathbf{Z}$. The set $\mathbf{Z}$ is given by $\mathbf{Z} := \mathbf{Z}_1 \times \mathbf{Z}_2 \times \mathbf{Z}_3$, where

$$\mathbf{Z}_1 := \left\{10^{-8},\ 10^{-8+\frac{8}{300}},\ 10^{-8+2\frac{8}{300}}, \ldots,\ 10^{-8+300\frac{8}{300}}\right\},$$
$$\mathbf{Z}_2 := \left\{10^{-3},\ 10^{-3+\frac{3+\log 0.3}{300}},\ 10^{-3+2\frac{3+\log 0.3}{300}}, \ldots,\ 10^{-3+300\frac{3+\log 0.3}{300}}\right\},$$
$$\mathbf{Z}_3 := \left\{10^{-2},\ 10^{-2+\frac{2}{300}},\ 10^{-2+2\frac{2}{300}}, \ldots,\ 10^{-2+300\frac{2}{300}}\right\}.$$

Meanwhile,

$$Q(\mu) := \begin{bmatrix} \mathrm{argmin}_{z_1 \in \mathbf{Z}_1 \text{ s.t. } z_1 \geq \mu_1} \| \log \mu_1 - \log z_1 \| \\ \mathrm{argmin}_{z_2 \in \mathbf{Z}_2 \text{ s.t. } z_2 \geq \mu_2} \| \log \mu_2 - \log z_2 \| \\ \mathrm{argmin}_{z_3 \in \mathbf{Z}_3 \text{ s.t. } z_3 \geq \mu_3} \| \log \mu_3 - \log z_3 \| \end{bmatrix},$$

where $\mu_i \in \mathbf{R}$ is the i-th element of $\mu \in \mathbf{R}^3$.

Then a solution to Problem 12.2 is given as Fig. 12.3 by solving the longest path problem for G_γ. The computation time is approximately 8 (min) by the computer with Intel Core i7-3960X processor (3.3GHz) and a 64GB memory unit. In this case, the output $w(t)$ of Σ_d is shown in Fig. 12.4. We see that the relapse of prostate cancer is delayed for more than 10 years and the solution delivers high performance in the approximate model.

Now, we apply the solution in Figure 12.3 to the original switched system. Fig. 12.5 depicts the output $y(t)$ (i.e., the PSA level). It is observed that the relapse of prostate cancer is delayed for more than 10 years also in the original system, and we can conclude that the proposed framework is useful in the medical application.

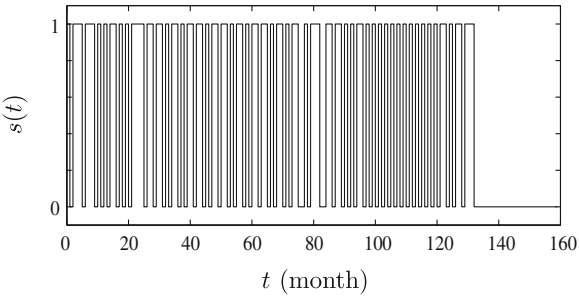

Fig. 12.3 Treatment schedule. It is given by solving the longest path problem for the graph G_γ

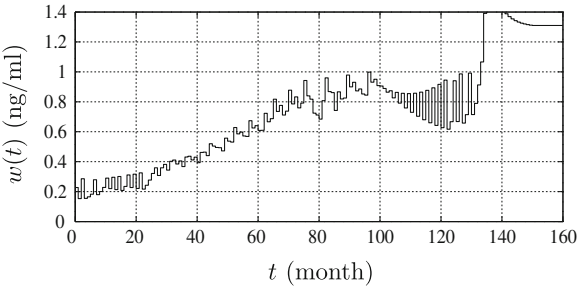

Fig. 12.4 PSA level for discrete-state system model. The relapse of prostate cancer is delayed for more than 10 years in the approximate model

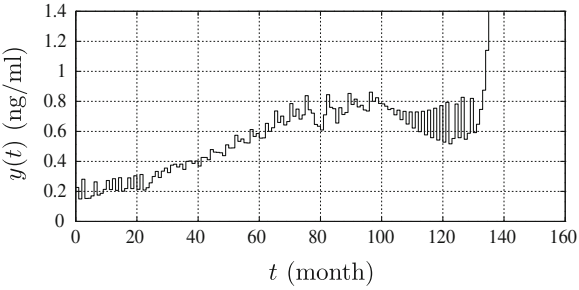

Fig. 12.5 PSA level for original switched system model. The relapse of prostate cancer is delayed for more than 10 years even in the original system

12.6 Conclusion

A control problem has been considered for unstabilizable switched systems. We have established a discrete-abstraction-based framework to approximately solve the problem. The performance is demonstrated for the scheduling problem of intermittent androgen suppression to delay the relapse of prostate cancer. We hope that our result is a foundation of control of unstabilizable systems.

In the future, it is expected to establish an exact and practical solution to the problem, since this paper has given an approximate solution. Also, the result should be extended to a more general class of unstabilizable systems.

References

1. Hirata, Y., Akakura, K., Higano, C.S., Brhchovsky, N., Aihara, K.: Quantitative mathematical modeling of PSA dynamics of prostate cancer patients treated with intermittent androgen suppression. J. Mol. Cell Biol. **4**, 127–132 (2012)
2. Hirata, Y., Azuma, S., Aihara, K.: Model predictive control for optimally scheduling intermittent androgen suppression of prostate cancer. Control of unstabilizable systems by discrete abstraction. Methods **67**, 278–281 (2014)
3. Takegami, T., Azuma, S., Hirata, Y., Sugie, T.: Control of unstabilizable systems by discrete abstraction. In: Proceedings of SICE 13th Annual Conference on Control Systems, P0906 (2013)
4. Tazaki, Y., Imura, J.: Bisimilar finite abstractions of interconnected systems. In: Proceedings of International Conference on Hybrid Systems: Computation and Control, pp. 22–24 (2008)
5. Cormen, T.H., Leiserson, C.E., Rivest, R.L., Stein, C.: Introduction to Algorithms, MIT Press, Cambridge (2009)
6. Hirata, Y., Bruchovsky, N., Aihara, K.: Development of a mathematical model that predicts the outcome of hormone therapy for prostate cancer. J. Theor. Biol. **264**, 517–527 (2010)

Part III
Complex Networks and Modeling for Control

Chapter 13
Clustered Model Reduction of Large-Scale Bidirectional Networks

Takayuki Ishizaki, Kenji Kashima, Jun-ichi Imura and Kazuyuki Aihara

13.1 Introduction

Dynamical systems that appear in both science and engineering are often modeled as interconnected systems. Examples of such interconnected systems include social networks, computer networks, biological networks and so forth [4, 11], whose interconnection topology is complex and large-scale in general. An approximation method is often used to relax their complexity [1, 13]. During the approximation, it is important to retain specific system properties/structures, such as stability and interconnection topology, for practical analyses and syntheses. In view of this, network structure-preserving model reduction is required and expected to be an efficient tool to simplify the analysis as well as control of large-scale interconnected systems.

In the literature, several network structure-preserving model reduction methods can be found. For instance, a Krylov projection method for interconnected systems is proposed in [15], where a block-diagonally structured projection is performed for

T. Ishizaki(✉)
Graduate School of Information Science and Engineering, Tokyo Institute of Technology, 2-12-1 Oh-Okayama, Meguro-ku, Tokyo 152-8552, Japan
e-mail: ishizaki@mei.titech.ac.jp

K. Kashima
Graduate School of Informatics, Kyoto University, Yoshida Honmachi, Sakyo-ku, Kyoto 606-8501, Japan
e-mail: kashima@amp.i.kyoto-u.ac.jp

J. Imura
Graduate School of Information Science and Engineering, Tokyo Institute of Technology, 2-12-1 Oh-Okayama, Meguro-ku, Tokyo 152-8552, Japan
e-mail: imura@mei.titech.ac.jp

K. Aihara
Institute of Industrial Science, University of Tokyo, 4-6-1 Komaba, Meguro-ku, Tokyo 153-8505, Japan
e-mail: aihara@sat.t.u-tokyo.ac.jp

K. Aihara et al. (eds.), *Analysis and Control of Complex Dynamical Systems*,
Mathematics for Industry 7, DOI 10.1007/978-4-431-55013-6_13

each subsystem to retain the interconnection topology among subsystems. However, since complete knowledge on the partition of the whole system into subsystems is necessary in advance, this method cannot deal with network systems in which subsystem partition is not apparent. As a similar way, a structured balanced truncation method for interconnected systems is proposed in [14], where the balanced truncation is performed for each subsystem. It should be noted that both of [15] and [14] do not theoretically discuss a relation between the subsystem partition and the resultant error caused by the the balanced truncation of each subsystem.

Against this background, the authors have developed a clustered model reduction method for interconnected linear systems, in which first-order subsystems are coupled over large-scale networks [7–9]. In this method, we introduce the notion of cluster reducibility, which is defined as the uncontrollability of disjoint subsets of state variables, called clusters. Furthermore, we provide an algorithm to find a set of reducible clusters. The aggregation of the reducible cluster produces an approximate model that preserves the interconnection topology among clusters as well as the stability of systems, with the provision of an error evaluation in terms of the $\mathscr{H}_2/\mathscr{H}_\infty$-norm. In this chapter, we overview the clustered model reduction method for bidirectional networks proposed in [9], and show several new numerical experiments from a viewpoint of the growth of computation time and comparison between a scale-free network and the Erdö-Rényi network. Furthermore, we provide detailed proofs to make the theoretical results easily comprehensible.

Notation. We denote the set of real numbers by $\mathbb{R}$, the set of nonnegative real numbers by $\mathbb{R}_{\geq 0}$, the n-dimensional identity matrix by I_n, the ith column of I_n by e_i^n, the cardinality of a set $\mathscr{I}$ by $|\mathscr{I}|$, the l_2-induced norm of a matrix M by $\|M\|$, and the maximum and minimum eigenvalues of a symmetric matrix M by $\lambda_{\max}(M)$ and $\lambda_{\min}(M)$, respectively. For a set of natural numbers $\mathscr{I} \subseteq \{1, \ldots, n\}$, let $e_{\mathscr{I}}^n \in \mathbb{R}^{n \times |\mathscr{I}|}$ denote the matrix composed of the column vectors of I_n compatible with $\mathscr{I}$, and the l_∞-induced norm of a matrix $M \in \mathbb{R}^{n \times m}$ is defined by

$$\|M\|_{l_\infty} := \max_{i \in \{1,\ldots,n\}} \sum_{j=1}^{m} |M_{i,j}|,$$

where $M_{i,j}$ denotes the (i, j)-element of M. A matrix M is said to be *Metzler* if all the off-diagonal entries of M are nonnegative. Furthermore, we denote the block diagonal matrix having matrices $M_1, \ldots, M_n$ on its block diagonal by $\mathrm{diag}(M_1, \ldots, M_N)$. Finally, the $\mathscr{H}_\infty$-norm of a stable transfer matrix G is defined by

$$\|G(s)\|_{\mathscr{H}_\infty} := \sup_{\omega \in \mathbb{R}} \|G(j\omega)\|.$$

13.2 Preliminaries

In this chapter, we deal with the following linear system evolving over bidirectional networks:

Definition 13.1 A linear system

$$\Sigma : \dot{x} = Ax + Bu, \quad A \in \mathbb{R}^{n\times n}, \quad B \in \mathbb{R}^{n} \tag{13.1}$$

is said to be a *bidirectional network* if A is symmetric.

For simplicity, we consider only single-input systems while a similar result can be obtained also for multi-input systems. Examples of bidirectional networks include a kind of reaction-diffusion systems evolving over a network that is given by

$$\dot{x}_i = -r_i x_i + \sum_{j=1, j\neq i}^{n} a_{i,j}(x_j - x_i) + b_i u, \quad i \in \{1, \ldots, n\}, \tag{13.2}$$

where r_i denotes the reaction rate of x_i, and $a_{i,j} = a_{j,i}$ for $i \neq j$ denotes the diffusion intensity between x_i and x_j. This system is often used as a primal model that represents diffusion processes evolving over a complex network [12]. Let $R := \mathrm{diag}([r_1, \ldots, r_n])$ be a reaction matrix and $\mathscr{L} := \{\mathscr{L}_{i,j}\}$ be a weighted graph Laplacian given by

$$\mathscr{L}_{i,j} = \begin{cases} -a_{i,j}, & i \neq j, \\ \sum_{j=1, j\neq i}^{n} a_{i,j}, & i = j. \end{cases}$$

By using them, (13.2) is expressed as a bidirectional network with

$$A = -(R + \mathscr{L}), \quad B = \begin{bmatrix} b_1 \\ \vdots \\ b_n \end{bmatrix}$$

and the state vector $x := [x_1, \ldots, x_n]^\mathsf{T}$. Note that (13.2) is stable if at least one r_i is strictly positive, all $a_{i,j}$ are nonnegative, and the associated graph is connected.

For the arguments below, we introduce the following state-space realization having a positive tridiagonal structure:

Definition 13.2 Let Σ in (13.1) be a bidirectional network. A coordinate transformation $\tilde{x} = H^\mathsf{T} x$ by a unitary matrix $H \in \mathbb{R}^{n\times n}$ is said to be *positive tridiagonalization* if the system matrices $\tilde{A} := H^\mathsf{T} A H \in \mathbb{R}^{n\times n}$ and $\tilde{B} := H^\mathsf{T} B \in \mathbb{R}^{n}_{\geq 0}$ of

$$\tilde{\Sigma} : \dot{\tilde{x}} = \tilde{A}\tilde{x} + \tilde{B}u \tag{13.3}$$

are in the form of

$$\tilde{A} = \begin{bmatrix} \alpha_1 & \beta_1 & & & \\ \beta_1 & \alpha_2 & \beta_2 & & \\ & \ddots & \ddots & \ddots & \\ & & \ddots & \ddots & \beta_{n-1} \\ & & & \beta_{n-1} & \alpha_n \end{bmatrix}, \quad \tilde{B} = \begin{bmatrix} \beta_0 \\ 0 \\ 0 \\ \vdots \\ 0 \end{bmatrix} \tag{13.4}$$

with $\beta_i \geq 0$ for all $i \in \{0, \ldots, n-1\}$. Moreover, $\tilde{\Sigma}$ in (13.3) is referred to as a *positive tridiagonal realization*.

Note that this realization belongs to a class of (internally) positive systems [2, 3, 5] because $\tilde{A}$ is Metzler and the entries of $\tilde{B}$ are all nonnegative. Based on this fact, the following result is proven:

Proposition 13.1 *Let $\tilde{\Sigma}$ in (13.3) be a positive tridiagonal realization, and define*

$$\tilde{X}(s) := (sI_n - \tilde{A})^{-1}\tilde{B}. \tag{13.5}$$

Then, it follows that

$$\|\tilde{X}_i(s)\|_{\mathscr{H}_\infty} = -e_i^{\mathsf{T}}\tilde{A}^{-1}\tilde{B} \tag{13.6}$$

for all $i \in \{1, \ldots, n\}$.

Furthermore, it has a *tridiagonal structure* representing serially cascaded autonomous systems equipped with a boundary input. The existence and uniqueness of positive tridiagonalization are shown as follows:

Proposition 13.2 *For every bidirectional network Σ in (13.1), there exists a unitary matrix $H \in \mathbb{R}^{n\times n}$ for positive tridiagonalization. Furthermore, for*

$$i^* := \begin{cases} \min\limits_{i\in\{1,\ldots,n-1\}} \{i : \beta_i = 0\}, & \text{if } \prod\limits_{i=1}^{n-1} \beta_i = 0, \\ n, & \text{otherwise}, \end{cases} \tag{13.7}$$

the submatrix $He^n_{1:i^*} \in \mathbb{R}^{n\times i^*}$ is uniquely determined among all transformation matrices.

Towards eigenvalue computation and model reduction, effective tridiagonalization procedures for large matrices, e.g., the Householder transformation and the controller Hessenberg transformation [6, 16], have been widely studied in the control and numerical linear algebra communities. From the structure of $\tilde{A}$ and $\tilde{B}$ in (13.4), we see that i^* in (13.7) coincides with the dimension of the controllable subspace of

Σ. In view of this, we see that the uniqueness of $He^n_{1:i^*}$ in Proposition 13.2 corresponds to the uniqueness of the transformation matrix for positive tridiagonalization for the controllable subspace of Σ.

In fact, most positive tridiagonalization procedures can be implemented without computationally expensive operations. For instance, the complexity of the primary algorithm based on the Householder transformation is at most $(2/3)n^3$ even for dense matrices. Furthermore, it is known that the computation can be done in linear time by explicitly considering the sparsity of matrices. In this sense, positive tridiagonalization can be implemented even for large-scale bidirectional networks.

13.3 Clustered Model Reduction

13.3.1 Problem Formulation

In this section, we provide a clustered model reduction method that can preserve the interconnection topology among clusters while guaranteeing a specified error precision. To formulate a clustered model reduction problem, we first introduce the following notion of network clustering:

Definition 13.3 Let $\mathbb{L} := \{1, \ldots, L\}$. The family of an index set $\{\mathscr{I}_{[l]}\}_{l\in\mathbb{L}}$ is called a *cluster set*, each of whose elements is referred to as a cluster, if each element $\mathscr{I}_{[l]} \subseteq \{1, \ldots, n\}$ satisfies

$$\bigcup_{l\in\mathbb{L}} \mathscr{I}_{[l]} = \{1, \ldots, n\}, \quad \mathscr{I}_{[l]} \cap \mathscr{I}_{[l']} = \emptyset, \quad l \neq l'.$$

Furthermore, an *aggregation matrix* compatible with $\{\mathscr{I}_{[l]}\}_{l\in\mathbb{L}}$ is defined by

$$P := \Pi \operatorname{diag}(p_{[1]}, \ldots, p_{[L]}) \in \mathbb{R}^{n\times L}, \tag{13.8}$$

where $p_{[l]} \in \mathbb{R}^{|\mathscr{I}_{[l]}|}$ such that $\|p_{[l]}\| = 1$, and the permutation matrix Π is defined as

$$\Pi := [e_{\mathscr{I}_{[1]}}, \ldots, e_{\mathscr{I}_{[L]}}] \in \mathbb{R}^{n\times n}, \quad e_{\mathscr{I}_{[l]}} \in \mathbb{R}^{n\times|\mathscr{I}_{[l]}|}.$$

In this definition, the aggregation matrix P clearly satisfies $P^\mathsf{T}P = I_L$, i.e., all column vectors of P are orthonormal. Using the aggregation matrix P in (13.8), we define the aggregated model of Σ in (13.1) by

$$\hat{\Sigma} : \begin{cases} \dot{\xi} = P^\mathsf{T}AP\xi + P^\mathsf{T}Bu, \\ \hat{x} = P\xi, \end{cases} \tag{13.9}$$

where $P^\mathsf{T}AP$ is symmetric and stable. Note that each state of the aggregated model $\hat{\Sigma}$ represents an approximant of the clustered states, given by $e_{\mathscr{I}_{[l]}}^\mathsf{T} x \in \mathbb{R}^{|\mathscr{I}_{[l]}|}$. The trajectory of each state of $\hat{\Sigma}$ aims to trace the trajectory of a kind of centroid compatible with the clustered states of Σ.

In this notation, we formulate the following clustered model reduction problem addressed below:

Problem 13.1 Let Σ in (13.1) be a stable bidirectional network. Given a constant $\varepsilon \geq 0$, find an aggregated model $\hat{\Sigma}$ in (13.9) such that

$$\|G(s) - \hat{G}(s)\|_{\mathscr{H}_\infty} \leq \varepsilon \tag{13.10}$$

where

$$G(s) := (sI_n - A)^{-1}B, \quad \hat{G}(s) := P(sI_L - P^\mathsf{T}AP)^{-1}P^\mathsf{T}B \tag{13.11}$$

denote the transfer matrices of Σ and $\hat{\Sigma}$, respectively.

In traditional model reduction methods, each state of the reduced model is usually obtained as a linear combination of *all* states of the original system [1]. This can be rephrased as that the projection matrix has no specific sparse structure. Note that the aggregation matrix (13.8) is *block-diagonally structured*. In this sense, our problem formulation clearly contrasts with the traditional model reduction problems.

13.3.2 Exact Clustered Model Reduction

In this subsection, we consider the case where no approximation error is caused by the cluster aggregation. To do this, we introduce the following notion of the reducibility of clusters:

Definition 13.4 Let Σ in (13.1) be a stable bidirectional network. A cluster $\mathscr{I}_{[l]}$ is said to be *reducible* if there exist a scalar rational function $G_{[l]}^\star$ and a vector $\eta_{[l]} \in \mathbb{R}^{|\mathscr{I}_{[l]}|}$ such that

$$e_{\mathscr{I}_{[l]}}^\mathsf{T} G(s) = \eta_{[l]} G_{[l]}^\star(s), \tag{13.12}$$

where G is defined as in (13.11).

This definition of cluster reducibility represents that the states corresponding to $\mathscr{I}_{[l]}$ have the same trajectories for all input signals. The following theorem shows that the cluster reducibility can be characterized by using positive tridiagonalization of bidirectional networks:

Theorem 13.1 *Let Σ in (13.1) be a stable bidirectional network. Consider its positive tridiagonal realization $\tilde{\Sigma}$ in (13.3) with the transformation matrix $H \in \mathbb{R}^{n\times n}$, and define*

$$\Phi := H\mathrm{diag}(-\tilde{A}^{-1}\tilde{B}). \tag{13.13}$$

Then, a cluster $\mathscr{I}_{[l]}$ is reducible if and only if there exist a row vector $\phi^{\star}_{[l]} \in \mathbb{R}^{1\times n}$ and a vector $\eta_{[l]} \in \mathbb{R}^{|\mathscr{I}_{[l]}|}$ such that

$$e^{\mathsf{T}}_{\mathscr{I}_{[l]}}\Phi = \eta_{[l]}\phi^{\star}_{[l]}. \tag{13.14}$$

In addition, if (13.14) holds, then $\eta_{[l]}$ coincides with a multiple of

$$-e^{\mathsf{T}}_{\mathscr{I}_{[l]}}A^{-1}B.$$

Moreover, if all clusters $\mathscr{I}_{[l]}$ are reducible, then the aggregated model $\hat{\Sigma}$ in (13.9) given by $p_{[l]} = \|\eta_{[l]}\|^{-1}\eta_{[l]}$ is stable and satisfies

$$G(s) = \hat{G}(s), \tag{13.15}$$

where G and $\hat{G}$ are defined as in (13.11).

Proof [Proof of the equivalence between (13.12) and (13.14)] We prove here that (13.12) implies (13.14). For the proof of the converse direction, see the proof of Theorem 13.2 because this is a special case of Theorem 13.2. Note that, if the equivalence is proven, we can confirm that $\eta_{[l]}$ is a multiple of $-e^{\mathsf{T}}_{\mathscr{I}_{[l]}}A^{-1}B$ by substituting $s = 0$ to (13.12).

Consider i^* in (13.7) that corresponds to the dimension of the controllable subspace of Σ, and define

$$\mathscr{K} := \{1, \ldots, i^*\}, \quad \overline{\mathscr{K}} := \{i^* + 1, \ldots, n\}.$$

Note that, owing to the uncontrollability, $\tilde{X}_k(s) \equiv 0$ for all $k \in \overline{\mathscr{K}}$, where $\tilde{X}_k$ denotes the kth entry of $\tilde{X}$ in (13.5). Thus, it follows that

$$\tilde{X}(s) = \begin{bmatrix} \tilde{X}_1(s) \\ \vdots \\ \tilde{X}_{i^*}(s) \\ 0 \end{bmatrix} = \mathrm{diag}(I_{i^*}, 0) \begin{bmatrix} \tilde{X}_1(s) \\ \vdots \\ \tilde{X}_{i^*}(s) \\ 0 \end{bmatrix} = e_{\mathscr{K}}e^{\mathsf{T}}_{\mathscr{K}}\tilde{X}(s). \tag{13.16}$$

By definition, we have

$$G(s) = H(sI_n - \tilde{A})^{-1}\tilde{B} = H\tilde{X}(s).$$

From this relation with (13.16), we see that (13.12) can be rewritten as

$$e_{\mathscr{I}_{[l]}}^{\mathsf{T}} H e_{\mathscr{K}} e_{\mathscr{K}}^{\mathsf{T}} \tilde{X}(s) = \eta_{[l]} G_{[l]}^{\star}(s). \tag{13.17}$$

Note that each of functions $\tilde{X}_k$ for $k \in \mathscr{K}$, i.e., each element of $e_{\mathscr{K}}^{\mathsf{T}} \tilde{X}(s)$, is *linearly independent* since any two of them do not have the same relative degree. This can be confirmed by the serially cascaded structure of the positive tridiagonal realization. Thus, the equality in (13.17) with a scalar rational function $G_{[l]}^{\star}$ implies that the rank of $e_{\mathscr{I}_{[l]}}^{\mathsf{T}} H e_{\mathscr{K}} \in \mathbb{R}^{|\mathscr{I}_{[l]}| \times i^*}$ must be one, and there exists a row vector $h_{[l]}^{\star} \in \mathbb{R}^{1 \times i^*}$ such that

$$e_{\mathscr{I}_{[l]}}^{\mathsf{T}} H e_{\mathscr{K}} = \eta_{[l]} h_{[l]}^{\star}. \tag{13.18}$$

Furthermore, since $\tilde{X}(0) = -\tilde{A}^{-1}\tilde{B}$, it follows from (13.16) that

$$\mathrm{diag}(-\tilde{A}^{-1}\tilde{B}) = e_{\mathscr{K}} e_{\mathscr{K}}^{\mathsf{T}} \mathrm{diag}(-\tilde{A}^{-1}\tilde{B}).$$

Multiplying (13.18) by $e_{\mathscr{K}}^{\mathsf{T}} \mathrm{diag}(-\tilde{A}^{-1}\tilde{B})$ from the right side, we have

$$e_{\mathscr{I}_{[l]}}^{\mathsf{T}} H e_{\mathscr{K}} e_{\mathscr{K}}^{\mathsf{T}} \mathrm{diag}(-\tilde{A}^{-1}\tilde{B}) = \eta_{[l]} h_{[l]}^{\star} e_{\mathscr{K}}^{\mathsf{T}} \mathrm{diag}(-\tilde{A}^{-1}\tilde{B}).$$

Note that the left-hand side is equal to $e_{\mathscr{I}_{[l]}}^{\mathsf{T}} \Phi$. Thus

$$\phi_{[l]}^{\star} = h_{[l]}^{\star} e_{\mathscr{K}}^{\mathsf{T}} \mathrm{diag}(-\tilde{A}^{-1}\tilde{B}) \in \mathbb{R}^{1 \times n}$$

satisfies (13.14). Hence, it follows that (13.12) implies (13.14).

[Proof of (13.15)] Let $\overline{p}_{[l]} \in \mathbb{R}^{|\mathscr{I}_{[l]}| \times (|\mathscr{I}_{[l]}|-1)}$ be an orthogonal complement of $p_{[l]}$, and define

$$\overline{P} := \Pi \mathrm{diag}(\overline{p}_{[1]}, \ldots, \overline{p}_{[L]}) \in \mathbb{R}^{n \times (n-L)}, \tag{13.19}$$

which is an orthogonal complement of P in (13.8). Note that $\overline{p}_{[l]}$ is allowed to be empty if $|\mathscr{I}_{[l]}| = 1$. The similarity transformation of the error system $G - \hat{G}$ yields

$$V A_e V^{-1} = \begin{bmatrix} P^{\mathsf{T}} A P & P^{\mathsf{T}} A \overline{P}\, \overline{P}^{\mathsf{T}} \\ 0 & A \end{bmatrix}, \quad V B_e = \begin{bmatrix} 0 \\ B \end{bmatrix}, \quad C_e V^{-1} = \begin{bmatrix} P & \overline{P}\, \overline{P}^{\mathsf{T}} \end{bmatrix}, \tag{13.20}$$

where

$$A_e := \begin{bmatrix} A & 0 \\ 0 & P A P^{\mathsf{T}} \end{bmatrix}, \quad B_e := \begin{bmatrix} B \\ -PB \end{bmatrix}, \quad C_e := \begin{bmatrix} I_n & P^{\mathsf{T}} \end{bmatrix}$$

and

$$V = \begin{bmatrix} P & I_L \\ I_n & 0 \end{bmatrix}, \quad V^{-1} = \begin{bmatrix} 0 & I_n \\ I_L & -P \end{bmatrix}.$$

From the block triangular structure of VA_eV^{-1} with the structure of VB_e and C_eV^{-1}, we see that the error system is factorized as

$$G(s) - \hat{G}(s) = \Xi(s)\overline{P}\,\overline{P}^{\mathsf{T}}G(s), \tag{13.21}$$

where

$$\Xi(s) := P(sI_L - P^{\mathsf{T}}AP)^{-1}P^{\mathsf{T}}A + I_n.$$

Note that $\overline{p}_{[l]}^{\mathsf{T}}\eta_{[l]} = 0$ from $p_{[l]} = \|\eta_{[l]}\|^{-1}\eta_{[l]}$. Hence, the reducibility of all clusters implies that

$$\overline{P}^{\mathsf{T}}G(s) = 0.$$

This guarantees (13.15). □

Theorem 13.1 shows that the cluster reducibility is characterized by linear dependence among the row vectors of Φ. However, the cluster reducibility is generally restrictive for the reduction of dimensions. This is because it represents a kind of structured uncontrollability representing that the controllable subspace of $e_{\mathscr{I}_{[l]}}^{\mathsf{T}}x$ is one-dimensional.

13.3.3 Approximation Error Evaluation for Clustered Model Reduction

Aiming at significant dimension reduction, let us relax the cluster reducibility through its equivalent representation in (13.14). To this end, we introduce the following weaker notion of cluster reducibility:

Definition 13.5 Let Σ in (13.1) be a stable bidirectional network. Consider its positive tridiagonal realization $\tilde{\Sigma}$ in (13.3) with the transformation matrix $H \in \mathbb{R}^{n\times n}$, and define Φ in (13.13). A cluster $\mathscr{I}_{[l]}$ is said to be θ-*reducible* if there exists a row vector $\phi_{[l]}^{\star} \in \mathbb{R}^{1\times n}$ such that

$$\left\| e_{\mathscr{I}_{[l]}}^{\mathsf{T}}\Phi - \eta_{[l]}\phi_{[l]}^{\star} \right\|_{l_\infty} \le \theta, \quad \theta \ge 0, \tag{13.22}$$

where $\eta_{[l]} = -e_{\mathscr{I}_{[l]}}^{\mathsf{T}}A^{-1}B$.

In Definition 13.5, the constant θ represents the degree of cluster reducibility. It can be easily verified that the θ-reducibility is equivalent to the cluster reducibility if $\theta = 0$. For the proof of Theorem 13.2 below, we first prepare the following lemma:

Lemma 13.1 *Let $A = A^\mathsf{T} \in \mathbb{R}^{n\times n}$ be stable and $B \in \mathbb{R}^{n\times m}$. Then, it follows that*

$$\|(sI_n - A)^{-1}B\|_{\mathscr{H}_\infty} = \|A^{-1}B\|.$$

Proof Denote $f(s) := (sI_n - A)^{-1}B$. By definition of the $\mathscr{H}_\infty$-norm, it follows that $\|f(s)\|_{\mathscr{H}_\infty} \geq \|f(0)\|$. Let γ be such that $\|f(0)\| < \gamma$. To prove $\|f(s)\|_{\mathscr{H}_\infty} \leq \|f(0)\|$, it suffices to show that $\|f(s)\|_{\mathscr{H}_\infty} < \gamma$, or equivalently, all eigenvalues of

$$J(\gamma) := \begin{bmatrix} A & -\gamma^{-1}BB^\mathsf{T} \\ \gamma^{-1}I_n & -A^\mathsf{T} \end{bmatrix}$$

are not on the imaginary axis [1]. By the symmetry of A, we have

$$J^2(\gamma) = \begin{bmatrix} A^2 - \gamma^{-2}BB^\mathsf{T} & * \\ 0 & A^2 - \gamma^{-2}BB^\mathsf{T} \end{bmatrix}.$$

Note that the block-diagonal entries

$$A^2 - \gamma^{-2}BB^\mathsf{T} = A(I_n - \gamma^{-2}f(0)f^\mathsf{T}(0))A^\mathsf{T}$$

are symmetric and positive definite since $\gamma > \|f(0)\|$. Therefore, all eigenvalues of J^2 are positive real. This implies that all eigenvalues of J are nonzero real. Hence, the claim follows. □

Now, we are ready to evaluate the approximation error caused by the aggregation of θ-reducible clusters as shown in the following theorem:

Theorem 13.2 *Let Σ in (13.1) be a stable bidirectional network. Consider its positive tridiagonal realization $\tilde{\Sigma}$ in (13.3) with the transformation matrix $H \in \mathbb{R}^{n\times n}$. If all clusters $\mathscr{I}_{[l]}$ are θ-reducible, then the aggregated model $\hat{\Sigma}$ in (13.9) given by $p_{[l]} = \|\eta_{[l]}\|^{-1}\eta_{[l]}$ is stable and satisfies*

$$\|G(s) - \hat{G}(s)\|_{\mathscr{H}_\infty} \leq \sqrt{\alpha}\|(P^\mathsf{T}AP)^{-1}P^\mathsf{T}A\|\theta, \tag{13.23}$$

where G and $\hat{G}$ are defined as in (13.11) and $\alpha := \sum_{l=1}^{L}|\mathscr{I}_{[l]}|(|\mathscr{I}_{[l]}| - 1)$.

Proof In the same notation as that in the proof of Theorem 13.1, it follows from (13.21) that

$$\|G(s) - \hat{G}(s)\|_{\mathscr{H}_\infty} \leq \|\Xi(s)\|_{\mathscr{H}_\infty}\|\overline{P}\,\overline{P}^\mathsf{T}G(s)\|_{\mathscr{H}_\infty}. \tag{13.24}$$

First, let us prove that

$$\|\Xi(s)\|_{\mathscr{H}_\infty} = \|(P^\mathsf{T}AP)^{-1}P^\mathsf{T}A\|.$$

Let

$$J(\gamma) := \begin{bmatrix} P^\mathsf{T} A P & -\gamma^{-1} P^\mathsf{T} A A^\mathsf{T} P \\ \gamma^{-1} I_L & -P^\mathsf{T} A^\mathsf{T} P \end{bmatrix}.$$

The inequality $\|\Xi\|_{\mathscr{H}_\infty} < \gamma$ holds if and only if $\gamma > \|I_n\| = 1$ and the Hamiltonian $\gamma^2(\gamma^2 - 1)^{-1} J(\gamma)$ of Ξ has no eigenvalue on the imaginary axis [1]. Note that this $J(\gamma)$ coincides with the Hamiltonian of

$$\hat{\Xi}(s) := (sI_L - P^\mathsf{T} A P)^{-1} P^\mathsf{T} A. \tag{13.25}$$

Therefore, we see that $\|\Xi\|_{\mathscr{H}_\infty} < \gamma$ is equivalent to $\gamma > 1$ and $\|\hat{\Xi}\|_{\mathscr{H}_\infty} < \gamma$. For the latter inequality, it follows that

$$\|\hat{\Xi}(0)\| = \|(P^\mathsf{T} A P)^{-1} P^\mathsf{T} A (P P^\mathsf{T} + \overline{P}\,\overline{P}^\mathsf{T})\| = \|P^\mathsf{T} + Z\| = \lambda_{\max}^{\frac{1}{2}}(I_L + Z Z^\mathsf{T}) > 1,$$

where we have used $P^\mathsf{T} Z^\mathsf{T} = 0$ for $Z := (P^\mathsf{T} A P)^{-1} P^\mathsf{T} A \overline{P}\,\overline{P}^\mathsf{T}$. Hence, $\|\Xi\|_{\mathscr{H}_\infty} < \gamma$ if and only if $\|\hat{\Xi}\|_{\mathscr{H}_\infty} < \gamma$ for all $\gamma \geq 0$, or equivalently $\|\Xi\|_{\mathscr{H}_\infty} = \|\hat{\Xi}\|_{\mathscr{H}_\infty}$. Thus, using Lemma 13.1, we obtain

$$\|\Xi(s)\|_{\mathscr{H}_\infty} = \|\hat{\Xi}(0)\| = \|(P^\mathsf{T} A P)^{-1} P^\mathsf{T} A\|. \tag{13.26}$$

Next, let us evaluate $\|\overline{P}\,\overline{P}^\mathsf{T} G\|_{\mathscr{H}_\infty}$. From

$$\|\overline{P}\,\overline{P}^\mathsf{T} G(s)\|_{\mathscr{H}_\infty} = \sup_{\omega \in \mathbb{R}} \lambda_{\max}^{\frac{1}{2}}(G^\mathsf{T}(-j\omega)\overline{P}\,\overline{P}^\mathsf{T}\overline{P}\,\overline{P}^\mathsf{T} G(j\omega)) = \|\overline{P}^\mathsf{T} G(s)\|_{\mathscr{H}_\infty},$$

where the second equality comes from $\overline{P}^\mathsf{T}\overline{P} = I_{n-L}$, it follows that

$$\|\overline{P}\,\overline{P}^\mathsf{T} G(s)\|_{\mathscr{H}_\infty} = \left\| \begin{bmatrix} \overline{p}_{[1]}^\mathsf{T} e_{\mathscr{I}_{[1]}}^\mathsf{T} G(s) \\ \vdots \\ \overline{p}_{[L]}^\mathsf{T} e_{\mathscr{I}_{[L]}}^\mathsf{T} G(s) \end{bmatrix} \right\|_{\mathscr{H}_\infty} \leq \sqrt{\textstyle\sum_{l=1}^{L} \|\overline{p}_{[l]}^\mathsf{T} e_{\mathscr{I}_{[l]}}^\mathsf{T} G(s)\|_{\mathscr{H}_\infty}^2}.$$

For the evaluation of $\|\overline{p}_{[l]}^\mathsf{T} e_{\mathscr{I}_{[l]}}^\mathsf{T} G\|_{\mathscr{H}_\infty}$, we first prove that

$$\|CG(s)\|_{\mathscr{H}_\infty} \leq \sqrt{p}\, \|C\Phi\|_{l_\infty} \tag{13.27}$$

for any $C \in \mathbb{R}^{p \times n}$. Note that

$$\|CG(s)\|_{\mathscr{H}_\infty} \leq \sqrt{\sum_{k=1}^{p} \|C_k G(s)\|_{\mathscr{H}_\infty}^2} \leq \sqrt{p} \max_k \|C_k G(s)\|_{\mathscr{H}_\infty},$$

where $C_k \in \mathbb{R}^{1\times n}$ denotes the kth row of C. Furthermore, it follows that

$$C_k G(s) = \sum_{i=1}^{n} C_{k,i} \sum_{j=1}^{n} H_{i,j} \tilde{X}_j(s),$$

where $H_{i,j}$ and $C_{i,j}$ denote the (i, j)-elements of H and C, respectively, and $\tilde{X}_j$ denotes the jth element of $\tilde{X}$ defined as in (13.5). Therefore, we have

$$\|C_k G(s)\|_{\mathscr{H}_\infty} = \left\| \sum_{i=1}^{n} C_{k,i} \sum_{j=1}^{n} H_{i,j} \tilde{X}_j(s) \right\|_{\mathscr{H}_\infty} \leq \sum_{j=1}^{n} \left| \sum_{i=1}^{n} C_{k,i} H_{i,j} \right| \tilde{X}_j(0) = \|C_k \Phi\|_{l_\infty}.$$

By the definition of the l_∞-induced norm, we see that

$$\max_k \|C_k \Phi\|_{l_\infty} = \|C\Phi\|_{l_\infty}.$$

This proves (13.27).

Using (13.27) with $C = \overline{p}_{[l]}^{\mathsf{T}} e_{\mathscr{I}_{[l]}}^{\mathsf{T}} \in \mathbb{R}^{(|\mathscr{I}_{[l]}|-1)\times n}$, we have

$$\|\overline{p}_{[l]}^{\mathsf{T}} e_{\mathscr{I}_{[l]}}^{\mathsf{T}} G(s)\|_{\mathscr{H}_\infty} \leq \sqrt{|\mathscr{I}_{[l]}| - 1}\, \|\overline{p}_{[l]}^{\mathsf{T}} e_{\mathscr{I}_{[l]}}^{\mathsf{T}} \Phi\|_{l_\infty}.$$

Let

$$\Delta_{[l]} := e_{\mathscr{I}_{[l]}}^{\mathsf{T}} \Phi - \eta_{[l]} \phi_{[l]}^{\star}.$$

Note that the assumption of θ-reducibility means that $\|\Delta_{[l]}\|_{l_\infty} \leq \theta$. Then, from the fact that $\overline{p}_{[l]}^{\mathsf{T}} p_{[l]} = 0$ and $p_{[l]} = \|\eta_{[l]}\|^{-1} \eta_{[l]}$, it follows that

$$\overline{p}_{[l]}^{\mathsf{T}} e_{\mathscr{I}_{[l]}}^{\mathsf{T}} \Phi = \overline{p}_{[l]}^{\mathsf{T}} \Delta_{[l]}.$$

Hence, we have

$$\|\overline{p}_{[l]}^{\mathsf{T}} e_{\mathscr{I}_{[l]}}^{\mathsf{T}} \Phi\|_{l_\infty} \leq \|\overline{p}_{[l]}^{\mathsf{T}}\|_{l_\infty} \|\Delta_{[l]}\|_{l_\infty} \leq \sqrt{|\mathscr{I}_{[l]}|}\, \|\overline{p}_{[l]}^{\mathsf{T}}\| \theta \leq \sqrt{|\mathscr{I}_{[l]}|}\, \theta,$$

where the second inequality stems from $\|M\|_{l_\infty} \leq \sqrt{m}\|M\|$ for any $M \in \mathbb{R}^{n\times m}$ and the third from $\|\overline{p}_{[l]}\| = 1$. Finally, we have

$$\|\overline{P}\,\overline{P}^{\mathsf{T}} G(s)\|_{\mathscr{H}_\infty} \leq \sqrt{\sum_{l=1}^{L} |\mathscr{I}_{[l]}| \left(|\mathscr{I}_{[l]}| - 1\right)}\, \theta, \tag{13.28}$$

which proves the claim. □

Theorem 13.2 shows a linear relation between the approximation error caused by cluster aggregation and the parameter θ expressing the degree of cluster reducibility. Thus, we can use θ as a criterion to regulate the the approximation error of the resultant aggregated model. Therefore, we can conclude that Theorem 13.2 gives a reasonable cluster determination strategy.

In what follows, based on the premise that $\theta \geq 0$ is given and Φ in (13.13) is calculated in advance, we propose an algorithm to construct a set of θ-reducible clusters. Assume that a set of clusters $\mathscr{I}_{[1]}, \ldots, \mathscr{I}_{[l-1]}$ are already formed. Let

$$\mathscr{N} := \{1, \ldots, n\} \backslash \bigcup_{i=1}^{l-1} \mathscr{I}_{[i]}.$$

When we construct a new cluster $\mathscr{I}_{[l]}$, we first select an index $j \in \mathscr{N}$. Then, we find all indices $i \in \mathscr{N}$ such that

$$\left\| \phi_i - \eta_i \eta_j^{-1} \phi_j \right\|_{l_\infty} \leq \theta, \tag{13.29}$$

where $\phi_i \in \mathbb{R}^{1\times n}$ denotes the ith row vector of Φ and $\eta_i \in \mathbb{R}$ denotes the ith entry of $\eta = -A^{-1}B$. Note that (13.29) is identical to give $\phi^\star_{[l]} = \eta_j^{-1}\phi_j$ for (13.22). Thus, we can verify that the cluster $\mathscr{I}_{[l]}$ is actually θ-reducible.

13.4 Numerical Example: Application to Complex Networks

We consider a diffusion process evolving over the Holme-Kim model [4] composed of 1000 nodes and 2000 edges, whose interconnection topology is depicted in Fig. 13.1. This network is an extension of the Barabási-Albert model, which is one of the well known complex network models and has a scale-free and small-world property as well as a high cluster coefficient. We give the bidirectional network Σ in (13.1) as follows. The input affects only one node, i.e., $B = [1, 0, \ldots, 0]^\mathsf{T}$. For $A \in \mathbb{R}^{1000\times 1000}$ in (13.2), we randomly choose $a_{i,j}$ from $(0, 1]$ if nodes i and j for $i \neq j$ are connected, otherwise they are given as 0, and we give $r_1 = 1$ and $r_i = 0$ for all $i \in \{2, \ldots, 1000\}$.

We apply our clustered model reduction method to this bidirectional network evolving over the Holme-Kim model. When $\theta = 1.5$ and $\theta = 3.0$, we obtain 47-dimensional and 27-dimensional aggregated models shown in Figs. 13.2 and 13.3, respectively. Comparing Figs. 13.2 and 13.3 with Fig. 13.1, we see that the interconnection topology of the aggregated models is much simpler than the original network. Since their relative approximation error $\|G - \hat{G}\|_{\mathscr{H}_\infty}/\|G\|_{\mathscr{H}_\infty}$ is 0.060 and 0.091, we can conclude that our clustered model reduction method successfully extracts meaningful inter-cluster connections in the sense of input-to-state mapping approximations.

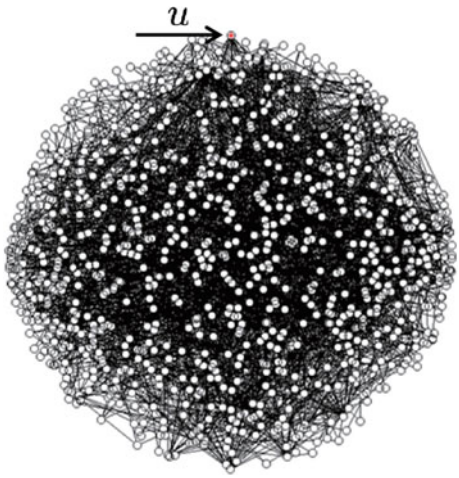

Fig. 13.1 Interconnection topology of the original bidirectional network evolving over the Holme-Kim model. This network is composed of 1000 nodes and 2000 edges, and the nonzero edge weights are randomly chosen from (0, 1]

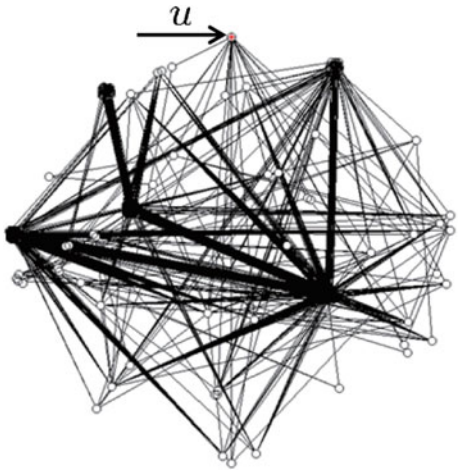

Fig. 13.2 Interconnection topology of the aggregated model. The resultant network is composed of 47 clusters (47 nodes). Meaningful inter-cluster connections in the sense of input-to-state mapping approximations are highlighted as *bold lines*

Next, we show the resultant computation time to construct aggregated models varying the dimensions of the original systems. Figure 13.4 shows the plot of the computation time versus the dimensions of the original systems, which are given in the same way as that to obtain the 1000-dimensional system above. From this figure, we see that the total calculation time grows in $O(n^3)$, which is mainly composed of computation to perform network clustering and positive tridiagonalization. This is implemented in MATLAB 2011b on a computer equipped with Intel Core i7 CPU-2620M, 2.60 GHz, RAM 16 GB, and a 64-bit operating system.

Finally, we compare the Holme-Kim model with the Erdö-Rényi model from a viewpoint of the degree of local uncontrollability. Figure 13.5 shows the plots of resultant relative errors caused by applying our clustered model reduction for 1000-dimensional network systems evolving over the Holme-Kim model (solid lines)

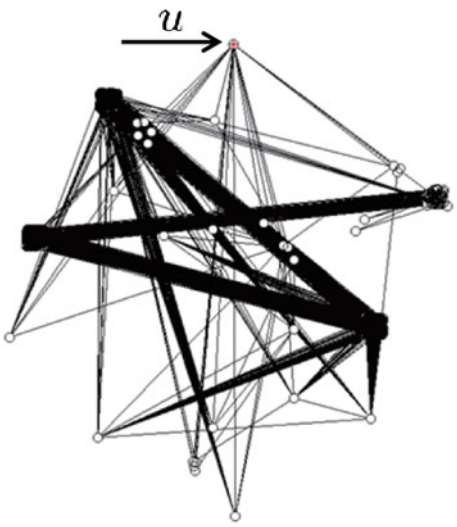

Fig. 13.3 Interconnection topology of the aggregated model The resultant network is composed of 27 clusters (27 nodes). Meaningful inter-cluster connections in the sense of input-to-state mapping approximations are highlighted as *bold lines*

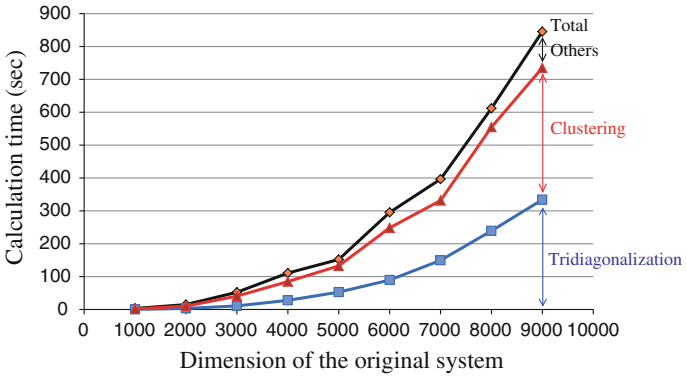

Fig. 13.4 Calculation time to construct aggregated model.The line with *squares* corresponds to the calculation of positive tridiagonal realization, the line with *triangles* corresponds to that of cluster construction, and the line with *diamonds* corresponds to the construction of a 1000-dimensional aggregated model

and the Erdö-Rényi model (dashed lines). To make the comparison fair, we give 2000 edges for both networks, which are produced by standard algorithms [4]. From Fig. 13.5, we see that the approximation errors for the Holme-Kim model are generally smaller than those for the Erdö-Rényi model. This result indicates that our clustered model reduction is more effective for scale-free networks. This is related to the fact shown in [10] that the degree of controllability of scale-free networks is generally less than that of the Erdö-Rényi network.

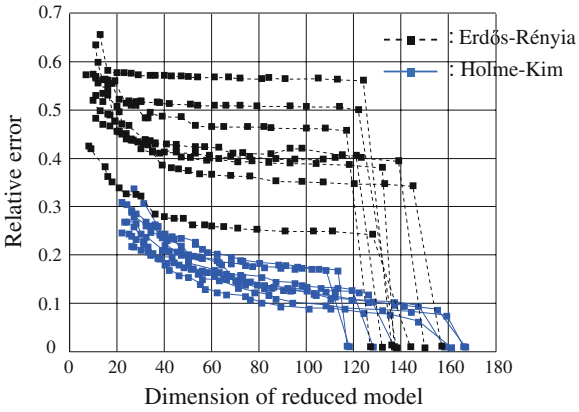

Fig. 13.5 Comparison of resultant approximation errors. The approximation errors for the Holme-Kim model (*solid lines*) are generally smaller than those for the Erdö-Rényi model (*dashed lines*)

13.5 Conclusion

In this chapter, we have overviewed a clustered model reduction method [8, 9] for interconnected linear systems evolving over undirected networks, which belongs to a kind of structured model reduction. In this type of structured model reduction, network clustering is performed according to a notion of uncontrollability of local states, called cluster reducibility. It is shown that the cluster reducibility is characterized based on positive tridiagonalization, and the aggregation of the reducible clusters yields an aggregated model that preserves an interconnection structure among clusters. Furthermore, we have shown that the approximation error caused by the cluster aggregation can be evaluated in terms of the $\mathscr{H}_\infty$-norm. Finally, in the numerical examples, we have applied our clustered model reduction to systems evolving over the Holme-Kim model and the Erdö-Rényi model, and have compared these models from a viewpoint of the degree of local uncontrollability.

References

1. Antoulas, A.C.: Approximation of Large-Scale Dynamical Systems. Society for Industrial and Applied Mathematics, Philadelphia (2005)
2. Astolfi, A., Colaneri, P.: A note on the existence of positive realizations. Linear Algebra Appl. **390**, 329–343 (2004)
3. Benvenuti, L., Farina, L.: A tutorial on the positive realization problem. IEEE Trans. Autom. Control **49**(5), 651–664 (2004)
4. Boccaletti, S., Latora, V., Moreno, Y., Chavez, M., Hwang, D.-U.: Complex networks: structure and dynamics. Phys. Rep. **424**(4), 175–308 (2006)
5. Farina, L., Rinaldi, S.: Positive linear systems: theory and applications. Wiley, New York (2000)
6. Grimme, E.J.: Krylov projection methods for model reduction. Ph.D. thesis, University of Illinois (1997)

7. Ishizaki, T., Kashima, K., Imura, J., Aihara, K.: Model reduction of multi-input dynamical networks based on clusterwise controllability. Proceedings of American Control Conference, pp. 2301–2306 (2012)
8. Ishizaki, T., Kashima, K., Girard, A., Imura, J., Chen, L., Aihara, K.: Clustering-based $\mathscr{H}$-state aggregation of positive networks and its application to reduction of chemical master equations. Proceedings of the 51st IEEE Conference on Decision and Control, pp. 4175–4180 (2012)
9. Ishizaki, T., Kashima, K., Imura, J., Aihara, K.: Model reduction and clusterization of large-scale bidirectional networks. IEEE Trans. Autom. Control **59**(1), 48–63 (2014)
10. Liu, Y.-Y., Slotine, J.-J., Barabási, A.-L.: Controllability of complex networks. Nature **473**(7346), 167–173 (2011)
11. Mesbahi, M. Egerstedt, M.: Graph theoretic methods in multiagent networks. Princeton University Press, Princeton (2010)
12. Newman, M.: Networks: an introduction. Oxford University Press, London (2009)
13. Obinata, G., Anderson, B.D.O.: Model reduction for control system design. Springer, London (2001)
14. Sandberg, H., Murray, R.M.: Model reduction of interconnected linear systems. Opt. Control Appl. Methods **30**(3), 225–245 (2009)
15. Vandendorpe, A., Van Dooren, P.: Model reduction of interconnected systems. In: Model Order Reduction: Theory, Research Aspects and Applications, pp. 305–321. Springer, Heidelberg (2008)
16. Wilkinson, J.H.: The algebraic eigenvalue problem, vol. 155. Oxford University Press, London (1965)

Chapter 14
Network Structure Identification from a Small Number of Inputs/Outputs

Masayasu Suzuki, Jun-ichi Imura and Kazuyuki Aihara

14.1 Introduction

In recent years, interest in analysis and control of large-scale network (NW) systems has been increasing rapidly. Against this background, developing methods to identify, we also say reconstruct, the NW structures, is required, and in fact, various interesting studies have been reported so far [1, 2, 4, 6, 7, 10, 11, 13–16, 18–20]. However, many methods proposed in such studies are based on the assumption that the state of every node can be accessible, that is, one can manipulate or monitor all the states [15, 18]. Since it is difficult to satisfy the above assumption in terms of technical and financial costs, inventing structure identification procedures using relatively smaller number of actuators/sensors than that of the states is quite important.

The NW structure reconstruction belongs to a class of the identification of gray-box models, and it has some features different from that of black-box models. In particular, we encounter the issues on identifiability for gray-box models [8, 9], and have been trying to overcome this problem by various approaches. The common

M. Suzuki (✉)
Graduate School of Engineering, Utsunomiya University,
7-1-2 Yōtō Utsunomiya-city, Tochigi 321-8585, Japan
e-mail: ma-suzuki@ieee.org

J. Imura
Graduate School of Information Science and Engineering,
Tokyo Institute of Technology, 2-12-1 O-Okayama, Meguro-ku,
Tokyo 152-8552, Japan
e-mail: imura@mei.titech.ac.jp

K. Aihara
Institute of Industrial Science, The University of Tokyo, 4-6-1 Komaba,
Meguro-ku, Tokyo 153-8505, Japan
e-mail: aihara@sat.t.u-tokyo.ac.jp

K. Aihara et al. (eds.), *Analysis and Control of Complex Dynamical Systems*,
Mathematics for Industry 7, DOI 10.1007/978-4-431-55013-6_14

way is to assume that the NW structure is sparse [1, 6], which often makes a sense, in particular, in biology. Some studies consider different types of NW systems: For example, in [10, 11], the class of NW topology has been restricted to the tree-type for the problem to be identifiable. In fact, Gonçalves and Warnick have shown that even if a problem is limited to reconstructing a NW structure among measurable nodes, one cannot uniquely reconstruct such a structure only from input/output data of the NW system [2, 4, 20]. Thus, we need to prepare some knowledge of the NW structure in advance, or to collect some other kinds of time-series data other than input/output data for the original NW system.

The gene-knock-out procedure in experimental biology may be a strong candidate following the later requirement. It is known that the gene-knock-out procedure works well to estimate the functions of nodes in gene networks where some specified nodes are killed (knocked-out), and the functions of the nodes are inferred by observing the difference between the original NW system and the knocked-out NW systems. Motivated by this operation, novel methods to identify NW structures have been proposed [4, 14, 17].

In this chapter, two approaches to identify NW structures are introduced. The first is a characteristic-polynomial-based method using the knock-out procedure, where we focus on a NW system that consists of identical multi-dimensional subsystems. We start to show what can be reconstructed from input/output data of the knocked-out NW systems and give some formulas based on [17]. One of keys is to use the generalized frequency variable, which enables us to treat the multi-dimensional subsystems as one-dimensional ones. Then, we demonstrate how the strength of a specified edge is estimated even if we do not know any information on the other nodes. Although some results shown here and in [17] are extensions for results in [14], the proposed method can be applied for a wider class of systems, and it provides a procedure to identify the connectivity between specified nodes.

The second approach focuses the reconstruction of the "dynamical structure function" that is defined as a structure of transfer functions with respect to measurable nodes. As explained later, this NW structure differs from usual NW graphs like a static adjacency matrix, and resides in between the transfer function of the NW system (the NW structure is invisible) and its realization with meaningful state valuables (the original NW structure completely appears). In [2], a necessary and sufficient condition for the reconstruction of the dynamical structure function was shown, and a special choice of control inputs that satisfies the condition was given. In this chapter, the formulation and some results in [2] will be introduced with comparison to the first approach.

The rest of this chapter is organized as follows: In Sect. 14.2, we introduce characteristic-polynomial-based method using knock-out procedure to identify the weight of edge between two specified subsystems. In Sect. 14.3, the problem to reconstruct the dynamical structure function is formulated for the NW of one-dimensional subsystems, and its analysis results are shown.

14.2 Characteristic-Polynomial-Based NW Structure Identification using Knock-Out

14.2.1 Problem Formulation

Consider a networked system consisting of the following N identical subsystems, each of which is a multi-dimensional, linear time-invariant, and single-input-single-output system:

$$\Sigma_k : \begin{cases} \dot{x}_k = Ax_k + bv_k, \\ z_k = cx_k, \end{cases} \quad k \in \{1, \ldots, N\},$$

where $x_k(t) \in \mathbb{R}^q$, $v_k(t) \in \mathbb{R}$, and $z_k(t) \in \mathbb{R}$. We denote by S the set of the indices $\{1, \ldots, N\}$. The input to each subsystem is given by

$$v_k = \sum_{l \in S} L_{kl} z_l + B_k u, \quad k \in S,$$

where $u(t) \in \mathbb{R}^m$ is an external input, and $L_{kl} \in \mathbb{R}$ and $B_k \in \mathbb{R}^{1 \times m}$ denote the strength of direct connections to Σ_k from the output of Σ_l and an external input u, respectively. In this section, we consider the matrix $[L_{kl}]$ to be given as a weighted graph Laplacian, that is, $L_{kl} = L_{lk} \geq 0$ for $k \neq l$ and $L_{kk} = -\sum_{l \in S \setminus \{k\}} L_{kl}$ hold.[1] In addition, we suppose that the output of the NW system, $y(t) \in \mathbb{R}^p$, is given by

$$y = \sum_{k \in S} C_k z_k,$$

where $C_k \in \mathbb{R}^p$, $k \in S$ are constant vectors. Thus the input u and output y are added and measured via the subsystems' input and output ports, respectively. By using the Kronecker product, the NW system is described as follows:

$$\Sigma : \begin{cases} \dot{x} = (I_N \otimes A + L \otimes bc)x + (B \otimes b)u, \\ y = (C \otimes c)x, \end{cases}$$

where $x(t) = \left[x_1(t)^\mathsf{T} \ \cdots \ x_N(t)^\mathsf{T}\right]^\mathsf{T} \in \mathbb{R}^{Nq}$, $B := \left[B_1^\mathsf{T} \ \cdots \ B_N^\mathsf{T}\right]^\mathsf{T} \in \mathbb{R}^{N \times m}$, and $C = [C_1 \ \cdots \ C_N] \in \mathbb{R}^{p \times N}$.

Knocking-out subsystem k is to keep the state x_k a steady value (e.g., the origin of the subspace). Denote by $\Delta \in 2^S$ and $|\Delta|$ a set of the indices of subsystems to be knocked-out and its cardinal number, respectively. Then, the state of the knocked-out NW system Σ^Δ, which is defined by removing the state variables of knocked-out subsystems as

[1] For the sake of consistency with the description in the next section, the adjacency matrix L has the reverse sign against the usual Laplacian matrix.

$$x^{\Delta} := \left[x_1^{\mathsf{T}} \ \cdots \ x_{i-1}^{\mathsf{T}} \ x_{i+1}^{\mathsf{T}} \ \cdots \ x_{j-1}^{\mathsf{T}} \ x_{j+1}^{\mathsf{T}} \ \cdots \ x_N^{\mathsf{T}} \right]^{\mathsf{T}}, \quad i, j, \ldots \in \Delta$$

satisfies

$$\Sigma^{\Delta} : \begin{cases} \dot{x}^{\Delta} = (I_{N-|\Delta|} \otimes A + L^{\Delta} \otimes bc)x^{\Delta} + (B^{\Delta} \otimes b)u, \\ y = (C^{\Delta} \otimes c)x^{\Delta}, \end{cases}$$

where B^{Δ}, C^{Δ}, and L^{Δ} are defined by removing columns, rows, and both corresponding to Δ, from B, C, and L, respectively. Since $\emptyset \in 2^S$ and $\Sigma^{\emptyset} = \Sigma$, we also regard the original NW system Σ as one of knocked-out NW systems for the sake of a simple description.

Now, we have the following assumptions:

Assumption For the NW system Σ,

A1. the number N and coefficients (A, b, c) of the subsystems are known,
A2. L is a weighted graph-Laplacian,
A3. L, B, and C are unknown other than the above knowledge, and
A4. the NW systems including knocked-out NW systems, which are used for the identification, are stable, controllable, and observable.

In the rest of this section, we address the following problem:

Problem 14.1 For given indices k and l $(k \leq l)$, and under Assumption A1–4, identify the weight of the edge between subsystem Σ_k and subsystem Σ_l, L_{kl}, from input/output data of knocked-out NW systems.

Nabi-Abdolyousefi and Mesbahi have proposed an identification method of the NW structure for a consensus-type undirectional NW system consisting of one-dimensional subsystems [14]. In addition to Assumption A1– 4, the literature [14] assumes that $(A, b, c) = (0, 1, 1)$ and $L \cdot 1_{N\times 1} = 0$, which means that the dynamics of the NW system Σ is given by (L, B, C). In [14], the transfer function matrix $(sI_N - L)^{-1}$ is identified by using knocked-out NW systems, and then, the NW structure L is estimated. In this section, we will extend the method in [14] to be able to apply to NW systems that consist of multi-dimensional subsystems, and also, introduce a procedure to identify the connectivity strength between two specified subsystems.

14.2.2 Representation Using the Generalized Frequency Variable

For the subsystem (A, b, c), denote by $h(s)$, $d(s)$, and $n(s)$ the transfer function, its denominator, and numerator, respectively: That is, $h(s) = c(sI_q - A)^{-1}b$, $d(s) = \det[sI_q - A]$, and $n(s) = c\mathrm{adj}[sI_q - A]b$. The transfer function G of the NW system Σ can be represented by using the generalized frequency variable $\phi(s) := 1/h(s)$ as follows [3, 12]:

Theorem 14.1 *For the NW system Σ, the following holds*:

$$G(s) = C(\phi(s)I_N - L)^{-1}B. \tag{14.1}$$

This theorem states that the transfer function $G(s)$ is equivalent to the transfer function of the system (L, B, C) (i.e., $C(sI_N - L)^{-1}B$), whose variable s is replaced by $\phi(s)$. For the identification of the NW structure, we focus on the inverse matrix part $(\phi(s)I_N - L)^{-1}$.

The Meaning of $(\phi(s)I_N - L)^{-1}$

The (k, l)-entry of $(\phi(s)I_N - L)^{-1}$ corresponds to the right-hand-side of (14.1) whose B and C matrices are chosen as

$$B = [0 \cdots 0 \overset{l}{\check{1}} 0 \cdots 0]^{\mathsf{T}} \quad \text{and} \quad C = [0 \cdots 0 \overset{k}{\check{1}} 0 \cdots 0].$$

Since $G(s) = (C \otimes c)(sI_{Nq} - I_N \otimes A - L \otimes bc)^{-1}(B \otimes b)$, it turns out

$$\begin{aligned}[(\phi(s)I_N - L)^{-1}]_{kl} = [0 \cdots 0 \overset{k}{\check{c}} 0 \cdots 0](sI_{Nq} - I_N \otimes A - L \otimes bc)^{-1} \\ \times [0 \cdots 0 \overset{l}{\check{b}}^{\mathsf{T}} 0 \cdots 0]^{\mathsf{T}}.\end{aligned}$$

Therefore, this (k, l)-entry implies a transfer function from the input[2] that is added to subsystem Σ_l to the output of subsystem Σ_k (see Fig. 14.1, and also compare to Fig. 14.3).

In the next two subsections, we consider how to identify the transfer function $(\phi(s)I_N - L)^{-1}$ and how to extract the weight of a specified edge from this transfer function.

14.2.3 Identification Method

14.2.3.1 How to Identify $(\phi(s)I_N - L)^{-1}$

A key idea is to use the fact that knocking-out subsystems $\{\Sigma_k\}_{k\in\Delta}$ corresponds to considering an inner dynamics described by $I_{N-|\Delta|} \otimes A + L^{\{\Delta\}} \otimes bc$. In addition, we apply a formula

$$\det\left[\phi(s)I_{N-|\Delta|} - L^{\Delta}\right] = \frac{\det\left[sI_{(N-|\Delta|)q} - (I_{N-|\Delta|} \otimes A + L^{\Delta} \otimes bc)\right]}{n(s)^{N-|\Delta|}}. \tag{14.2}$$

[2] This does not mean that there is a real input port.

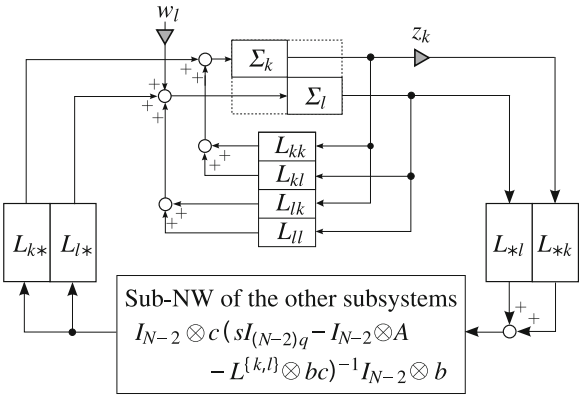

Fig. 14.1 The transfer function $[(\phi(s)I_N - L)^{-1}]_{kl}$ means the transfer function from w_l to z_k. This block diagram depicts the inner dynamics of the whole NW system. Here, symbol "$*$" denotes indices $(1, \ldots, k-1, k+1, \ldots, l-1, l+1, \ldots, N)$; e.g., L_{k*} denotes $[L_{k1} \cdots L_{kN}]$, where (k, k) and (k, l)-entry are removed

Note that the numerator of the right hand side of (14.2) is the characteristic polynomial of Σ^{Δ}.

First, we focus on the diagonal of $(\phi(s)I_N - L)^{-1}$. Since the kth diagonal of $(\phi(s)I_N - L)^{-1}$ can be calculated as

$$\begin{aligned}\left[(\phi(s)I_N - L)^{-1}\right]_{kk} &= \frac{\mathrm{adj}_{kk}[\phi(s)I_N - L]}{\det[\phi(s)I_N - L]} \\ &= \frac{\det\left[\phi(s)I_{N-1} - L^{\{k\}}\right]}{\det[\phi(s)I_N - L]},\end{aligned}$$

we have the following from (14.2):

Theorem 14.2 *For the NW system Σ,*

$$\left[(\phi(s)I_N - L)^{-1}\right]_{kk} = \frac{n(s)\det\left[sI_{(N-1)q} - (I_{N-1} \otimes A + L^{\{k\}} \otimes bc)\right]}{\det[sI_{Nq} - (I_N \otimes A + L \otimes bc)]} \tag{14.3}$$

holds.

A calculation procedure for the off-diagonals of $(\phi(s)I_N - L)^{-1}$, which is more complicated than that for the diagonal, is given as follows:

Theorem 14.3 *For the NW system Σ, the following holds*:

$$\left[(\phi(s)I_N - L)^{-1}\right]_{kl}^2 = \frac{n(s)^2\Psi_{kl}(s)}{\left(\det[sI_{Nq} - (I_N \otimes A + L \otimes bc)]\right)^2}, \quad k \neq l,$$

where

$$\begin{aligned}\Psi_{kl}(s) = &\det\left[sI_{(N-1)q} - \left(I_{N-1} \otimes A + L^{\{k\}} \otimes bc\right)\right] \\ &\times \det\left[sI_{(N-1)q} - \left(I_{N-1} \otimes A + L^{\{l\}} \otimes bc\right)\right] \\ &- \det\left[sI_{Nq} - (I_N \otimes A + L \otimes bc)\right] \\ &\times \det\left[sI_{(N-2)q} - \left(I_{N-2} \otimes A + L^{\{k,l\}} \otimes bc\right)\right].\end{aligned}$$

This relation can be derived from a special version of the Jacobi's identity for determinants [5]

$$\det\left[M^{-1}\right]_{(\{k,l\},\{k,l\})} = \frac{\det M_{(S\setminus\{k,l\},S\setminus\{k,l\})}}{\det M},$$

and (14.2) and (14.3). Here, M is a square non-singular matrix, and $M_{(\mathscr{S}_1,\mathscr{S}_2)}$ denotes a matrix including entries of M in which the rows and columns are specified by $\mathscr{S}_1$ and $\mathscr{S}_2$. Note that to derive the formula in Theorem 14.3, the symmetric property of the NW was used. Thus for the calculation of a off-diagonal, four characteristic polynomials of the original NW system Σ, NW systems $\Sigma^{\{k\}}$ and $\Sigma^{\{l\}}$ in which subsystem k and l are knocked-out, respectively, and NW system $\Sigma^{\{k,l\}}$ in which both k and l are knocked-out.

14.2.3.2 Identification of the Weight of a Specified Edge

Suppose that we derived a rational function matrix $F(s)$ as a result of the identification of $(\phi(s)I_N - L)^{-1}$:

$$(\phi(s)I_N - L)^{-1} = F(s) \text{ for each } s. \tag{14.4}$$

Then, by substituting some value $\bar{s}$ for (14.4), L can be derived as $L = F(\bar{s})^{-1} + \phi(\bar{s})I_N$. However, this requires the calculation of the inverse matrix, which means that all entries of $F(s)$ have to be used in general: i.e., one has to identify them. On the other hand, we often encounter situations in which the identification of the whole NW structure is not necessary, namely, just want to estimate the connectivity strength between specified subsystems. For such a case, it is meaningful to estimate the target with few procedures as possible. In this subsection, it is shown that the weight of edge L_{kl} between subsystems Σ_k and Σ_l can be extracted from the (k,l)-entry of $(\phi(s)I_N + L)^{-1}$ in fact.

As mentioned in Sect. 14.2.2, the (k,l)-entry of $(\phi(s)I_N - L)^{-1}$ is the transfer function from the input for subsystem Σ_l to the output of subsystem Σ_k. Therefore this entry can be represented as follows:

$$\left[(\phi(s)I_N - L)^{-1}\right]_{kl} = \frac{L_{kl} + L_{k*}\Theta^{\{k,l\}}(s)L_{*l}}{\Gamma(s)}, \tag{14.5}$$

$$\begin{aligned}\Gamma(s) = &\left[\phi(s) - L_{kk} - L_{k*}\Theta^{\{k,l\}}(s)L_{*k}\right] \\ &\times \left[\phi(s) - L_{ll} - L_{l*}\Theta^{\{k,l\}}(s)L_{*l}\right] \\ &- \left[L_{lk} + L_{l*}\Theta^{\{k,l\}}(s)L_{*k}\right] \\ &\times \left[L_{kl} + L_{k*}\Theta^{\{k,l\}}(s)L_{*l}\right],\end{aligned}$$

$$\Theta^{\{k,l\}}(s) = \left(\phi(s)I_{N-2} - L^{\{k,l\}}\right)^{-1}.$$

Let the transfer function of the subsystem be given as

$$h(s) = \frac{\sum_{i=0}^{f} \beta_i s^i}{\sum_{i=0}^{e} \alpha_i s^i},$$

where $\alpha_0 = 1$. Denote by r the relative degree of $h(s)$, i.e., $r = e - f$. Then, taking into account the fact that $\Theta^{\{k,l\}}$ is strictly proper, we find that the relative degree of the rational function of (14.5) is equal to $2r$ if $L_{kl} \neq 0$, and larger than $2r$ if $L_{kl} = 0$. Consequently, it turns out that

$$\lim_{s\to\infty} s^{2r}\left[(\phi(s)I_N - L)^{-1}\right]_{kl} = \beta_f^2 L_{kl} \tag{14.6}$$

holds, which can be used to extract L_{kl} from $\left[(\phi(s)I_N - L)^{-1}\right]_{kl}$. From Theorem 14.3, what can be derived from input/output identification for knocked-out NW systems is the square of a rational function corresponding to $[(\phi(s)I_N + L)^{-1}]_{kl}$, $F_{kl}(s)^2$. Note that $L_{kl}^2 = \lim_{s\to\infty} s^{4r} F_{kl}(s)^2/\beta_f^4$. Then denoting by ν_{kl} the coefficient of the $2(Nq - 2r)$-order term of the numerator of $F_{kl}(s)^2$, we find $L_{kl}^2 = \nu_{kl}/\beta_f^4$. Since $L_{kl} \geq 0$, $k \neq l$, we have

$$L_{kl} = \frac{\sqrt{\nu_{kl}}}{\beta_f^2}. \tag{14.7}$$

Next we consider a problem to extract the weight of the self-loop, L_{kk}, from the diagonal entry $\left[(\phi(s)I_N - L)^{-1}\right]_{kk}$. For the diagonal entry, we have

$$\left[(\phi(s)I_N - L)^{-1}\right]_{kk} = \frac{1}{\phi(s) - L_{kk} - L_{k*}\Theta^{\{k\}}(s)L_{*k}}.$$

Note that the form of this rational function differs from that of (14.5), and the relation of (14.6) is invalid for the diagonal case. However, it is still possible to extract L_{kk} if ϕ is known. In fact, applying the following recursive calculation to $\left[(\phi(s)I_N - L)^{-1}\right]_{kk}$

$$\begin{cases} H_0(s) = s^{r-1}\left[(\phi(s)I_N - L)^{-1}\right]_{kk}, \\ H_n(s) = sH_{n-1}(s) - \xi_{n-1}, & n = 1, \ldots, r, \\ \xi_0 = \beta_f, \\ \xi_n = \beta_{f-n} - \sum_{k=0}^{n-1} \alpha_{e-n+k}\xi_k, & n = 1, \ldots, r, \end{cases} \tag{14.8}$$

where β_l ($l < 0$) is zero when $r > f$, we derive

$$H_r(s) = \frac{\left(\beta_f^2 L_{kk} + \xi_r\right) s^{e-1} + (\text{less than } (e-1)\text{-order terms})}{\sum_{i=0}^{e} \alpha_i s^i - \left(\sum_{i=0}^{f} \beta_i s^i\right)\left[L_{kk} + L_{k*}\Theta^{\{k\}}(s)L_{*k}\right]},$$

and

$$\lim_{s\to\infty} sH_r(s) = \beta_f^2 L_{kk} + \xi_r. \tag{14.9}$$

Thus, one can extract L_{kk} from $\left[(\phi(s)I_N - L)^{-1}\right]_{kk}$ using the information on $\phi(s)$.

14.2.3.3 Algorithm (Summary)

Summarizing the above discussion, we derive an algorithm as follows:

Algorithm From the knowledge of subsystem (A, b, c), calculate the transfer function $h(s) = n(s)/d(s)$.
$\langle\langle$ Case $k = l$ $\rangle\rangle$

- d1 For the NW system Σ and knocked-out NW system $\Sigma^{\{k\}}$, identify their characteristic polynomials, and denote them as $p(s)$ and $p_k(s)$, respectively.
- d2 Calculate $n(s)p_k(s)/p(s)$, and denote it by $F_{kk}(s)$, which is an estimate for $[(\phi(s)I_N - L)^{-1}]_{kk}$.
- d3 Calculate (14.8) for F_{kk} instead of $[(\phi(s)I_N - L)^{-1}]_{kk}$. Then, from (14.9), we derive an estimate for L_{kk} as

$$\tilde{L}_{kk} = \frac{-\xi_r + \lim_{s\to\infty} sH_r(s)}{\beta_f^2}.$$

$\langle\langle$ Case $k \neq l$ $\rangle\rangle$

- o1 For the NW system Σ, knocked-out NW systems $\Sigma^{\{k\}}$, $\Sigma^{\{l\}}$, and $\Sigma^{\{k,l\}}$, identify their characteristic polynomials, and denote them as $p(s)$, $p_k(s)$, $p_l(s)$, and $p_{kl}(s)$, respectively.

o2 Calculate $n(s)^2[p_k(s)p_l(s) - p(s)p_{kl}(s)]$, and let $\tilde{\nu}_{kl}$ be the coefficient of its $2(Nq - 2r)$-order term, which is an estimate for the corresponding coefficient for the numerator of $[(\phi(s)I_N - L)^{-1}]^2_{kl}$.
o3 From (14.7), we derive an estimate for L_{kl} as

$$\tilde{L}_{kl} = \frac{\sqrt{\tilde{\nu}_{kl}}}{\beta_f^2}.$$

14.3 Identification of a Transfer Characteristic Among Measurable Nodes

In this section, we discuss a NW structure reflecting transfer characteristics among measurable nodes in which other unmeasurable nodes are treated together as a hidden subsystem. We start to define the NW structure, and confirm its meaning. Then, the identification problem will be formulated, and some analysis results will be shown.

14.3.1 Network System and Its Dynamical Structure Function

Consider N one-dimensional systems

$$\Sigma_k : \begin{cases} \dot{x}_k = \alpha_k x_k + v_k, \\ z_k = x_k, \end{cases} \quad k \in S = \{1, \ldots, N\},$$

where $x_k(t) \in \mathbb{R}$, $v_k(t) \in \mathbb{R}$ and $z_k(t) \in \mathbb{R}$ are the state, the input and the output, respectively. Suppose that these systems construct a NW. The input to each subsystem is given by

$$v_k = \sum_{l \neq k} L_{kl} z_k + B_k u,$$

where $u(t) \in \mathbb{R}^m$ is an external input, and $L_{kl} \in \mathbb{R}$ and $B_k \in \mathbb{R}^{1\times m}$ denote the connectivity strength to subsystem Σ_k from the output of subsystem Σ_l and u, respectively. Moreover, suppose that the output signals of p ($\leq N$) subsystems are measurable Without loss of generality, one can consider Σ_k, $k = 1, \ldots, p$ to be the measurable subsystems. Letting $B_1 := \begin{bmatrix} B_1^\mathsf{T} & \cdots & B_p^\mathsf{T} \end{bmatrix}^\mathsf{T}$, $B_2 := \begin{bmatrix} B_{p+1}^\mathsf{T} & \cdots & B_N^\mathsf{T} \end{bmatrix}^\mathsf{T}$, and $L_{kk} := \alpha_k$, and defining a weighted adjacency matrix by

$$A = \begin{bmatrix} A_{11} & A_{12} \\ A_{21} & A_{22} \end{bmatrix} := [L_{kl}]_{k,l\in S},$$

we derive the following representation of the NW system:

$$\Sigma : \begin{cases} \begin{bmatrix} \dot{y} \\ \dot{x}_h \end{bmatrix} = \begin{bmatrix} A_{11} & A_{12} \\ A_{21} & A_{22} \end{bmatrix} \begin{bmatrix} y \\ x_h \end{bmatrix} + \begin{bmatrix} B_1 \\ B_2 \end{bmatrix} u, \\ y = [I \;\; 0] \begin{bmatrix} y \\ x_h \end{bmatrix}, \end{cases} \tag{14.10}$$

where $y = [x_1 \;\cdots\; x_p]^\mathsf{T}$ and $x_h = [x_{p+1} \;\cdots\; x_N]^\mathsf{T}$.

Applying the Laplace transformation $\mathscr{L}$ to (14.10) under the assumption that the initial value is zero, and canceling variable X_h ($:= \mathscr{L}\{x_h\}$), we have

$$sY(s) = [A_{11} + A_{12}(sI - A_{22})^{-1}A_{21}]Y(s) + [B_1 + A_{12}(sI - A_{22})^{-1}B_2]U(s), \tag{14.11}$$

where $Y = \mathscr{L}\{y\}$ and $U = \mathscr{L}\{u\}$. Let

$$W(s) = A_{11} + A_{12}(sI - A_{22})^{-1}A_{21},$$
$$V(s) = B_1 + A_{12}(sI - A_{22})^{-1}B_2,$$

and define a diagonal matrix D consisting of the diagonal of W by

$$D(s) = \mathrm{diag}_{k\in\{1,\ldots,p\}}\{W_{kk}(s)\}.$$

Then transform (14.11) as follows:

$$Y(s) = Q(s)Y(s) + P(s)U(s),$$

where

$$Q(s) = (sI - D(s))^{-1}(W(s) - D(s)), \tag{14.12}$$
$$P(s) = (sI - D(s))^{-1}V(s). \tag{14.13}$$

Note that the diagonal elements of Q are zero. The function Q, P, and the pair (Q, P) are called the *internal structure function*, *control structure function*, and *dynamical structure function*, respectively.

The meaning of these functions will be explained below. To this end, we denote by Σ^m and Σ^h a sub-NW consisting of the measurable subsystems $\{\Sigma_k\}_{k=1}^p$ and one consisting of the hidden subsystems $\{\Sigma_k\}_{k=p+1}^N$, respectively. Furthermore, let $L_{k*} := [L_{k,p+1} \cdots L_{kN}]$, and $L_{*l} := [L_{p+1,l} \cdots L_{Nl}]^\mathsf{T}$. Then, the NW system Σ can be regarded as a closed-loop system as shown in Fig. 14.2.

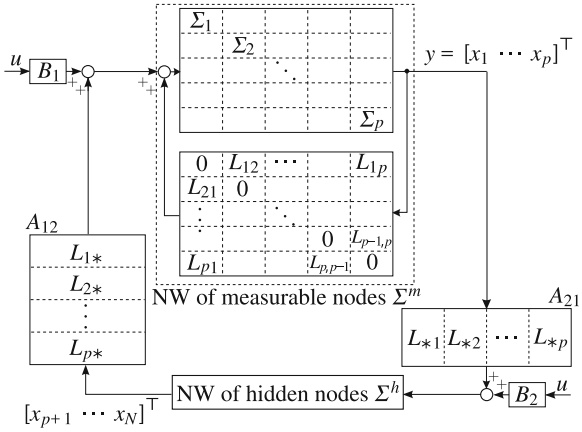

Fig. 14.2 Block diagram of the NW system Σ. The NW is divided into the sub-NW of the measurable nodes, Σ^m, and that of the hidden nodes, Σ^h. The symbol "$*$" denotes indices $(p+1, \ldots, N)$; e.g., L_{k*} denotes $[L_{k,p+1} \cdots L_{kN}]$

The meaning of the inner structure function Q

The rational function Q_{kl} $(1 \leq k, l \leq p, k \neq l)$ can be calculated as

$$Q_{kl}(s) = [(sI - D(s))^{-1}]_{kk} W_{kl}$$
$$= \underbrace{\frac{\frac{1}{s-L_{kk}}}{1 - \frac{1}{s-L_{kk}} \cdot L_{k*}(sI - A_{22})^{-1} L_{*k}}}_{\text{(i)}} \cdot \underbrace{\left[L_{kl} + L_{k*}(sI - A_{22})^{-1} L_{*l} \right]}_{\text{(ii)}}.$$

The part of (i) means the transfer function of a closed-loop system that consists of subsystem Σ_k and sub-NW of the hidden subsystems, Σ^h, from an input to the inner state. The part of (ii) is the sum of two transfer operator from x_l to the input for Σ_k: One is the feedthrough operator (i.e., constant scalar L_{kl}), and the other is the transfer operator via Σ^h (i.e., $L_{k*}(sI - A_{22})^{-1} L_{*l}$). Then it turns out that Q_{kl} corresponds to the transfer function from x_l to x_k in the block diagram shown in Fig. 14.3. In other words, Q_{kl} implies the transfer function of the sub-NW system derived by removing measurable subsystems other than Σ_k and the external input ports from the whole NW system in Fig. 14.2.

Thus, as explained in [2], the matrix Q represents a weighted adjacency matrix among "measurable" nodes. The weights are strictly proper transfer functions, and hence, this representation of Q preserves the causality of the measurable variables. Moreover, it can be said that, this representation is indirect in the sense that measurable nodes may influence each other through hidden nodes, while it is direct in the sense that each weight does not depend on any other measurable nodes. Transfer function $\left[(\phi(s) I_N - L)^{-1}\right]_{kl}$ in Sect. 14.2 does not have the later property, because $\left[(\phi(s) I_N - L)^{-1}\right]_{kl}$ includes the dynamics of subsystems other than Σ_k and Σ_l, regardless of whether they are measurable or not.

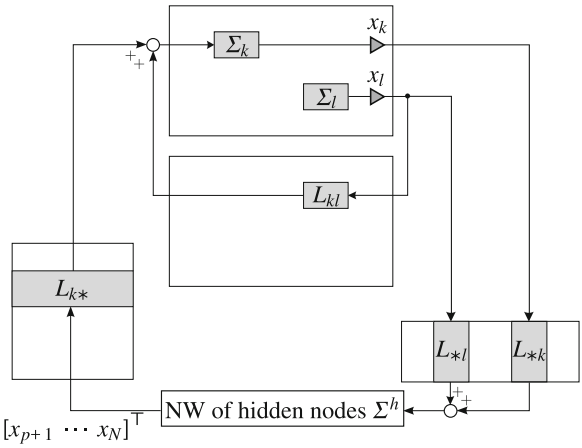

Fig. 14.3 Block diagram representing the (k, l)-entry of the inner structure function Q: the rational function of Q_{kl} is the transfer function from x_l to x_k in this diagram. Note that Q_{kl} does not include the dynamics of Σ_l

The meaning of the control structure function P

In a similar way to the inner structure function, we find that P_{kr} $(1 \leq k \leq p,$ $1 \leq r \leq m)$ can be calculated as

$$P_{kr}(s) = [(sI - D(s))^{-1}]_{kk} V_{kr}$$
$$= \underbrace{\frac{\frac{1}{s-L_{kk}}}{1 - \frac{1}{s-L_{kk}} \cdot L_{k*}(sI - A_{22})^{-1} L_{*k}}}_{\text{(i)}} \cdot \underbrace{\left[(B_1)_{kr} + L_{k*}(sI - A_{22})^{-1}(B_2)_{*r}\right]}_{\text{(ii)}'}.$$

Again, the part of (i) describes the same closed-loop of Σ_k and Σ^h as above. The part of (ii)$'$ is composed of the feedthrough-and Σ^h-through-operators from u_r to the input of Σ_k, i.e., $(B_1)_{*r}$ and $L_{k*}(sI - A_{22})^{-1}(B_2)_{*r}$, respectively. Thus P_{kr} corresponds to the transfer function from u_r to x_k in Fig. 14.4, which does not include the inner dynamics among the measurable nodes.

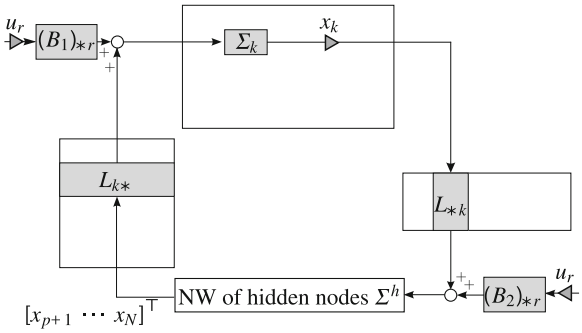

Fig. 14.4 The block diagram representing (k, r)-entry of the control structure function P: The rational function P_{kr} is the transfer function from u_r to x_k in this diagram. Two u_r's are identical

14.3.2 Reconstruction of Dynamical Structure Function from the Transfer Function of the NW System

14.3.2.1 Necessary and Sufficient Condition for the Reconstruction

Denote by G the transfer function of the NW system of (14.10) from the input u to the output y. Since $(I - Q(s))Y(s) = P(s)U(s)$,

$$G(s) = (I - Q(s))^{-1} P(s) \tag{14.14}$$

holds. Recall that G can be uniquely identified by using appropriate input/output data in general. As we saw above, (Q, P) possesses valuable properties as a NW structure, and hence, it makes a sense to discuss the reconstruction of (Q, P) from G. Gonçalves and Warnick have formulated this problem in [2]. In the formulation, "reconstruction" refers to (Q, P) being found as a pair of matrices specified from a realization of G by (14.12) and (14.13). Therefore, the diagonal elements of Q must be zero, and (Q, P) must be strictly proper. Unfortunately, for a given G, (Q, P) is not uniquely determined in general. Thus, we have the following question:

Problem 14.2 Suppose that a $p \times m$ transfer function G is given. When can (Q, P) be reconstructed from G?

To find the reason why the existence of (Q, P) satisfying (14.14) is not unique, consider a transformation of (14.14)

$$G^{\mathsf{T}} = M_G [Q \ P]^{\mathsf{T}}, \tag{14.15}$$

where

$$M_G : \mathbb{C}^{p+m} \to \mathbb{C}^m : w \mapsto \begin{bmatrix} G^{\mathsf{T}} & I \end{bmatrix} w.$$

Since the nullspace of a linear operator M_G is p-dimensional, there exist an infinite number of pairs (Q, P) satisfying (14.14) in general. More specifically, the following can be shown:

Proposition 14.1 (Gonçalves and Warnick [2]) *Given a $p \times m$ transfer function G, a set $\mathscr{S}_G$ of dynamical structure functions (Q, P) that satisfy (14.14) can be parameterized by $p \times p$ inner structure functions $\tilde{Q}$ as follows*:

$$\mathscr{S}_G = \left\{ (Q, P) : \begin{bmatrix} Q^{\mathsf{T}} \\ P^{\mathsf{T}} \end{bmatrix} = \begin{bmatrix} 0 \\ G^{\mathsf{T}} \end{bmatrix} + \begin{bmatrix} I \\ -G^{\mathsf{T}} \end{bmatrix} \tilde{Q}^{\mathsf{T}}, \ \tilde{Q} \in \mathscr{Q} \right\}.$$

Here, $\mathscr{Q}$ is a set of inner structure functions.

Since the diagonal of the inner structure function is zero, the choice of $\tilde{Q}$ has $p^2 - p$ degree of freedom. Thus, if one has no information on the NW structure in advance it is impossible to reconstruct (Q, P) from G. Conversely, when we

know the component of (Q, P) in the nullspace of M_G from a priori knowledge, (Q, P) can be uniquely determined.

Theorem 14.4 (Gonçalves and Warnick [2]) *Given a $p \times m$ transfer function G, the dynamical structure function (Q, P) can be reconstructed (by some knowledge of the structure) if and only if, for each column of $[Q\ P]^{\mathsf{T}}$, $p-1$ entries that uniquely determine the components of the column in the nullspace of M_G are known.*

The necessary and sufficient condition in Theorem 14.4 can be checked using the given transfer function G as follows. Suppose that γ and $p-\gamma$ entries in kth rows of Q and P, respectively, are known. Here, the known entries include $Q_{kk}\ (=0)$. Denote by S and T the indices of these known entries as

$$\begin{aligned} S &:= (s_1, \ldots, s_\gamma), \quad 1 \le s_1 < \cdots < s_\gamma \le p, \quad \text{for } Q, \\ T &:= (t_1, \ldots, t_{p-\gamma}), \ 1 \le t_1 < \cdots < t_{p-\gamma} \le m, \ \text{for } P. \end{aligned}$$

Meanwhile, denote by $\bar{S}$ and $\bar{T}$ the indices of the other unknown entries as

$$\begin{aligned} \bar{S} &:= (\bar{s}_1, \ldots, \bar{s}_{p-\gamma}), \quad 1 \le \bar{s}_1 < \cdots < \bar{s}_{p-\gamma} \le p, \quad \text{for } Q, \\ \bar{T} &:= (\bar{t}_1, \ldots, \bar{t}_{m-p+\gamma}), \ 1 \le \bar{t}_1 < \cdots < \bar{t}_{m-p+\gamma} \le m, \ \text{for } P. \end{aligned}$$

Furthermore, for index-sets E and F of length $|E|$ and $|F|$, respectively, let G_{EF} be a $|E| \times |F|$ matrix arraying entries of G that are specified by E and F for the row and column, respectively. Then transforming the following equation

$$M_G \begin{bmatrix} Q_{k*} & P_{k\dagger} \end{bmatrix}^{\mathsf{T}} = 0, \quad * = (1, \ldots, p), \quad \dagger = (1, \ldots, m),$$

we derive

$$\underbrace{\begin{bmatrix} Q_{k\bar{S}} & P_{k\bar{T}} \end{bmatrix} \begin{bmatrix} G_{\bar{S}T} & G_{\bar{S}\bar{T}} \\ 0 & I \end{bmatrix}}_{(\star)} = -\underbrace{\begin{bmatrix} Q_{kS} & P_{kT} \end{bmatrix}}_{\text{known}} \begin{bmatrix} G_{ST} & G_{S\bar{T}} \\ I & 0 \end{bmatrix}.$$

For any given entries $[Q_{kS}\ P_{kT}]$, entries $\begin{bmatrix} Q_{k\bar{S}} & P_{k\bar{T}} \end{bmatrix}$ are uniquely determined. This means that a vector $\begin{bmatrix} Q_{k*} & P_{k\dagger} \end{bmatrix}^{\mathsf{T}}$ in the nullspace is determined, if and only if matrix of $(\star)$ is non-singular. In summary, we have the following:

Proposition 14.2 *The entries $\{Q_{ks}\}_{s\in S}$ and $\{P_{kt}\}_{t\in T}$ specify the components of kth columns of $[Q\ P]^{\mathsf{T}}$ in the nullspace of M_G if and only if $(p-\gamma)\times(p-\gamma)$ transfer function matrix $G_{\bar{S}T}$ is nonsingular.*

In the same way as above, we can calculate $\begin{bmatrix} Q_{k\bar{S}} & P_{k\bar{T}} \end{bmatrix}$ by

$$\begin{bmatrix} Q_{k\bar{S}} & P_{k\bar{T}} \end{bmatrix} = \left(\begin{bmatrix} G_{kT} & G_{k\bar{T}} \end{bmatrix} - \begin{bmatrix} Q_{kS} & P_{kT} \end{bmatrix} \begin{bmatrix} G_{ST} & G_{S\bar{T}} \\ I & 0 \end{bmatrix} \right) \begin{bmatrix} G_{\bar{S}T} & G_{\bar{S}\bar{T}} \\ 0 & I \end{bmatrix}^{-1}$$

when $G_{\bar{S}T}$ is nonsingular.

14.3.2.2 Reconstruction Using Independent Inputs to Measurable Nodes

As a special case, we suppose that $m = p$, G is nonsingular, the external inputs are added to the measurable nodes independently, and moreover, these inputs do not affect hidden nodes (i.e., $B_2 = 0$). Without loss of generality, one can consider that the inputs are numbered such that the control structure function P is diagonal. Note that $p^2 - p$ off-diagonal entries are zeros. Since the condition of Theorem 14.4 holds, the dynamical structure function can be uniquely reconstructed. In fact, the following is true.

Proposition 14.3 (Gonçalves and Warnick [2]) *Assume that $m = p$, G is full rank, and each external input is added to a measurable node independently. Then the dynamical structure function can be uniquely determined. Moreover, letting $H(s) := G(s)^{-1}$, we have*

$$Q_{kl} = -\frac{H_{kl}}{H_{kk}}, \quad P_{kk} = \frac{1}{H_{kk}}.$$

14.3.2.3 Extension to NW of Multi-Dimensional Subsystems

The discussions in this section can be extended to NW systems of multi-dimensional subsystem (Λ, b, c). Consider the following NW system:

$$\Sigma : \begin{cases} \begin{bmatrix} \dot{x}^m \\ \dot{x}^h \end{bmatrix} = \left(I_N \otimes \Lambda + \begin{bmatrix} A_{11} & A_{12} \\ A_{21} & A_{22} \end{bmatrix} \otimes bc \right) \begin{bmatrix} x^m \\ x^h \end{bmatrix} + \begin{bmatrix} B_1 \\ B_2 \end{bmatrix} u, \\ y = \left(\begin{bmatrix} I_p & 0 \end{bmatrix} \otimes c \right) \begin{bmatrix} x^m \\ x^h \end{bmatrix}. \end{cases}$$

Using the generalized frequency variable of the subsystem, $\phi(s) := 1/c(sI - \Lambda)^{-1}b$, and (Q, P) of (14.12)–(14.13), we define

$$\hat{Q}(s) = Q(\phi(s)) \quad \text{and} \quad \hat{P}(s) = P(\phi(s)),$$

that is, $\hat{Q}(s)$ and $\hat{P}(s)$ are defined by replacing s of $Q(s)$ and $P(s)$ with $\phi(s)$. Recall from Sect. 14.2.2 that the transfer function of Σ is given by $G(\phi(s))$ $(:= \hat{G}(s))$, in which G is the transfer function of (14.10). Then it turns out that $\left(\hat{Q}, \hat{P}\right)$ is the dynamical structure function of the NW system Σ, and satisfies

$$\hat{G} = \left(I_p - \hat{Q}\right)^{-1} \hat{P}.$$

Since algebraic structure is the same as NW of one-dimensional subsystems, the results shown above are still valid.

14.4 Conclusions and Discussions

In this chapter, for linear NW systems with unmanipulable/unmeasurable nodes, a problem to identify their NW structures was considered, and two approaches to the problem were introduced. One was a characteristic-polynomial-based method using the knock-out procedure, and the other was a study on the reconstruction of the dynamical structure function.

The former focuses on a matrix $(\phi(s)I - L)^{-1}$, where L is the adjacency matrix of NW system and $\phi(s)$ is the reciprocal number of the transfer function of nodes. Preparing knocked-out NW systems in which some subsystems are kept steady states, and using the characteristic polynomials estimated by the existing system identification method, entries of $(\phi(s)I - L)^{-1}$ can be calculated. Then, the weights of the edges are individually extracted from the entries of $(\phi(s)I - L)^{-1}$. The main advantage is that one can identify the strength of connectivity between two nodes even if they are unmanipulable and unmeasurable. However, since this method is on the basis of the identification of the characteristic polynomials, we assumed that the NW system is controllable and observable to derive consistent estimates of the characteristic polynomials. It is needed to investigate how the estimates are affected by uncontrollable/unobservable modes, which is one of the future issues.

The second approach focuses on a NW structure reflecting transfer properties among measurable nodes, which is called the dynamical structure function. The hidden nodes are treated as a sub-NW system, and the dynamical structure function does not give any information on the individual hidden nodes. Nevertheless, the dynamical structure function preserves the original causality of the NW system. Moreover, the reconstruction of the dynamical structure function is formulated as a decomposition of the NW system's transfer function, one needs not take into account the controllable/observable property.

Acknowledgments We would like to express our gratitude to Mr. Nobuki Takatsuki, Mr. Soshi Katsuta and Mr. Shota Mizuta, Tokyo Institute of Technology, for giving valuable comments.

References

1. August, E., Papachristdoulou, A.: Efficient, sparse biological network determination. BMC Syst. Biol. **3**(1), 25 (2009)
2. Gonçalves, J., Warnick, S.: Necessary and sufficient conditions for dynamical structure reconstruction of LTI networks. IEEE Trans. Autom. Control **53**(7), 1670–1674 (2008)
3. Hara, S., Hayakawa, T., Sugata, H.: Stability analysis of linear systems with generalized frequency variables and its applications to formation control. Proceedings of IEEE Conference on Decision and Control (2007)
4. Hayden, D., Yuan, Y., Gonçalves, J.: Network reconstruction using knock-out and over-expression data. Proceedings of European Control Conference (2013)
5. Horn, R.A., Johnson, C.R.: Matrix Analysis. Cambridge University Press, Cambridge (1985)
6. Julius, A., Zavlanos, M., Boyd, S., Pappas, G.J.: Genetic network identification using convex programming. IET Syst. Biol. **3**(3), 155–166 (2009)

7. Liu, H., Lu, J.A., Lu, J., Hill, D.J.: Structure identification of uncertain general complex dynamical networks with time delay. Automatica **45**(8), 1799–1807 (2009)
8. Ljung, L.: System Identification: Theory for the User. Prentice-Hall, Englewood Cliffs (1987)
9. Lyzell, C., Enqvist, M., Ljung, L.: Handling certain structure information in subspace identification. Proceedings of IFAC Symposium on System Identification (2009)
10. Materassi, D., Innocenti, G.: Topological identification in networks of dynamical systems. IEEE Trans. Autom. Control **55**(8), 1860–1871 (2010)
11. Materassi, D., Salapaka, M.V.: Network reconstruction of dynamical polytrees with unobserved nodes. Proceedings of IEEE Conference on Decision and Control (2012)
12. Mullis, C.T., Roberts, R.A.: Roundoff noise in digital filters: frequency transformations and invariants. IEEE Trans. Autom. Control **24**(6), 538–550 (1976)
13. Nabi-Abdolyousefi, M., Fazel, M., Mesbahi, M.: A graph realization approach to network identification. Proceedings of IEEE Conference on Decision and Control (2012)
14. Nabi-Abdolyousefi, M., Mesbahi, M.: Network identification via node knock-out. IEEE Trans. Autom. Control **57**(12), 3214–3219 (2012)
15. Napoletani, D., Sauer, T.D.: Reconstructing the topology of sparsely connected dynamical networks. Phys. Rev. E. **77**, 026, 103 (2008)
16. Su, R.Q., Wang, W.X., Lai, Y.C.: Detecting hidden nodes in complex networks from time series. Phys. Rev. E. **85**, 065, 201 (2012)
17. Suzuki, M., Takatsuki, N., Imura, J., Aihara, K.: Node knock-out based structure identification in networks of identical multi-dimensional subsystems. Proceedings of European Control Conference (2013)
18. Timme, M.: Revealing network connectivity from response dynamics. Phys. Rev. Lett. **98**, 224101 (2007)
19. Yeung, E., Gonçalves, J., Sandberg, H., Warnick, S.: The meaning of structure in interconnected dynamic systems. arXiv preprint. arXiv:1108.2755 (2011)
20. Yuan, Y., Stan, G.B., Warnick, S., Goncalves, J.: Robust dynamical network structure reconstruction. Automatica **47**(6), 1230–1235 (2011)

Index

K. Aihara et al. (eds.), *Analysis and Control of Complex Dynamical Systems*,
Mathematics for Industry 7, DOI 10.1007/978-4-431-55013-6